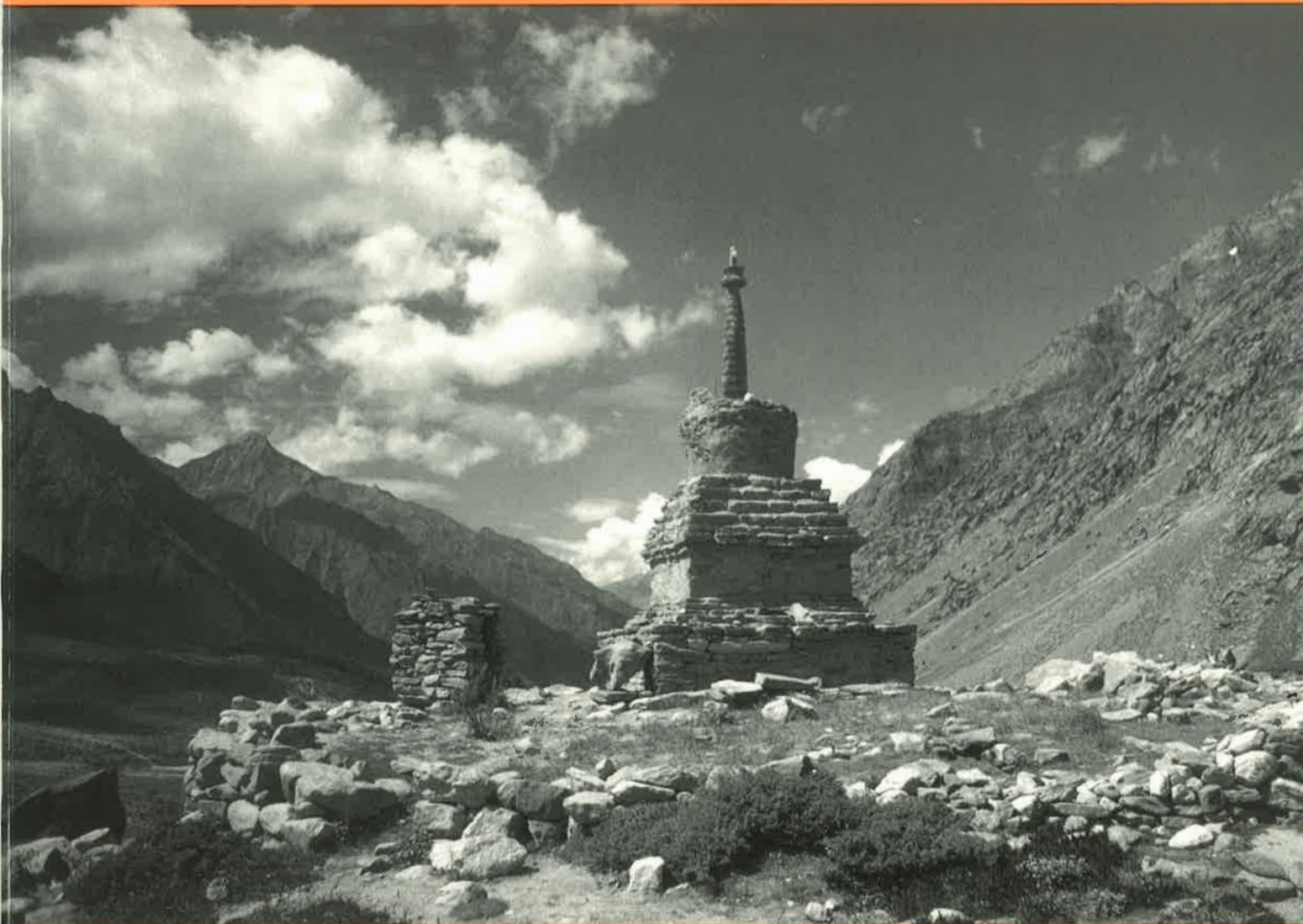


# **Thrusting, extension and doming in the High Himalaya of Lahul-Zaskar area (NW India) : structural and pressure-temperature constraints.**

par Martin Robyr



# Mémoires de Géologie (Lausanne)

*Section des Sciences de la Terre*  
*Université de Lausanne*  
BFSH-2, 1015 Lausanne, Suisse



This work is licensed under a Creative Commons  
Attribution 4.0 International License  
<http://creativecommons.org/licenses/by-nc-nd/4.0/>

40

# Mémoires de Géologie (Lausanne)

EDITEUR DE LA SERIE

Jean Guex  
Institut de Géologie et Paléontologie  
BFSH-2 Université de Lausanne  
CH-1015, Lausanne SUISSE

COMITE EDITORIAL

Clark Blake  
U.S. Geological Survey  
345 Middlefield Road  
94025 Menlo Park, California, U.S.A.

Francis Hirsch  
Geological Survey of Israel,  
30 Malkhe Israel Street  
95501 Jerusalem, ISRAEL

Gilles S. Odin  
Géochronologie et Sédimentologie  
Université P. et M. Curie, 4 Place Jussieu  
75252 Paris Cedex 05 FRANCE

Hugo Bucher  
Paleontologisches Institut  
Universität Zürich  
8006 Zürich

Alan R. Lord  
Department of Earth Science  
University College, Gower Street  
WC1E 6BT, London, U.K.

José Sandoval  
Dpto. Estratigrafía y Paleontología  
Universidad de Granada  
18002, Granada, ESPAGNE

David Taylor  
ODOT  
Portland, Oregon  
USA

Jean Marcoux  
Géologie Paris VII et IPGP  
Tour 25/24 1er étage, 2 place Jussieu  
75251 Paris Cedex 05 FRANCE

Rudolph Trümpy  
Geologisches Institut, ETH-zentrum  
Sonneggstrasse 5  
CH-8092, Zürich, SUISSE

Giorgio Martinotti  
Dipartimento di Scienze della Terra  
Università, Via Valperga Caluso 37  
10125 Torino ITALIE

Mémoires de Géologie (Lausanne)  
Section des Sciences de la Terre  
Institut de Géologie et Paléontologie  
Université de Lausanne  
BFSH-2, CH-1015 Lausanne

ROBYR Martin

Titre : Thrusting, extension and doming in the High Himalaya of Lahul-Zaskar area (NW India)  
Mém. Géol. (Lausanne), n° 40, 2002, 127 pp., 62 text-figs., 1 pl.  
ISSN: 1015-3578

Imprimeur : Chabloz S.A., Tolochenaz

**THRUSTING, EXTENSION AND  
DOMING IN THE HIGH HIMALAYA OF  
LAHUL-ZANSKAR AREA (NW INDIA)**

Martin Robyr

Mémoires de Géologie (Lausanne), No 40, 2002

# CONTENT

## ABSTRACT

## RESUME

|  |           |
|--|-----------|
| <b>CHAPTER 1: INTRODUCTION</b>                                   | <b>1</b>  |
| 1.1. PREAMBLE  | 1         |
| 1.2. GEOGRAPHICAL SETTING  | 2         |
| <b>CHAPTER 2: GEOLOGICAL SETTING</b>                             | <b>7</b>  |
| 2.1. INTRODUCTION  | 7         |
| 2.2. MAIN TECTONIC SUBDIVISIONS OF THE HIMALAYA                  | 7         |
| 2.2.1. The main Himalayan structures                             | 8         |
| 2.2.1.1. <i>The Main Frontal Thrust (MFT)</i>                    | 8         |
| 2.2.1.2. <i>The Main Boundary Thrust (MBT)</i>                   | 8         |
| 2.2.1.3. <i>The Main Central Thrust (MCT)</i>                    | 8         |
| 2.2.1.4. <i>The South Tibetan Detachment System (STDS)</i>       | 8         |
| 2.2.2. The main tectono-metamorphic units                        | 9         |
| 2.2.2.1. <i>The Subhimalaya</i>                                  | 10        |
| 2.2.2.2. <i>The Lesser Himalaya</i>                              | 10        |
| 2.2.2.3. <i>The High Himalayan Crystalline</i>                   | 10        |
| 2.2.2.4. <i>The Tethyan Himalaya</i>                             | 11        |
| 2.2.2.5. <i>The Indus-Tsangpo Suture Zone</i>                    | 11        |
| 2.3. HISTORY OF GEOLOGICAL INVESTIGATIONS                        | 12        |
| <b>CHAPTER 3: PURPOSE OF THE STUDY</b>                           | <b>15</b> |
| <b>CHAPTER 4. STRATIGRAPHY</b>                                   | <b>21</b> |
| 4.1. INTRODUCTION  | 21        |
| 4.2. THE PHE FORMATION   | 21        |
| 4.2.1. Introduction  | 21        |
| 4.2.2. Age of the Phe Formation                                  | 23        |
| 4.2.3. Origin and depositional environment of the Phe Formation. | 24        |
| <b>CHAPTER 5: TECTONICS</b>                                      | <b>25</b> |
| 5. 1. INTRODUCTION   | 25        |
| 5. 2. TECTONIC FRAMEWORK OF THE LAHUL AND ZANSKAR AREA           | 25        |

|   |           |
|---|-----------|
| 5. 2. 1. Introduction   | 25        |
| 5. 2. 2. Phase D1: The NE-directed Shikar Beh nappe                                 | 28        |
| 5. 2. 3. Phase D2: The SW-directed Nyimaling-Tsarap nappe                           | 28        |
| 5. 2. 4. Phase D3: The SW-directed High Himalayan nappe                             | 30        |
| 5. 2. 5. Phase D4: The doming phase   | 31        |
| 5. 3. STRUCTURAL GEOLOGY OF THE MIYAR VALLEY SECTION                                | 31        |
| 5. 3. 1. Introduction   | 31        |
| 5. 3. 2. Phase D1: The NE-directed Shikar Beh structures                            | 32        |
| 5. 3. 2. 1. <i>The Miyar Thrust Zone and associated structures</i>                  | 32        |
| 5. 3. 2. 2. <i>The earliest phase and associated structures</i>                     | 42        |
| 5. 3. 2. 3. <i>Discussion</i>   | 45        |
| 5. 3. 3. Phase D2: The SW-directed Nyimaling-Tsarap structures                      | 45        |
| 5. 3. 4. Phase D3: The SW-directed High Himalayan Nappe structures                  | 47        |
| 5. 3. 4. 1. <i>Crenulation cleavage S3 and F3 chevron folds</i>                     | 47        |
| 5. 3.4. 2. <i>Discussion</i>  | 48        |
| 5. 3. 5. Phase D4: The doming phase and the Khanjar Shear Zone                      | 48        |
| 5. 3. 5. 1. <i>The Khanjar Shear Zone and associated structures</i>                 | 48        |
| 5. 3. 5. 2. <i>Discussion</i>   | 51        |
| 5. 3. 6. Additional late phases   | 51        |
| 5. 3. 6. 1. <i>Phase D<sub>A</sub> : Dextral Strike-Slip Shearing</i>               | 52        |
| 5. 3. 6. 2. <i>Phase D<sub>B</sub> :Late NW-directed folding</i>                    | 52        |
| 5. 3. 6. 3. <i>Phase D<sub>C</sub> :Late vertical movements</i>                     | 55        |
| 5. 3. 7. Pre-Himalayan and Tertiary pegmatitic and leucogranitic dykes              | 55        |
| 5.3.7.1. <i>Pre-Himalayan pegmatitic dykes</i>                                      | 56        |
| 5.3.7.2. <i>Tertiary leucogranitic dykes and sills</i>                              | 56        |
| 5. 3. 8. Conclusions of the structural investigations in the Miyar Valley section   | 60        |
| 5. 4. STRUCTURAL GEOLOGY OF THE GIANBUL VALLEY SECTION                              | 61        |
| 5. 4. 1. Introduction   | 61        |
| 5. 4. 2. Phase D2: The SW-directed Nyimaling-Tsarap structures                      | 61        |
| 5. 4. 3. Phase D3: The NE-directed extensional Zanskar Shear Zone                   | 62        |
| 5. 4. 4. Phase D4: The doming phase and the High-angle normal faults                | 64        |
| 5. 4. 5. Conclusions of the structural investigations in the Gianbul Valley section | 64        |
| 5. 5. CHRONOLOGY OF THE TECTONIC EVENTS   | 64        |
| 5. 6. CONCLUSIONS   | 66        |
| <b>CHAPTER 6: METAMORPHISM</b>  | <b>69</b> |
| 6. 1. INTRODUCTION  | 69        |
| 6.2. MIYAR VALLEY SECTION   | 73        |
| 6.2.1. Prograde metamorphic field gradient (M1)                                     | 73        |

|   |            |
|---|------------|
| 6.2.1.1. Chlorite and biotite zones                                       | 78         |
| 6.2.1.2. Garnet zone  | 79         |
| 6.2.1.3. Kyanite and staurolite zone                                      | 81         |
| 6.2.1.4. Sillimanite zone   | 81         |
| 6.2.1.5. Migmatite zone   | 82         |
| 6.2.2. Thermobarometry  | 83         |
| 6.2.2.1. Methodology  | 83         |
| 6.2.2.2. Results  | 83         |
| 6.2.3. Oxygen isotope thermometry   | 87         |
| 6.2.4. Discussion   | 91         |
| 6.2.5. Retrograde metamorphic evolution (M4)                              | 91         |
| 6.3. GIANBUL VALLEY SECTION   | 94         |
| 6.3.1. SW-directed Nyimaling –Tsarap nappe and prograde metamorphism (M2) | 94         |
| <i>Discussion</i>   | 95         |
| 6.3.2. Zaskar Shear Zone and retrograde metamorphism (M3)                 | 97         |
| 6.4. SYNTHESIS  | 100        |
| 6.5. CONCLUSIONS  | 102        |
| 6.6. APPENDIX   | 104        |
| <b>CHAPTER 7: MECHANISM OF THE GIANBUL DOME FORMATION</b>                 | <b>109</b> |
| <b>CHAPTER 8: CONCLUSIONS</b>   | <b>113</b> |
| <b>ACKNOWLEDGEMENTS</b>   | <b>115</b> |
| <b>BIBLIOGRAPHY</b>   | <b>117</b> |

## ABSTRACT

Along the Miyar Valley - Gianbul Valley transect in NW Lahul – SE Zaskar area, the High Himalayan Crystalline Zone crops out as a large-scale dome structure, called the Gianbul dome. Although the metamorphic field zonation is comparable on both sides of the dome, detailed petrographic, geothermobarometric and structural observations reveal a succession of four events, related to NE-directed and SW-directed contractional and extensional tectonic movements.

The first event corresponds to a crustal thickening associated with the NE-directed Shikar Beh nappe emplacement. This event is responsible for a prograde Barrovian-type metamorphism on the southern limb of the Gianbul dome in the Miyar Valley, characterized by peak conditions increasing gradually from the chlorite zone, to the SW, to the sillimanite-migmatite zone, to the NE. In the central part of the Gianbul dome, partial melting related to the M1 phase occurred at temperatures between 700 and 800°C. The main structures related to this event is the Miyar Thrust Zone, a 20 km wide ductile shear zone characterized by the presence of mylonites, in which shear sense criteria indicate a clear top-to-the-NE thrusting. A similar shear sense is confirmed by sigmoidal inclusion trails in syntectonic M1 garnet porphyroblasts.

A second event of crustal thickening is observed only in the northern part of the transect, in the footwall of the Zaskar Shear Zone in the Gianbul Valley. This phase is associated with a M2 Barrovian metamorphism, responsible for a gradual zonation increasing from the chlorite zone, to the NE, to the sillimanite-migmatite zone, to the SW. Thermobarometry results indicate peak conditions evolving from 650°C / 7 kbar for the kyanite zone to 800 °C / 12 kbar for the sillimanite-migmatite zone. Sigmoidal inclusion trails in M2 garnets porphyroblasts indicate a syntectonic growth during a SW-directed shearing, and these microfabrics are superposed by the extensional structures associated to the NE-dipping Zaskar Shear Zone. These observations implies that: (1) the M2 prograde metamorphism in the northern limb of the Gianbul dome is the consequence of a SW-directed crustal thickening, in contrast to the M1 tectono-metamorphic evolution in the southern limb of the dome; and (2) the Zaskar Shear Zone reactivates an older SW-directed thrust zone as a NE-directed ductile extensional shear zone during the exhumation of the High Himalayan Crystalline Zone. The M2 crustal thickening phase most likely reflects the underthrusting of the High Himalayan beneath the frontal part of the SW-directed Nyimaling-Tsarap nappe affecting the sedimentary series of the Tethyan Himalaya.

Two phases of extension and retrograde metamorphism are superposed on the contractional M1 and M2 tectono-metamorphic events. In the northern limb of the Gianbul dome, NE-directed extension is responsible for the shearing of the M2 isograds along the Zaskar Shear Zone, and for the sharp metamorphic contrast between the high grade High Himalayan Crystalline Zone and the overlying low grade Tethyan Himalaya. This event is related to the exhumation of the High Himalayan Crystalline Zone controlled by extension along the Zaskar Shear Zone, as well as by SW-directed thrusting of the High Himalayan nappe along the Main Central Thrust. In the footwall of the Zaskar Shear Zone, this rapid exhumation is characterized by a nearly isothermal decompression and enhanced partial melting during the M3 retrograde metamorphism. The fourth and last major tectono-metamorphic phase affecting the studied area corresponds to the creation of the Gianbul dome. In the northern limb of the dome, this event is associated with high-angle, brittle-ductile normal faults superposed on the Zaskar Shear Zone. In the Miyar Valley to the south, this large-scale doming is associated with a SW-dipping extensional structure, the Khanjar Shear Zone. This extensional event is marked by high T-low P retrograde conditions superposed on the prograde M1 assemblages in the Miyar Valley.



Although characterized by an apparently simple, symmetrical geometry and metamorphic zonation, the large-scale doming commonly observed in the High Himalayan Crystalline Zone of Zaskar appears to be the consequence of a complex, polyphase tectono-metamorphic evolution.

## RESUME

Dans les régions du Haut-Lahul et du SE Zaskar, le Cristallin du Haut-Himalaya est exposé à la faveur d'une grande structure de dôme appelé le Gianbul dôme. Bien que la zonation métamorphique soit comparable de part et d'autre du dôme, une étude structurale, pétrographique, et thermobarométrique détaillée, le long des vallées de la Miyar et de la Gianbul, révèle une suite de quatre événements tectoniques, associés successivement à des mouvements tectoniques en compression de vergence NE et SW suivi d'une tectonique en extension.

Le premier événement correspond à un épaississement crustal associé à la mise en place de la nappe de Shikar Beh à vergence NE. Cet événement est responsable d'un métamorphisme prograde de type Barrovien sur le flanc sud du dôme. Le gradient métamorphique de terrain associé à ce métamorphisme M1 est caractérisé par une zonation métamorphique augmentant graduellement de la zone à chlorite au sud, à la zone à sillimanite-migmatite au nord. Dans la partie centrale du Gianbul dôme, de la fusion partielle relié à la phase M1 s'est produite à des températures comprises entre 700 et 800° C. La "Miyar Thrust Zone" est la principale structure associée à cet événement. Cette large zone de cisaillement, se caractérise par la présence de mylonites, dans lesquelles les critères de cisaillement indiquent clairement un chevauchement en direction du NE. Un tel sens de cisaillement est confirmé par des inclusions hélicitiques dans des porphyroblastes de grenats syntectoniques.

Le deuxième événement d'épaississement crustal se manifeste uniquement sur le flanc nord du dôme, dans le mur de la "Zaskar Shear Zone", dans la Gianbul vallée. Cette phase est associée à un métamorphisme Barrovien M2, responsable de la zonation métamorphique allant de la zone à chlorite, au nord jusqu'à la zone à sillimanite-migmatite au sud. Les résultats de thermobarométrie indiquent des conditions du pic du métamorphisme évoluant de 650° C / 7 kbar pour la zone à disthène à 800° C / 12 kbar pour la zone à sillimanite-migmatite. Des inclusion hélicitiques dans des porphyroblastes de grenats M2 indiquent une croissance syntectonique lors d'un cisaillement en direction du SW. Ces microfabriques sont superposées par des structures d'extension associées à la "Zaskar Shear Zone". Ces observations impliquent que: (1) le métamorphisme prograde M2 sur le flanc nord du dôme est la conséquence de la mise en place d'une nappe à vergence SW contrairement à l'évolution métamorphique M1 sur le flanc sud du dôme, et (2) la "Zaskar Shear Zone" réactive une ancienne zone de cisaillement à vergence SW en une zone d'extension durant l'exhumation du Cristallin du Haut-Himalaya. La phase d'épaississement crustal M2 reflète très vraisemblablement le sous-charriage du Cristallin du Haut-Himalaya sous la partie frontal de la nappe de Nyimaling-Tsarapp affectant les sédiments de l'Himalaya téthysien.

Deux phases d'extension et de métamorphisme rétrograde sont superposées aux événements tectono-métamorphiques M1 et M2. Sur le flanc nord du dôme, de l'extension en direction du NE est responsable du cisaillement des isogrades M2 le long de la "Zaskar Shear Zone" ainsi que du saut métamorphique net entre le Cristallin du Haut-Himalaya et l'Himalaya Téthysien. Cet événement est associé à l'exhumation du Cristallin du Haut-Himalaya contrôlé à la fois par de l'extension le long de la "Zaskar Shear Zone" et par du chevauchement vers le SW le long du "Main Central Thrust". Dans le mur de la "Zaskar Shear Zone", cette exhumation rapide se caractérise par une décompression isothermale et de la fusion partielle durant le métamorphisme rétrograde M3.

Le quatrième événement correspond à la formation du Gianbul dôme. Sur le flanc nord du dôme, cet événement est associé à la formation de failles normales cassantes à fort angle superposées à la "Zaskar Shear Zone". Dans la vallée de la Miyar, ce doming est associé à une structure d'extension avec un sens de cisaillement top vers le SW, appelée la Khanjar Shear Zone". Cette événement en extension est marqué par un métamorphisme rétrograde de haute température et de basse pression superposé dans la vallée de la Miyar au métamorphisme prograde M1.

Bien que caractérisée par une géométrie et une zonation métamorphique apparemment simple et symétrique, la structure de dôme observée dans le Cristallin du Haut Himalaya du Zaskar apparaît être la conséquence d'une évolution tectono-métamorphique polyphasée et complexe.

## CHAPTER 1: INTRODUCTION

### 1.1. PREAMBLE

The Himalaya called by the Tibetans "roof of the world" means in fact "abode of snows" for the Indians (from the Sanskrit *hima* for snow and from *alaya* for abode). This range was from time immemorial one of the most mysterious areas of our planet. Its summits are considered by the Hindus and the Buddhists as the eternal residence of the gods, haunted by the evil geniuses and the legendary Yeti. For us the Himalaya is rather synonymous with adventures, cold and wild spaces. Everyone still has in his mind the staggering accounts of the first explorers to the conquest of the first 8000 m

However, the Himalaya is not restricted to its snow-clad peaks, but its charm arise from the diversity of its landscapes, the authenticity of its villages (Fig.1.1) and the kindness of its inhabitants.



**Fig. 1.1:** The village of Khanjar in the upper reaches of the Miyar Valley

For the travellers arriving from the Indian plain, the frenzy and the agitation which rhythm the life of the populations living in the plain grow blurred quickly while venturing inside the range. To the green valleys and the fascinating hill stations located on the foothills ranges of Himachal

Pradesch range quickly succeed the powerful rivers and deep gorges of the Lahul and Zaskar regions. The tiny mountain villages are renowned for their hospitality and it's not unusual to be invited to a family home for a cup of tchai, or to a colourful village religious celebration. The buddhist Gompas, repositories of the rich Tibetan culture scattered across the Himalaya, give to this range a sacred dimension. With its beautiful mountains, its inaccessible valleys, its unique flora and fauna, its magnificent gompas and quiet places for reflection and meditation, it's not surprising that the Himalaya is also known as Dhevbumi – the abode of the gods.

## 1.2. GEOGRAPHICAL SETTING

The Himalayan range s.l (with the Karakorum range) extends as an arc for more than 3000 km from the Pakistan to the west to the Indian State of Arunachal Pradesh, to the east. With its 14 peaks over 8000 m high, this range forms the most spectacularly mountainous barrier of our planet (Fig. 1.2). The width of the range varies from 200 km to 300 km, separating the Indian sub-continent to the south from the Tibetan Plateau to the north. The range is surrounded by two of the most important rivers of the Asian continent: the Indus river and the Tsang Po – Brahmaputra river.

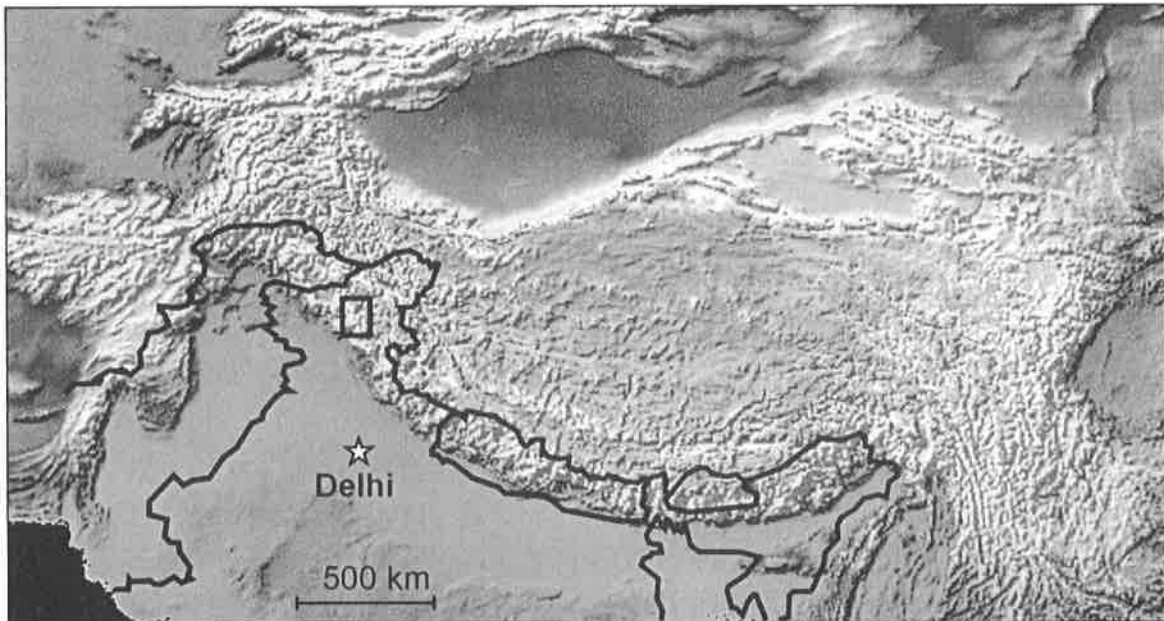


**Fig 1.2:** Digital Elevation Model of the Himalayan Range. The studied area is shown in the bold lined box (C. Duncan)

Although the source of this two rivers is located in the same area near the Mount Kailash in Tibet, the way they follow across the range is very different. The Indus river begins its way running towards the north-west, before changing its course towards the south through Pakistan, to finally flow into the Arabian Sea. In contrast, the Tsang-Po river flows towards the east behind the Great Himalayan range, and turns towards the south where it takes the name of Brahmaputra river before flowing into the Bengal Gulf.

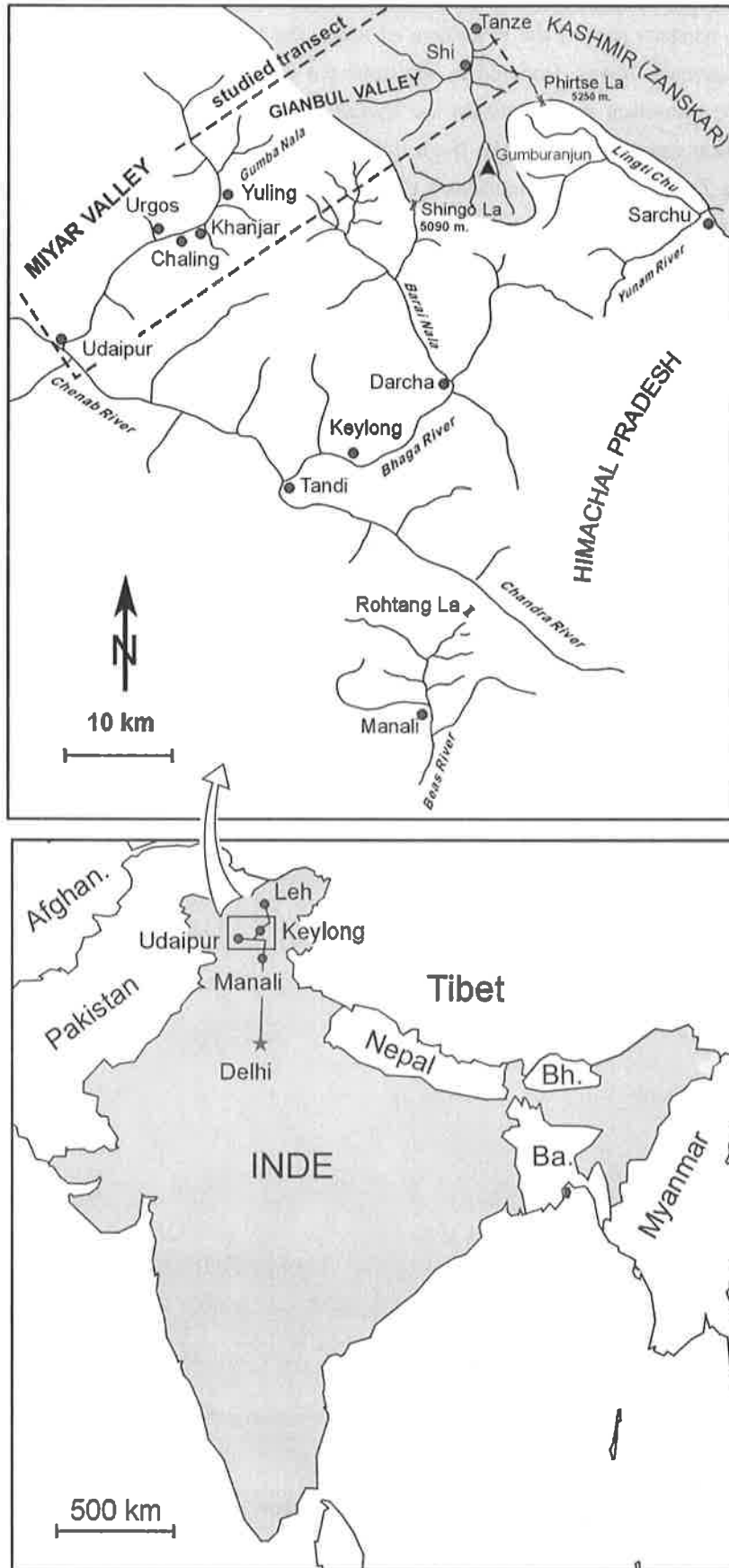
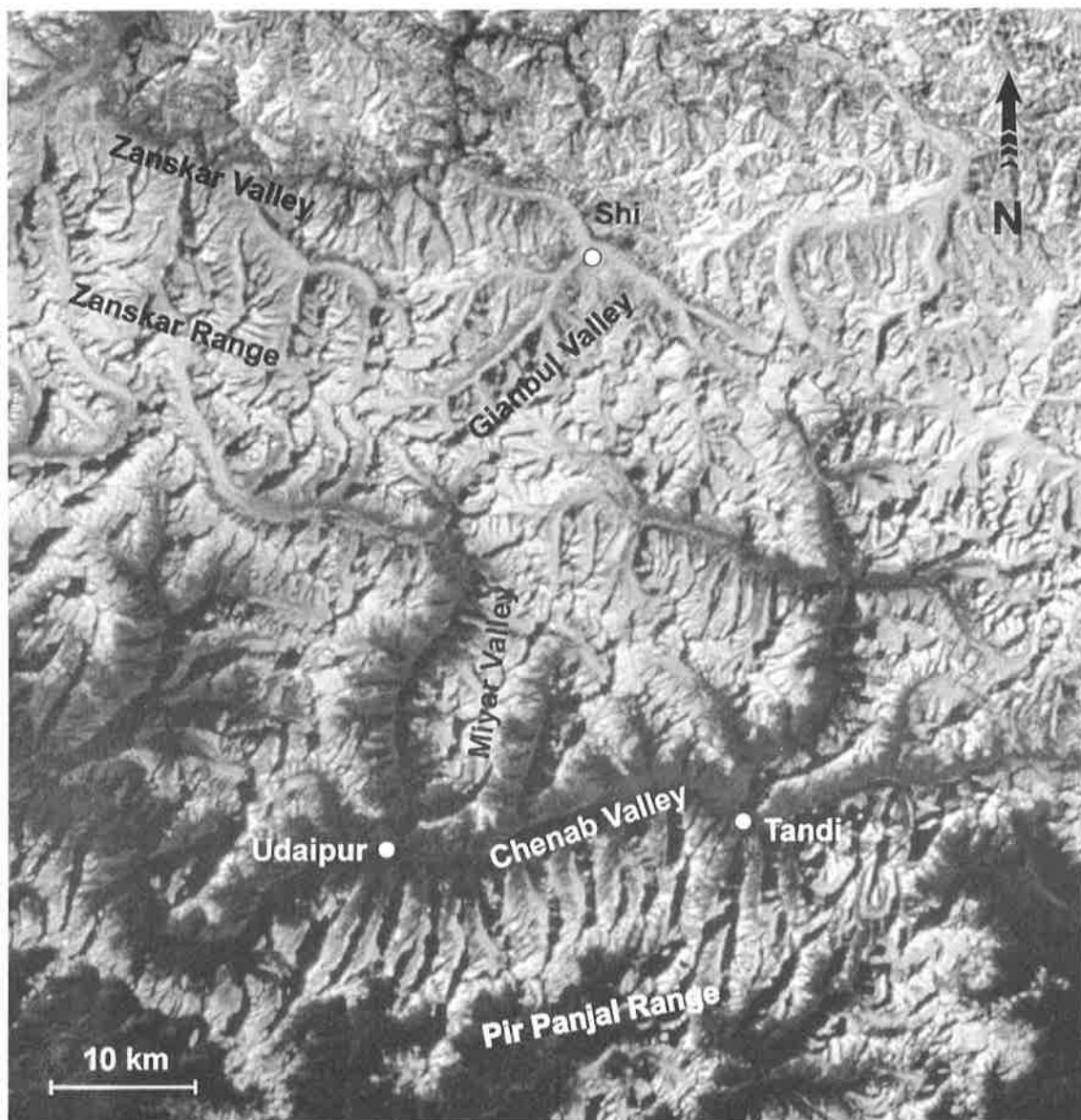


Fig. 1.3: Geographic map showing the location of the studied area in NW India. Afghan = Afghanistan; Bh = Bhutan; Ba = Bangladesh

In the north-western part of the Himalaya of India, the range can be subdivided in four more or less parallel mountain zones. Located in the northern part of the Himalaya of India, the Ladakh range marks the transition zone between the Indian sub-continent and the Tibetan Plateau. To the south, the Zanskar range, is part of the High Himalayan range characterized by its eternally snow-clad peaks. The Zanskar range constitutes a real barrier separating the State of Himachal Pradesh to the south from the Zanskar to the north.

Farther to the south, the transition zone between the Indian plain and the Zanskar range is formed by two less important ranges: the Pir Panjal range and the Siwaliks range. The Pir Panjal range is constituted by mountains peaks reaching between 4000 and 5000 m, and marks the natural boundary between the Chenab Valley to the north, and the Chamba and Kullu Valleys to the south. The Siwaliks range is located at the front of the Himalayan range and these foothills represent the first slopes reach by those heading north from the Indian plain.



**Fig. 1.4:** The studied area as seen from the space. The Gianbul dome forms the crest which separates the Miyar Valley to the south from the Gianbul Valley to the north

These different topographic features strongly influence the climate of this part of the Himalaya. In a general way, the NW Himalaya can be climatically divided into two regions located on both sides of the Zaskar range. The northern region including Zaskar and Ladakh have a high altitude desert climate. Humidity is always low and rainfall no more than a few cm each year. In summer, however, the monsoon can reach the Zaskar area and can provoke more abundant precipitation. In contrast, the regions situated on the southern limb of the Great range are subjected to the monsoon. In this regions, dramatic rainfall can occur and cause important damage for the populations living on this side of the range.

Set against the massive snow-capped peaks of the Zaskar Mountains, the studied area skirts the flowered Miyar Valley (Figs. 1.3 and 1.4). To the narrow gorges which marks the entrance to the Miyar Valley from Udaipur, succeed rapidly the flowered meadows and pea and millet fields gathered around the main villages of the valley. Moving up the valley, we leave behind us the fields and the coniferous forests to reach the grazing pastures where yak herds graze peacefully with wide herds of sheep. From this area, we get a wonderful view on some of the 6000 m peaks of the Great Himalaya. Ascending gradually toward the Kang La, the huge frontal moraine of the Miyar glacier marks the limit of the wild flowered meadows. Beyond this point, the scenery changes radically and we enter a desert of ice, stones and peaks.

The landscape and the flora and fauna of the Miyar Valley are typical of a well preserved Himalayan valley: unspoilt villages, tiny hand-cultivated fields, meadows with wildflowers and high altitude pastures with nomadic shepherds and their flock. The valley is also very impressive for a vast array of unspoilt alpine and himalayan flora, including the delightful blue poppy (Fig. 1.5)

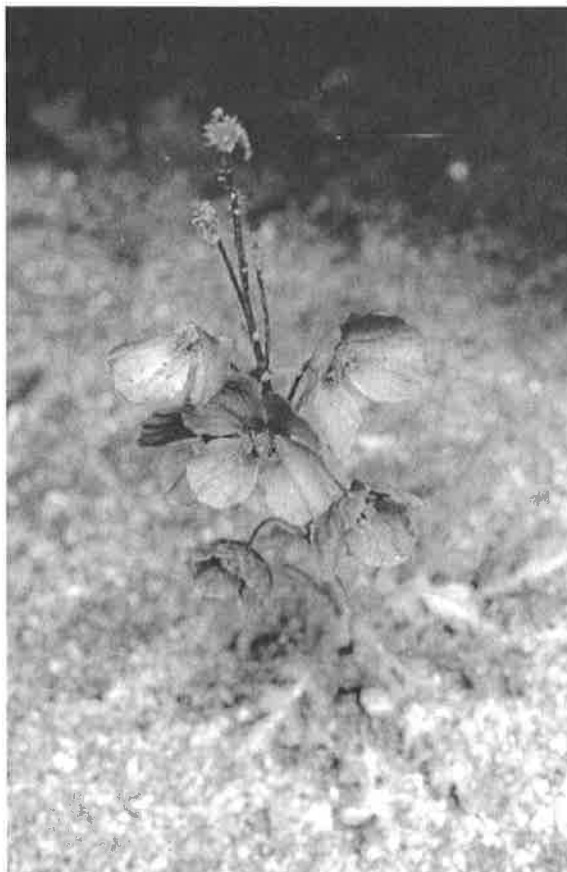


**Fig. 1.5:** The blue poppy is a classic flower of the Himalayan valleys

## CHAPTER 2: GEOLOGICAL SETTING

### 2.1. INTRODUCTION

The history of the Himalayan range starts during Early Cretaceous about 103 millions years ago (Honegger et al. 1982). At this time, the Indian plate spreads away from the Pangea continent and begins to derive towards the north. A subduction occurs then at the edge of the position of the actual Tibet. The oceanic crust of the Indian plate, heavier than the continental plate, subducts then beneath the continental Eurasian plate. The first consequences of this event correspond to the appearance of an Andean-type volcanic range into the Tibetan continental crust. Until the Eocene, the shortening of the Neotethys ocean was accommodated by subduction of the oceanic crust towards the north. From this time, the oceanic lithosphere is absorbed and a major change occurs. The both plates in confrontation are now continental. The downward pulling forces exerted by the subducting oceanic crust is then counteracted by the high buoyancy of the continental Indian plate. The subduction is thus strongly slowed down. The converging rate data between the Indian and Eurasian plates demonstrate in a spectacular way the deceleration of the Indian plate motion 50 millions years ago (Patriat and Achache 1984). At this time, the average speed of convergence decreases from 16 cm/year to 5 cm/year. The crustal shortening requests by the continued convergence between India and Asia is accommodated by thrusting and folding as well in the Himalayan as in the mountain ranges to the north of the suture zone. Across the Himalayan range, the shortening of the north Indian continental margin is accommodated by several major SW-directed thrusts, the principal ones being, from south to north, the Main Frontal Thrust (MFT), the Main Boundary Thrust (MBT), and the Main Central Thrust (MCT).

### 2.2. MAIN TECTONIC SUBDIVISIONS OF THE HIMALAYA

One of the characteristics of the Himalayan range is this rather simple geometry. All along the belt, the tectonic units and the metamorphic zones are thrust towards the south over the more frontal units along the main Himalayan thrusts. In spite of several decades of intensive and detailed geological investigations, the general structure of the Himalayan orogen is still based on the main major divisions established by Gansser (1964). Generally, the transition between two domains is expressed by the presence of a major tectonic structure. However, in some cases, the transition between two domains is gradual and this is marked by a progressive variation in the metamorphic conditions. According to this divisions, the Himalayan belt is classically subdivided in six major domains from the Indian plain to the south to the Tibetan Plateau to the north.



### **2.2.1. The main Himalayan structures**

From south to north and from younger to older structures, the architecture of the Himalayan range is based on the following main structural elements:

#### ***2.2.1.1. The Main Frontal Thrust (MFT)***

As its name indicates, this still active structure is the most frontal thrust of the range. It is along this structure that the Subhimalaya, thrusts towards the SW over the alluvial deposits of the Indo-Gangetic plain.

#### ***2.2.1.2. The Main Boundary Thrust (MBT)***

This thrust separates the Lesser Himalaya (hanging wall) from the Subhimalaya (footwall). The cataclasites associated with this thrust indicate a SW-directed thrusting of the Lesser Himalaya over the Subhimalaya along this structure.

#### ***2.2.1.3. The Main Central Thrust (MCT)***

This major structure marks the limit between the Lesser Himalaya and the High Himalayan Crystalline. This important tectonic element consists of a major intra-continental crustal-scale thrust zone developed in the Indian plate margin during Early Miocene (c. 23 Ma, Frank et al., 1977; Hubbard & Harrison, 1989; Coleman, 1998). It is along this structure that the medium to high grade metamorphic rocks of the High Himalayan Crystalline thrust over the weakly metamorphosed series of the Lesser Himalaya. Shear sense indicators on both sides of this thrust indicate a clear SW-directed shearing. This structure exhibits a striking continuity along the entire 2000 km length of the orogen, and is characterized by an intense mylonitic shear zone and inverted metamorphism. Although the Main Central Thrust can be mapped along the entire frontal zone of the range, it is nevertheless occasionally exposed in more internal positions around tectonic windows, such as the Kishtwar window and the Larji-Kulu-Rampur window.

#### ***2.2.1.4. The South Tibetan Detachment System (STDS)***

This major structure consists of a north-dipping extensional shear zone separating the High Himalayan Crystalline from the Tethyan Himalaya (Caby et al., 1983; Burg and Chen, 1984). A detailed structural analysis of this shear zone clearly demonstrates the ductile and extensional deformation related to this structure. Contrary to the other structures referred above, the South Tibetan Detachment System is not continuous along the entire Himalayan range. In different parts of the range, this extensional structure is nevertheless relayed by local equivalent structures such as the Zaskar Shear Zone exposed in the north-western part of the Himalaya of India. This major syn-orogenic extensional structure, first identified by Herren (1987), corresponds to a ductile

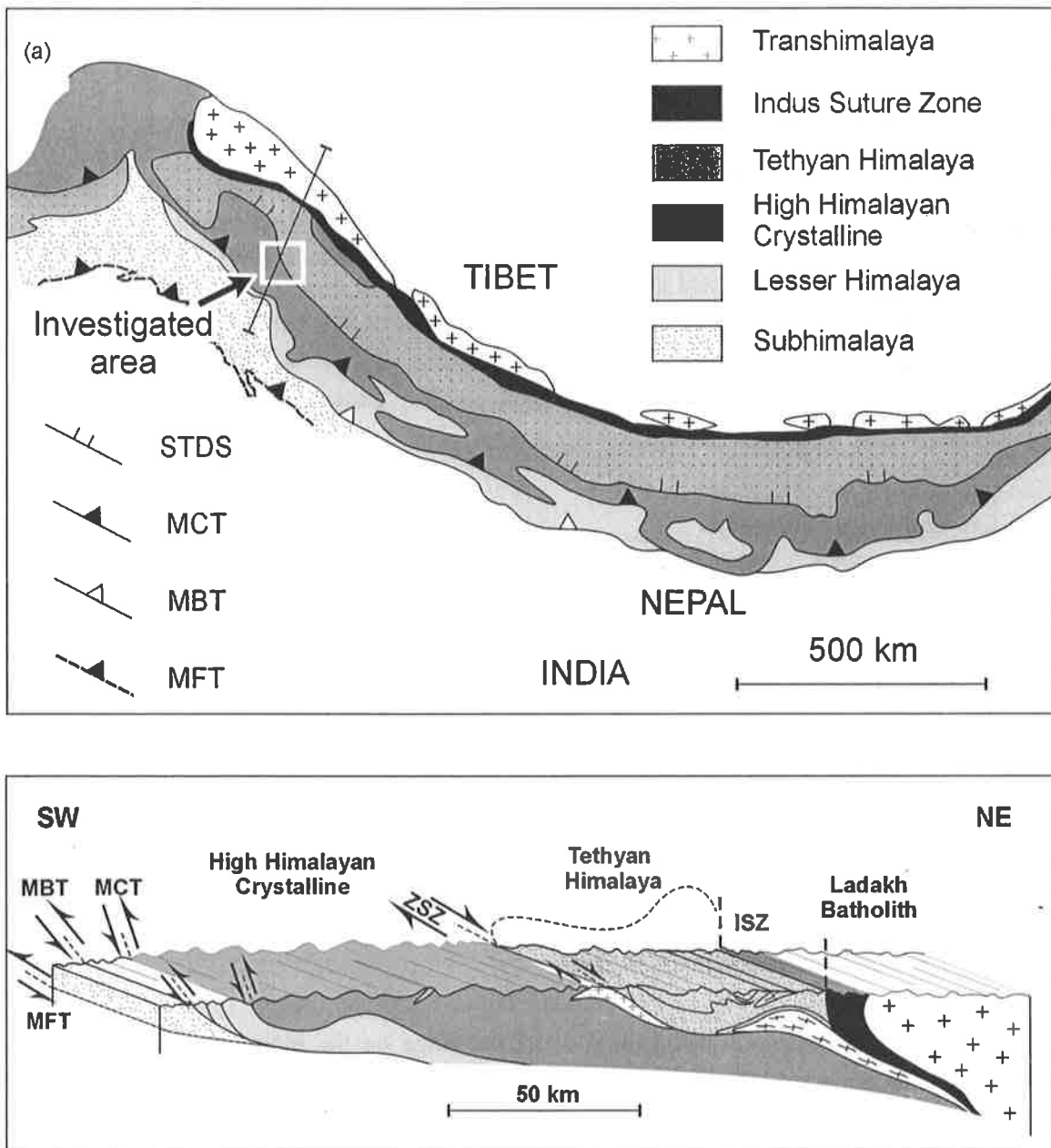


Fig. 2.1: Simplified tectonic map of the Himalaya modified after Gansser (1964) and Dèzes (1999) (b) Geological profile through the north-western part of the Himalaya of India showing the main tectonic units and structural elements (modified after Dèzes 1999). MBT = Main Boundary Thrust; Main Central Thrust; ZSZ = Zaskar Shear Zone; ISZ = Indus Suture Zone.

extensional shear zone which accommodated a minimum slip of about 35 km during Early Miocene (Dèzes et al., 1999).

### 2.2.2. The main tectono-metamorphic units

The Himalayan orogen is subdivided in five laterally continuous tectonometamorphic units (Gansser 1964). These are from south to north:

### **2.2.2.1. The Subhimalaya**

The Subhimalaya corresponds to the Tertiary Molasse which forms the first foothills of the Himalayan belt moving up from the Indian plain. In the north-western Indian section, this unit is mainly constituted by a clastic sequence of conglomerate overlaid by much thinner grained sequence (Frank et al., 1995). This unit is composed of Paleogene and Neogene sediments eroded from the rising orogen and deposited in the foreland basin in front of the mountain belt (Najman and Garzanti, 2000 and references therein). As these sediments are conglomerates and cross-laminated sandbars, the depositional environment of these deposits seems to have been an meandering river system. This Subhimalayan Molasse also known as Murree and Siwaliks Formation thrust over the Quaternary alluvial deposits along the Main Frontal Thrust.

### **2.2.2.2. The Lesser Himalaya**

Mainly formed by low-grade Upper Proterozoic to Lower Cenozoic detrital sediments (Valdiya, 1980; Parrish and Hodges, 1996) this unit thrusts on the Subhimalaya domain along a major thrust called the Main Boundary Thrust (MBT). Considered as the sedimentary cover of the Indian continental plate, the Lesser Himalaya is also characterized by the presence of granitic gneiss and acid volcanic rocks (1840 $\pm$ 70 Ma, Frank et al., 1977) intercalated in the detrital metasediments. Generally located in the frontal part of the range, this unit appears sometimes in a more internal position at the favour of tectonic windows, such as the Kishtwar window and the Larji-Kulu-Rampur window.

### **2.2.2.3. The High Himalayan Crystalline**

This unit consists mainly of sedimentary rocks deposited on the Indian continental margin during Late Proterozoic to Early Cambrian (Frank et al., 1995; Parrish and Hodges, 1996; Whittington et al., 2000). In most sections along the range, this unit formed the metamorphic core zone of the orogen. In the literature, several names are used to describe this unit, the most used being the Tibetan Slab, the Central Crystalline Zone or the Great Himalayan Sequence. However, the term of High Himalayan Crystalline (or High Himalayan Crystalline Sequence) is the name generally used to designate this domain bounded along the top by the South Tibetan Detachment System and at the base by the main Central Thrust. This metamorphic core zone consists of an up to 40 km thick sequence of amphibolite facies to migmatitic paragneiss, with minor orthogneiss, metabasites and calc-silicate gneiss. In the central and eastern part of the range, this High Himalayan Crystalline forms a monoclinical metamorphic slab which thrusts over the low to medium grade sedimentary series of the Lesser Himalaya along the Main Central Thrust. In the north-western part of the Himalaya of India, the metamorphic zonation of the High Himalayan Crystalline contrasts significantly with what is observed in the central and eastern part of the Himalaya. In the Zaskar-Lahul region, the High Himalayan Crystalline represents the product of a multiphase structural and metamorphic evolution and can be subdivided in two metamorphic zones: (1) the low-grade metamorphic Chamba Zone in the frontal part of the range and (2) the high-grade

metamorphic High Himalayan Crystalline Zone of Zaskar which is exposed in a more internal part of the range .

Above the Main Central Thrust, the High Himalayan Crystalline is characterized by the presence of several, kilometric scale dome structures, generally centred on granitic gneiss bodies cropping out in the amphibolite facies to migmatitic paragneiss (e.g. Kündig, 1989). Farther to the NE, the contact between the High Himalayan Crystalline and the low-grade sediments of the Tethyan Himalaya corresponds to the 150 km long Zaskar Shear Zone (Herren, 1987). A major feature of this area is a general decrease of the metamorphic grade toward the SE. In the Zaskar-Lahul area, the High Himalayan Crystalline Zone is characterized by the presence of the Gianbul dome, a large-scale dome structure centred on the Tertiary Gumburanjun leucogranite (22.2 +/- 0.2 Ma., U-Pb monazite) (Dèzes et al., 1999).

#### ***2.2.2.4. The Tethyan Himalaya***

The Tethyan Himalaya (Auden, 1937) is composed of a more or less complete stratigraphic column from Upper Precambrian to Eocene sediments deposited on the Indian continental margin (Gaetani and Garzanti, 1991). This stratigraphic succession is very well preserved in the Zaskar and Spiti basin where most of the sedimentary formations were defined ( Stoliczka, 1866; Lydekker, 1878; Hayden, 1904; Nanda and Singh, 1977; Srikantia et al., 1980; Baud et al., 1984; Gaetani et al., 1990). This unit exhibits an approximately 100 km wide synclinorium formed by weakly metamorphosed sediments. Several nappes termed North Himalayan nappes have been recognised in this unit (Bassoulet et al., 1980; Steck et al., 1993 and 1998). The North Himalayan nappes emplacement is responsible of the main phase of deformation affecting the sedimentary sequences of the Tethyan Himalaya in the northern part of the range. The name of Nyimaling-Tsarap nappe was introduced for the first time by Steck et al. (1993) to designate the whole thrust pile of sedimentary rocks located between the Indus Suture Zone, near Leh, to the north and the Baralacha La to the south. The internal structure of the Tethyan Himalaya is characterized by a progressive change in the style of the deformation, evolving from ductile shearing in the northern part of the unit to development of ramps and flats and imbricate structures at its southern limb.

The transition between the low-grade sediments of the Tethyan Himalaya and the high-grade metamorphic rocks of the High Himalayan Crystalline Zone is usually progressive. Nevertheless, in many places along the range, the transition zone is marked by a major NE-dipping extensional structure termed the South Tibetan Detachment System (STDS; Caby et al., 1983; Burg and Chen, 1984).

#### ***2.2.2.5. The Indus-Tsangpo Suture Zone***

The Indus-Tsangpo Suture Zone, defined by Gansser (1964), is the zone of collision between India and Asia and represents the scar of the oceanic domain (Neotethys) separating, during the Mesozoic, the Indian plate from the continental block forming the Tibet at present. This complex zone is mainly composed by remains of oceanic crust (Jurassic-Cretaceous ophiolitic melanges,

Gansser, 1980) and island arcs (Dras volcanics; Robertson and Degnan, 1994) mixed with molassic deposits (Indus Molasse, Garzanti and Van Haver, 1988). This suture zone constitutes the northern limit of the Himalayan range. Farther to the north, the Transhimalaya batholiths referred to as the Ladakh batholith in the north-western part of the Himalaya, result from the partial melting of the Asian mantle above the subducting Neotethyan oceanic crust below the Tibetan block. This batholith massif was formed in several magmatic phases from 100 Ma to Late Palaeocene (Honegger et al., 1982; Schärer et al., 1984). The Transhimalaya batholith consequently represents the relics of an ancient calc-alkali volcanism of Andean type.

### **2.3. HISTORY OF GEOLOGICAL INVESTIGATIONS**

From time immemorial, and the Himalaya more than others, the mountains exerted an attraction on people. Some wanted to conquer them by climbing them, others wanted to dominate them by understanding their history and their structure. Until the second middle of the XIX century, most of the Himalayan range is remained *terra incognita* for the Westerners. These areas were presented then as a kind of vast *No man's land* between two strongly developed powers, India and China. However this gap on the geographical map of this time was for ages a way of passage. Separating two thousand-year-old civilizations, the Himalayan belt was however used as a link between these two populations which in spite of the topographic difficulties succeeded in maintaining constant commercial and cultural exchanges through the centuries.

It is only from the years 1860's that the first geologists of the Geological Survey of India dared to venture inside the range, in the areas of Zaskar and Ladakh. The first reports of these expeditions were the work of Ferdinand Stoliczka (1866) then that of his successor Lydekker (1883). The closing of these areas to the foreigners during most of the XX century explains the fact that the geology of this range remained ignored a long time. Nevertheless, during the first middle of the XX century, several works of Dainelli (1933-1934) brought several and rich observations along the Kashmir-Leh road. We also have to note the excellent geological transect of Berthelsen (1953) through the Tso Moriri area and finally the splendid work of Augusto Gansser (1964) that allowed the future geologists to profit from some references before tackling the geology of these areas. It is nevertheless only from the beginning of the Eighties with the opening of the Ladakh and Zaskar area to the foreigners that the knowledge of the Himalayan geology really took its rise.

Since 1979, a Himalayan research program was undertaken by the Earth Sciences Department of the University of Lausanne in order to understand the relations between tectonics and metamorphism during the Himalayan orogen (Baud et al., 1982; Stutz and Steck, 1986; Stutz and Thöni, 1987; Stutz, 1988; Spring and Crespo, 1992; Spring, 1993; Spring et al., 1993; Steck et al., 1993a and b; Vannay, 1993; Epard et al., 1995; Vannay and Steck, 1995; Steck et al., 1998; Dèzes, 1999; Dèzes et al., 1999; Girard and Bussy, 1999; Girard et al., 1999; Steck et al., 1999; Wyss et al., 1999; Wyss, 2000). This research program focused along a complete transect from the Indus Suture Zone to the north and the Main Central Thrust to the south. The different studies demonstrated that: (1) the Tethyan Himalaya corresponds to a large-scale, SW-directed nappe system (Nyimaling-Tsarap nappe) as already proposed by Bassoulet et al. (1980) in NW Zaskar;

(2) in the Sarchu-Baralacha La region, the frontal nappe stack is overprinted by younger extensional structures, representing the south-eastern continuation of the Zaskar Shear Zone; (3) the tectono-metamorphic evolution of the High Himalayan Crystalline in Kulu-Lahul-Spiti region is the consequence of two major phases, associated respectively with the emplacement of the NE-directed Shikar Beh nappe and with the subsequent thrusting of the High Himalayan nappe along the Main Central Thrust towards the southwest; (4) the Zaskar Shear Zone accommodated a minimum extensional slip of about 35 km during Early Miocene (Dèzes et al. 1999).

At the same time as the works of the Lausanne group, most studies focused on the Zaskar and Kishtwar region. As the Zaskar basin represents an excellent region for the study of the sedimentary series deposited on the northern margin of the Indian continental plate, a lot of stratigraphic studies were undertaken in the Zaskar area ( Stoliczka, 1866; Lydekker, 1878; Hayden, 1904; Pickett et al, 1975; Nanda and Singh, 1977; Srikantia et al., 1980; Baud et al., 1984; Gaetani et al., 1990; Brookfield et al., 1993; Vannay, 1993). Herren (1987) highlighted that the contact zone between the Tethyan Himalaya to the north and the high-grade metasediments of the High Himalayan Crystalline to the south corresponded to a strongly developed extensional shear zone; the so-called Zaskar Shear Zone. The tectonic and metamorphic relation between the High Himalayan Crystalline and the underlying Lesser Himalaya exposed in the Kishtwar tectonic window in SW Zaskar have been studied by Stäubli (1989) and Guntli (1993). Kündig (1989) established that the exhumation of the high-grade metamorphic rocks of the High Himalayan Crystalline Zone exposed in SW Zaskar are mainly controlled by doming processes. In the same area, several works by Searle (Searle and Rex, 1989; Searle et al., 1992; 1999) and Stephenson (Stephenson et al., 2000; 2001) focused on the inverted metamorphism. They proposed a thermal model for the evolution of the Main Central Thrust Zone in Kishtwar-Zaskar region. In contrast, the south-eastern part of the High Himalayan Crystalline in Lahul region was less studied. A reconnaissance mapping, structural and metamorphic investigations were undertaken by Frank et al., (1995) and by Fuchs and Linner (1995). In the Miyar Valley-Kurgiakh Valleys area, Lombardo et al., (1987), Pognante and Lombardo (1989), and Pognante et al. (1990), studied the metamorphic evolution of the High Himalayan Crystalline Zone of Zaskar. On the basis of early relic assemblages in metabasites, they suggest the possible existence of a pre-Himalayan metamorphic event. A such pre-Himalayan metamorphic stage was also suggested by Wyss (1999) on the basis of comparable arguments in olivine gabbro and amphibolite layers intruded within the Precambrian to Lower Cambrian metasediments of the High Himalayan Crystalline of the Tos Valley (Himachal Pradesh).

## CHAPTER 3: PURPOSE OF THE STUDY

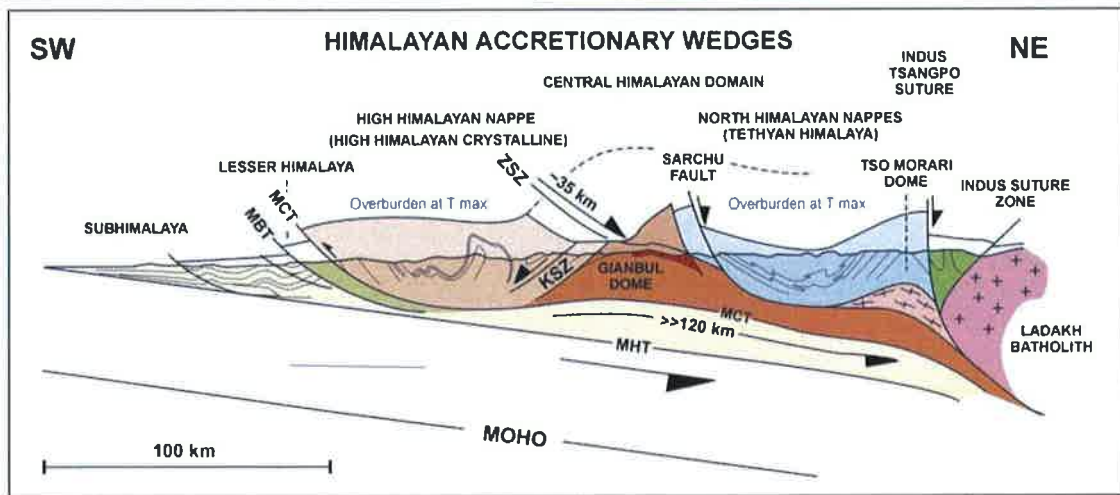
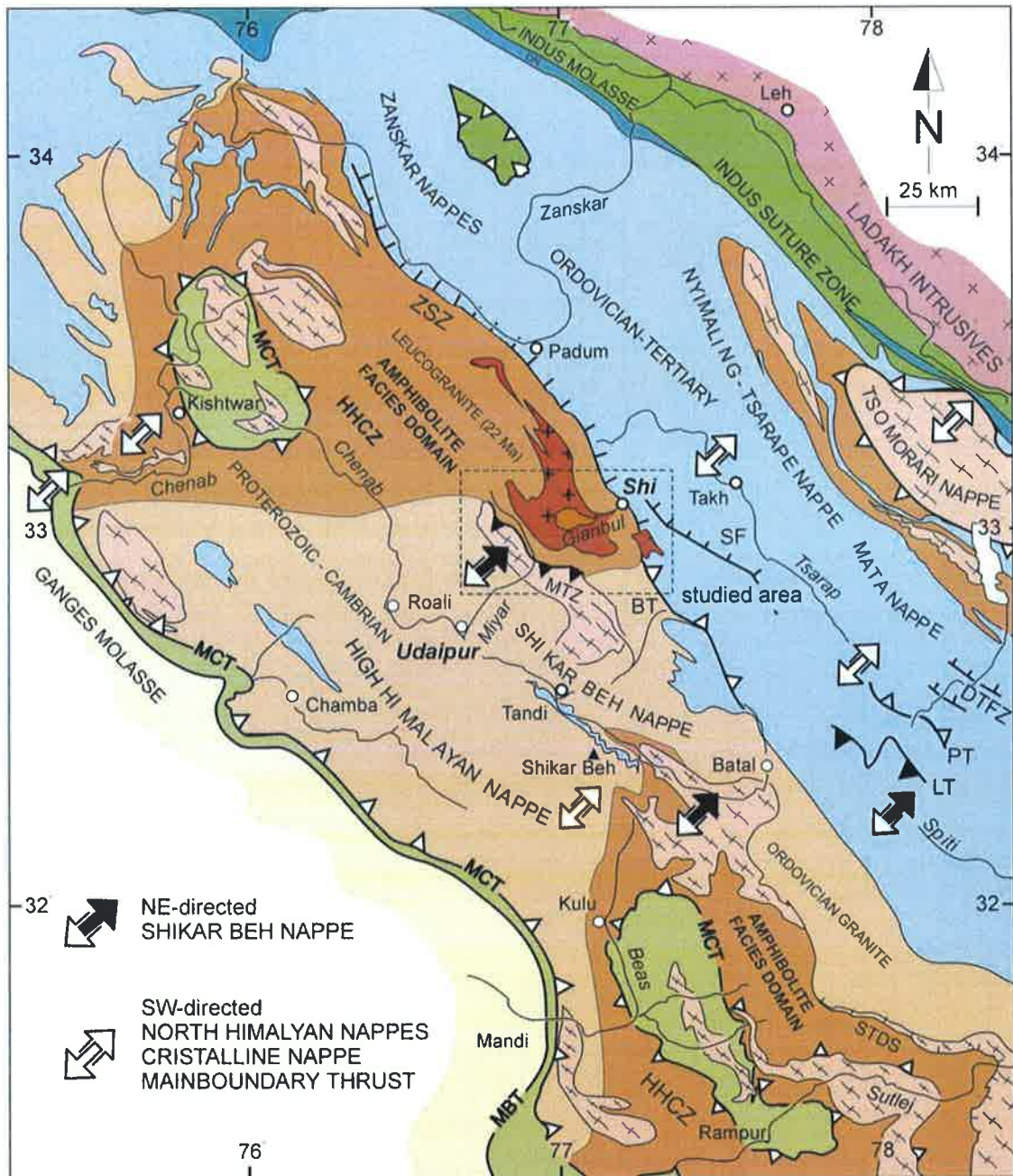
The metamorphic core zone of the Himalayan orogen consists of a 5 to 20 km thick sequence of amphibolite facies to migmatitic paragneiss, with minor orthogneiss, metabasite and calcsilicate gneiss. This High Himalayan Crystalline Zone (HHCZ) thrusts over the low- to medium-grade sedimentary series of the Lesser Himalaya along the Main Central Thrust (MCT), a major intra-continental thrust developed within the Indian plate margin during Early Miocene, since c. 23 Ma (e.g. Frank et al., 1977; Hubbard and Harrison, 1989; Coleman, 1998) (Fig.1). In numerous sections along the range, the HHCZ is separated from the overlying, low-grade sediments of the Tethyan Himalaya by the extensional structures of the South Tibetan Detachment System (STDS, Burchfiel et al., 1992). Geochronological and structural results indicate that STDS was activated during Early Miocene, around 23 Ma (e.g. Hodges et al., 1992; Dèzes et al., 1999). Broadly contemporaneous movements along both the MCT and the STDS reflect consequently a tectonically-controlled exhumation of the HHCZ.

For more than 1400 km along the range, in the central and eastern parts of the Himalaya, this metamorphic core corresponds to a fairly monoclinical slab, 5 to 20 km thick, and dipping to the NE. This unit is mainly exposed in the frontal part of the orogen and it overthrusts the low to medium grade sedimentary series of the Lesser Himalaya along the Main Central Thrust. This rather simple geometry contrasts significantly with what is observed in the NW part of the Himalaya of India. In this region, between the Kulu and the Chenab Valleys, the amphibolite facies to migmatitic gneiss are mainly exposed in a more internal part of the orogen, broadly forming a 180 km long and 60 km large dome structure in the Zaskar region (Fig. 1). These high-grade gneiss metasediments are almost completely surrounded by lower grade metasediments and they are not directly connected to the similar high-grade rocks cropping out as a thick sheet in the frontal part of the belt, from the Kulu Valley to the SE. In contrast, between the Kulu Valley and the Chenab Valley, the hanging wall of the MCT in the frontal part of the orogen mainly consists of greenschist facies (chlorite to biotite zones) metasediments of the Tethyan Himalaya (e.g. Frank et al., 1973; Steck et al., 1993; Epard et al., 1995; Vannay et Steck, 1995)

Consequently, two main metamorphic zones have been reported in the following discussion (Fig. 3.1). We will refer to the low-to medium-grade metasediments as the Chamba zone, whereas the term of High Himalayan Crystalline Zone (HHCZ) will be used to describe the sequence of amphibolite facies to migmatitic gneiss in the central part of the orogen further to the NE.

**Fig. 3.1:** (a) Geological map of the north-western part of the Himalaya of India (modified after Steck et al. 1999) showing the main structural elements discussed in the text. HHCZ = High Himalayan Crystalline Zone, MTZ = Miyar Thrust Zone, BT = Baralacha La Thrust, DTFZ = Dutung-Thaktote Fault Zone, LT = Lagudarsi La Thrust, MBT = Main Boundary Thrust, MCT = Main Central Thrust, SF = Sarchu Fault, ZSZ = Zaskar Shear Zone, KSZ = Khanjar Shear Zone, PT = Parang Thrust. (b) Geological profile through the north-western part of the Himalaya of India (modified after Epard et al., in prep.). MHT = Main Himalaya Thrust.





In the Himalaya of Zaskar, the contact between the HHCZ and the overlying low-grade sediments of the Tethyan Himalaya corresponds to the 150 km long Zaskar Shear Zone (ZSZ), a ductile extensional shear zone which accommodated a minimum slip of c. 35 km during Early Miocene (c. 23-19 Ma; Herren, 1987; Dèzes et al., 1999). Since the description of this spectacular tectonic setting, most geological studies have been focussed on the NE border and central part of the HHCZ of Zaskar (e.g. Honegger et al., 1982; Stäubli, 1989; Kündig, 1989; Dèzes et al., 1999; Searle et al., 1999; Walker et al., 1999; Stephenson et al. 2000). In contrast, only limited work has been done along the southern border of this unit (Pognante et al., 1990; Steck et al., 1999) and the tectonic and metamorphic transition between the amphibolite facies to migmatitic metamorphic rocks of the HHCZ and the greenschist facies metasediments of the Chamba zone exposed to the south remains still poorly constrained.

The aim of the present study is to provide new constraints on the tectono-metamorphic evolution of the south-easternmost limit of the HHCZ of Zaskar, on the basis of detailed petrographic and thermobarometric investigations in the Miyar Valley in the Upper Lahul region. Together with comparable data for the NE limit of the HHCZ along the Gianbul Valley in SE Zaskar (Dèzes, 1999; Dèzes et al., 1999), these new results allow us to propose a reconstruction of the tectono-metamorphic evolution along a complete transect across the Gianbul dome and the structures of the HHCZ of Zaskar.

## CHAPTER 4. STRATIGRAPHY

### 4.1. INTRODUCTION

Whereas the Zaskar-Spiti basin constitutes an exceptional area for the study of the sedimentary sequences deposited on the northern margin of the Indian continental plate, the Upper-Lahul area, to the south of this basin, is mainly formed by a thick and monotonous series of detrital sediments of Precambrian to Lower Cambrian age belonging to the Phe Formation (Nanda and Singh 1977). These sediments form the most abundant sedimentary protolith cropping out in the studied area.

### 4.2. THE PHE FORMATION

#### 4.2.1. Introduction

The Phe Formation, introduced by Nanda and Singh (1977) as an equivalent of the Haimantas (Griesbach 1891, Hayden 1904, Frank et al. 1995) constitutes the base of all the sedimentary sequence of the Tethyan Himalaya. This formation is mainly made up of an alternation of centimetric to metric thick beds of clastic rocks such as graywackes, siltstones and pelites. However, in spite of the presence of more pelitic levels, the sandier lithologies dominate in this formation. In the studied area, the monotony of this serie is only broken by three regional marker horizons (Steck et al., 1999) which are from bottom to top: 1) a diamictite pebbly mudstone level, 2) a dolomitic carbonates level, 3) two levels of graphitic quartzites (Fig 4.1).

The diamictite pebbly mudstones, also called “boulder slates” crops out in the Lohani area and constitutes the core of the Lohani anticline. This thick massive level of boulder slates is attributed to the Manjir Formation (Rattan 1973; Frank et al., 1995; Draganits et al., 1998). These conglomerates are interpreted as glaciomarine deposits (Frank et al., 1995; Draganits et al., 1998). Because of its stratigraphic position within the Haimantas sequence, Frank et al.(1995) suggest that this level belongs to the Middle Haimantas. These sediments are the oldest rocks along the Chenab-Miyar Valley transect and constitute the base of the stratigraphic column of Fig. 4.1. These conglomerates are topped by dolomitic beds of variable thickness forming a characteristic brownish horizon.

This kind of dolomitic beds is comparable with several Proterozoic carbonate horizons following glaciogenic sequences in other parts of the world (Draganits et al., 1998). In the Upper Haimantas, only two graphitic quartzite levels break the monotony of the Phe sedimentary sequence. Following Frank et al. (1995), these horizons are diagnostic for the Upper Haimantas. They consist of black cherts, black graphitic quartzites and white quartzites intercalated with layers

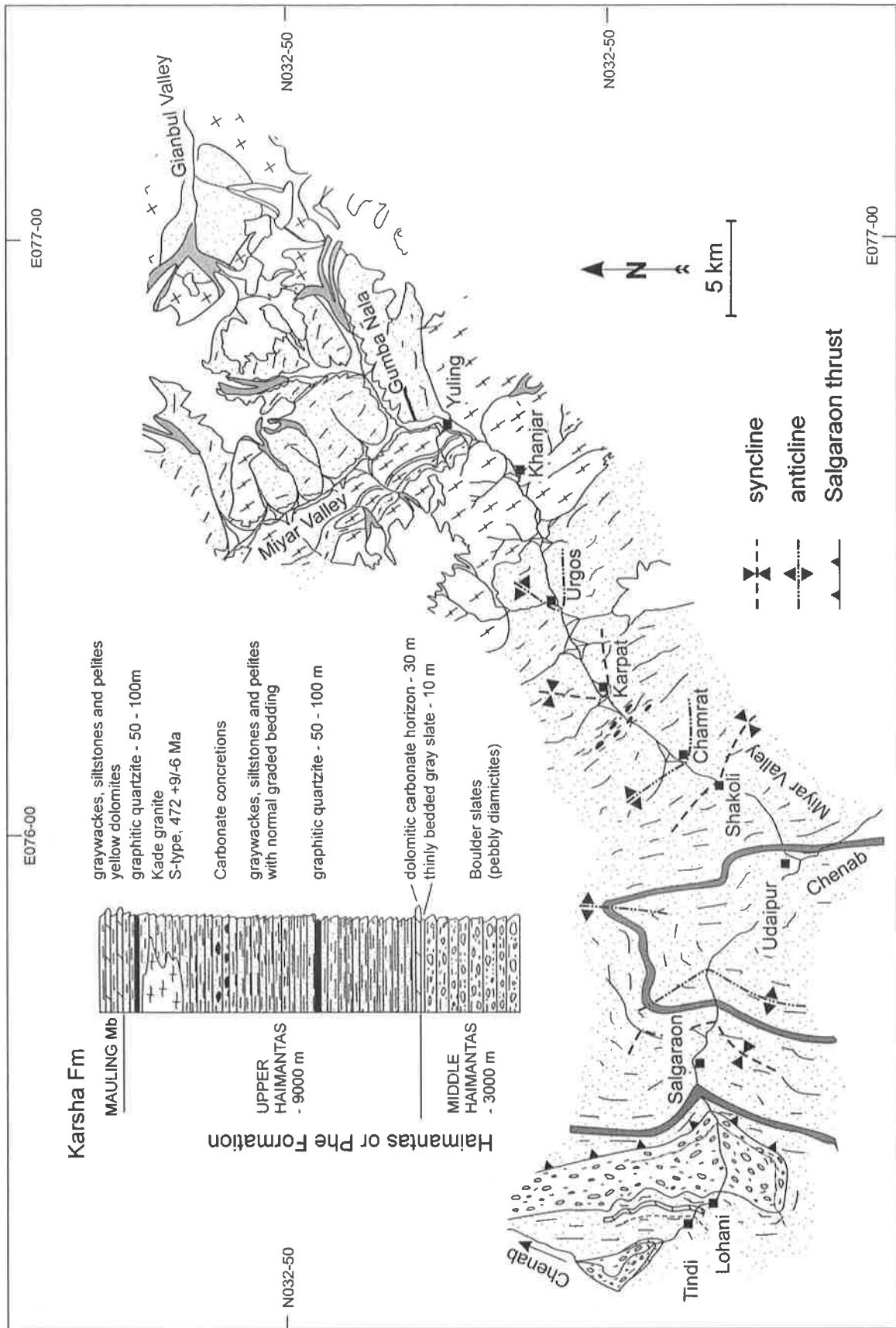


**Fig. 4.1:** Geological map and stratigraphic profile of the Proterozoic to Cambrian Haimantas or Phe Fm. of the Miyar Valley transect after Steck et al. (1999). The thickness estimates of the Haimantas lithologies is based on a detailed geological mapping and profiles.

of pyritous slates. In the Tamlu–Karpāt area, the stratigraphic succession is disturbed by the presence of a level with carbonate concretions of uncertain origin.

These three horizons constitute the only stratigraphic markers we can use to outline a stratigraphic column. Moreover, because of the intense folding, it is difficult to reconstruct a precise stratigraphic succession for the Miyar Valley area. Nevertheless, based on detailed geological map and profiles, Steck et al. (1999) measured the thickness of the sedimentary sequence for the Chenab-Miyar Valley transect. The thickness they obtain for the different lithologies as well as the stratigraphic succession they propose are presented in the Fig. 3.1.

In the Miyar Valley between the localities of Chaling and Yuling (Fig. 3.1), this sedimentary sequence is intruded by the Ordovician Kade granite (472 ±9/-6, U-Pb monazite age; Pognante et al., 1990). This granitic intrusion contains several lenses of basic rocks. The granite of Kade is a porphyritic two micas granite with a S-type geochemistry (Pognante et al., 1990). The transition between the Phe Formation and the overlying lower to middle Cambrian Karsha Formation crops out to the north of Miyar Valley transect in the Shi area, in the Kurgiakh Valley. This transition is gradual and is defined by the first appearance of dolomitic levels.

#### **4.2.2. Age of the Phe Formation**

The metamorphic core zone of the Himalayan orogen (HHCZ) is mainly composed by metasediments (metagreywackes, metasiltstones, and metapelites) which belongs to the Phe Formation or to its south-eastern equivalents. This metasediments show a striking lithologic similarity all along the Himalayan range. Moreover, the  $\delta^{18}\text{O}$  values of quartz in the High Himalayan Crystalline Zone of Zaskar (Roby et al., 2002) are comparable with the isotopic compositions obtained by Vannay et al. (1999) for the High Himalayan Crystalline Zone of the Sutlej Valley, about 150 km to the SE and with the data obtained by Massey et al. (1994) in the High Himalayan Crystalline Zone of the Langtang Valley in Nepal. These results indicate that the High Himalayan Crystalline Zone preserved a characteristic isotopic composition over large distances, despite high-grade metamorphism. This isotopic composition most likely reflects the composition of the pre-metamorphic protolith. Therefore, it seems that the sediments of the High Himalayan Crystalline Zone exposed now in different parts of the range, were deposited contemporaneously in the same basin.

An Upper Precambrian to Lower Cambrian age is generally assigned to this formation on the basis of its stratigraphic position below the fossiliferous Middle Cambrian Karsha Formation. However, in some sections in India and Nepal, isotopic data allowed to adjust the age of the metasediments of the Phe Formation and of its lateral equivalents. In the Langtang area, in the Nepalese Himalaya, the existence of 0.8-1.0 Ga detrital zircon (U-Pb) in the metasediments of the High Himalaya confirm an Upper-Precambrian age for this formation (Parrish and Hodges 1996). In the north-western part of the Himalaya of India, detrital micas from the Upper-Haimantas series yielded plateau type Ar/Ar ages between 800-900 Ma with typical values at 860 Ma (Frank et al., 1995). Rb/Sr whole-rock model ages were calculated for some samples from the metasediments of the High Himalayan Crystalline Zone of the Miyar Valley section (Whittington et al., 2000). These

authors obtain ages going from 630 to 720 Ma which correspond nearly to the values recorded in several other area of the Himalayan range.

These overall results demonstrate that the depositional age of the Upper-Haimantas is not older than Neoproterozoic. On the other hand, no direct evidence concerning the end of the sedimentary cycle exists. However, the gradual transition between the siliciclastic deposition characterizing the Phe Formation and the dolomitic beds of the Karsha Formation marks the end of the sedimentation of the Phe Formation. The presence of middle Cambrian brachiopods, trilobites, and conodontes in the Karsha Formation zone suggests a early to middle Cambrian age for the upper boundary of the Phe Formation (Hayden 1904; Bhatt and Kumar 1980; Garzanti et al., 1986; Hughes and Jell 1999). Moreover, the upper part of the formation is regularly intruded by 500 Ma Cambro-Ordovician granites. These observations reveal that the end of the depositional phase of the Phe Formation occurs before the Middle Cambrian.

#### **4.2.3. Origin and depositional environment of the Phe Formation.**

One of the main feature of the Proterozoic of the High Himalaya is the occurrence of similar lithological formations along the whole range indicating a long and roughly contemporaneous depositional history within a vast clastic intracontinental sedimentary basin. In the metasediments of the Phe Formation, paleocurrent directions defined by flute casts, chevron marks, and foreset-dip show a dominant sediment transport direction to the SW-SE. It means that the source area of the sediments of the Phe Formation was to be situated in a yet unlocated Gondwana fragment in the North of the sedimentary basin (Draganits et al., 1998). Although the exact source region remains at present obscure, it must have been a composite metamorphic/granitic basement with a last thermal event between 900 and 700 Ma. (Frank et al., 1994).

The relationship between the Palaeozoic and Mesozoic sediments of the Tethyan and their Precambrian basal part, the so-called High Himalaya, is still debated. It is still regularly thought that the High Himalayan Crystalline Zone represents a pre-himalayan crystalline basement for the Tethyan sediments. The reason is that, in the majority of the sections, a tectonic contact (e.g. STDS) masks the transition between the High Himalayan Crystalline and the overlying formations. However, some sections of the Himalaya of India, e.g. Parahio valley (Spiti) or Kurghiak valley (Zanskar), reveal that the northern Indian continental margin recorded a continuous stratigraphic sequence from the Precambrian to Lower Cambrian Phe Formation up to Eocene formations (Gansser 1964; Brookfield 1993; Steck et al., 1993; Draganits et al., 1998). At present, no clear real basement with a pronounced regional unconformity and metamorphic break has been reported in the Himalaya.

## CHAPTER 5: TECTONICS

### 5. 1. INTRODUCTION

Most data suggest that the Himalayan range is essentially the consequence of a single orogenic cycle associated with the Eocene India-Asia continental collision. Since the collision, a shortening of about 1800-2500 km occurred between the Indian plate and the stable Eurasia. One-third to one-half of this contraction seems to have been accommodated by shortening in the Indian crust (Hodges, 2000) along a series of parallel major thrust-faults and extensional detachments which divide the Himalayan range into a succession of sub-parallel tectonic units all along the Himalayan belt. In the Zaskar-Lahul region, one of this unit, the High Himalayan nappe, has recorded a polyphase tectonic history which can be subdivided in two major episodes. A first phase of crustal shortening is recorded in the sedimentary sequence of the Indian continental margin. This shortening was accommodated by thrusting, folding, and formation of both NE and SW-directed nappes. The second major phase is related to syn-orogenic extension. This phase is expressed by the formation of ductile normal shear zones, brittle normal faults and dome structures.

### 5. 2. TECTONIC FRAMEWORK OF THE LAHUL AND ZANSKAR AREA

#### 5. 2. 1. Introduction

Many authors have already worked in the Lahul and Zaskar area in order to resolve the rather complex tectonic evolution of these regions (Frank et al., 1973, 1977, 1987; Thöni, 1977; Bassoulet et al., 1980; Fuchs, 1982, 1987, 1989; Honegger et al 1982; Honegger, 1983; Baud et al., 1984; Gaetani et al., 1985; Colchen et al., 1986; Gilbert, 1986; Searle, 1986; Stutz and Steck, 1986; Herren, 1987; Pognante et al., 1987, 1990; Kündig, 1989; Searle et al., 1988; McElroy et al., 1990; Pêcher, 1991; Gapais et al., 1992; Gütli, 1993; Patel et al., 1993; Steck et al., 1993, 1998; 1999; Spring, 1993; Vannay, 1993; Epard et al., 1995; Vannay and Steck, 1995; Dèzes, 1999; Wyss et al., 1999; Walker et al., 1999; Stephenson et al., 2000; 2001).

**Fig. 5.1:** Geological map of the north-western part of the Himalaya of India after Steck et al. 1999 showing the main structural elements discussed in the text. BT = Baralacha La Thrust, DTFZ = Ditung-Thaktote Fault Zone, HHCZ = High Himalayan Crystalline Zone, KSZ = Khanjar Shear Zone, LT = Lagudarsi La Thrust, MBT = Main Boundary Thrust, MCT = Main Central Thrust, MT = Miyar Thrust, PT = Parang Thrust, SF = Sarchu Fault, ZSZ = Zaskar Shear Zone.

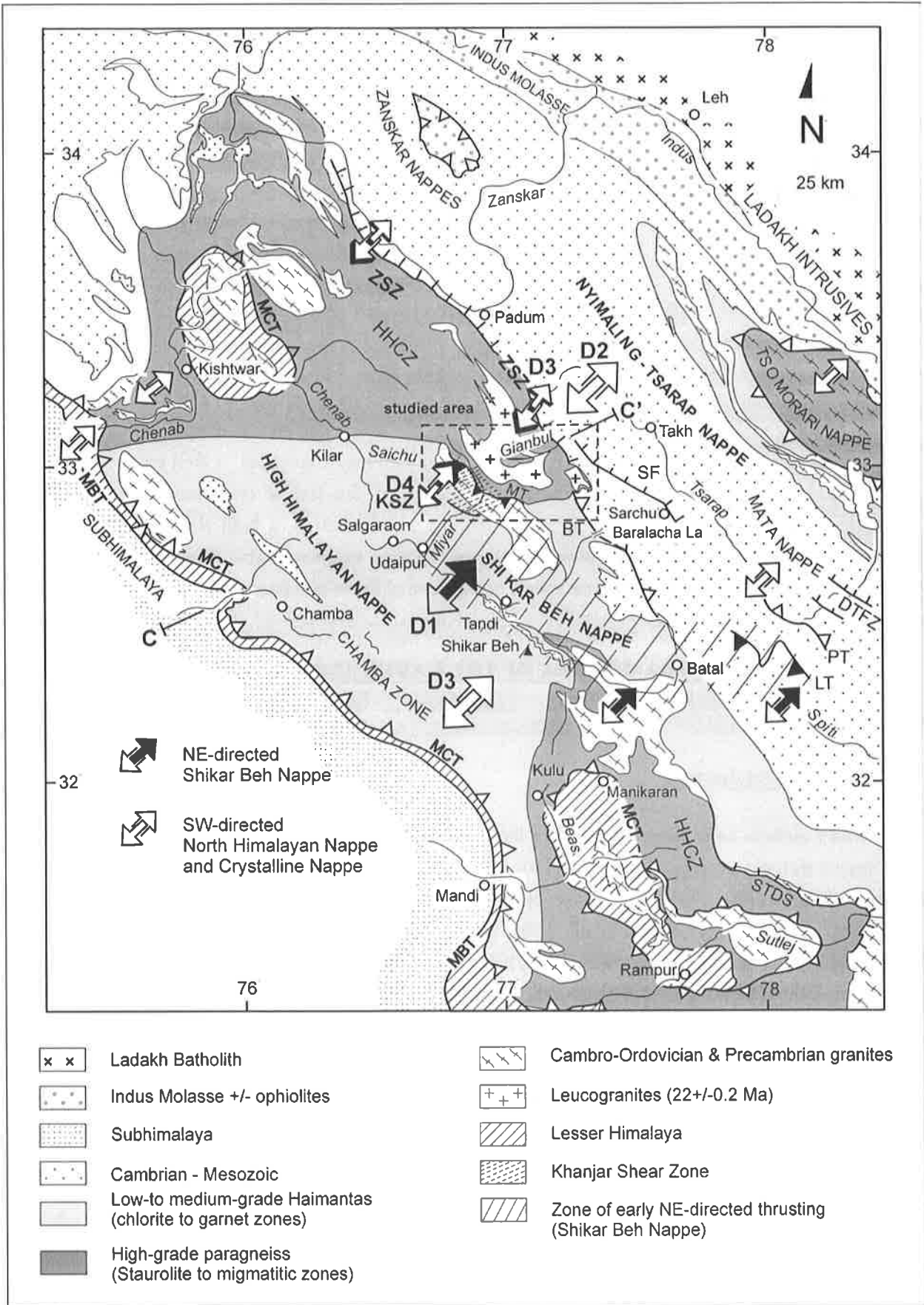




Table 5.1: Tertiary structures of the Miyar Valley - Gianbul Valley transect

|                | Small-scale structures       |                                     |                | Large-scale structures |                            | Age                    |
|----------------|------------------------------|-------------------------------------|----------------|------------------------|----------------------------|------------------------|
|                | Foliation                    | Lineation                           | Folds          |                        |                            |                        |
| D1a            | NE-directed fold             | Schistosity S1a                     | L1a            | F1a                    | Shikar Beh Nappe           | Eocene                 |
| D1b            | NE-directed fold             | Main schistosity S1b                | L1b            | F1b                    | Miyar Thrust Zone          | Eocene                 |
|                |                              |                                     |                |                        | Salgaraon Thrust           |                        |
| D2             | SW-directed fold             | Main schistosity S2                 | L2             | F2                     | Nymaling-Tsarap Nappe      | Eocene to<br>Oligocene |
| D3             | SW-directed fold             | Crenulation cleavage S3             |                | F3                     | Crystalline Nappe          | Early Miocene          |
|                |                              |                                     |                |                        | Zanskar Shear Zone         |                        |
| D4             | SW-directed extension        | Shear bands S4                      |                |                        | Khanjar Shear Zone         | Miocene                |
|                |                              |                                     |                |                        | Gianbul dome               |                        |
| D <sub>A</sub> | Dextral Strike-Slip Shearing |                                     |                |                        | Chandra Dextral Shear Zone | Lower Miocene          |
| D <sub>B</sub> | Late NW-directed foldings    | Crenulation cleavage SB             | L <sub>B</sub> | F <sub>B</sub>         |                            | Lower Miocene          |
| D <sub>C</sub> | Late vertical movements      | dome and basin interference pattern |                |                        |                            | Lower Miocene          |

These studies, although sometimes contradictory, have allowed to lay the bases of the tectono-metamorphic evolution of this part of the Himalayan range. It comes out from these previous works that the Himalayan structures are dominated by SW-directed thrustings and foldings. However, in the Spiti and the Chenab Valley area, early NE-directed verging structures have also been described. Following these works, four major tectonic events are considered to explain the tectonic evolution of the Zaskar and Lahul area (Fig 5.1 and 5.2). The principal characteristics of these deformations are summarised in table 5.1. For the description of the structural elements, the studied transect is subdivided in two sections:

- the Miyar Valley section
- the Gianbul Valley section

### **5. 2. 2. Phase D1: The NE-directed Shikar Beh nappe**

The early NE-directed Shikar Beh nappe was proposed for the first time by Steck et al. (1993 a,b). Their arguments are based on the regional distribution of the metamorphic facies in the lower part of the Chandra Valley, near Khoksar (Fig. 6.1). Indeed, in this area, the metamorphic grade reaches the amphibolite facies conditions and decreases gradually northward, in the direction of the frontal part of the North Himalayan nappes (Nyimaling-Tsarap nappe). According to Steck et al. (1993), this decrease in the metamorphic conditions likely results from the overthrusting of a pile of nappes from the SW towards the NE. Other arguments for an early NE-directed nappe are based on the unusual vergence of the Tandi syncline. Although the enigmatic character of this syncline was already recognised by several authors, the interpretations that they proposed are often contradictory. In 1883 already, Lyddecker recognised this structure as a syncline. One century later, a detailed structural analysis by Powell and Connaghan (1973) showed the polyphase nature of this structure and they demonstrated that the Tandi syncline is associated with a first phase of deformation. Nevertheless, they interpreted it as an antiform closing to the NE. Frank et al. (1973) and Srikantia and Bhargava (1976 and 1979) recognised the NE-directed vergence of the Tandi Syncline. For Frank et al. (1973), this unusual NE-vergence only represents a local perturbation of the SW-directed foldings associated with the SW-directed thrusting along the Main Central Thrust. At the beginning of the nineties, detailed structural analysis of the Tandi syncline confirmed that this structure corresponded to a NE verging fold (Steck et al., 1993; Vannay 1993; Vannay and Steck, 1995). These authors associated this phase with an early NE-directed nappe referred to as the Shikar Beh nappe. In the last ten years, others detailed petrographic and structural investigations in the Lahul and Spiti regions confirmed the existence of the Shikar Beh nappe (Epard et al., 1995; Steck et al., 1998, 1999; Wyss et al., 1999, 2000).

### **5. 2. 3. Phase D2: The SW-directed Nyimaling-Tsarap nappe**

In the northern part of the Indian Himalaya, in the Zaskar and Ladakh area (Fig.5.1), the first phase of folding is associated with the SW-directed North Himalayan nappes emplacement. Nappes tectonics in this part of the Himalaya was described for the first time by the French geologists (Bassoulet et al., 1980). Although confirmed later by several works (Baud et al., 1984; Stutz, 1988;

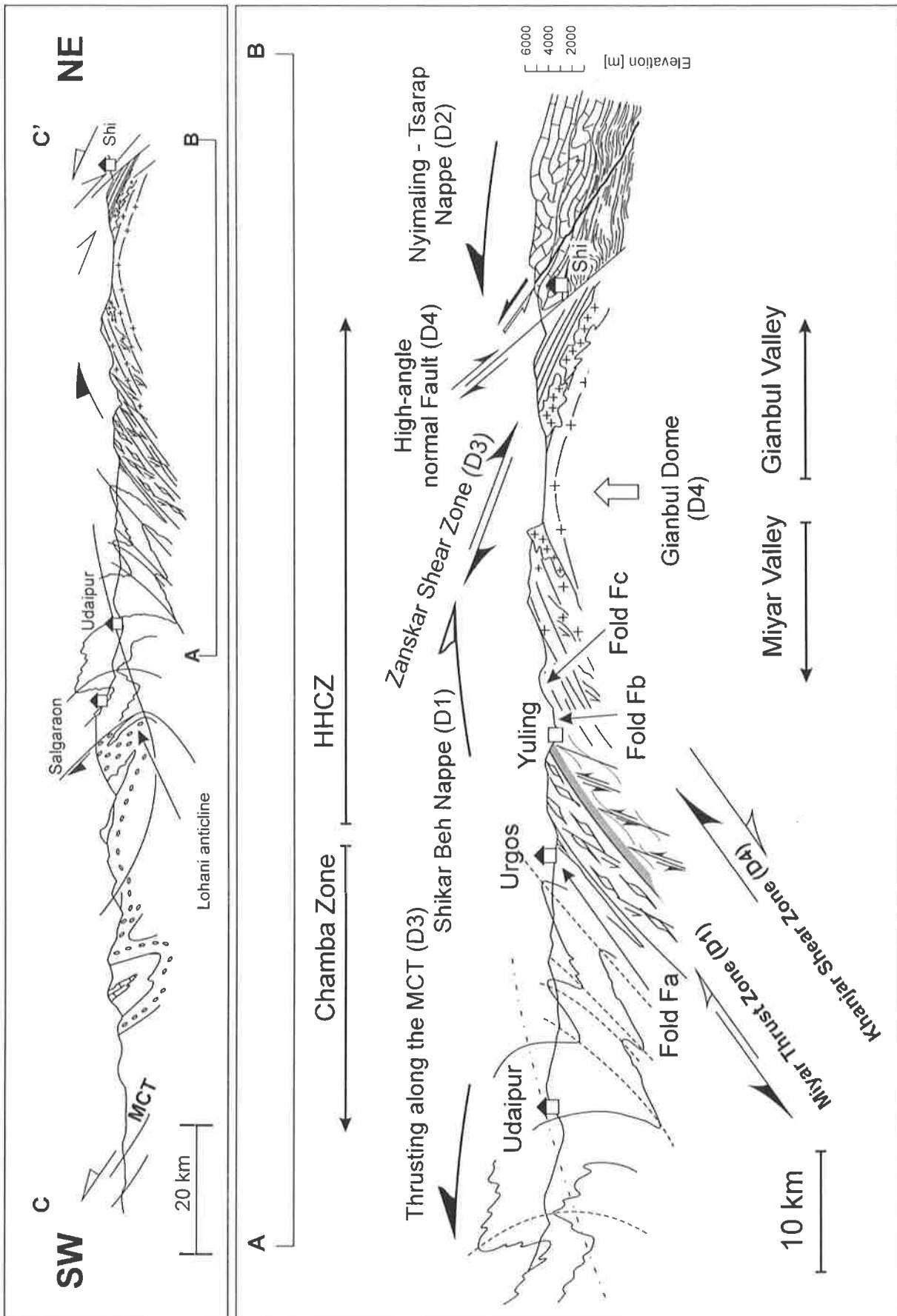


**Fig. 5.2:** (a) General cross-section of the High Himalayan nappe in the north-western part of the Himalaya of India after Steck et al. (1999). See Fig 5.1 for location. (b) Geological cross-section for the Miyar Valley -Gianbul Valley transect after Steck et al. 1999.

Steck et al., 1993 a,b; Vannay and Steck, 1995; Steck et al., 1998; Dèzes, 1999; Steck et al., 1999; Wyss et al., 1999; Girard, 2001), nappe tectonics in the northern part of the Indian Himalaya are still debated by Fuchs and Linner (1995) and Fuchs (2001). For these authors, the term of nappe is not appropriate to describe the tectonics in the Zaskar region. They consider that prevalent tectonics in Zaskar only consist of folds and imbricated structures. On basis of a two dimensional shear model, Steck et al. (1993) calculated a total crustal shortening of about 87 km within the Tethyan Himalaya of Zaskar. On the base of their map and structural observations, these authors concluded that the geometry and the kinematic of the Tethyan Himalaya in Zaskar is comparable with the tectonic style of alpine nappes, as described by Argand (1916). Consequently the term of nappe is justified for the tectonic occurring in the Tethyan Himalaya.

The North Himalayan nappes emplacement is responsible for the main phase of deformation affecting the sedimentary sequences of the Tethyan Himalaya (or Tibetan Himalaya, Argand 1924) in the northern part of the range. The name of Nyimaling-Tsarap nappe was introduced by Steck et al. (1993) for the whole thrust pile of sedimentary rocks located between the Indus Suture Zone to the north and the Baralacha La to the south.

The internal structure of this nappe stack is characterized by a progressive change in style of deformation. The northern part of the range, close to the suture zone, corresponds to the root zone of the Nyimaling-Tsarap nappe. In this region, the deformation is primarily accommodated by ductile shearing and folding. In contrast, in the frontal part of the nappe, the deformation becomes more and more brittle and is characterized by the development of imbricated structures.

#### **5. 2. 4. Phase D3: The SW-directed High Himalayan nappe**

In the Lahul and Spiti area (Fig. 5.1), the early NE-directed structures of the Shikar Beh nappe (D1) are overprinted by SW-directed folding (Steck et al., 1993a,b; Vannay 1993; Epard et al., 1995 Vannay and Steck, 1995; Steck et al., 1998; 1999; Wyss et al., 1999; Wyss, 2000). These D3 structures are observed in the central and southern part of Upper Lahul, and the intensity of the deformation increases from the NE toward the SW. Whereas no D3-large-scale structures was highlighted in the Chenab Valley area, this D3 phase is, on the other hand, responsible of the spectacular SW-directed Kalath fold in the Kulu valley (Thöni, 1977). On the basis of its vergence, its style and its location, this D3 phase is interpreted as related to the SW-directed folding and thrusting of the High Himalayan nappe along the Main Central Thrust (Crystalline nappe; Frank et al., 1973 and 1977). This SW-directed nappe is generally formed of the metamorphic core zone of the Himalayan orogen. In numerous sections along the range, the Crystalline nappe is separated from the low-grade metamorphic sediments of the Tethyan Himalaya by the extensional Zaskar Shear Zone (Herren 1987; Dèzes et al.,1999) considered as a local equivalent of the South Tibetan Detachment System (Burchfiel et al., 1992).

### **5. 2. 5. Phase D4: The doming phase**

In the central and eastern part of the Himalaya, the metamorphic core zone of the range corresponds to a 5 to 40 km thick, NE-dipping monoclinial slab. In contrast, in the north-western part of the Himalaya of India, the high-grade metamorphic rocks are mainly exposed in a more internal part of the orogen. A major characteristic of this high-grade metamorphic zone in the Zaskar area is the presence of several large-scale dome structures, cored by Cambro-Ordovician granitic gneisses and/or Tertiary migmatites and leucogranites (e.g. Kündig, 1989; Searle et al., 1999; Dèzes, 1999). This particular setting implies that the exhumation of high-grade rocks in this part of the range was for a large part controlled by doming. The exhumation of these rocks back to the surface and the mechanism of dome formation are a complicated and still debated problem. In the studied area, structural relations suggest that the doming phase probably occurred shortly after the activation of the extensional Zaskar Shear Zone during Early Miocene.

## **5. 3. STRUCTURAL GEOLOGY OF THE MIYAR VALLEY SECTION**

### **5. 3. 1. Introduction**

The Miyar Valley in the Upper Lahul region represents a natural cross-section through the southern limb of the High Himalayan Crystalline dome defined by Dèzes et al. (1999) as the Gianbul Dome (Fig. 5.1; 5.2). In the Miyar Valley, the stratigraphic column is essentially composed by a thick and monotonous series of Upper Proterozoic to Cambrian detrital sediments (graywackes, siltstones and pelites), generally referred to as Haimantas (e.g. Griesbach, 1891; Frank et al., 1995) or Phe Formation (Nanda and Singh, 1977). These sediments preserved a typical Barrovian metamorphic field gradient indicating a gradual increase of metamorphic conditions from SW to NE. Moving upsection, from the village of Udaipur in the Chenab Valley to the south to the Gumba glacier to the north, the increase in the metamorphic grade gradually transforms these sediments into amphibolite facies to migmatitic paragneiss.

Two types of intrusive granites are also observed in the studied transect. In the Miyar Valley, a thick sheet of granitic gneiss crops out in the northern part of the Chamba zone. This Kade orthogneiss is a porphyric two micas granitic gneiss, characterized by a S-type geochemistry, and derived from an Ordovician protolith ( $496 \pm 16$  Ma, Rb/Sr whole rock, Frank et al., 1977). In the northern part of the Miyar Valley, the HHCZ migmatitic paragneiss are cross-cut by numerous leucogranitic dykes and small plutons. These granitic intrusions are in cartographic continuity with similar granites cropping out in the footwall of the ZSZ in the Gianbul Valley to the NE, as well as with the Lower Miocene Gumburanjun leucogranite ( $22.2 \pm 0.2$  Ma, U-Pb monazite) to the E (Ferrara et al., 1991; Dèzes et al., 1999).

Following the first fieldwork carried out during the summer 1998, we already published the first results of the structural investigations of this area (Steck et al., 1999). This preliminary work already demonstrated that 1) a SW-dipping zone of NE-directed folds and thrusts, the Miyar Thrust

Zone (MTZ), represents the oldest synmetamorphic structure in the Miyar Valley; 2) this Miyar Thrust Zone represents the frontal structure of the early NE-directed Shikar Beh nappe; 3) during a late stage of synmetamorphic deformation, the high grade metamorphic rocks of the Miyar Valley were overprinted by the SW-dipping Khanjar Shear Zone probably related to the late exhumation of the Gianbul dome structure.

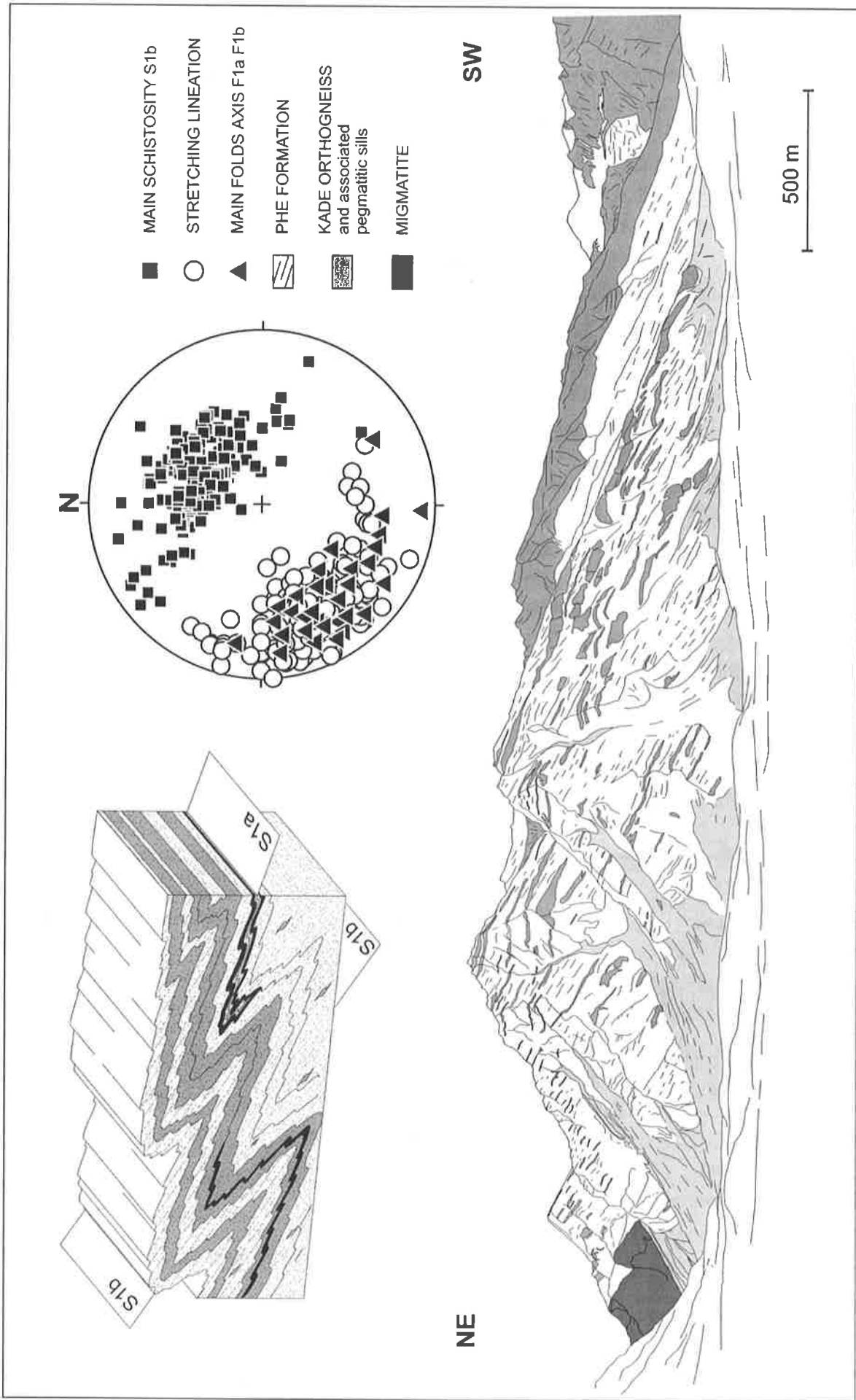
The aim of the following chapter is to provide new constraints on the tectonic evolution of the southern limb of the Gianbul crystalline dome on basis of detail structural investigations in the Miyar Valley area. Together with comparable data from the north-eastern side of the dome (Dèzes et al 1999; Dèzes 1999) in the Gianbul Valley, these new results allow us to unravel the complex tectonic evolution of the High Himalayan Crystalline of Zaskar along a complete transect across the Gianbul dome structures.

### **5. 3. 2. Phase D1: The NE-directed Shikar Beh structures**

#### ***5. 3. 2. 1. The Miyar Thrust Zone and associated structures***

The main tectonic structure in the Miyar Valley corresponds to the SW-dipping Miyar Thrust Zone (MTZ), initially described by Pognante et al. (1990) as a up to a few tens of meter thick synmetamorphic shear zone which separates the weakly metamorphosed Chamba Zone from the high-grade metasediments of the High Himalayan Crystalline Zone (Fig. 5.1). Steck et al. (1999) confirmed that the mylonitic zone affecting the metasediments near the pasture ground called Yuling in the upper Miyar Valley indicates the presence of a thrust shear zone at this structural level. This Miyar Thrust Zone consists in a 10 to 15 km wide ductile shear zone located on the southern limb of the Gianbul Dome (Fig. 5.2). This shear zone is characterised by an increase of the strain intensity with respect to the structural depth from the south towards the north. The increase of the strain intensity is expressed by the development of a mylonitic zone in the northern part of the valley and by the modification of the geometry of the folds which tend to become tighter in the northern part of the section.

**Fig.5.3:** View of the Miyar Thrust Zone near the pasture ground of Yuling. This panorama shows the lower contact between the Kade orthogneiss and the staurolite-kyanite-bearing metasediments of the Phe Formation. Note that the pegmatitic and leucogranitic dykes are oriented with a constant SW-directed dip. No discordant leucogranitic dykes are observed in this area. The structural orientation of the main structural elements associated with the NE-directed Shikar Beh nappe is projected on the stereogram (equal-area stereographic plots; lower hemisphere). The block diagram summarizes the style and the relation between the D1a and D1b structures.



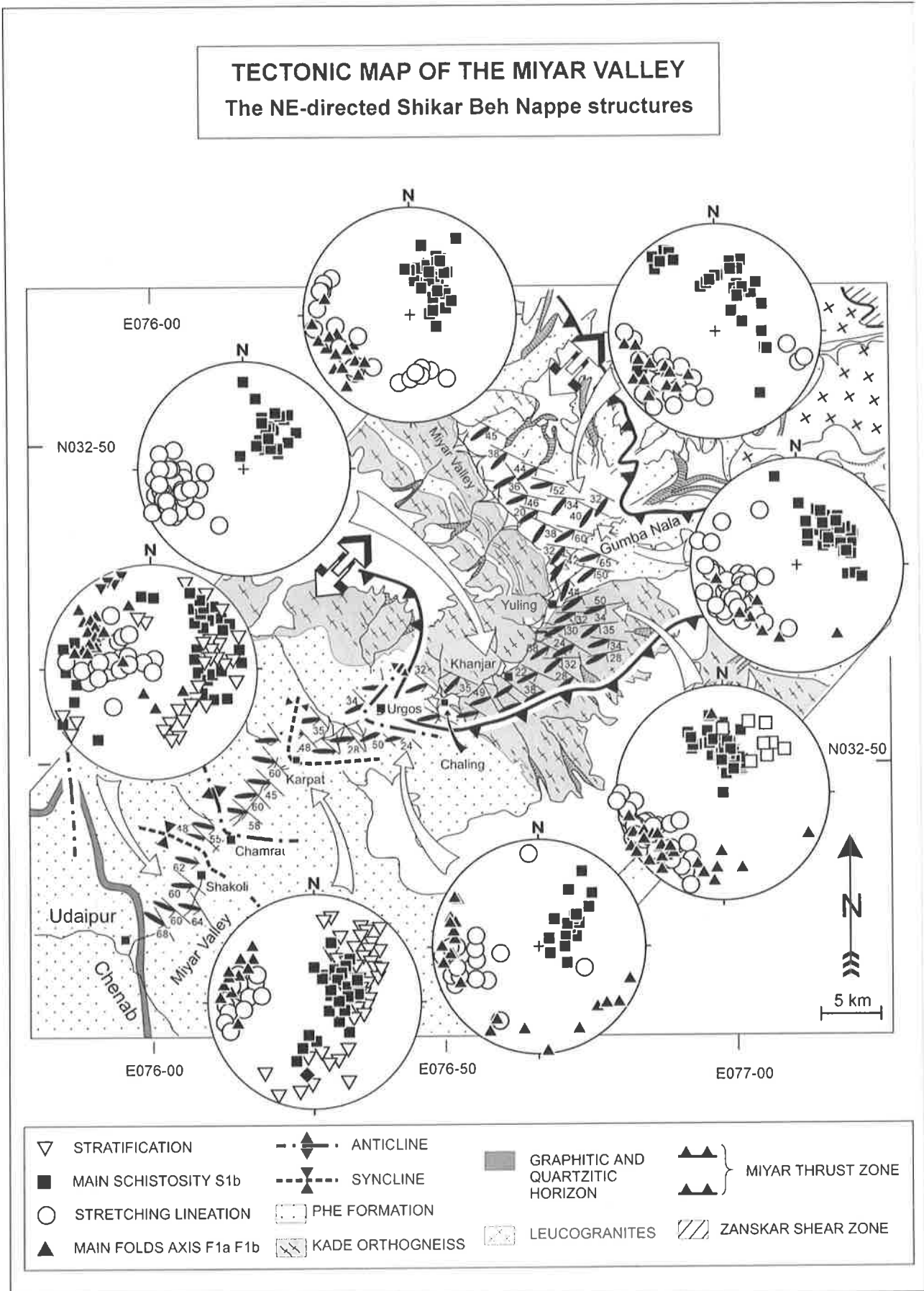


**Fig. 5.4:** Tectonic map of the Miyar Valley, modified after Steck et al. (1999), showing the orientation of the main D1 NE-directed Shikar Beh structures (equal-area stereographic plots, lower hemisphere).



### ***Main schistosity S1b and stretching lineation L1b***

In the downstream part of the valley, the main schistosity (S1b) corresponds to the axial surface structure of the map scale folds. In this part of the section, the bedding (So) and the sedimentary structures are generally preserved and the relationships between the main schistosity and bedding can be used to determine the stratigraphic orientation and the position of the main fold structures. Moving up the valley, with increasing the structural depth, the angle between bedding and main schistosity decreases and the two foliations are gradually transposed parallel into a shear zone defined as Miyar Thrust Zone (Fig 5.2). In the Yuling area, beneath the orthogneiss-paragneiss contact (Fig. 5.1 and 5.3), this shear zone is well exposed and includes the development of a mylonitic fabric synchronous with amphibolite-facies metamorphism. The mean orientation of the dominant S1b mylonitic foliation dips constantly 30° to the S-SW and is marked mainly by biotite, white micas, staurolite and kyanite. Within the shear zone, an associated mineral-stretching lineation plunges approximately 20° to the SW (Figs. 5.3 and 5.4). This L1b lineation is defined by aligned biotite and muscovite aggregates, by aligned prismatic minerals such as staurolite, kyanite, or by the elongation of quartz pebbles and quartz ribbons, and by stretched K-feldspar porphyroclasts in the Kade granite gneiss. Quartz veins and metabasite lenses exposed within the schists are commonly boudinaged parallel to the L1b stretching lineation.

### ***Shear sense criteria***

Within the mylonitic zone, numerous fabric elements providing good kinematic indicators, have been used to decipher the sense of displacement along the Miyar Thrust Zone.

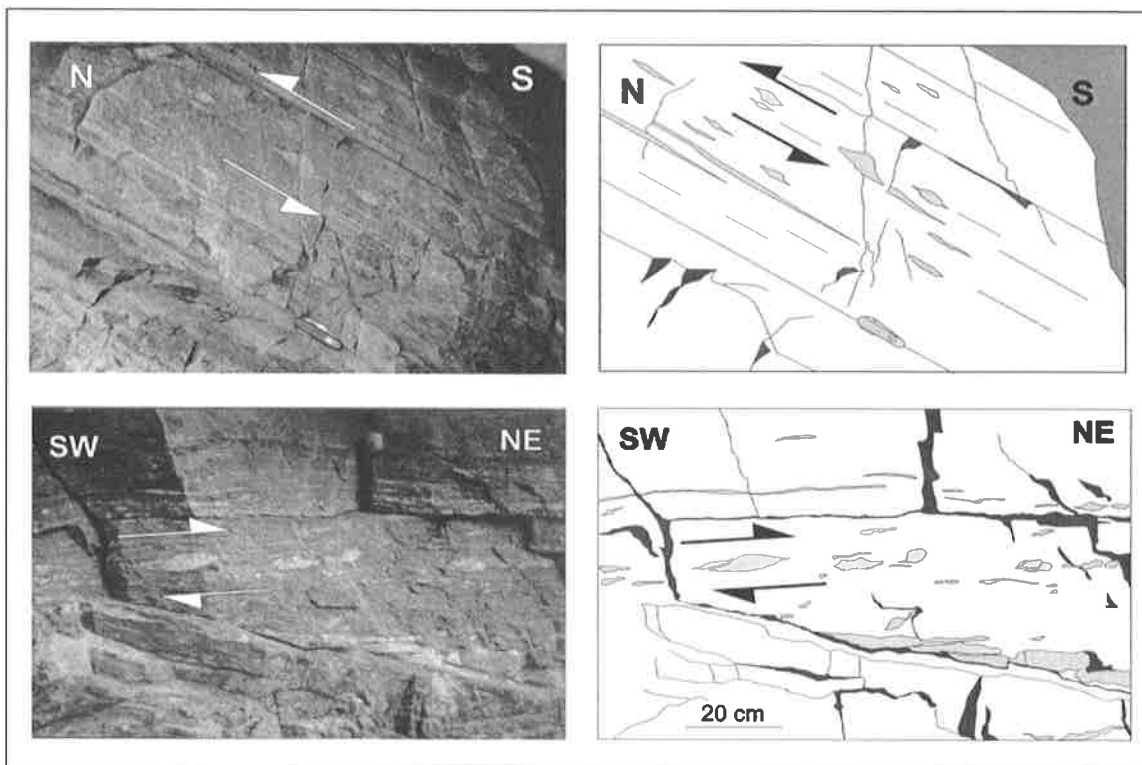


**Fig. 5.5:** Mylonitic sandstone with  $\sigma$ -type porphyroclasts of quartz showing a top-to-the NE shear sense in a finer-grained recrystallised matrix (Gumba Nala area). The section is parallel to the stretching lineation and normal to the tectonic foliation.

One of the most abundant kinematic indicators observed in the Miyar Thrust Zone are asymmetrical augen structures of  $\sigma$ -type such as K-feldspar porphyroclasts in the Kade orthogneiss or quartz pebbles in the schists. The geometrical analysis of the position of their wings relative to the main foliation reveals a top-to-the-NE movement (Fig. 5.5).

Pinch-and-swell structures and boudinage of layer of different compositions are also common in the Miyar Thrust Zone. As the consequence of the non-coaxial deformation, the more competent levels acquire the geometry of fish-shape ellipsoidal volumes (Fig 5.6). The non-coaxial deformation also produces the formation of discrete extensional shear bands in the pinches of the boudins. These extensional asymmetrical shear bands have an angle lesser than 30 degrees with respect to the main foliation. The top-to-the-NE sense of shear deduced from these structures is consistent with the movements revealed by  $\sigma$ -type structures.

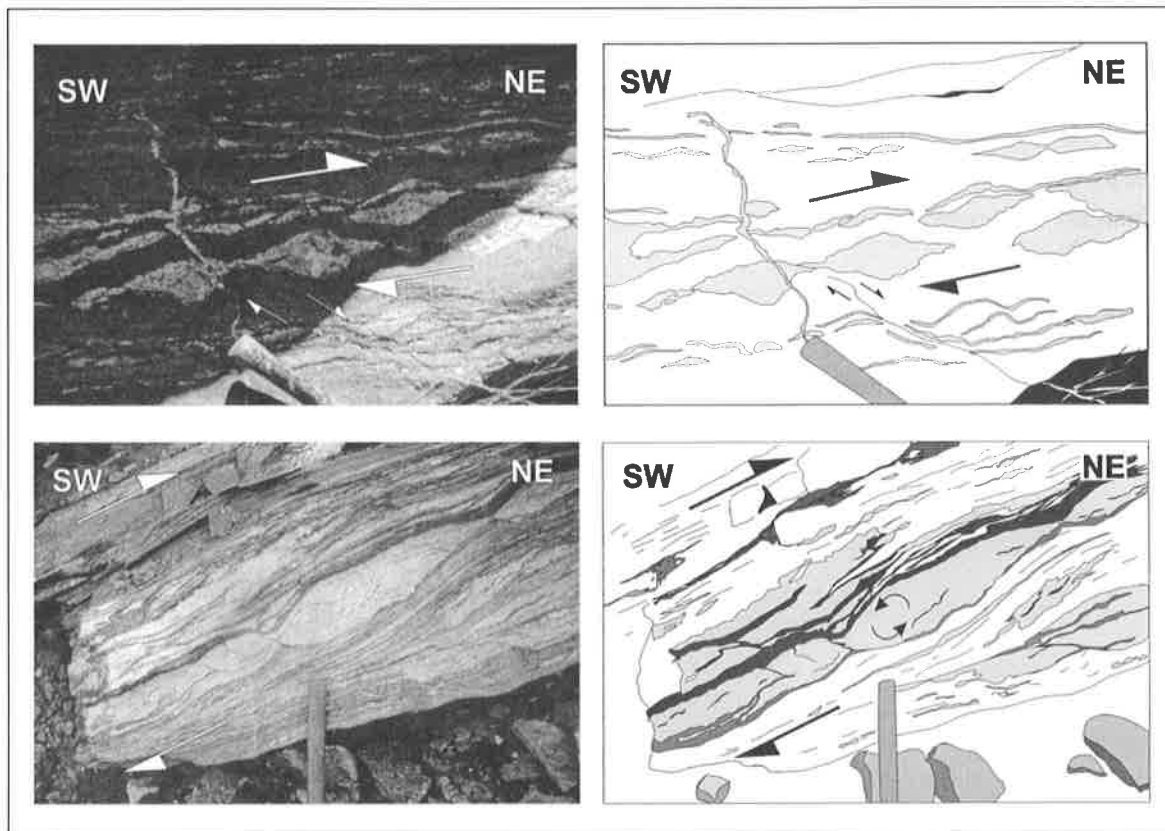


**Fig. 5.6:** Asymmetrical boudinage of quartzo-felspathic layers in the migmatitic zone (Gumba Nala area). Note the presence of discrete extensional shear bands between the boudins showing a top-to-the-NE shear sense. (bottom) The back rotated boudins indicate top-to-the-NE ductile extensional movements

However, the most reliable shear-sense indicator in the Miyar Thrust Zone is the occurrence of sigmoidal inclusion trails in syntectonic garnet porphyroblasts. In the Gumba Nala area, at the base of the Miyar Thrust Zone, inclusion trails in garnet porphyroblaste indicate a clear top-to-the-NE sense of shear (Fig. 5.7).

Consequently, these overall kinematic indicators, together with NE-vergence of the map-scale folds associated with the Miyar Thrust Zone (Fig. 5.2) suggest hanging wall movement to the NE relative to the footwall along the SW-dipping Miyar Thrust Zone.

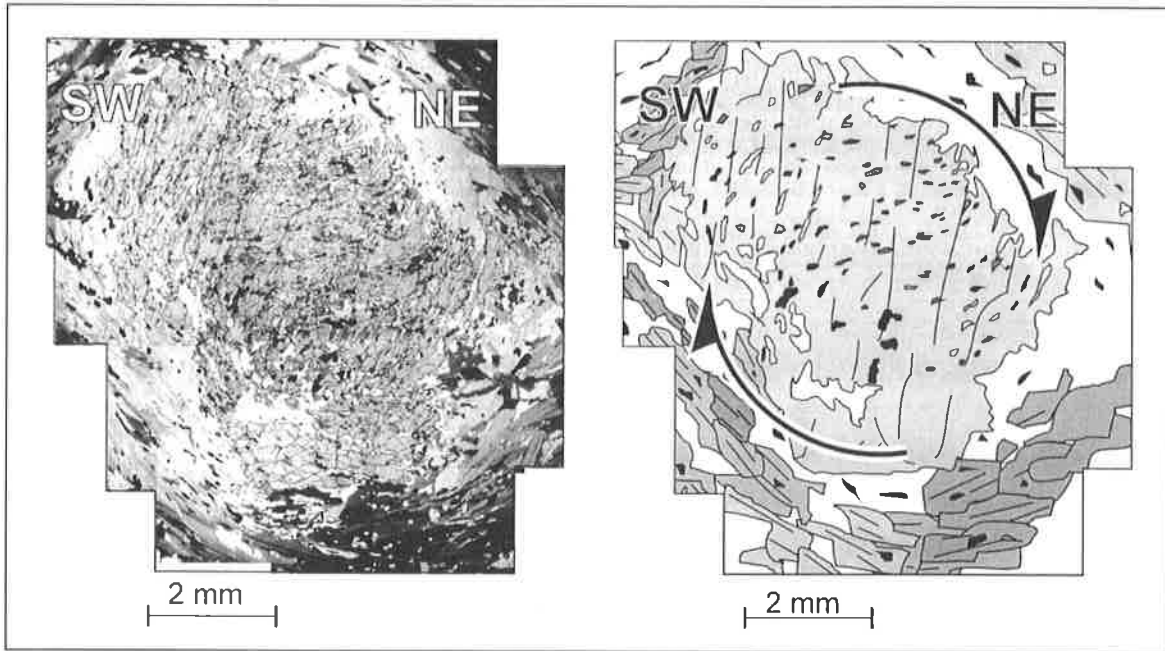


**Fig. 5.7:** D1 syntectonic garnet porphyroblast in micaschist from the migmatitic zone (Gumba Nala area) showing an almost 120° of top-to-the NE rotation with respect to the main schistosity.

### ***Strain intensity and folds F1b***

The strain intensity increases northwards together with the gradual increase of the metamorphic conditions ranging from chlorite, kyanite-staurolite up to sillimanite-migmatite zone. Throughout the Miyar Thrust Zone, the tightening of intrafolial folds reveals the increase of the strain intensity.

Structurally above the shear zone, downstream from the village of Chaling (Fig. 5.4), the main schistosity becomes less penetrative compare to the mylonitic foliation observed within the shear zone. Indeed, in the downstream part of the Miyar Valley, the metasediments generally preserve their sedimentary features, such as graded bedding, load casts and ripple marks (Steck et al., 1999). Because of the monotony of the detrital Phe Formation and the scarcity of good marker horizons, sedimentological criteria, such as graded bedding, were systematically used to determine the stratigraphic polarity. The position of the axial surface of the main folds and therefore the position of the large-scale fold structures were determined using the structural relations between schistosity and bedding. Locally, the presence of more competent levels, such as sandstones allowed us to observe second order folds and to precisely describe their geometry.

The geometry of the folds is described using the classification of Ramsay (1967) based on the shape of the profile section of the folded layers. Following the Ramsay's method, it is possible to express the changes in shape within the folds and to classify the folded layers using the orthogonal thickness  $t$  which corresponds to the perpendicular distance between the two parallel tangents. In contrast, the isogon corresponds to the line connecting two point of equal dip on opposite surface of the layer (Fig. 5.8). Using the orthogonal thickness method, every folded layer can be drawn as a single line and can be classified into five important classes of folds (Fig. 5.8). This method is based

on the hypothesis that the folds start by being parallel and the modifications of the fold geometry occur by superimposed homogeneous strain.

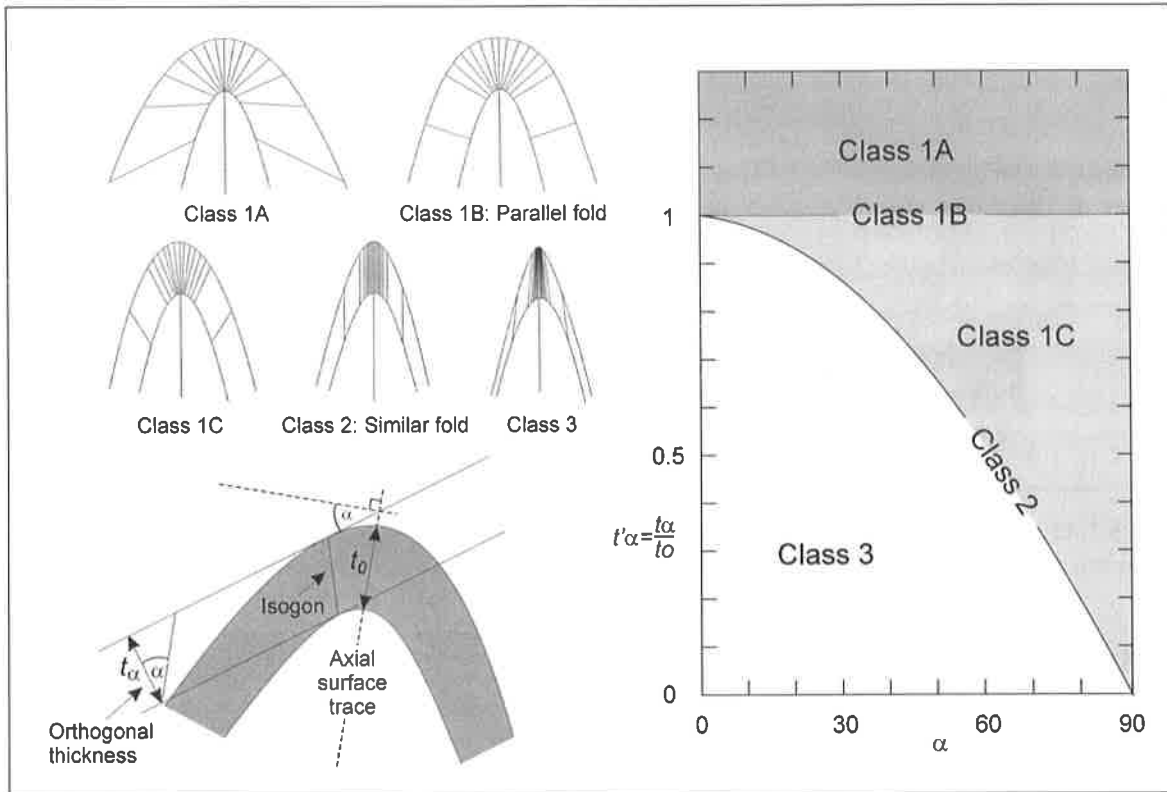


**Fig. 5.8:** Ramsay's classification of folded layer. (top) Fundamental types of fold classes. Dip isogons have been drawn at  $10^\circ$  intervals from the lower to the upper surface X and Y. (bottom) Geometrical representation of the layer inclination  $\alpha$ , the dip isogons, and the orthogonal thickness  $t_\alpha$ . (right) Classification of folded layers according to the thickness of the layer with increasing  $\alpha$  (that is from hinge to limb). Fold classes are distinguished by the normalized orthogonal thickness  $t' = t_\alpha/t_0$ , where  $t_0$  is the orthogonal thickness at the hinge where  $\alpha = 0$ .

Three folds (Fa; Fb; Fc) were examined for this geometrical study (Fig. 5.2). These folds are located at different structural levels across the shear zone. The fold Fa is located at a weak structural depth whereas the folds Fb and Fc are respectively located at increasing depths within the shear zone.

Following this classification, the geometry of the folds observed in the hanging wall of the Miyar Thrust Zone (fold Fa) corresponds to the 1C class (Fig. 5.9). According to this classification, this kind of folds is named folds with weakly convergent isogons. It means that the orthogonal thickness of the folded layer in the limb of the folds is always smaller than at the fold hinge. In general, it is assumed that folds of 1C class are formed by homogeneous flattening of parallel folds (isopachyte), and they have been termed *flattened parallel folds* by Ramsay (1962).

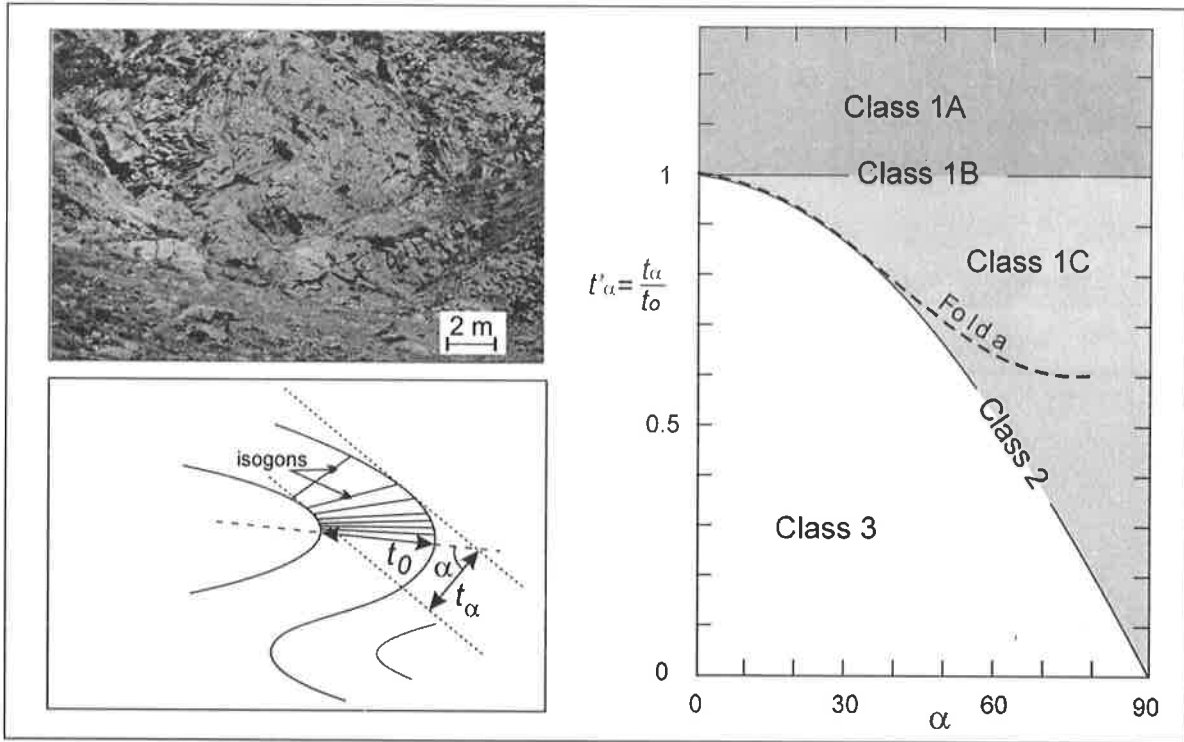


**Fig. 5.9:** (top) Profile of the Fa fold within the hanging wall of the Miyar Thrust Zone near Urgos. (bottom) The decrease of the orthogonal thickness  $t_\alpha$  from hinge to limb, together with the convergence of the dip isogons toward the inner side of the fold, characterizes the class 1C folds. (right) Graphical plot of the orthogonal thickness  $t_\alpha$  for the Fa fold in a  $t'_\alpha$  versus  $\alpha$  graph.

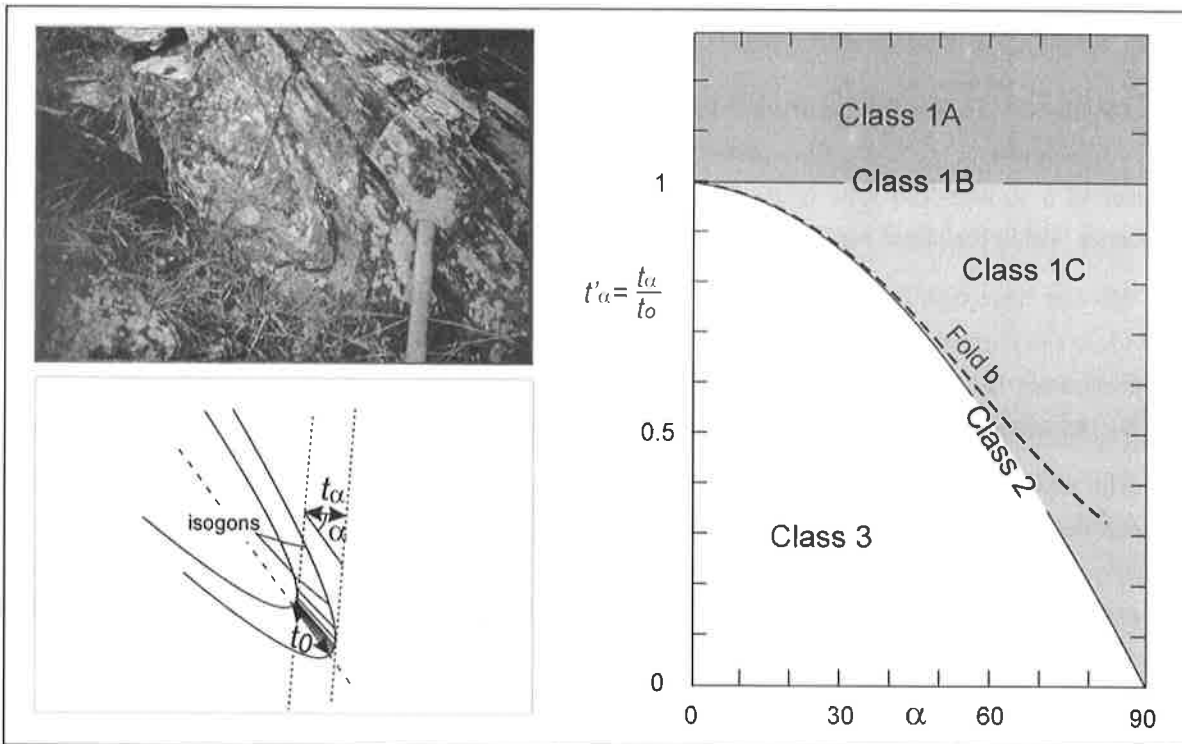


**Fig. 5.10:** (top) Profile of the Fb fold within the Miyar Thrust Zone near Yuling. (bottom) The decrease of the orthogonal thickness  $t_\alpha$  from hinge to limb, together with the convergence of the dip isogons toward the inner side of the fold, characterizes the class 1C folds. (right) Graphical plot of the orthogonal thickness  $t_\alpha$  for the Fa fold in a  $t'_\alpha$  versus  $\alpha$  graph showing a geometry which tends to become close to a similar fold type (class 2).

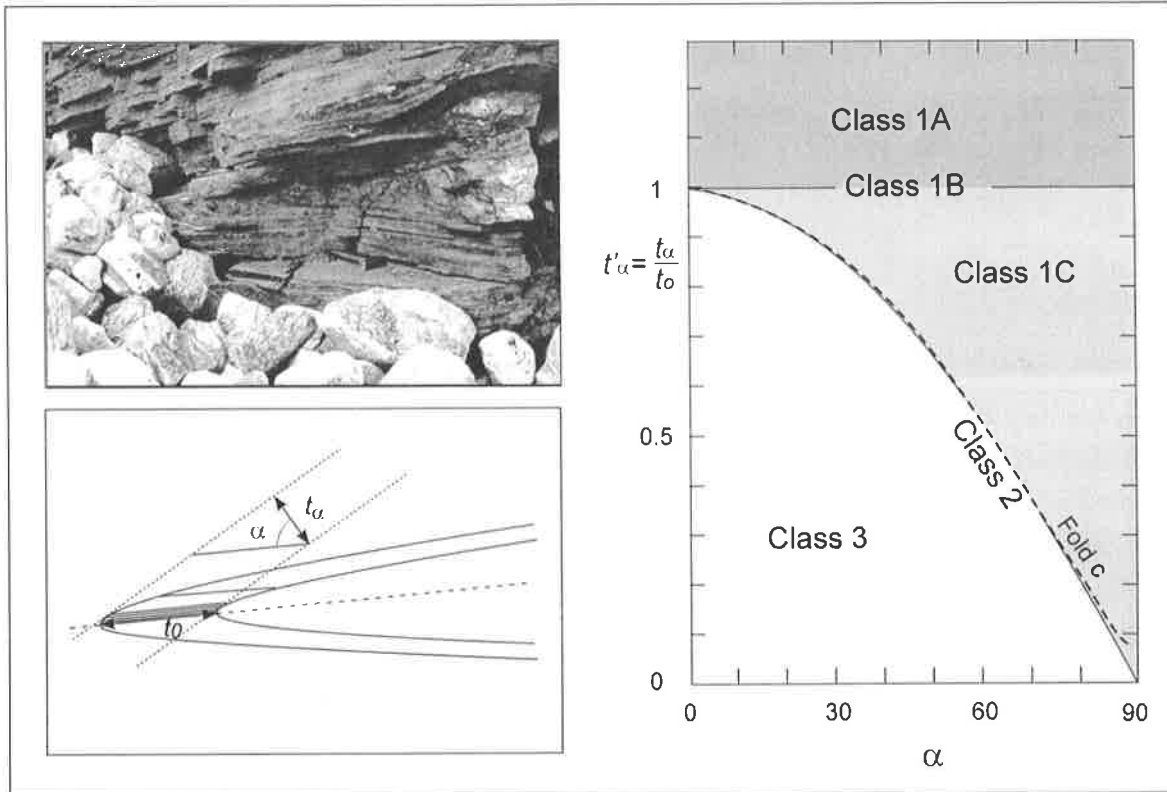


**Fig. 5.11:** (top) Profile of the Fc fold near the deepest part of the Miyar Thrust Zone in the Gumba Nala area. (bottom) The average isogon pattern for this fold is approximately parallel to the axial surface and testifies that the geometry of this fold closely approximates the similar fold type (class 2). (right) Graphical plot of the orthogonal thickness  $t_\alpha$  for the Fa fold in a  $t'_\alpha$  versus  $\alpha$  graph showing a geometry which closely approximates a similar fold type (class 2).

Structurally inside the shear zone (fold Fb), near the Yuling area, the geometry of the fold becomes tighter (Fig. 5.10). This fold belongs also to the class 1C but its geometry tends to come closer to a similar-fold type (class 2). It means that the flattening on the limbs of the folds is stronger within the shear zone than in the hanging wall.

Moving upsection along the Miyar Valley, the geometry of the folds becomes still tighter (Fig. 5.11). In the Gumba Nala, towards the bottom of the Miyar Thrust Zone, the fold geometry closely approximates the geometry of similar folds (fold Fc). These results testify of a significant increase of the deformation towards the deeper part of the Miyar Thrust Zone.

The progressive increase in the deformation through the Miyar Thrust Zone can be estimated using the graphical method proposed by Ramsay (1967). This method allows to estimate the total compressive strain that has acted along the layer of the initial parallel folds. For this calculation, it is assumed that the original shape of the fold was a parallel fold. Consequently, this graphical method aims to quantify exclusively the shape modification of an initially parallel fold by superimposed homogeneous strain. This method is based on the following mathematical relation between the orthogonal thickness  $t$ , the angle  $\alpha$  between the isogons and the axial surface, and  $\lambda_1$  and  $\lambda_2$ , the quadratic extensions parallel and perpendicular to the axial surface respectively :

$$t'_\alpha = (\cos^2 \alpha + \lambda_2/\lambda_1 \sin^2 \alpha)^{1/2}$$

Using this equation, a graph of  $t'$  versus  $\alpha$  can be built for 1C type folds and for various values of  $\lambda_2/\lambda_1$  (Fig. 5.12). The lowest curve where  $\lambda_2/\lambda_1 = 0$  correspond to similar fold type (class 2) and the highest ( $\lambda_2/\lambda_1$ ) represent the parallel fold geometry (class 1B).

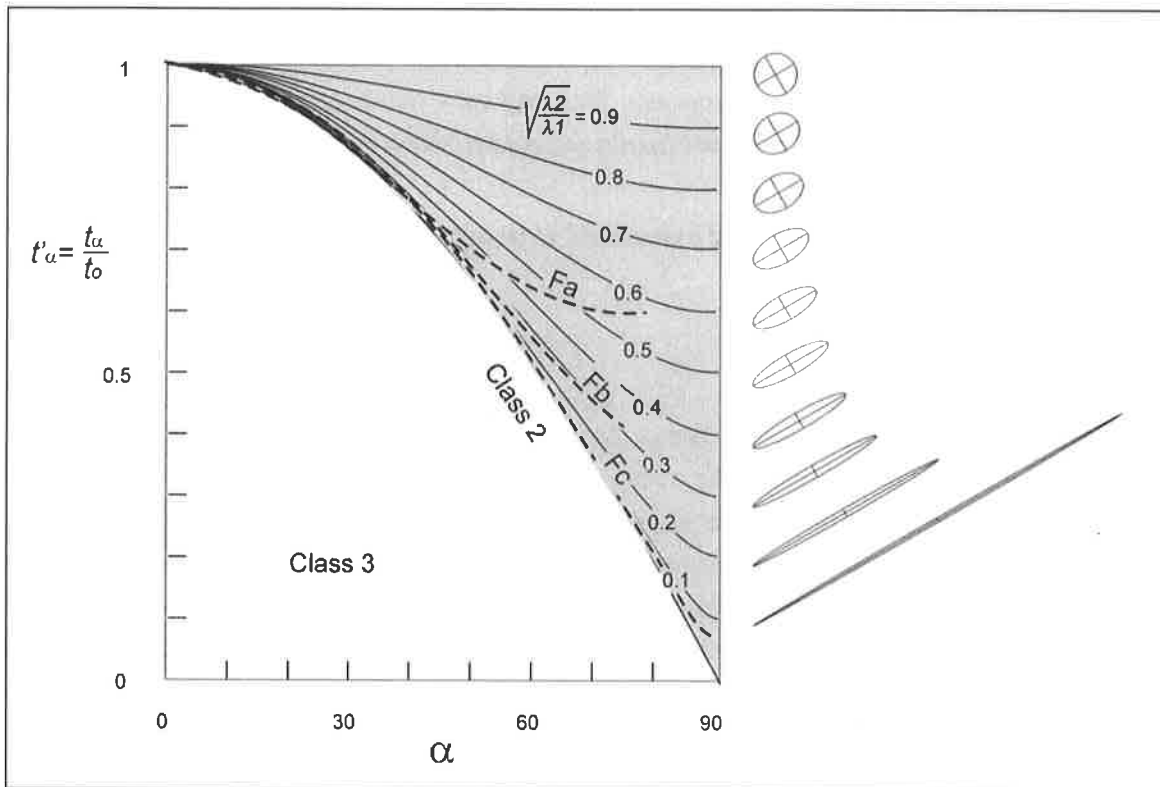


**Fig. 5.12:** Values of  $t'/\alpha$  in flattened parallel folds with variation in  $\lambda_2/\lambda_1$ . The continuous curves represent the initial parallel folds modified by superimposed strain with various values of  $\lambda_2/\lambda_1$ . The highest curve where  $\lambda_2/\lambda_1 = 1$  gives the parallel fold geometry and the lowest curve  $\lambda_2/\lambda_1 = 0$  corresponds to the similar fold model (class 2). The dashed curves represent the position of the Fa, Fb, and Fc folds with respect to the  $\lambda_2/\lambda_1$  superimposed strain. (right) Representative strain ellipse relative to the variation in  $\lambda_2/\lambda_1$

On the graph of the Fig. 5.12, the fold Fa, located in the hanging wall of the Miyar Thrust Zone, has a  $\lambda_2/\lambda_1$  values between 0.5 and 0.6. It means that the quadratic extension  $\lambda_1$  parallel to the axial surface is three to four times longer than the quadratic extension  $\lambda_2$  normal to the axial surface. The fold Fc cropping out in the bottom of the shear zone indicates that the quadratic extension  $\lambda_1$  should be hundred times longer than the normal quadratic extension  $\lambda_2$ . It means that the superimposed homogeneous strain was more significant of a factor six on the limb of the fold Fc than on the limb of the fold Fa. In agreement with these results, the fold Fb, located in the middle of the shear zone, corresponds to a stage of intermediate modification compared to folds Fa and Fc. Therefore, the geometrical analyses of the different shape of the intrafolial folds throughout the Miyar Thrust Zone provides evidences on the increase of the intensity of the deformation through the Miyar Thrust Zone.

On a regional scale, the ductile Miyar Thrust Zone is interpreted as the ductile equivalent of the more brittle and discrete Salgaraon thrust structure described for the first time by Steck et al. (1999) in the Chenab Valley (Fig. 5.2). Close to the village of Salgaraon, at a higher tectonic level,

the SW-directed Lohani anticline (Fig 5.1 and 5.2) is characterized by a strong asymmetry in the thickness of its limbs, the upper limb being clearly thinner than the lower limb. This asymmetry is explained by Steck et al. (1999) as the effect of a discrete thrust structure: the Salgaraon thrust. Initially refolded towards the NE, the originally NE-verging Lahoni anticline was first thrust towards the NE, causing strong deformation and reduction of its overturned northern limb along the Salgaraon thrust. Then this thrust anticline was rotated to its present position during the SW-directed High Himalayan nappe emplacement. This originally NE-directed thrusting is interpreted as being the brittle equivalent of the more ductile and deeper Miyar Thrust Zone.

### 5. 3. 2. 2. *The earliest phase and associated structures*

#### *The S1a schistosity*

In the hanging wall of the Miyar Thrust Zone, some interference fold patterns highlight the existence of a first phase, preceding the main schistosity (Fig. 5.13). In most of the case, the S1a schistosity related to this first phase is parallel to the bedding and to the main schistosity. Consequently, it is difficult to distinguish the two foliations. However, in some more competent hornblende-bearing volcanoclastic levels, the S1a schistosity is highlighted by aligned amphibole aggregates. The chronological relation between the two schistositities can thus be clearly illustrated (Fig. 5.13 and 5.15). The chronological relations between these two schistositities reveal that the main schistosity on the regional scale already corresponds to a second schistosity (S1b). Although in most of the cases the S1a schistosity is parallel to bedding, an angle between the S1a schistosity and bedding (S0) can be locally observed. The rare outcrops where the bedding/schistosity relationship can be observed reveal that the S1a schistosity dips more steeply towards the south than the stratification (Fig. 5.14). This S1a schistosity-stratification relation suggests that the formation of this first schistosity is related to a NE-directed thrusting (Steck et al., 1999). Indeed, if we draw the F1a fold associated with to the S1a schistosity and that we unfold the S1b intrafolial fold, we note that the F1a fold should have a NE-directed vergence.

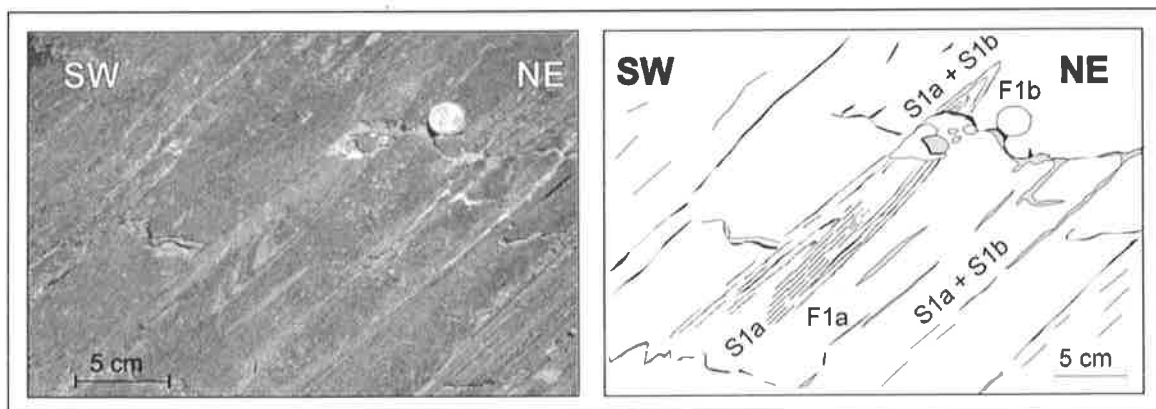


**Fig. 5.13:** F1a-F1b fold interference pattern from the normal F1b fold limb between Shakoli and Chamrat (from Steck et al., 1999)



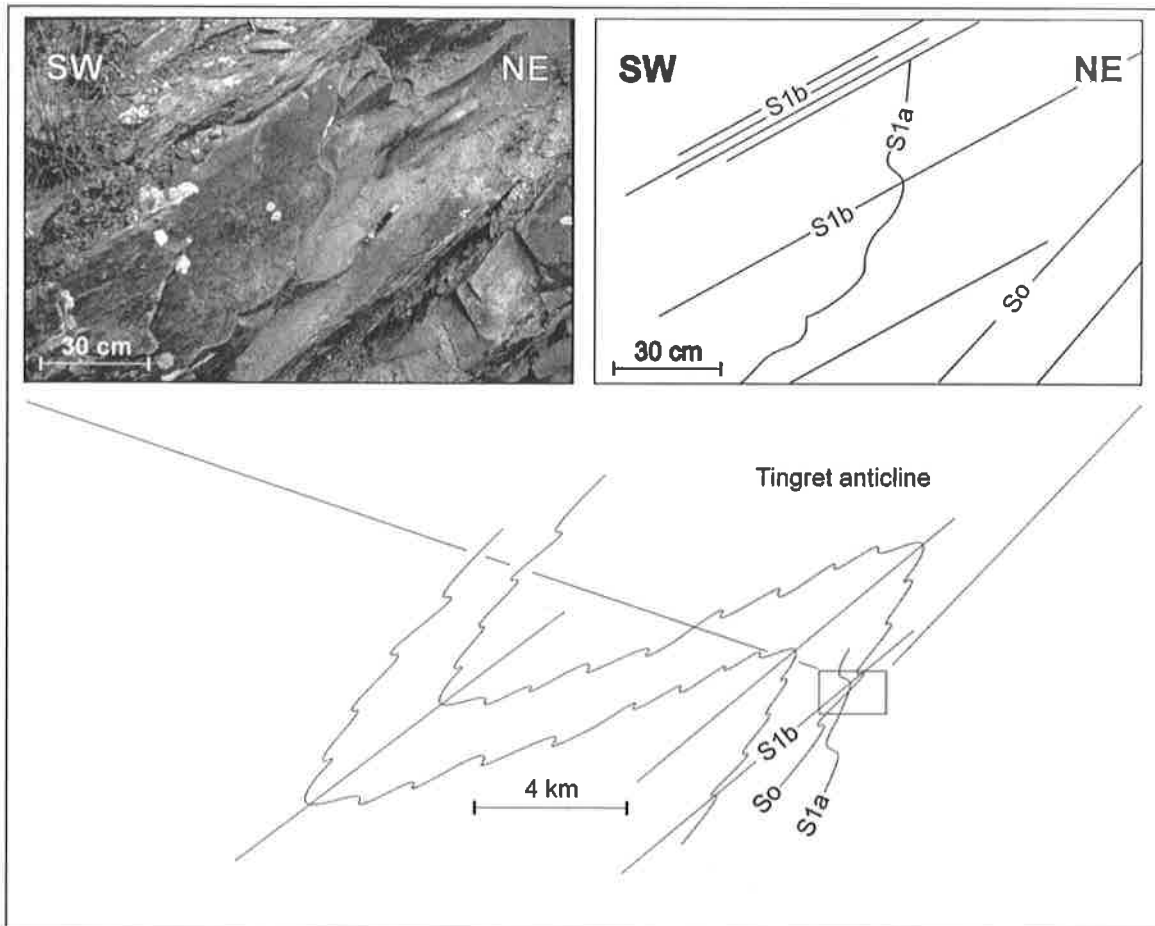


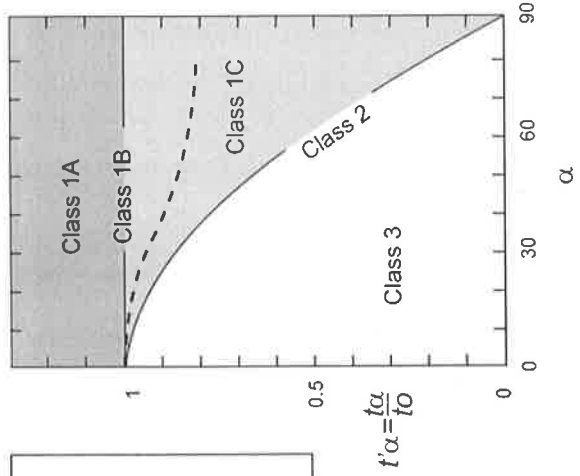
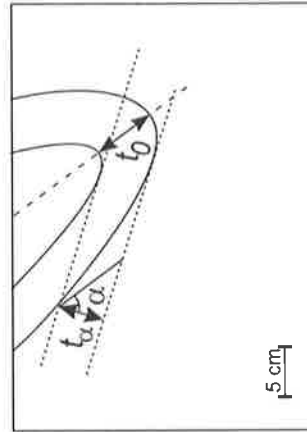
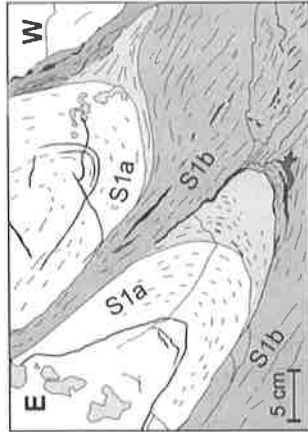
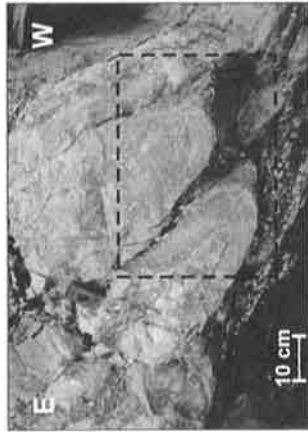
**Fig. 5.14:** S1a-S1b and F1a-F1b interference pattern in the inverted northern limb of the Tingret anticline near Urgos. Note that the S1a schistosity dips steeper southward than bedding. This bedding-schistosity relationship together with rare NE-verging F1a folds suggest that the formation of the S1a schistosity is related to NE-directed thrusting (from Steck et al. 1999).

### *The F1a Fold*

The F1a fold structures are scarce and have been observed at small scale only (Fig. 5.13 and 5.15). If we compare the F1a folds with the F1b folds located in levels of equal competence and exposed in an identical geographical as well as structural position (near the village of Urgos), the geometric analysis of these various folds reveals different types of folds (Fig. 5.13). Whereas the F1b folds correspond to *flattened parallel folds* of 1C class-fold model as discussed previously, the F1a folds generally show a shape of a similar-fold model (class 2) or a geometry which closely approximates it (very flattened 1C-class) (Fig. 5.15). The difference of geometry between the F1a and F1b folds comes probably from the fact that the F1a fold has undergone at least two phases of deformation. It seems that the geometry of the F1a folds had to correspond to 1C class-fold type whose flatness of the limbs approaches the similar-fold model. Therefore, the closely approximation of similar-fold model exhibited by the F1a folds most likely reflects the modification of shape of the originally F1a folds by superimposed homogeneous strain relative to the occurrence of the main D1b NE-directed phase.

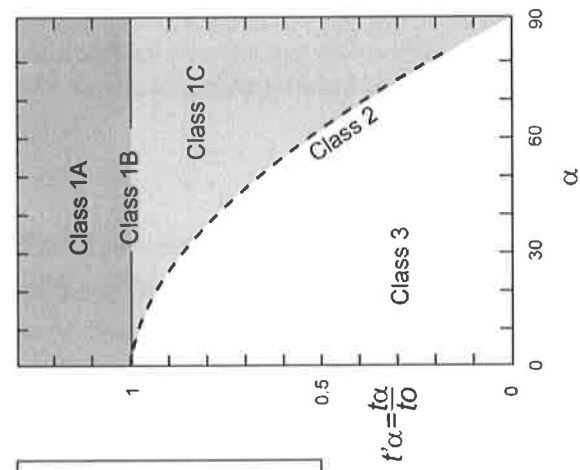
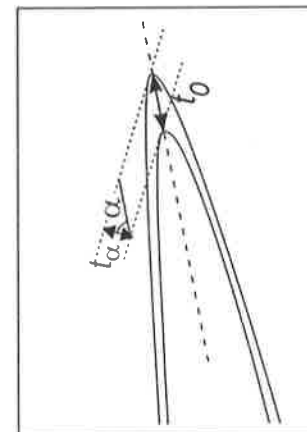
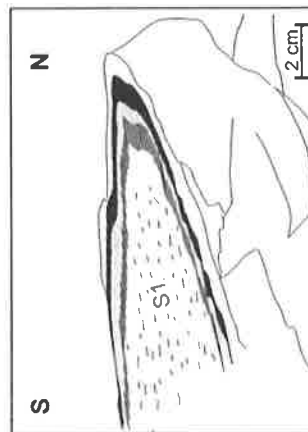
**Fig. 5.15:** Comparison between the F1a folds and the F1b folds near the village of Urgos, in the hanging wall of the Miyar Thrust Zone. (a) The F1a fold shows a shape which closely approximates the similar fold type. The syntectonic foliation is marked by hornblende. (b) The F1b fold shows a typical 1C class type geometry. Note that in this fold, the S1a hornblende-bearing schistosity is refolded by the D1b phase.

F1b Fold (Urgos)



(b)

F1a Fold (Urgos)



(a)

### 5. 3. 2. 3. Discussion

In the Miyar valley section, the D1 phase is characterized by NE-verging structures which can be divided into the D1a and the D1b sub-phases. The D1b phase is documented by the main S1b schistosity and by a 10 to 15 km wide ductile shear zone defined by Steck et al. (1999) as the Miyar Thrust Zone. This structure is characterised by sheath folds, mylonitic structures and well-developed top-to-the-NE shear sense criteria. The S1b schistosity corresponds to the main schistosity which forms the axial surface structures of the map-scale folds along the whole Miyar Valley section. This phase strongly overprints and transposes the D1a structures.

One of the main conclusions of the Miyar Valley structural analyses is that the earliest deformations, the D1a phase as well as the D1b phase, both exhibit clear NE-directed movements. The main implication of this unusual vergence is that it attest to an early NE-directed tectonic phase contrasting with the dominant SW-directed tectonic phases observed in most of the sections along the Himalayan range. In the Miyar Valley, this early NE-directed phase is responsible for the northward prograde metamorphic field gradient as well as for the progressive increase of the strain intensity towards the north. Consequently, this first phase is of great importance for both the deformational and the metamorphic evolution of this part of the Himalayan range and has to be associated with a significant NE-directed crustal thickening event.

In the Lahul and Spiti region, 50 to 90 km farther to the SE, several researchers have found evidence for an early Himalayan NE-directed tectonics (Steck et al., 1993; Vannay 1993; Vannay and Steck, 1995; Epard et al., 1995; Steck et al., 1998, 1999; Wyss et al., 1999, Wyss, 2000). Along the Spiti and Chandra valleys, structural interferences patterns demonstrate that these structures predate the predominant SW-directed thrusting observed along the Himalayan range (Steck et al., 1993, 1998; Wyss et al., 1999). On basis of structural and metamorphic observations, these authors interpreted the NE-directed structures found in these regions as testifying to an early NE-directed crustal thickening event associated with the emplacement of the Shikar Beh nappe. With respect to their relative age, to their stretching direction and to their sense of shear, the NE-directed structures observed in the Miyar Valley can be correlated to the structures exposed in the Lahul and Spiti regions and can be consequently associated with the NE-thrusting of the Shikar Beh nappe. A such a NE-directed tectonic movement could be the consequence of a reactivation, during the early stage of collision, of SW-dipping normal faults pre-existing in the north Indian margin and related to the Late Palaeozoic Neo-Tethys rifting (Steck et al., 1993).

### **5. 3. 3. Phase D2: The SW-directed Nyimaling-Tsarap structures**

Structures associated with this event are only preserved in the northern limb of the Gianbul dome; they do not affect the geology of the Miyar Valley section. This phase is responsible of the main phase of deformation in the sedimentary sequences of the Tethyan Himalaya in the northern part of the range. A more precise structural analysis of the D2 associated structures will be presented in the chapter on the structural geology of the Gianbul Valley section.

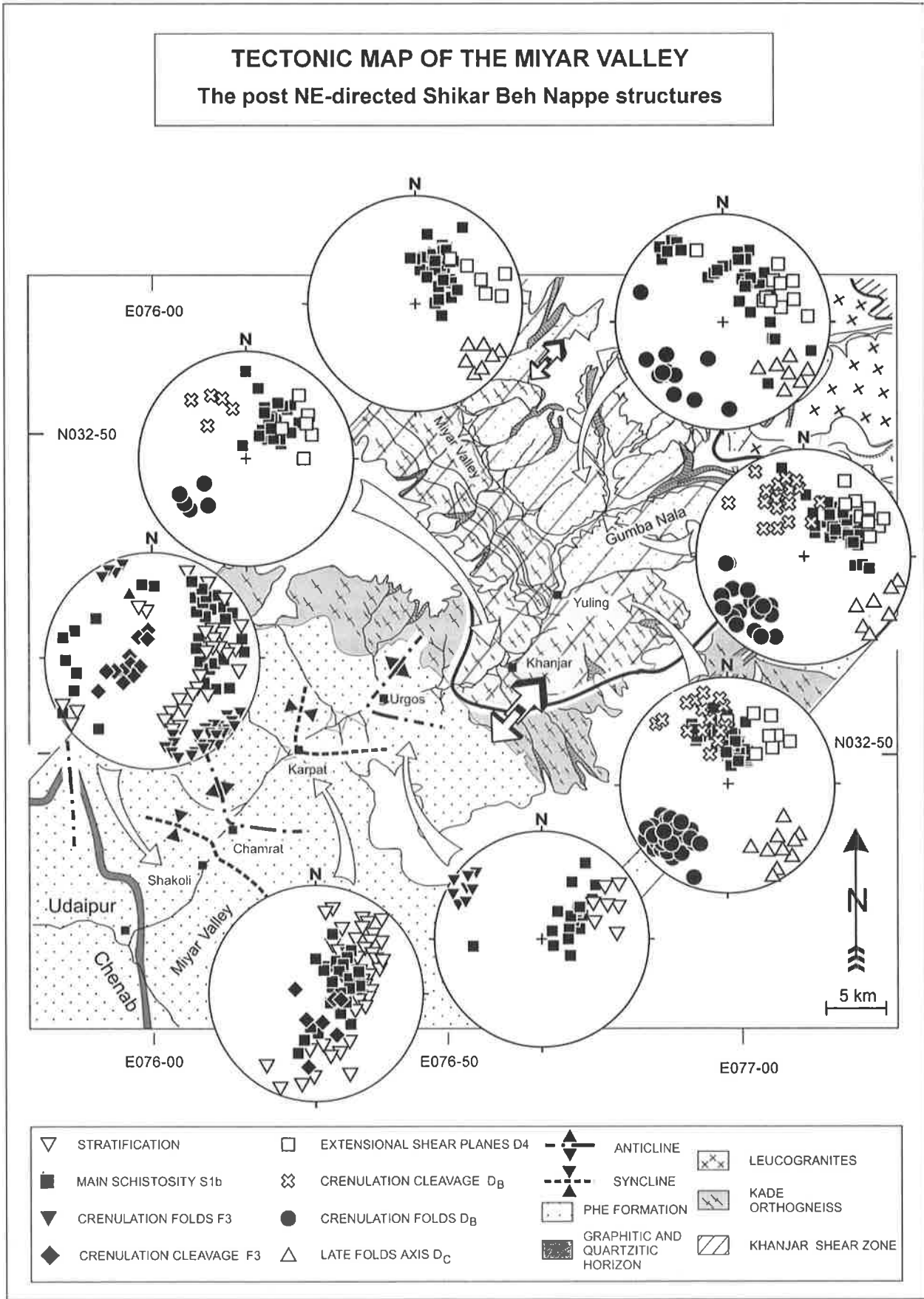


Fig. 5.16: Tectonic map of the Miyar Valley, modified after Steck et al. (1999), showing the orientation of the main post-D1 structural elements (equal-area stereographic plots, lower hemisphere).

### 5.3.4. Phase D3: The SW-directed High Himalayan Nappe structures

#### 5.3.4.1. Crenulation cleavage S3 and F3 chevron folds

The D3 fabrics are well developed in the downstream part of the section, between Udaipur and Karpāt. In this area, a strong S3 crenulation cleavage slightly dipping to the NE, and associated to open F3 folds, overprints the main S1b schistosity (Fig. 5.16). The deformation relative to this event is documented by characteristic F3 kink and chevron fold structures which deform the axial surface of the main F1b folds (Fig 5.2 and Fig. 5.17). The F3 fold axes are oriented toward the NW-SE and dip weakly towards the NW. These folds are generally of low amplitude, ranging from centimetre to meter size. The F3 folds are restricted to the downstream part of the valley, in the low-grade metasediments. In some outcrops, a N-S stretching oriented lineation L3 is observable

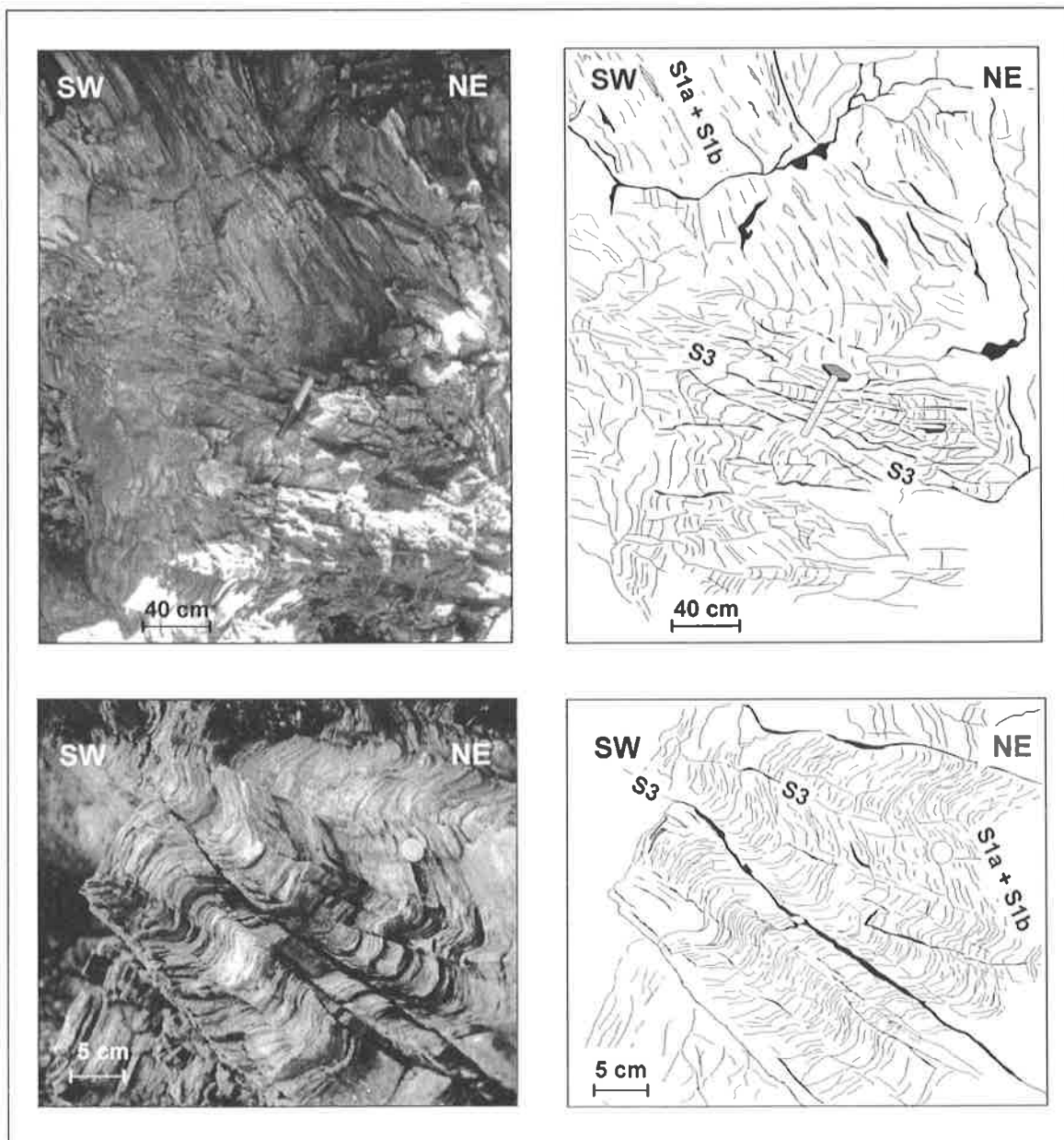


Fig. 5.17: Discrete S3 crenulation cleavage gently dipping to the NE and associated F3 kink folds of overprinting the main S1a + S1b schistosity. Miyar gorge between Udaipur and Shakoli

on the limbs of the folds. This lineation is likely formed by slip along the folded layers. In this part of the valley, the regular alternation of competent and incompetent layers with high ductility contrast provides the favourable conditions to form chevron and kink folds.

As we saw before, in this part of the section the D1b phase produces F1b flattened parallel folds. The difference in the geometry between the F1b and the F3 folds is probably due to the variation in the metamorphic conditions between the D1b and D3 tectonic phases. The phase D1b occurs in a burial context. The slightly higher metamorphic conditions prevailing during the formation of the F1b folds than during the D3 phase, probably reduces the contrast of viscosity between the various layers and does not allow the creation of chevron folds during the D1b phase.

### **5. 3.4. 2. Discussion**

At the regional scale, the D3 folding is responsible for the overturning toward the SW of the initially F1b NE-verging folds (Fig.5.2). South-eastward, outside of the studied area, the intensity of this phase of deformation increases and the S3 crenulation cleavage evolves to a more penetrative foliation associated with intense SW-directed folds such as the Kalath fold in the Kulu Valley (Thöni et al., 1977). In the Kulu Valley, the phase is associated with the SW-directed significant tectonic movements related to the High Himalayan nappe emplacement (or Crystalline nappe, Frank et al., 1973, 1977; Thöni 1977; Epard et al., 1995).

The extrusion of the High Himalayan nappe along the Main Central Thrust is also controlled by broadly contemporaneous extensional movements along the Zaskar Shear Zone farther to the north. We will describe later, in the Gianbul Valley section, this spectacular 150 km long extensional shear zone which separates the low-grade sediments of the Tethyan Himalaya from the high-grade metamorphic rocks of the High Himalayan Crystalline Zone.

### **5. 3. 5. Phase D4: The doming phase and the Khanjar Shear Zone**

#### **5. 3. 5. 1. The Khanjar Shear Zone and associated structures**

In the upstream part of the Miyar Valley, from the village of Chaling to the Gumba glacier, the initial top-to-the-NE thrusting movements associated with the Miyar Thrust Zone are partly overprinted by late top-to-the-SW extensional structures (Fig. 5.16). These structures occur rather sporadically as SW-extensional shear bands, dipping at about 50 degrees to the SW, which concentrate the strain in narrow bands of about up to several millimetres thick by up to several meters long. This late fabric clearly cross-cut the S1a and S1b schistosity associated with the Miyar Thrust Zone (Fig. 5.18). The main S1b schistosity is deflected in the vicinity of the shear bands. As a general rule, particularly in the sillimanite-migmatitic zone, the main S1b foliation can be followed through the shear bands and no discontinuities can be observed. This last observation means that these structures are associated with a ductile shear zone and have been formed under medium to high metamorphic conditions.

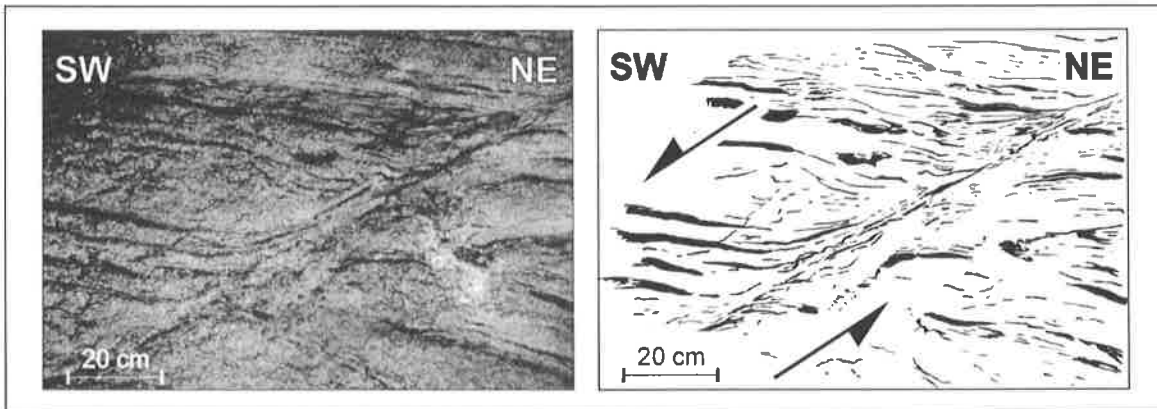


**Fig. 5.18:** Asymmetrical extensional shear bands overprinting the main foliation in the paragneiss from the migmatitic zone (Gumba Nala area). Section parallel to the stretching lineation and normal to the main foliation showing a top-to-the SW movement associated with the Khanjar Shear Zone.

In order to establish the sense of displacement along the shear bands, we have considered the deflection of the main S1b schistosity as it enters the shear bands. The apparent deflection of the main foliation draws a sigmoidal pattern through the shear zone which defines the sense of shear as documented on the Fig. 5.18. The curvature of the main schistosity at the boundary of the shear band clearly indicates a top-to-the-SW sense of displacement along the shear bands.

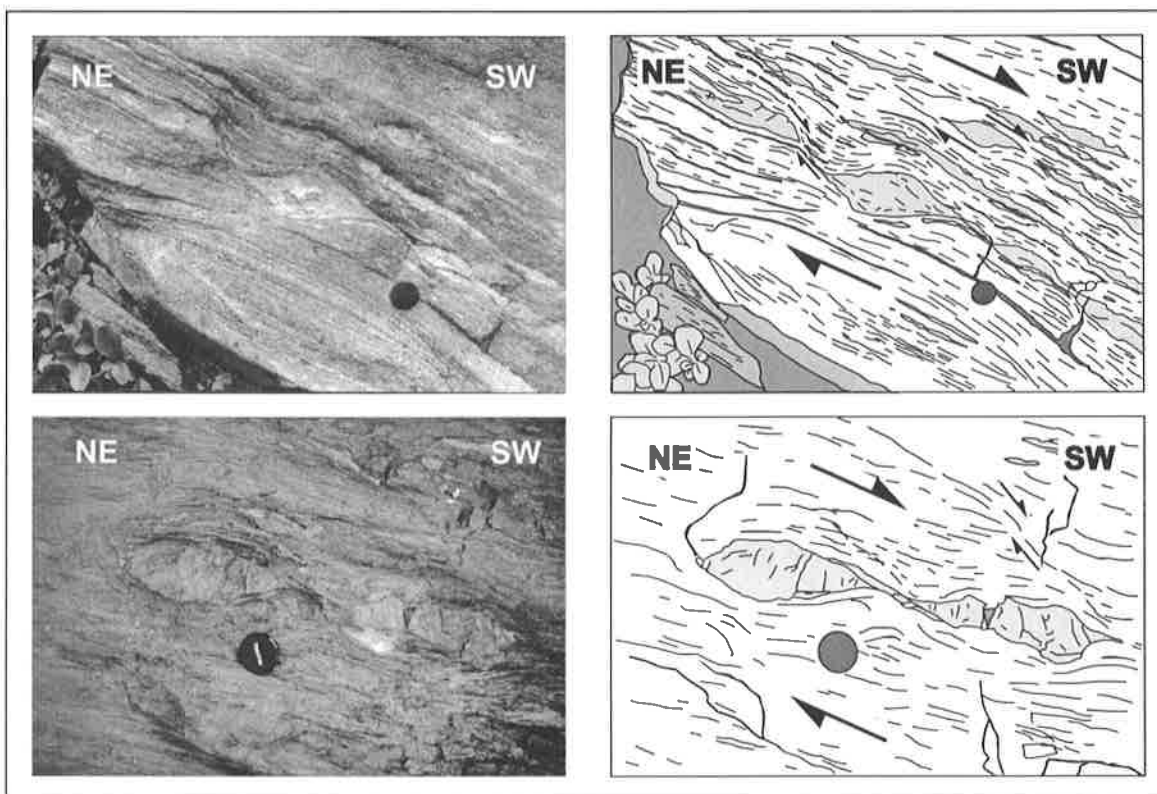


**Fig. 5.19:** (top) Asymmetrical boudinage of quartzo-felspathic layers in the migmatitic zone indicating a top-to-the SW ductile extensional movements associated with the SW-directed D4 phase (Gumba Nala area). Note the presence of discrete extensional shear bands between the boudins showing a top-to-the SW shear sense. (bottom) Elongated and boudinaged quartz ribbons in the kyanite-staurolite-bearing metasediments near Yuling testifying of a top-to the SW displacement associated with the Khanjar Shear Zone. Sections parallel to the stretching lineation and normal to the main foliation.

Boudined veins of quartz also give good indications about the shear sense along the extensional shear bands (Fig. 5.19). Such asymmetrical boudinaged veins are frequent in the upstream part of the Miyar Valley and they clearly highlight the D4 top-to-the-SW shearing.

Inter-boudin shear bands as well as the shear bands recutting the main schistosity are dipping towards the SW with an angle of approximately 50 degrees. Generally, the set of asymmetrical extensional shear bands are commonly oblique to the slip plane with a dominant angle at 15-25 degrees to the shear zone boundary (Platt and Vissers 1980; Platt 1984; Hanmer and Passchier 1991). It consequently means that the D4 bulk flow plane at the regional scale is dipping towards the SW with an angle of about 25-30 degrees. Such a dip corresponds to those developed by the main S1b schistosity. This observation suggests that the NE-directed shear zone associated with the D1 Shikar Beh nappe was reactivated as a late SW-directed extensional shear zone during the D4 phase. This interpretation is also confirmed by the presence, along the pervasive D1 mylonitic foliation, of some asymmetrical augen structures showing a top-to-the-SW movement of shearing (Fig.5.19; 5.20). Such a reactivation of a shear zone was also described by Patel et al. (1993) for the Zanskar Shear Zone, to the north of the Miyar Valley section.

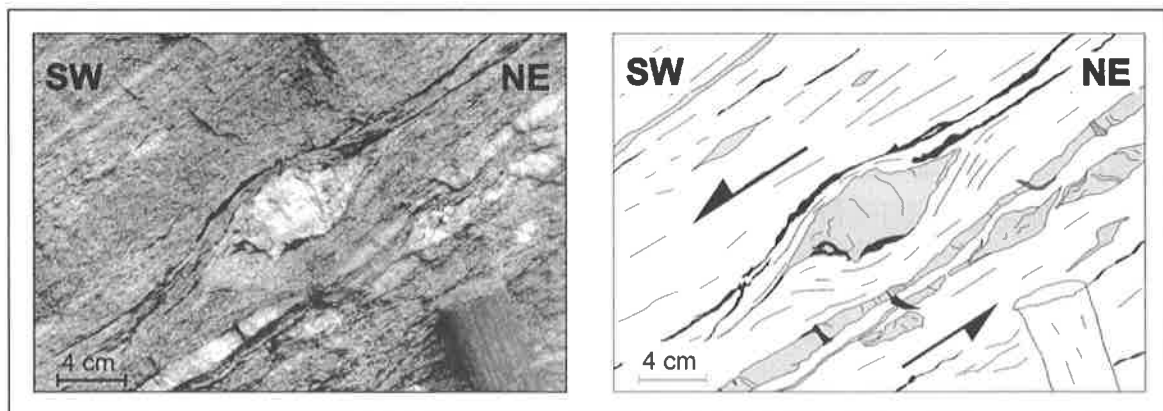


**Fig. 5.20:** Top-to-the SW  $\sigma$ -type porphyroclasts of quartz showing a top-to-the NE shear sense in a finer-grained recrystallised matrix (Gumba Nala area). The section is parallel to the stretching lineation and normal to the tectonic foliation.

At the regional scale, this SW-dipping extensional structure overprints the main foliation over a width of approximately 15 km. This structure is located at nearly the same geographical position as the Miyar Thrust Zone, on the southern limb of the Gianbul dome. The boundaries of the shear zone are not sharply defined but the strain intensity is reduced gradually from Chaling toward the south.

The name of Khanjar Shear zone was proposed by Steck et al. (1999) for this SW-dipping extensional shear zone situated on the southern limb of the Gianbul dome. For these authors, the Khanjar Shear Zone is closely associated with the Gianbul dome formation described by Dèzes (1999).



### 5. 3. 5. 2. Discussion

In the Miyar Valley, the structures of the main D1 deformation clearly shows top-to-the-NE movement. These movements are well documented by the Miyar Thrust Zone and its associated structures. However, a detailed analysis of the various structures through the Miyar Thrust Zone reveals the presence of younger SW-dipping structures indicating a direction of shearing towards the SW. As a consequence, the wide shear zone along the southern limb of the Gianbul dome, cropping out in the Miyar Valley, can be interpreted as a polyphase ductile shear zone with a initial top-to-the-NE sense of thrusting (MTZ) followed by the later superposition of top-to-the-SW extension (KSZ). The reversal in the shear sense along the Miyar Thrust Zone has a major effect in the metamorphic evolution of the Miyar Valley. As described by Pognante et al. (1990), lower grade rocks (chlorite to garnet zone) are superposed onto higher grade rocks (kyanite zone and higher) along the Miyar Thrust Zone and no metamorphic gap, as we will see later, occurs between the footwall and the hanging-wall as it is generally the case along a thrust contact. This discrepancy is likely the consequence of the reactivation of the Miyar Thrust Zone.

Farther to the west, in the Kilar area (Fig. 5.1), along the Chenab river, such top-to-the-S extensional shear structures were also described by Stephenson et al. (2001). This Kilar Shear Zone is described by these authors as a broad zone of deformation which separates the amphibolite facies metamorphic rocks from the low-grade and unmetamorphosed sediments of the Chamba syncline. This Kilar Shear Zone may correspond to the lateral equivalent of the Khanjar Shear Zone. In a lateral continuity, between the Kilar Shear Zone and the Khanjar Shear Zone, Frank et al. (1995) described in the Saichu Valley (Fig. 5.1) some shear sense criteria which document a displacement of the hanging wall towards the south. This zone of distributed deformation also likely corresponds to the Khanjar Shear Zone.

A comparable reactivation of a shear zone has been proposed for the South Tibetan Detachment System where structural arguments demonstrate that this NE-directed extensional shear zone is superposed on earlier SW-verging compressional structures (Patel et al. 1993; Vannay and Hodges, 1996). Extension along the STDS are interpreted as associated with the extrusion of the High Himalayan Crystalline toward the SW. In contrast, the SW-directed extension along the Khanjar Shear Zone suggests a sub-vertical exhumation of the metamorphic rocks in the northern part of the Miyar Valley as a domal structure referred to as the Gianbul dome (Dèzes 1999).

### **5. 3. 6. Additional late phases**

Three other less important, but nevertheless well documented, phases were also observed in the Miyar Valley area. As the chronological relation between these latter phases and the other major phases is not well constrained, D<sub>A</sub>, D<sub>B</sub> and D<sub>C</sub> are assigned to these phases.

### 5. 3. 6. 1. Phase $D_A$ : Dextral Strike-Slip Shearing

Moving up the Miyar Valley, the orientation of the stretching lineations varies from the south towards the north. Whereas in the north-eastern part of the section the stretching lineations related to the D1 deformation show a NE-SW orientation, in the downstream part of the section, between Udaipur and Urgos, the stretching lineation progressively turns into an unusual E-W orientation (Fig. 5.4). The change between the two orientations of the stretching lineations is not documented by intense strike-slip shear strains or by a distinct contact. On the contrary, the transition occurring around the village of Urgos occurs in a rather progressive way by reorientation of the NE-SW stretching lineations towards an E-W direction. The geometrical analysis of the new E-W orientation of the stretching lineations located between Udaipur and Urgos compared to the NE-SW orientations documented in the upstream part of the valley suggests a clockwise rotation of the structures in the downstream part of the section.

Further to the west, in the Tandi-Khoksar area along the Chenab river, such E-W stretching lineations were also documented by Vannay (1993) and Vannay and Steck (1995). These studies revealed that the localisation of these E-W lineations corresponded to an approximately 20 km wide corridor, bordering the Chenab valley (Fig. 5.21).

This zone of unusual E-W orientation is described by these authors as a NW-SW-oriented broad zone of dextral shearing that they named the Chandra Dextral Shear Zone. They interpret this corridor as the consequence of a progressive reorientation of syn-metamorphic lineations, initially NE-SW-oriented. This interpretation is consistent with the observations from the Miyar Valley section. Consequently, the dextral shear zone observed in the downstream part of the Miyar Valley may correspond to the lateral equivalent of their Chandra Dextral Shear Zone.

In the Lahul area, the classical NE-SW oriented syn-metamorphic stretching lineation is interpreted as mainly associated with the SW-directed overthrusting of the High Himalayan nappe along the Main Central Thrust (Frank et al., 1973;1977; Thöni 1977; Epard et al., 1995; Wyss et al., 1999). As this dextral shear zone causes the passive reorientation of the syn-metamorphic lineation relative to the SW-directed D3 phase, the  $D_A$  dextral strike-slip shear zone has to be consequently younger than the D3 phase and could correspond to a Miocene phase. Similar dextral shear zones have also been revealed throughout the range (Pêcher et al., 1991). Pêcher (1991) associates these dextral movements with a Miocene clockwise motion of Tibet relative to the Greater Himalaya and proposes that these strike-slip shear zones represent a Miocene ductile equivalent of the Quaternary dextral strike-slip faults observed in the southern part of Tibet, such as the Karakorum Fault.

### 5. 3. 6. 2. Phase $D_B$ :Late NW-directed folding

The  $D_B$  phase corresponds to a NW-verging post-metamorphic folding event which is restricted in the upstream part of the Miyar Valley. The structures relative to this phase are frequent in the Yuling-Gumba area and the associated deformation is documented by metric amplitude, asymmetric open flattened NW-verging  $F_B$  folds (Fig. 5.22). In the weak competent levels like the

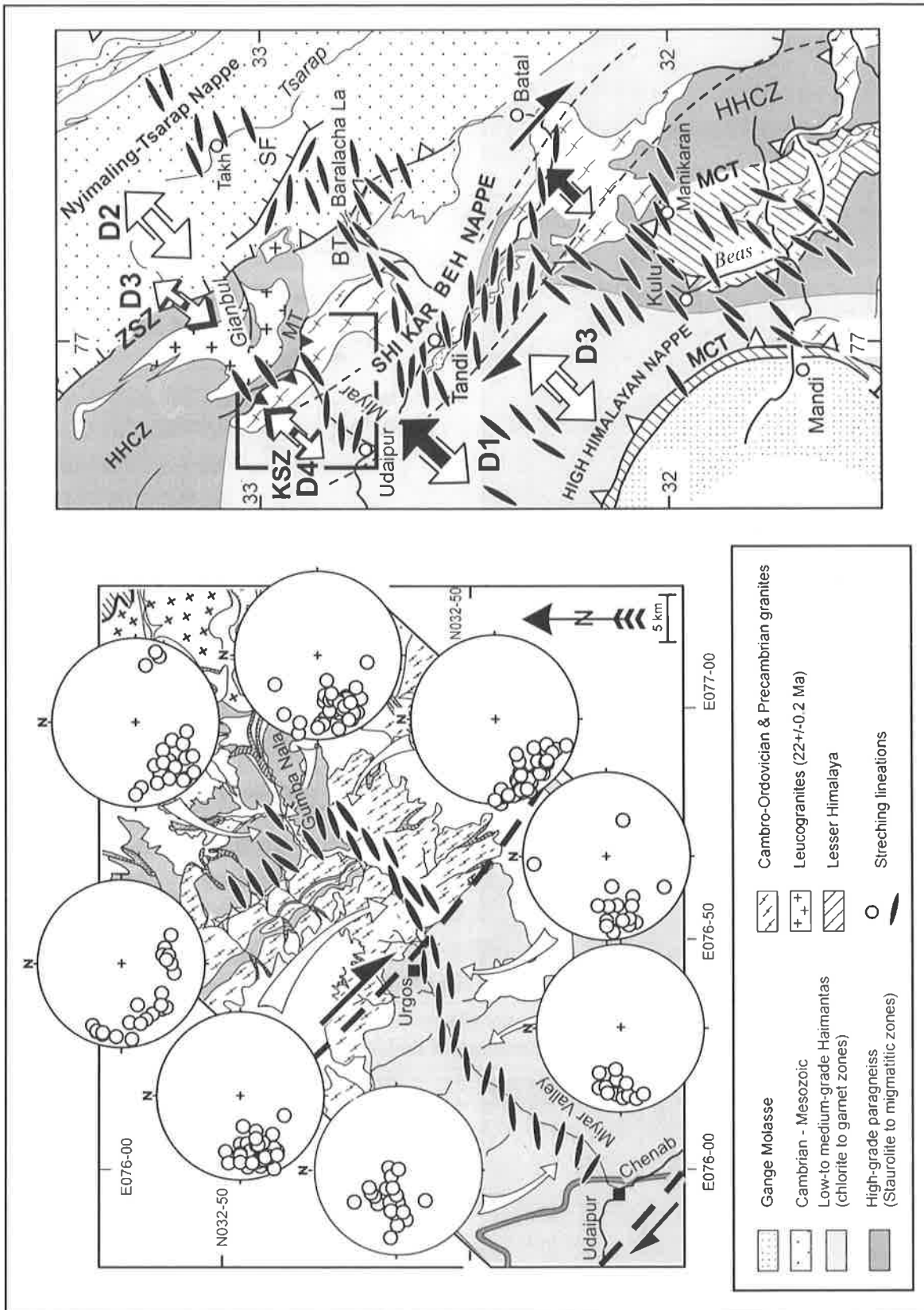


**Fig. 5.21:** Structural map showing the main large-scale shearing structure observed in the NW Himalaya (from Vannay and Steck 1995). Black ellipses represent the syn-metamorphic stretching lineations. HHCZ = High Himalayan Crystalline Zone, MT = Miyar Thrust, BT = Baralacha La Thrust, MCT = Main Central Thrust, SF = Sarchu Fault, ZSZ = Zanskar Shear Zone, KSZ = Khanjar Shear Zone.

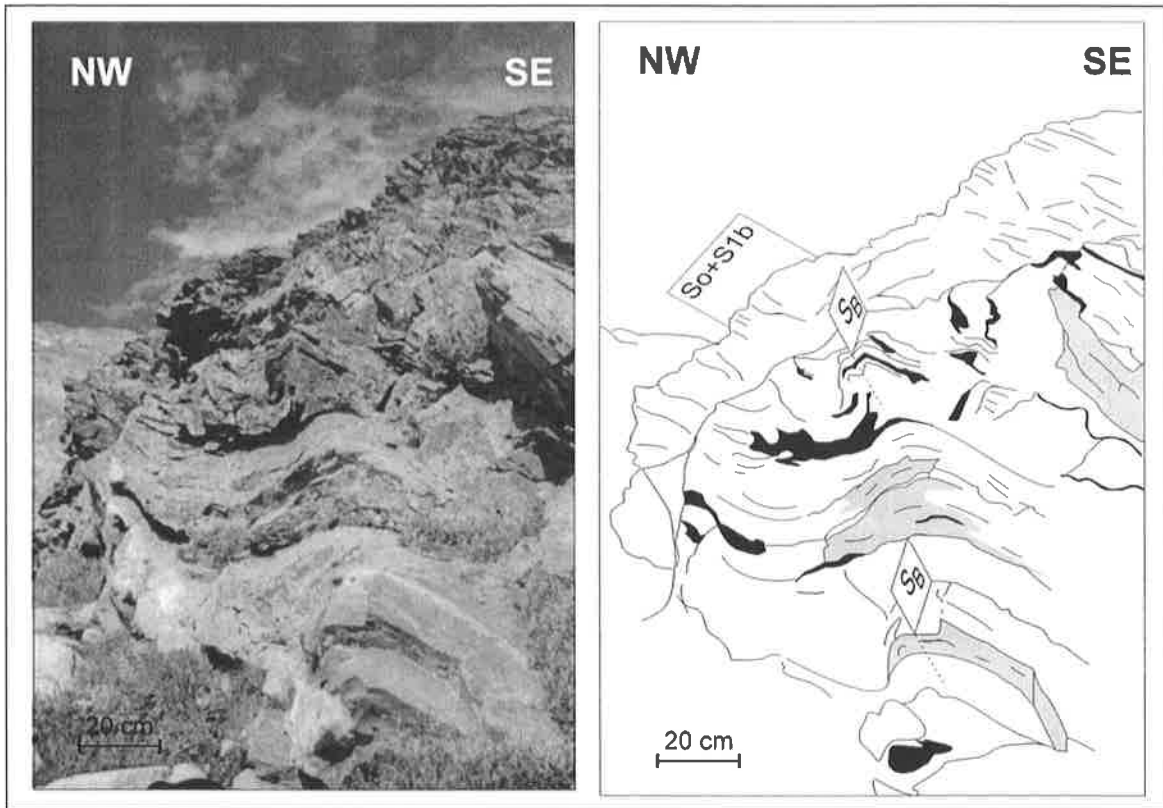


**Fig. 5.22:** NW-directed DB folds from the staurolite-kyanite zone in the Yuling-Gumba area.

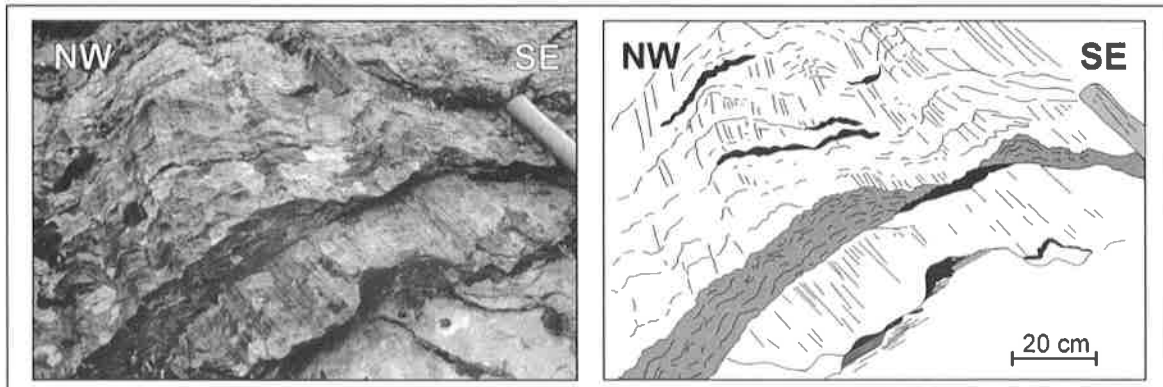


**Fig. 5.23:** LB crenulation lineations in the metapelites from the staurolite-kyanite zone in the Yuling-Gumba area. The lineation is marked by the appearance of the hinges of the FB folds on the main foliation.

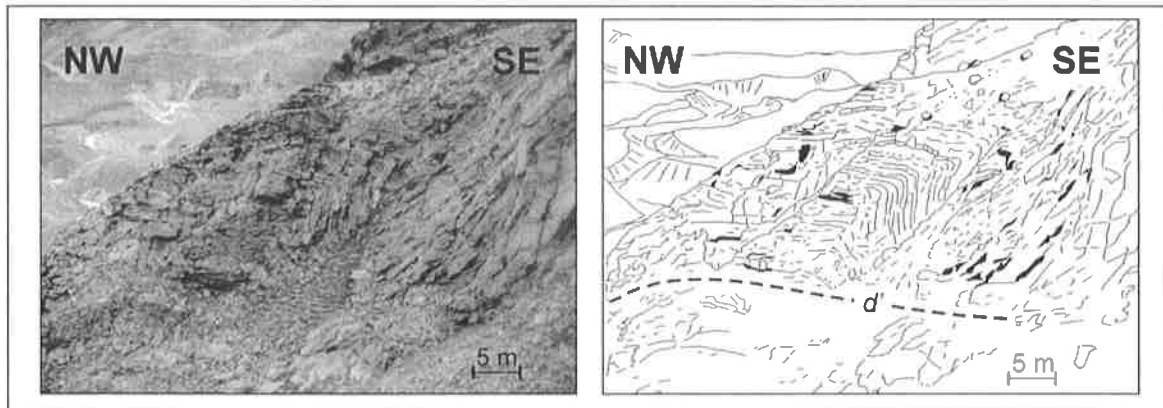


**Fig. 5.24:** DB Chevron fold in metapelites from the sillimanite zone (Gumba Nala). Note that the chevron folds damp and are gradually transposed parallel into the décollement structure  $d'$ .

and gradually transposed parallel into a décollement structure (Fig. 5.24). As these folds refold clearly the syn-metamorphic S1b schistosity as well as the associated migmatitic gneiss, and that moreover this phase does not produce new metamorphic assemblages, it seems that this event corresponds to a late post-metamorphic stage.

Late N-verging structures were revealed at several places in the northern part of Upper-Lahul (Vannay, 1993; Vannay and Steck, 1995). These structures are interpreted as back-folds resulting from the tectonic doming which deforms the units of the central and northern parts of Upper-Lahul. However, such NE-directed back-folds are only restricted on the northern limb of this dome. In the Miyar Valley section, the late NW-directed folds are oddly located on the southern limb of the Gianbul dome. Consequently, these  $D_B$  structures do not seem directly related to the exhumation of the Gianbul dome. The SW-NE trending axial surface of the  $F_D$  folds most likely indicates a NW-SE directed shortening. This shortening could be the result of late tectonic readjustments following the exhumation of the numerous domal structures which occur in the Kishtwar-Zaskar area.

### **5. 3. 6. 3. Phase $D_C$ :Late vertical movements**

The  $D_C$  phase does not produce spectacular structures, but slightly undulates the main S1b schistosity. In some outcrops, this  $D_C$  phase associated with the  $D_B$  phase induces interference pattern of dome and basin type with a very low amplitude. The wide wavelength of these structures complicates the measurements of these structures. These foldings are characterized by a sub-vertical axial surface and by NW-SE-oriented sub-horizontal fold axis (Fig. 5.16).

The dome and basin interference pattern between  $D_B$  and  $D_C$  phases does not allow to define the relative chronology of these two events. However the sub-vertical axial surface of the  $F_C$  folds seem to indicate that this event is related to late vertical movements.

### **5. 3. 7. Pre-Himalayan and Tertiary pegmatitic and leucogranitic dykes**

As mentioned previously, two types of intrusive granites are observed in the Miyar Valley section (Fig. 5.1; 5.2 and 5.3). In the central part of the valley, a thick sheet of granitic gneiss crops out between Urgos and Yuling. This Kade orthogneiss is a porphyric two micas granitic gneiss, characterized by a S-type geochemistry, and derived from a Cambro-Ordovician protolith ( $496 \pm 16$  Ma, Rb/Sr whole rock, Frank et al., 1977). In the northern part of the Miyar Valley, the migmatitic paragneiss are cross-cut by numerous leucogranitic dykes and small plutons. This intrusive complex is in cartographic continuity with similar granites cropping out in the footwall of the Zaskar Shear Zone in the Gianbul Valley to the NE, as well as with the Early Miocene Gumburanjun leucogranite ( $22.2 \pm 0.2$  Ma, U-Pb monazite) to the E (Ferrara et al., 1991; Dèzes et al., 1999).

### 5.3.7.1. Pre-Himalayan pegmatitic dykes

Several pegmatitic dykes crop out on both sides of the Kade granite. From the Yuling area to the upstream part of the Gumba Nala, in the kyanite-sillimanite-bearing metasediments, these dykes are abundant and form centimetres to several meters wide lenticular bodies slightly dipping towards the SW (Fig. 5.3). These pegmatitic bodies are cut at a low angle by the main S1b schistosity. Therefore, this structural relation implies that the intrusion of these dykes is older than the formation of the main schistosity. The pegmatites located at the edges of the Kade granite are likely related to the intrusion of this granite in the sedimentary series of the Phe Formation, about 500 Ma ago.

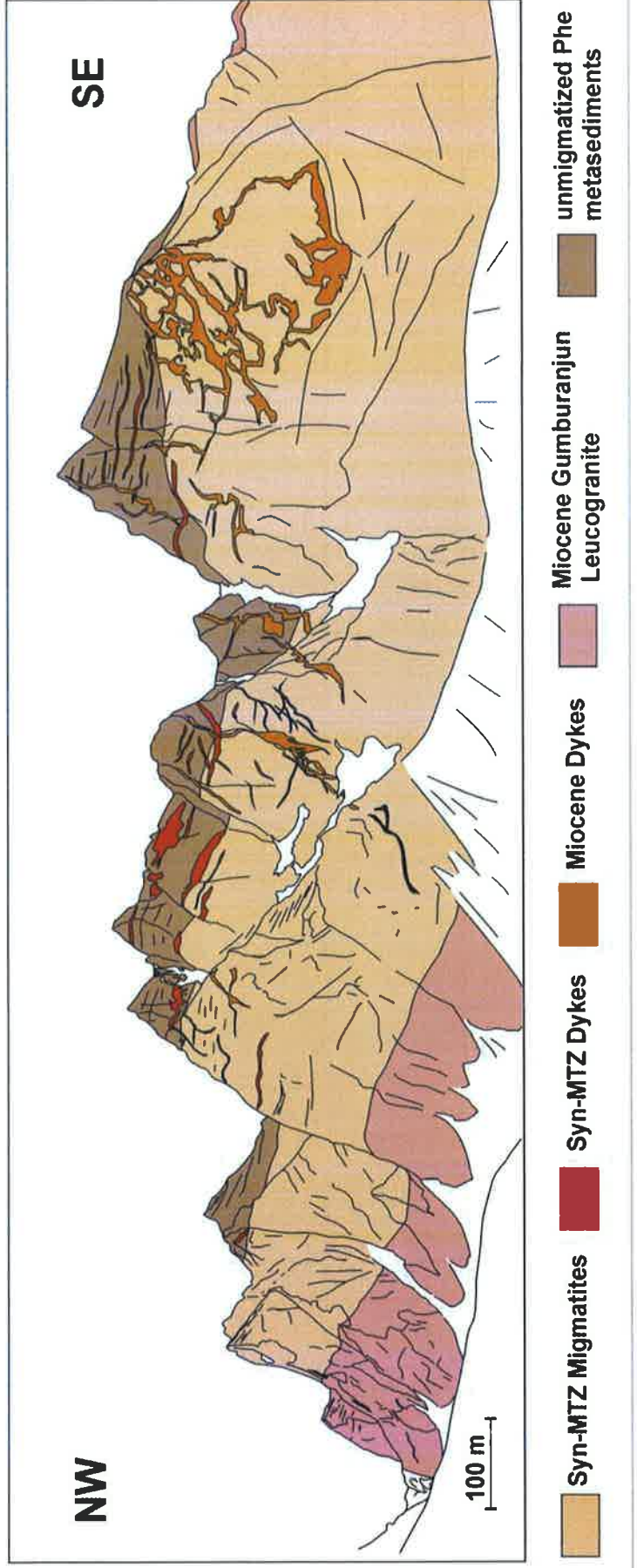
### 5.3.7.2. Tertiary leucogranitic dykes and sills

The tertiary Gumburanjun Leucogranite (Dèzes, 1999) forms a large pluton composed of several intrusions located at the top of the High Himalayan Crystalline Zone and bounded to the north by the extensional Zaskar Shear Zone. One of these intrusions with many peripheral dykes is very well exposed in the most northern part of the Gumba Nala, near the crest between the Miyar Valley and the Gianbul Valley. In this area, the leucogranites and their associated dykes together with the migmatitic set are exposed in the south face of the crest as an intrusion complex as shown in Fig. 5.25. The undeformed leucogranites which form the basal part of the complex are topped by sillimanite bearing migmatites which constitute the greatest part of the cliff. The mean orientation of the dominant foliation in the migmatite dips about 50° to the S-SW, consistently with the main foliation at the regional scale. Above the migmatitic zone, unmigmatized sillimanite bearing metasediments form the top of the cliff. Within these metasediments, pegmatitic and leucogranitic veins are transposed parallel to the main foliation. In contrast, several vertical dykes crosscut all the cliff. These dykes are undeformed and seem to be fed by the leucogranitic body.

In the Gianbul Valley, the natural cross-section through this intrusion complex provides information about the deepest part of the complex. In this valley, a migmatitic zone forms the basal part of the complex (Fig. 5.2 and 5.27). This migmatite zone appears to be the source of vertical dykes which feed the leucogranitic body. In contrast with what is observed in the Miyar Valley, the leucogranitic pluton is directly topped by unmigmatized kyanite-bearing metasediments (Dèzes, 1999). Through the observations from the both valleys, the intrusion complex can be represented as the following schematic lithological succession (Fig. 5.26).

The deepest structural part is composed by a Miocene migmatite zone which probably corresponds to the production zone of the leucogranitic melts responsible for the feeding of the leucogranitic body (Dèzes 1999). As explained by Dèzes (1999), this lower migmatitic zone seems to be the consequence of a Miocene isothermal decompression associated with the SW-directed extensional movements along the Zaskar Shear Zone.

**Fig. 5.25:** View of the southwest face of the crest which separates the Miyar Valley from the Gianbul Valley. Approximately 1500 m of relief exists between the Gumba glacier and the summit of the cliff. The leucogranite forms the white basal part on the left side of the cliff. Massive ochre sillimanite-bearing migmatites immediately above the leucogranites are overlain by brownish unmigmatized sill-bearing metasediments with leucogranitic sills and dykes. Note the vertical undeformed dykes cutting through the migmatitic part.



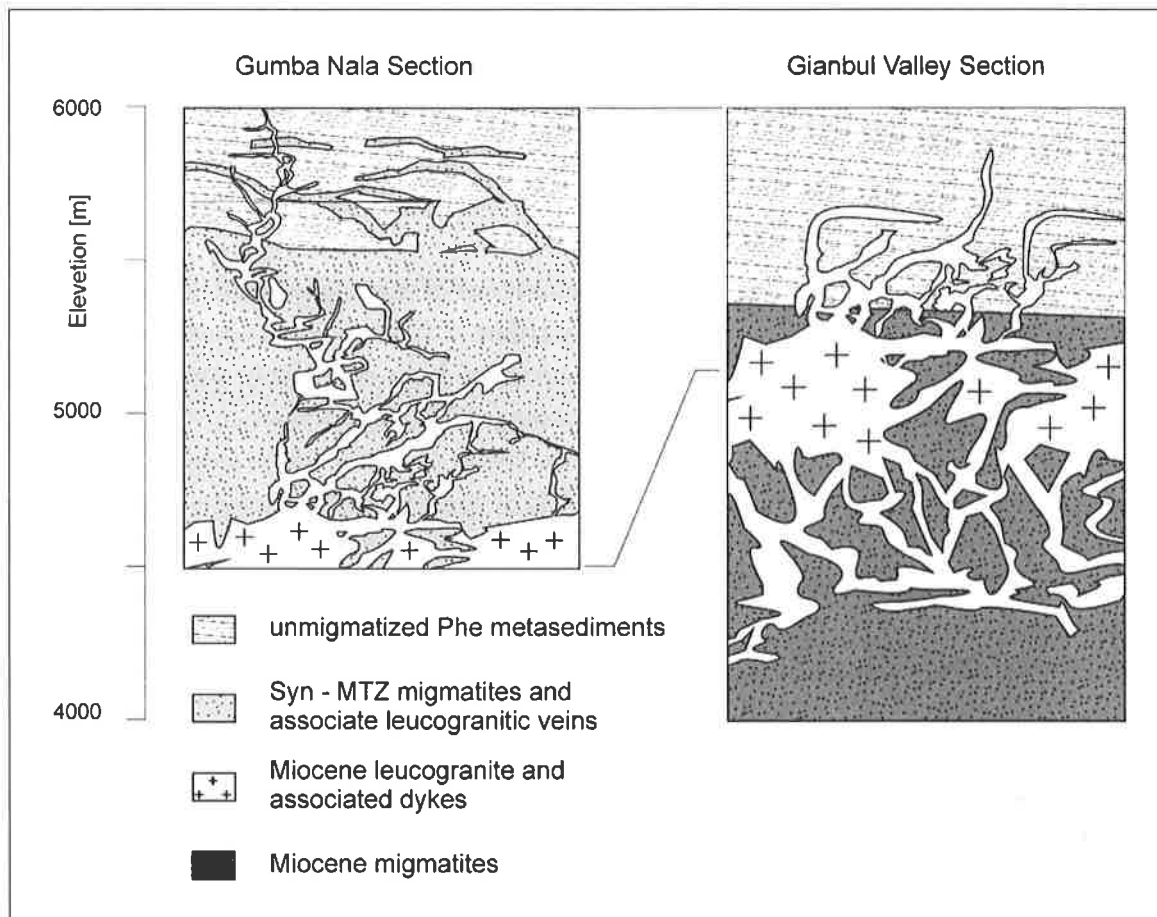


**Fig. 5.26:** Schematic profiles of the intrusion complex in the Gumba Nala area and in the Gianbul Valley area. Note the reduction of thickness of the migmatites overlying the leucogranite in the Gianbul Valley with respect to the Gumba Nala area.

In the Gumba glacier area, the Miocene leucogranites are overlaid by a second migmatitic zone which probably corresponds to the syn-Miyar Thrust Zone prograde migmatitic zone cropping out in the downstream part of the Gumba Nala. This second migmatitic zone which preserved some NE-directed D1 structures is intruded by Miocene undeformed dykes probably coming from the subjacent leucogranitic body. This zone is also likely the probable source for a part of the pegmatites and leucogranites which intrude the unmigmatized sillimanite-bearing overlying metasediments. Another part of these dykes are probably related to the pre-himalayan pegmatitic dykes associated with the Kade granite.

Consequently, two generations of migmatites and leucogranitic dykes can be distinguish in the Gumba Nala area.

The first generation of migmatites which forms the greatest part of the cliffs bordering the Gumba Nala is related to the prograde barrovian-type metamorphism associated with the NE-directed Shikar Beh Nappe emplacement. This interpretation is in agreement with the geological observations from the Gianbul Valley, where the absence of thick portions of migmatites covering the leucogranites coincides with the lack of structures related to the Shikar Beh Nappe (Fig. 5.2).



The second generation corresponds to the migmatites forming the deepest part of the intrusion complex. These basal migmatitic zone is the probable production zone of the leucogranitic melt and feed the leucogranitic body through vertical dykes. This second generation of migmatites likely results from a regional isothermal decompression consecutive to the Miocene extensional movements along the Zaskar shear Zone. We will see later in the metamorphic chapter that this decompression path is also well documented by typical retrograde metamorphic assemblages occurring in the kyanite-staurolite zone.

Pognante et al. (1987) already suggested two generations of migmatites in the High Himalayan Crystalline of Zaskar. In the High Himalayan Crystalline of Zaskar, these authors reported that migmatization and associated leucocratic granitoids have been pervasively recrystallized into leucocratic orthogneiss during the SW-directed thrusting of the High Himalayan nappe along the Main Central Thrust. On basis of these observations, Pognante et al. (1987) recognised two main metamorphic events in the High Himalayan Crystalline of Zaskar, and suggested a major time-gap between events 1 and 2. Because of this time-gap, these authors interpreted the first generation of migmatites as the result of a pre-Himalayan event. Although pre-Himalayan acid magmatism could be associated with a pre-Himalayan tectonic activity (Girard and Bussy, 1999; Wyss, 1999), no clear evidence for a pre-Himalayan metamorphism and deformation is recorded in the High Himalayan Crystalline.

### **5. 3. 8. Conclusions of the structural investigations in the Miyar Valley section**

The main tectonic structure in the Miyar Valley corresponds to a wide SW-dipping shear zone which recorded two divergent phases. Early NE-directed compressional movements resulted in the development of mylonitic fabric synchronous with the prograde Barrovian-type metamorphic zonation increasing from chlorite zone to the SW, to the sillimanite-migmatitic zone to the NE. Late stage structures in the shear zone include SW-directed extension superimposed the NE-directed movements.

This Miyar Thrust Zone is the main structure which documents the NE-directed movements. It is associated with the crustal shortening phase. It consists of 20 km wide SW-dipping shear zone in which shear sense criteria and structural fabrics clearly demonstrate top-to-the-NE movements. The shear strain within the thrust zone is progressively distributed through the shear zone with an increase of the strain northwards from the top to the bottom of the shear zone. The increase of the shear strain and the top-to-the-NE movements together with the metamorphic mineral zonation increasing from the South towards the North demonstrate that this structure is closely associated with the emplacement of a NE-directed nappe. By comparison with other similar NE-directed structures described in the Upper-Lahul area, we associate these movements with the Shikar Beh Nappe emplacement.

One of the most significant structural feature of this area is that the NE-directed shear zone is overprinted by widespread extensional structures we have defined as the extensional Khanjar Shear Zone. An important characteristic of these late extensional structures is that they only occur within the ductile Miyar Thrust Zone. Outside this zone, no extensional structures were observed. This

observation leads us to consider the Khanjar Shear Zone and the Miyar Shear Zone as a single structure which initially acted as a ductile thrust zone later reactivated as a ductile extensional shear zone.

## **5. 4. STRUCTURAL GEOLOGY OF THE GIANBUL VALLEY SECTION**

### **5. 4. 1. Introduction**

In order to have a more complete view and a better understanding of the tectonic evolution of the Lahul-Zaskar area, we have incorporated in our study the data from the Gianbul Valley area, in the northern limb of the Gianbul dome.

The main tectonic structure observed in the Gianbul Valley corresponds to the Zaskar Shear Zone, which marks the transition between the high-grade metamorphic rocks of the Gianbul dome and the low-grade sediments of the Tethyan Himalaya to the NE (Fig. 5.1 and 5.2).

In the Gianbul Valley, in the footwall of the Zaskar Shear Zone, the High Himalayan Crystalline Zone is formed by Upper Proterozoic to Cambrian detrital sediments (graywackes, siltstones and pelites). The structurally deepest zone of these area recorded a high grade metamorphism which transformed these sediments into amphibolite facies to migmatite paragneiss. Toward the top of the High Himalayan Crystalline Zone, the metasediments are intruded by a massive leucogranitic pluton referred to as the Tertiary Gumburanjun Leucogranite (Fig. 5.27). The leucogranitic body is overlaid by the Zaskar Shear Zone. Within the shear zone, the metamorphic field gradient is characterized by a very rapid decrease of the metamorphic grade from the amphibolite facies at the base of the Zaskar Shear Zone to lower greenschist facies at its top. The hanging-wall of the Zaskar Shear Zone is composed by the sedimentary formations of the Tethyan Himalaya.

On basis of the structural data obtained by Dèzes (1999), the following chapters aim to describe the main tectonic events recorded on the northern limb of the Gianbul dome.

### **5. 4. 2. Phase D2: The SW-directed Nyimaling-Tsarap structures**

In the sedimentary series of the Tethyan Himalaya, the development of SW-verging folds characterizes the first tectonic event. This event is responsible for the main compression phase affecting the sedimentary of the Tethyan Himalaya and corresponds to the development of the SW vergent Nyimaling-Tsarap nappe (Steck et al., 1993).

The internal structure of this nappe is characterized by a progressive change in the style of deformation. The northern part of the range, close to southern edge of the Indus Suture Zone (Fig. 5.1), corresponds to the root zone of this nappe. The deformation is here primarily accommodated by ductile shearing. Moving southwards to the frontal part of the nappe, the deformation becomes

more and more brittle and is documented by the development of ramp-and-flat and imbricate structures.

This phase is related to the underthrusting of the basal series of the Tethyan Himalaya, which will subsequently become the metamorphic rocks of the High Himalayan Crystalline Zone, beneath the frontal part of the Nyimaling-Tsarap Nappe. In the Gianbul Valley area, the D2 SW-directed structures are associated with this burial and the associated structures are essentially gathered along a ductile shear zone which concentrates the compression force at the base of the Nyimaling-Tsarap Nappe. Structures testifying a SW-directed motion along this ductile thrust zone are scarce and are preserved only as inclusion trails in synmetamorphic SW-rotated garnet porphyroblasts. The presence of these SW rotated syntectonic garnets inside the currently NW-directed Zaskar Shear Zone reveals that this major regional NE-directed extensional structure acted first as a ductile thrust zone during the D2 phase. Patel et al. (1993) already recognised such superposition of extensional shearing over an earlier thrust zone at the top of the High Himalayan Crystalline Zone along other segments of the Zaskar Shear Zone.

#### **5. 4. 3. Phase D3: The NE-directed extensional Zaskar Shear Zone**

In the Gianbul Valley section, the NE-directed D2 compressional structures are overprinted by a D3 tectonic phase documented by asymmetrical extensional shear bands which indicate top-to-the-NE extension. The shearing surface associated with this extensional structure defines a 1 km wide NE-dipping extensional shear zone which was described for the first time by Herren (1987) as the Zaskar Shear Zone and which is interpreted as a local equivalent of the South Tibetan Detachment System (STDS). In the Gianbul Valley, the Zaskar Shear Zone defines the main tectonic foliation which constantly dips 20° to the NE (Fig. 5.27). Throughout the shear zone, shear sense markers such as back-rotated boudins, micas fishes and  $\sigma$ -type porphyroblasts systematically indicate a top-to-the-NE shear sense.

Thermobarometric data indicate a difference in equilibration depths of  $12 \pm 3$  km between the hanging wall and the footwall of the shear zone (Dèzes et al., 1999). On basis of a simple geometrical model, these data together with the present-day dip of the shear zone (20°) indicate a minimum slip of  $35 \pm 9$  km along the structure (Dèzes et al., 1999). Geochronological results from Dèzes (1999) and Dèzes et al. (1999) indicate that the main ductile deformation along the Zaskar Shear Zone took place between  $22.2 \pm 0.2$  and  $19.8 \pm 0.1$  Ma.

Such results are in agreement with the data obtained in other segments along the South Tibetan Detachment System in central Nepal. Several studies (Hodges et al., 1992; Guillot et al., 1994; Harrison et al., 1995; Coleman, 1996; Hodges et al., 1996) showed that this structure of extension was active during the 24-21 time interval. These data thus indicate that the movements of extension along the South Tibetan Detachment System are contemporary along the range. Moreover, the same type of geochronological data on the Main Central Thrust also reveals that the movements along this ductile thrust zone began during Early Miocene ( $\approx 23$  Ma; Frank et al., 1977; Hubbard and Harrison, 1989; Harrison et al., 1995; Hodges et al., 1996). Consequently, these geochronological data indicates that the movements along both the Main Central Thrust and the

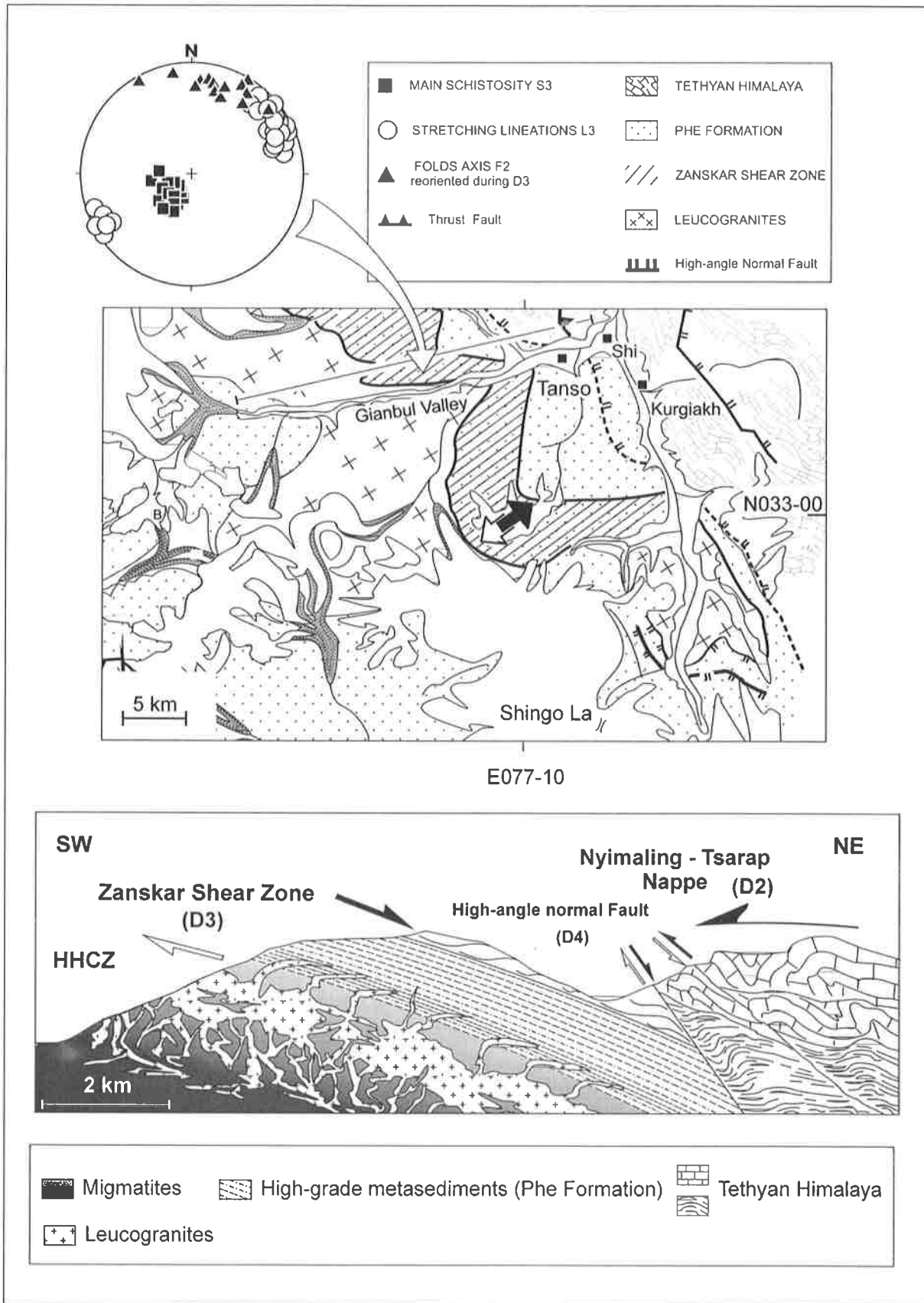


**Fig. 5.27:** (a) Tectonic map of the Gianbul Valley after Dèzes (1999), showing the orientation of the main structural elements. The structural orientation of the main structures is projected on the stereogram (equal area stereographic plots; lower hemisphere). (b) Geological cross-section for the Gianbul Valley transect after Dèzes (1999)

South Tibetan Detachment System were broadly contemporaneous. The contemporaneousness of the movements along both of these detachment likely reflects a tectonically-controlled extrusion of the High Himalayan Crystalline Zone.

#### **5. 4. 4. Phase D4: The doming phase and the High-angle normal faults**

The last tectonic phase affecting the geology of the Gianbul Valley area corresponds to the exhumation of the Gianbul dome (Fig. 5.27). The question about the chronological relationship between extension along the Zaskar Shear Zone and the exhumation of the Gianbul dome is still open. For Kündig (1989), the ductile extensional shearing along the Zaskar Shear Zone is the consequence of doming. In contrast, Dèzes (1999) observes a warping of the Zaskar Shear Zone and interprets this warping as the consequence of the doming. Our observations along the Miyar Valley do not allow to solve this problem. In the Gianbul Valley, the doming is associated with further extension documented by the occurrence of more brittle high-angle normal fault dipping towards the NE at an angle of about 60°. In the Tanso-Shi area, these D4 NE-dipping faults cross-cut the Zaskar Shear Zone and propagate through the overlying sedimentary series of the Tethyan Himalaya (Dèzes 1999). We interpret these high-angle normal faults as the brittle equivalent of the ductile extensional Khanjar Shear Zone in the Miyar Valley. It consequently appears that the doming phase and the associated extensional movements along the Khanjar Shear Zone likely occur shortly after the activation of the Zaskar Shear Zone.

#### **5. 4. 5. Conclusions of the structural investigations in the Gianbul Valley section**

The main tectonic structure observed in the Gianbul Valley corresponds to the Zaskar Shear Zone, which marks the transition between the high-grade metamorphic rocks of the Gianbul dome and the low-grade sediments of the Tethyan Himalaya to the NE (Fig. 5.1 and 5.2). The structural and petrographic constraints acquired by Dèzes (1999) indicate that the tectono-metamorphic history in the Gianbul section is the result of two main events: (1) an initial phase of crustal thickening related to the emplacement of the SW-directed Nyimaling–Tsarap nappe; and (2) the subsequent exhumation of the HHCZ as a consequence of NE-directed extension along the Zaskar Shear Zone and of later doming.

In contrast with what is observed in the Miyar Valley, the Gianbul Valley is not affected by the NE-directed D1 structures. It seems that the structures associated with this phase are restricted to the southern limb of the dome.

### **5. 5. CHRONOLOGY OF THE TECTONIC EVENTS**

From the Miyar Valley to the Kulu Valley, the NE-verging structures associated with the Shikar Beh nappe are overprinted by the SW-verging structures associated with the thrusting of the HHCZ toward the foreland along the Main Central Thrust (Steck et al., 1993; Vannay and Steck, 1995; Steck et al., 1999; Wyss et al., 1999). In the studied transect, the relative chronology of the Shikar

Beh nappe emplacement relative to the SW-directed Nyimaling-Tsarap nappe cannot be established because of a lack of structural interference between these tectonic phases. Such a structural interference is, however, observed in the Chandra Valley near Batal, about 90 km to the SE of the studied area and in the upper Spiti Valley, and it indicates that the structures of the frontal part of the Nyimaling-Tsarap nappe overprint those related to the Shikar Beh nappe (Steck et al., 1993; Steck et al., 1998; Wyss et al., 1999). Geochronological results from the northernmost part of the HHCZ of Zaskar indicate on-going metamorphism between 33-28 Ma, as constrained by Sm-Nd dating of garnet (Vance and Harris, 1999). According to Vance and Harris (1999), this thermal event is interpreted as the consequence of SW-directed thrusting and crustal thickening occurring south of the Indus Suture Zone during Late Eocene to Early Oligocene (c. 40-35 Ma). The thrust responsible for this crustal thickening must be located between the HHCZ and the Tethyan Himalaya that is not affected by high-grade metamorphism. Consequently, the high-grade metamorphism in the HHCZ is most likely the consequence of the NE-directed underthrusting of this unit beneath the Tethyan Himalaya, along a thrust which was subsequently re-activated as the extensional ZSZ, as proposed by Patel et al. (1993). This event was most likely coeval with the SW-directed nappe tectonics in the Tethyan Himalaya (e.g. Nyimaling-Tsarap nappe), in the hanging wall of the Zaskar Shear Zone. This interpretation is supported by  $^{40}\text{Ar}/^{39}\text{Ar}$  data indicating that SW-verging folding and thrusting in the Tethyan Himalaya of Spiti took place during Middle Eocene (45-42 Ma; Wiesmayr and Grasemann, 1999). Consistently with these ages, illite K/Ar dating, ranging between 44 to 47 Ma, in the Sarchu area (Fig. 5.1) suggests that the Tethyan sedimentary sequence was affected by a Barrovian metamorphism shortly after the collision (Bonhomme and Garzanti, 1991)

The main ductile extension along the Zaskar Shear Zone occurred between 22.2 and 19.8 Ma (Dèzes et al., 1999), contemporaneously with the Early Miocene thrusting along the MCT (Frank et al., 1977; Hodges et al., 1992; Coleman, 1998). In the Gianbul section, brittle extension along high angle normal faults outlasted the ductile extension along the Zaskar Shear Zone. In the Miyar Valley, extensional shear bands intruded by granitic segregations and cross-cut by late pegmatitic and aplitic dykes indicate that extension along the Khanjar Shear zone was coeval with partial melting in the HHCZ (Steck et al., 1999). The relative chronological relation between the Zaskar Shear Zone and the Khanjar Shear zone cannot be established precisely because of the lack of structural interferences between these tectonic phases. Structural analysis and geometric modelling indicates that the large-scale fold interference pattern mapped in the Miyar Valley required a succession of three deformation phases (Steck et al., 1999): (1) NE-verging folding related to the Shikar Beh nappe emplacement (D1 phase); (2) SW-verging folding induced by thrusting along the Main Central Thrust (D3 phase); and (3) doming associated to the exhumation of the migmatitic Gianbul Dome (D4 phase). Extension along the SW-dipping Khanjar Shear Zone was obviously related to the D4 phase of doming and it most likely post-dates the extension along the Zaskar Shear Zone (D3 phase). It cannot be completely ruled out, however, that both the Zaskar Shear Zone and the Khanjar Shear Zone developed as a consequence of the doming (Kündig, 1989). In any cases, the rapid cooling of the HHCZ of Zaskar during Early Miocene (Dèzes et al., 1999; Searle et al., 1999) implies that the exhumation of these high-grade rocks controlled by extension and doming most likely occurred in a short time interval of a few M.y.

## **5. 6. CONCLUSIONS**

The structural evolution of the High Himalayan Crystalline Zone in the Lahul – Zaskar area can be divided into four important phases (Fig. 5.28)

The first phase of deformation produces NE-verging folds associated with clear top-to-the-NE movements (Fig. 5.28a). In the Miyar valley, this phase is documented by a ductile thrust zone called the Miyar Thrust Zone. The well-established top-to-the-NE thrust movement, highlighted by kinematic indicators within the shear zone, is related to the NE-directed Shikar Beh nappe emplacement. This vergence contrasts with the main SW-directed thrusting observed all along the Himalayan belt. Such a NE-directed tectonic movement could be the consequence of a reactivation, during the early stages of collision, of SW-dipping normal faults pre-existing in the north Indian margin and related the Late Paleozoic Neo-Tethys rifting (Steck et al., 1993).

A second phase of deformation is recorded in the Gianbul Valley (Fig. 5.28b). This phase is characterized by SW-directed folds associated with the thrusting of the Nyimaling – Tsarap nappe. In the Gianbul Valley, this phase is only preserved as inclusion trails in syntectonic rotated garnet porphyroblasts showing a top-to-the-SW sense of shear.

These two first events are related to the crustal shortening, thickening, and Barrovian metamorphism recorded by the sedimentary sequence of the Indian continental margin. They are associated with the tectonic compression and overburden due to the collision between India and Asia at ca 50-55 Ma (Patriat and Achache, 1984; Garzanti et al., 1987).

The third and the fourth phases are related to syn-orogenic extension superposed on the two first contractional tectonic events. These two last phases contribute to the exhumation of the high grade metamorphic rocks of the High Himalayan Crystalline Zone. The third event is related to the extrusion of the High Himalayan nappe controlled by extension along the Zaskar Shear Zone, as well as by SW-directed thrusting of the High Himalayan nappe along the Main Central Thrust (Fig. 28c). The last phase leads to the formation of the Gianbul dome (Fig. 28 d). It is expressed in the Miyar Valley by the development of the SW-directed extensional Khanjar Shear Zone. In the Gianbul valley, this event is characterized by the formation of high angle normal faults which cross-cut the Zaskar Shear Zone. These faults are interpreted as the brittle equivalent of the ductile extensional Khanjar Shear Zone. Structural data indicate consequently that the tectonic evolution of the High Himalayan Crystalline Zone in SE Zaskar is associated with a complex tectonic history involving converging nappe structures superimposed by opposite-directed extensional structures.

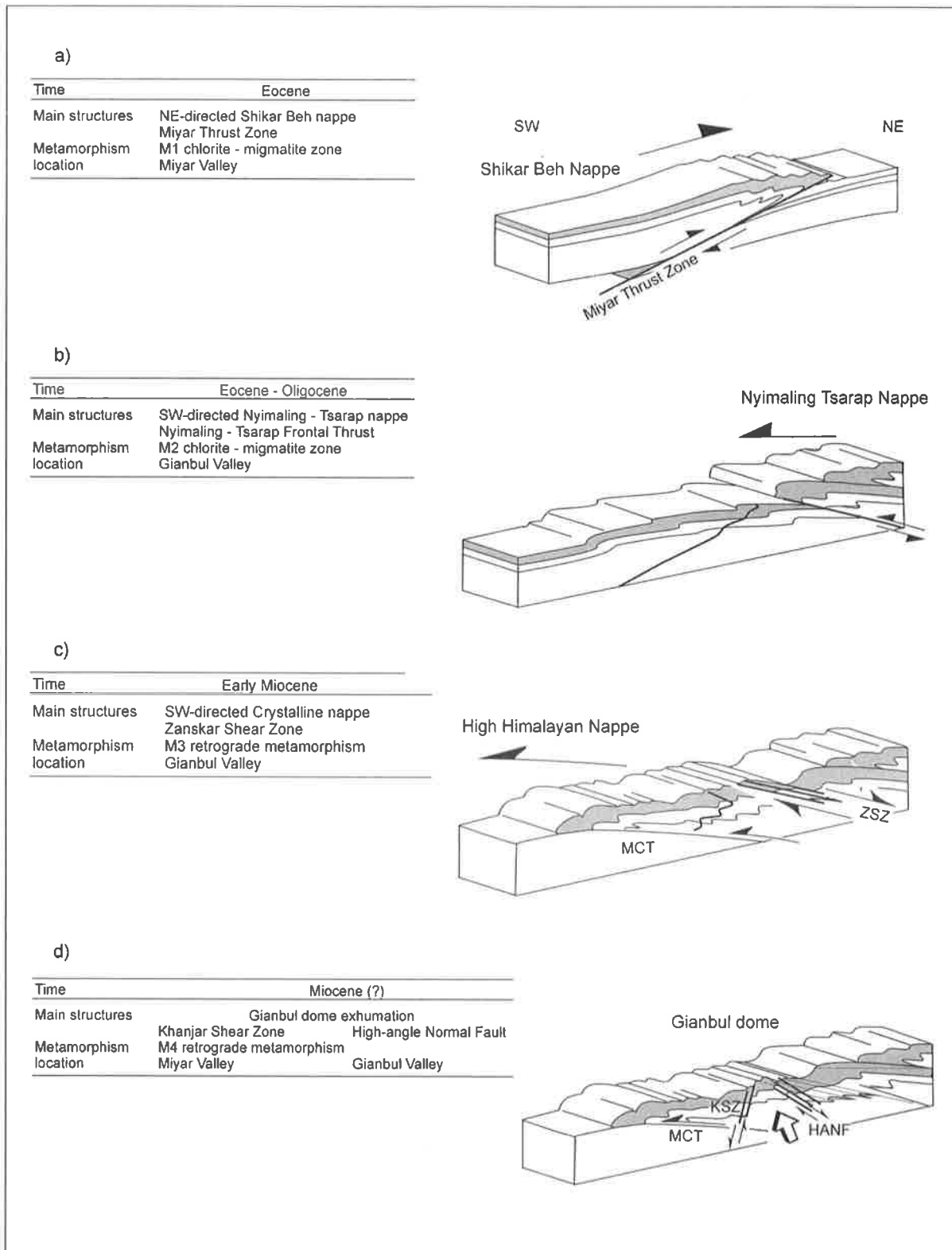


**Fig. 5.28:** Tectonic model for the High Himalayan Crystalline in the Gianbul dome area. HANF = High-angle Normal Fault; KSZ = Khanjar Shear Zone; MCT = Main Central Thrust; ZSZ = Zanskar Shear Zone

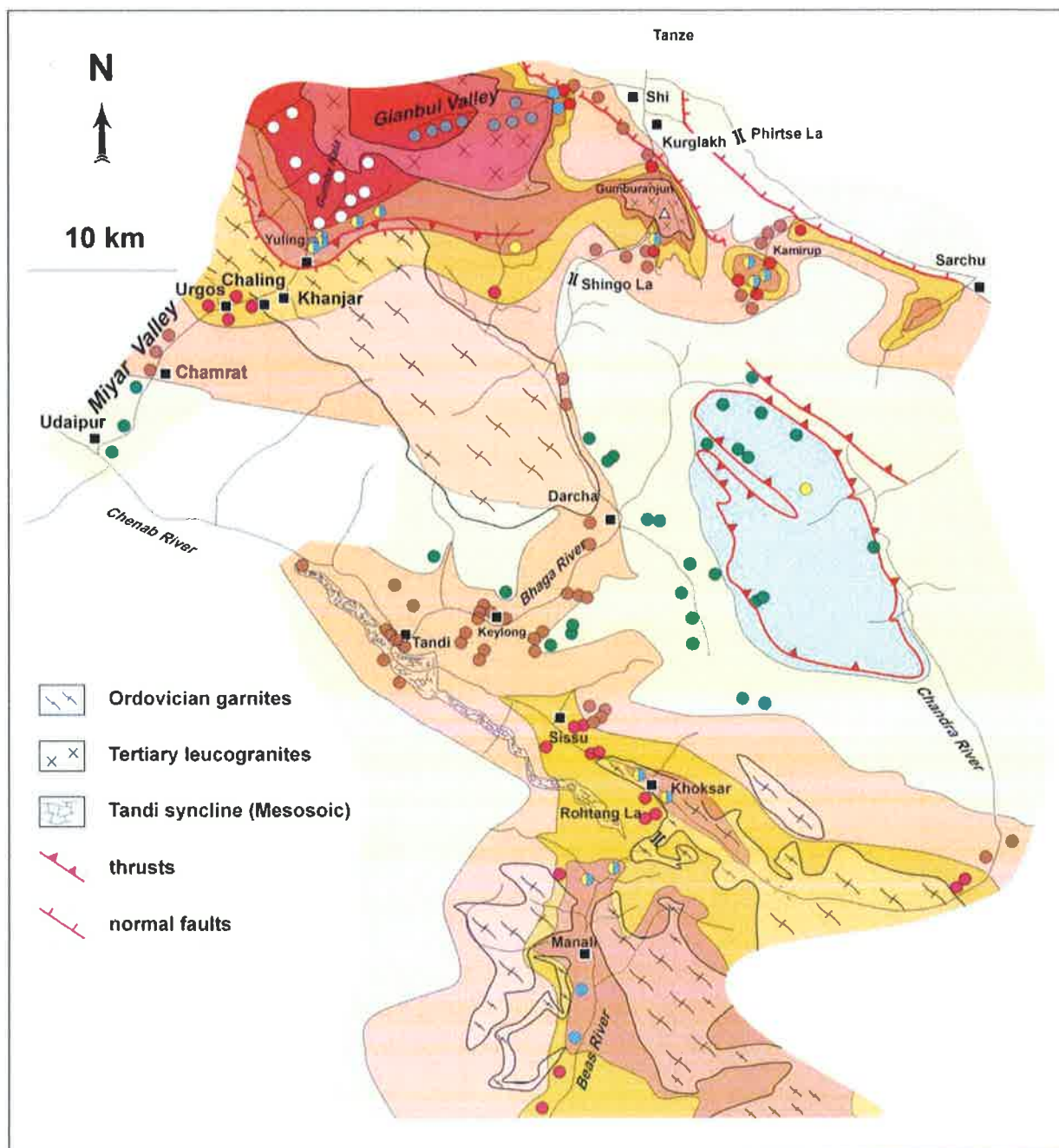


## CHAPTER 6: METAMORPHISM

### 6. 1. INTRODUCTION

Along the Miyar Valley – Gianbul Valley transect, the Himalayan orogen consists mainly of one tectonic unit, the so-called High Himalayan Nappe. For more than 1400 along the range, in the central and eastern part of the Himalaya, this nappe forms a fairly monoclinical crystalline slab up to 20 km thick, constituted by ductile deformed, high grade metamorphic rocks. In these regions, the High Himalayan nappe corresponds to the metamorphic core zone of the orogen and it is exposed in the frontal part of the range, superposed on the greenschist rocks of the Lesser Himalaya along the Main Central Thrust. Farther to the north, this nappe is generally separated from the low-grade sedimentary series of the Tethyan Himalaya by the extensional structures of the South Tibetan Detachment System. In contrast, in the north-western part of the Himalaya of India, the High Himalayan nappe doesn't correspond any more to a monoclinical crystalline slab. In this region, the High Himalayan nappe represents the product of a multiphase structural and metamorphic evolution (Steck et al., 1993 a and b; Vannay, 1993, Epard et al., 1995) and can be roughly divided into two metamorphic zones: (1) the low-grade metamorphic Chamba Zone in the frontal part of the range and (2) the High Himalayan Crystalline Zone of Zaskar which are exposed in a more internal part of the orogen (Fig. 5.1 and Fig. 6.1).









The Chamba Zone is mainly composed by weakly metamorphosed Haimantas sediments. In these sediments, the metamorphic overprint is expressed by the recrystallisation of the fine grained argillaceous matrix in white micas chlorite  $\pm$  biotite. This anchizone – biotite zone is extended northward in the Baralacha La area and broadly forms a 35 km wide, E-W oriented corridor of low-grade metamorphic rocks separating the high-grade metamorphic metasediments of the High Himalayan Crystalline Zone of Zaskar from similar high-grade rocks cropping out as a thick sheet in the frontal part of the belt, from the Kulu Valley to the east (Fig. 5.1). From the Baralacha La to the north, the increase of the metamorphic condition, evolving from the anchizone to the kyanite zone in the Sarchu area (Fig. 6.1), is interpreted as reflecting the underthrusting of the basal series of the Tethyan Himalaya, which will ultimately form the High Himalayan nappe, beneath the frontal part the Nyimaling – Tsarap nappe. In contrast, the high-grade metamorphic rocks exposed in the Khoksar area likely results from a significant overburden from south toward the north associated with the NE-directed Shikar Beh nappe emplacement (Steck et al., 1993; Vannay 1993; Epard et al., 1995). Farther to the north-west, the high-grade metamorphic rocks of High Himalayan Crystalline Zone of Zaskar are mainly exposed as a large-scale metamorphic dome which is referred to as the Gianbul dome (Dèzes, 1999). Since the last decade, most studies focused on the NE half of the Gianbul dome and on the northern metamorphic transition between the high-grade metamorphic rocks of the High Himalaya Crystalline Zone of Zaskar and the low-grade metamorphic zone of the Tethyan Himalaya is well constrained. It appears from these previous studies that the metamorphic gap observed in the SE Zaskar (Fig 6.2) results from the rapid exhumation of the High Himalayan Crystalline Zone controlled by extension along the Zaskar Shear Zone. In contrast, the metamorphic transition between the high-grade rocks of the High Himalayan Crystalline of Zaskar and the lower grade metasediments of the Chamba Zone exposed to the south remains however poorly constrained.



**Metamorphic zones**

- |  |  |
|--|--|
|  anchizone    |  garnet zone                |
|  chorite zone |  kyanite-staurolite zone    |
|  biotite zone |  sillimanite-migmatite zone |

**Metamorphic index minerals**

- |   |  |
|---|--|
|  pumpellyite |  kyanite-staurolite     |
|  chorite     |  kyanite                |
|  biotite     |  sillimanite            |
|  garnet      |  retrograde sillimanite |

**Fig 6.1:** Metamorphic zones in the Lahul - Zaskar area. Modified after Vannay (1993), Epard et al. (1995), Dèzes (1999), Wyss (1999) and data of this study for the Miyar Valley area. This map shows the high-grade metamorphic domains of the Khoksar - Manali area to the south and of the Gianbul - Sarchu area to the north.

The aim of the present chapter is to provide new constraints on the metamorphic evolution of the southernmost limit of the High Himalayan Crystalline Zone of Zaskar on the basis of petrographic, thermobarometric, and isotopic investigations in the Miyar Valley. Together with comparable data from the north-eastern limit of the High Himalayan Crystalline Zone in the Gianbul Valley area, these new data, combined with the structural data, allow us to proposed a reconstruction for the tectono-metamorphic evolution of the High Himalayan Crystalline Zone of Zaskar along a complete transect across the Gianbul dome.

## **6.2. MIYAR VALLEY SECTION**

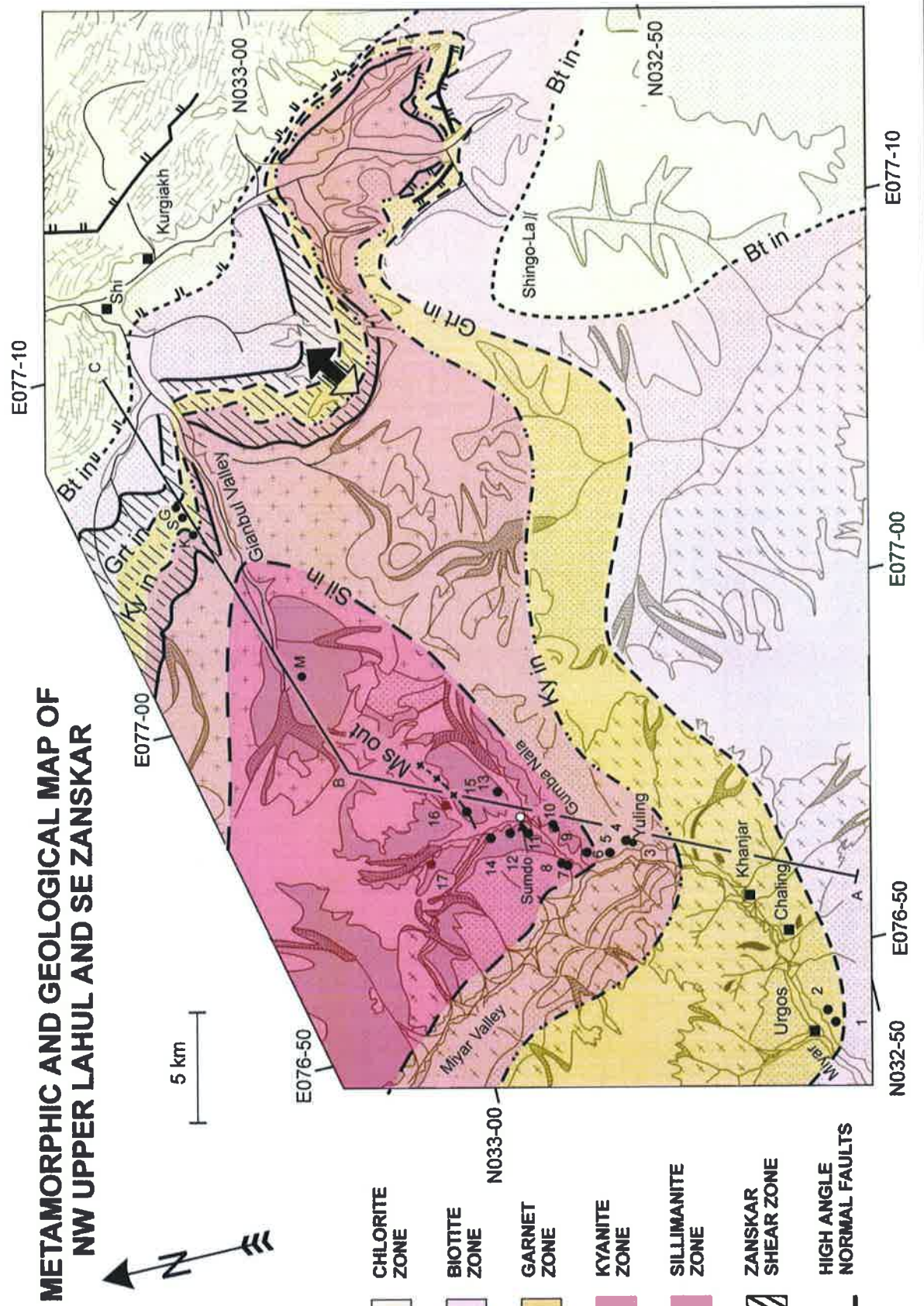
### **6.2.1. Prograde metamorphic field gradient (M1)**

The metapelites of the HHCZ in the Miyar Valley preserve a typical Barrovian metamorphic field gradient indicating a gradual increase of metamorphic conditions from SW to NE (Figs. 6.2 and 6.3). Moving upsection along the valley, from the village of Udaipur to the Gumba glacier upstream, a gradual succession of chlorite, biotite, garnet, kyanite + staurolite, sillimanite and migmatite zones can be observed. This continuous metamorphic field gradient indicates a gradual, although rapid, transition between the greenschist facies metasediments of the Chamba zone to the SW, and the amphibolite facies to migmatitic paragneiss of the HHCZ to the NE. Below the staurolite-kyanite isograd, the metasediments generally preserve their sedimentary features, such as the bedding and other sedimentary structures. Above the staurolite-kyanite isograd, the metamorphic assemblages and fabric dominate in the HHCZ paragneiss, as a consequence of pervasive recrystallisation and ductile deformation at high temperatures. Consequently, we arbitrarily define the staurolite-kyanite isograd as the limit between the HHCZ and the Chamba zone (Fig. 5.1). Sigmoidal inclusion trails in synkinematic garnet blasts indicate prograde growth during a NE-directed shearing (Fig. 5.7), in accordance with the numerous NE-directed shear sense criteria observed in the Miyar Thrust Zone. The Barrovian metamorphism observed in the Miyar Valley is consequently interpreted as reflecting the crustal thickening related to the emplacement of the NE-directed Shikar Beh nappe.

The stability of the observed diagnostic mineral assemblages in a KFMASH petrogenetic grid allows a first estimation of the P-T conditions associated with the metamorphic field gradient in the Miyar Valley (Fig. 6.4). Because most of the isograd reactions are characterized by steep  $dP/dT$  slopes in the grid, the peak temperature field gradient is relatively well constrained. The stability of either kyanite or sillimanite in the studied assemblages provides informations about the minimum or maximum peak pressure, respectively.

**Fig 6.2:** Geological and metamorphic map of the NW Upper Lahul and SE Zaskar. Labelled black dots corresponds to the location of the samples collected for thermobarometry (incorporating data from Dèzes 1999). The A-B-C transect corresponds to the location of the cross section on Fig 6.3.

# METAMORPHIC AND GEOLOGICAL MAP OF NW UPPER LAHUL AND SE ZANSKAR



- CHLORITE ZONE
- BIOTITE ZONE
- GARNET ZONE
- KYANITE ZONE
- SILLIMANITE ZONE
- ZANSKAR SHEAR ZONE
- HIGH ANGLE NORMAL FAULTS

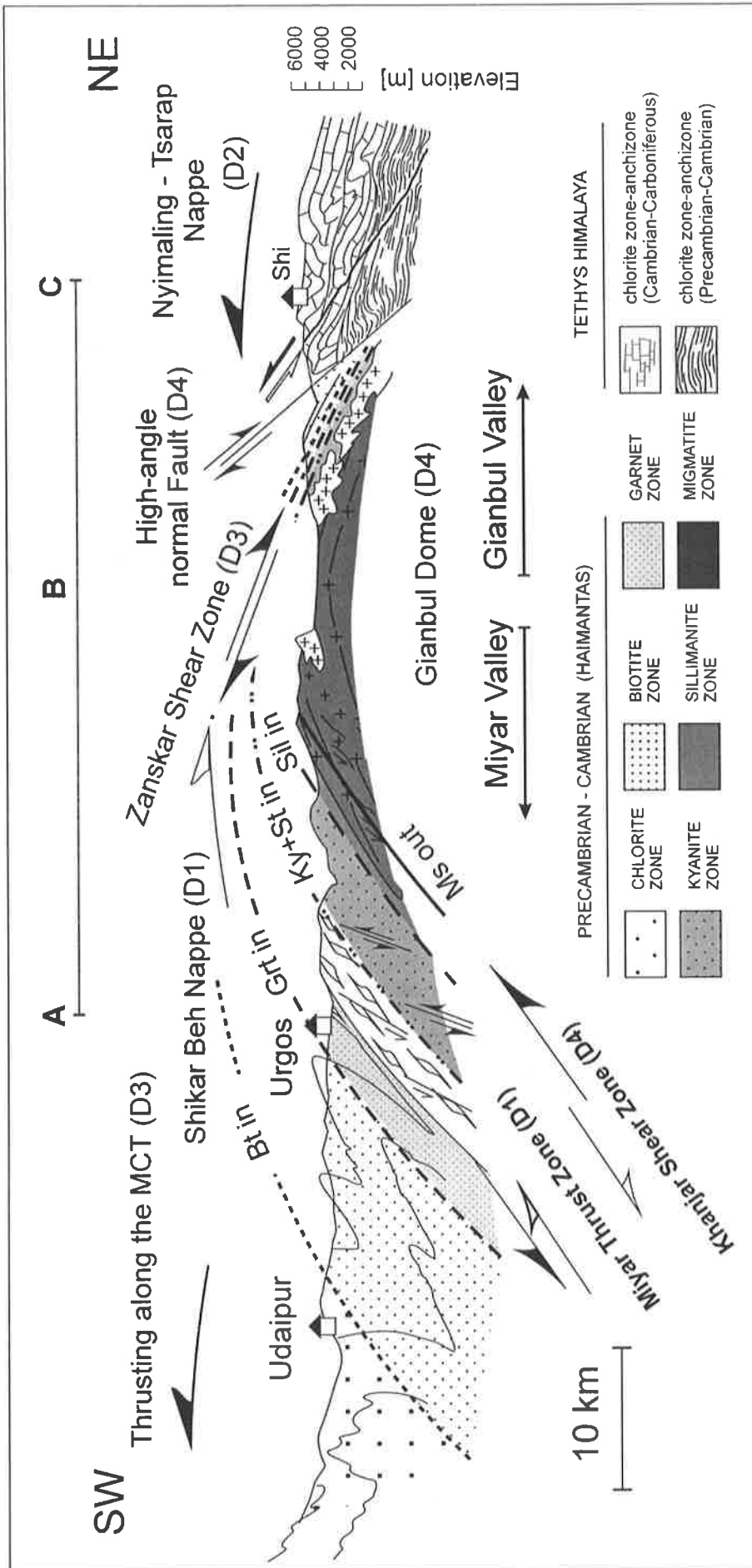
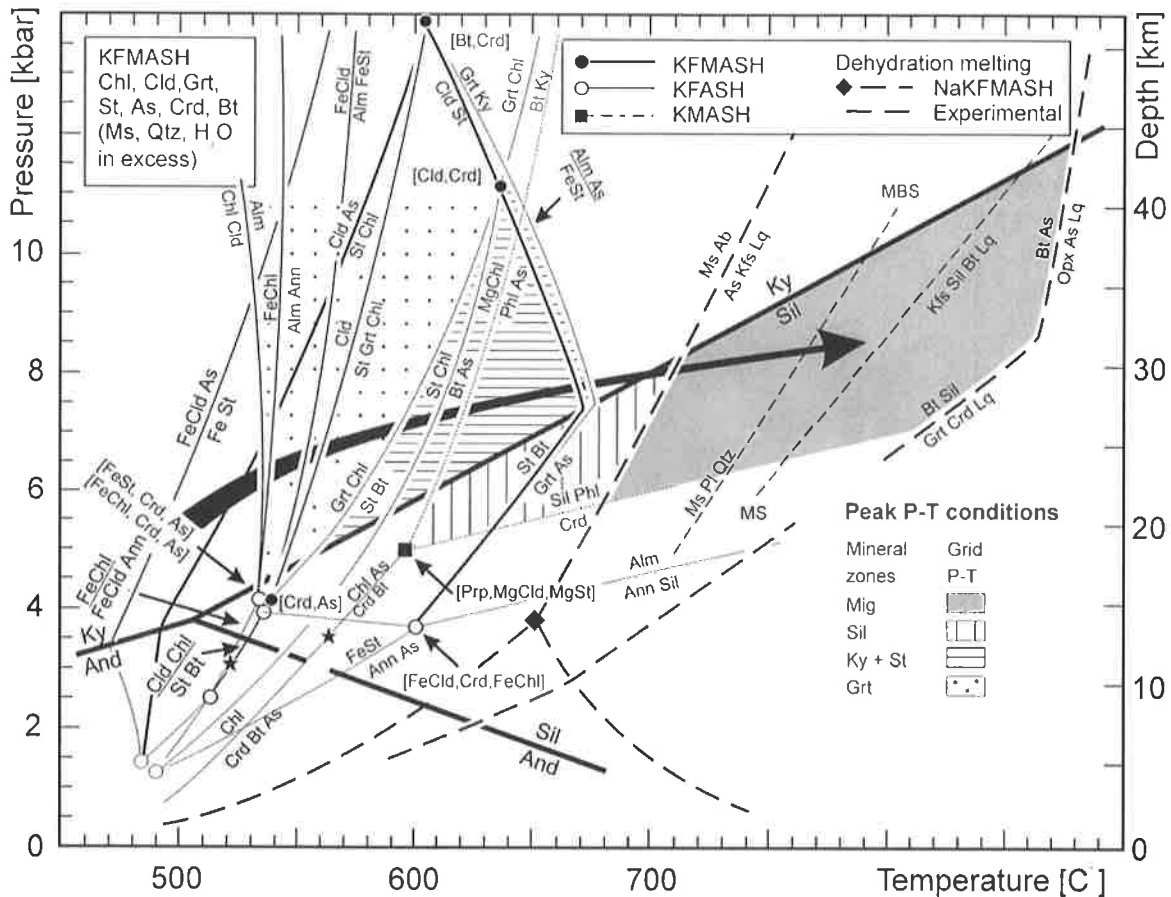


Fig. 6.3: Geological cross-section through the Gianbul dome along the Miyar Valley and Gianbul Valley (see Fig. 2 for location). Abbreviations: Bt = biotite, Grt = garnet, Ky = kyanite, Ms = muscovite, Sil = sillimanite, St = staurolite. See Fig. 6.2 for location



**Fig. 6.4:** Peak P-T estimates from the metamorphic assemblages of the metapelites from the A-B transect of the Miyar Valley (see on Fig 6.2 for location), reported in a KFMASH petrogenetic grid. All reactions calculated according to the thermodynamic database of Holland and Powell (1998), except the partial melting reactions. The muscovite dehydration reactions labelled "MBS" and "MS" correspond to the experimentally-determined partial melting conditions for muscovite + biotite bearing and muscovite-bearing Himalayan metapelites, respectively (Patiño-Douce and Harris, 1998). The additional muscovite and biotite dehydration melting reactions are taken from Spear et al. (1999). The black arrow represents the prograde metamorphic field gradient in the Miyar Valley. Abbreviations: Alm = almandine; And = andalusite; Ann = annite; As = aluminosilicate; Bt = biotite; Chl = chlorite; Cld = chloritoid; Crd = cordierite; Grt = garnet; Kfs = K-feldspar; Ky = kyanite; Lq = liquid (melt); Ms = muscovite; Opx = orthopyroxene; Phl = phlogopite; Prp = pyrope; Sil = sillimanite;

### 6.2.1.1. Chlorite and biotite zones

In the southern part of the Miyar Valley, as well as farther to the SW, the low-grade metasediments contain mainly chlorite zone assemblages. Moving up the Miyar Valley, in the Chamrat area, the first apparition of biotite crystal defines the biotite in isograd (Fig 6.1). In this part of the section, the rocks mainly consist of alternation of psammitic and slaty beds. The chlorite and micas define the main foliation generally subparallel to bedding (Fig. 6.5). This preferred orientation corresponds to the main schistosity (S1a+ S1b) at the regional scale (Fig 6.3). This schistosity is sometimes crenulated and a discrete crenulation cleavage mainly defines by biotite and white micas crystals can be locally observed (Fig. 6.6). Consequently, two generations of

micas occur in this part of the section. The first generation together with the chlorite crystallisation, correspond to the S1a + S1b main schistosity which forms the axial plane foliation of the regional scale folds. This generation reflects the M1 metamorphism associated with the NE-directed Shikar

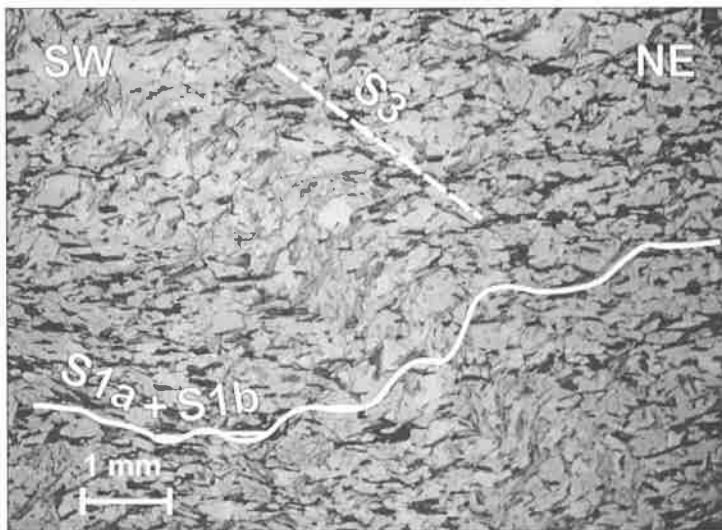


**Fig. 6.5:** A fine-grained slate composed of an association of chlorite, biotite, muscovite, plagioclase and quartz. The S1a+S1b main foliation is folded by the D3 phase referred to as the SW-directed High Himalayan nappe emplacement. This D3 phase produces a slightly S3 crenulation cleavage. Southern part of the Miyar Valley between Chamrat and Urgos.

Beh nappe emplacement. The second generation is likely associated with to the SW-directed thrusting of the High Himalaya nappe along the Main Central Thrust.

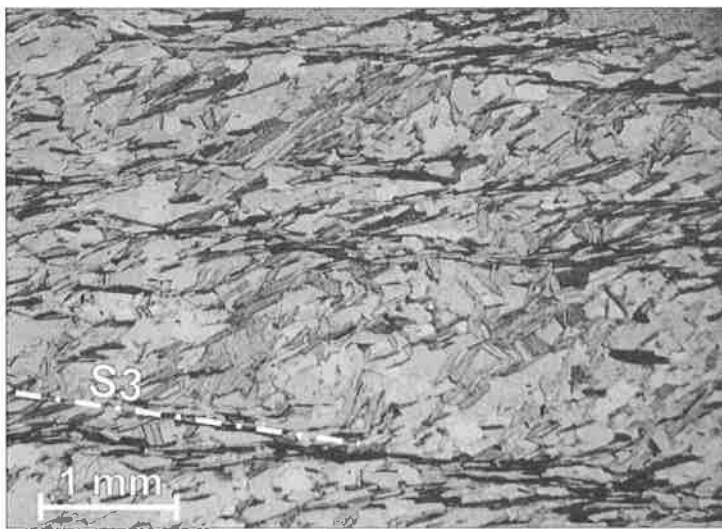


**Fig. 6.6:** Discrete crenulation cleavage overprinting the slaty S1a+S1b main foliation. The S3 crenulation cleavage is mainly underlined by biotite and white micas. Chlorite is lacking in this crenulation cleavage. Southern part of the Miyar Valley between Chamrat and Urgos

The typical assemblage defining the main schistosity in the metapelites of the biotite zone consists of biotite + chlorite + quartz + white mica  $\pm$  epidote  $\pm$  albite. This stable assemblage implies, in first estimation, a temperature exceeding 300 to 400°C for the M1 prograde metamorphism in this part of the section.

#### 6.2.1.2. Garnet zone

Proceeding up the valley, the first garnets appear at the level of the village of Urgos (Fig. 6.2). The metapelitic rocks of the garnet zone generally contain the diagnostic mineral assemblage garnet + biotite + muscovite + quartz + plagioclase  $\pm$  epidote  $\pm$  chlorite. In these rocks, the garnets appear as sporadic and small crystals (Fig 6.7). Shear sense indicators, such as sigma clasts and the



systematic NE-directed vergence of the synmetamorphic fold, show that the penetrative schistosity, marked by the micas, is associated with a NE-directed tectonic movement (Shikar Beh nappe). Garnet is also observed in assemblage with quartz + plagioclase + K-feldspath + muscovite +

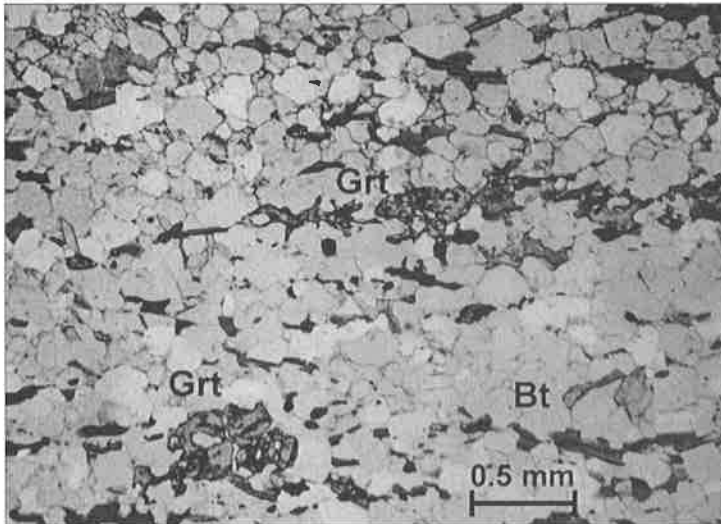


**Fig. 6.7:** Garnet and biotite-bearing metapsammite from the garnet zone near the village of Urgos. The biotite crystals weakly marks the S1b schistosity.

biotite + tourmaline in the Kade granitic gneiss, cropping out as a thick sheet between the villages Chaling and Yuling (Figs 6.2 and 6.3).

Within the metasediments, thin mafic horizons, representing volcanoclastic levels and/or metamarls, contain garnet + hornblende + plagioclase + biotite + titanite. Together with the biotite, the amphibole defines a penetrative schistosity in these rocks (Fig. 6.8). Following the classification of Leake et al. (1997), these amphiboles have chemical compositions characteristic of aluminotschermakite to aluminomagnesian hornblende. The average garnet composition is alm = 40-45%, grs = 25-30%, pyr = 5-10%, and sps = 15-20%. The plagioclase is Ca-rich (anorthite = 70-90%). Together with the lack of chlorite, the critical stable hornblende + plagioclase assemblage in these metabasites indicates peak conditions in the amphibolite facies, broadly constraining the peak temperature between c. 500 and 600°C (Eskola 1939).

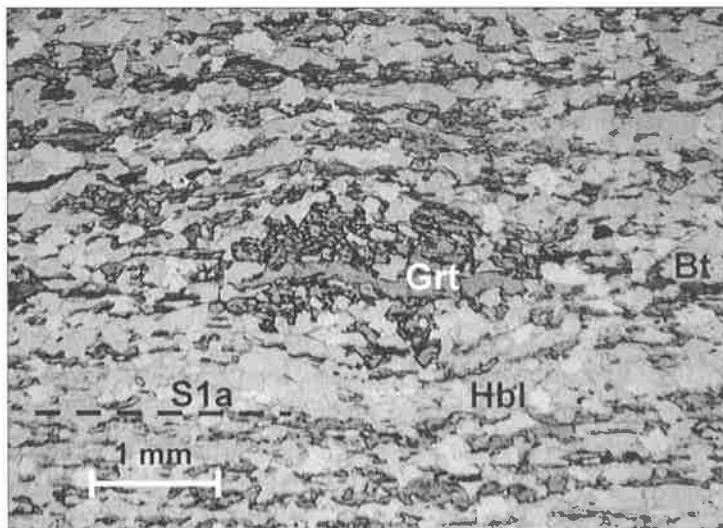


**Fig. 6.8:** Metabasite level intercalated in the metapsammite of the garnet zone near the village of Urgos, in the central part of the valley. The structural observations clearly indicate that the hornblende crystals marks the S1a foliation. These metabasite levels likely result from a volcanogenic origin or from a metamorphic marl transformation.

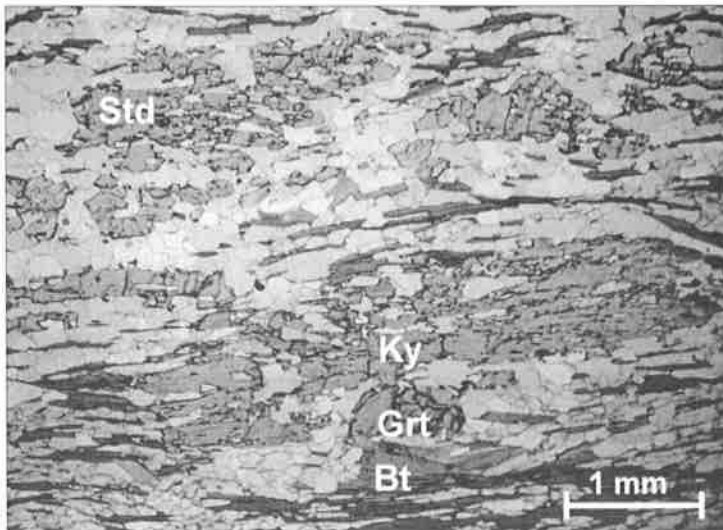


**Fig. 6.9:** Garnet, staurolite, and kyanite bearing assemblage of the metapelites from the Staurolite-Kyanite zone (Yuling area). In the metapelite level, the garnet crystals are rather scarce but they are abundant in the more psammitic levels. The crystals are elongated along the main mylonitic S1b foliation.

### 6.2.1.3. Kyanite and staurolite zone

Underlying the Kade orthogneiss, farther to the NE, the paragneiss of the HHCZ consists of metapsammites alternating with pelitic beds. The massive psammitic levels contain the assemblage garnet + biotite + muscovite + quartz + plagioclase, whereas kyanite and staurolite appear in the mica-rich pelitic horizons. Kyanite and staurolite are both stable in these rocks and they form prismatic blasts reaching centimetric size, whereas garnet is relatively rare (Fig. 6.9). Abundant kyanite and staurolite are observed at the margins of quartz veins in the metapelites. The diagnostic assemblage of this kyanite + staurolite zone is kyanite + staurolite + biotite + muscovite + quartz + plagioclase ± garnet. The stability conditions for this typical assemblage is well constrained in a KFMASH grid (Fig. 6.4) by the kyanite-in isograd (staurolite + muscovite + chlorite = biotite + kyanite) and the staurolite-out reaction (staurolite + biotite = garnet + aluminosilicate), indicating a peak temperature c. 600-670°C and a pressure in excess of c. 6 kbar.

### 6.2.1.4. Sillimanite zone

The typical assemblage of the sillimanite zone is sillimanite + garnet + muscovite + biotite + quartz + plagioclase. Prograde sillimanite forms long prismatic crystals marking the penetrative schistosity together with the biotite and muscovite (Fig. 6.10). Such rocks also contain a fine-grained fibrolitic sillimanite associated with the retrograde history. The prograde sillimanite isograd coincides with the disappearance of both kyanite and staurolite in the metapelites, indicating a metamorphic field gradient crossing the kyanite = sillimanite equilibria at the level of the staurolite-out reaction (staurolite + biotite = garnet + aluminosilicate) at about 670°C / 7.5 kbar.

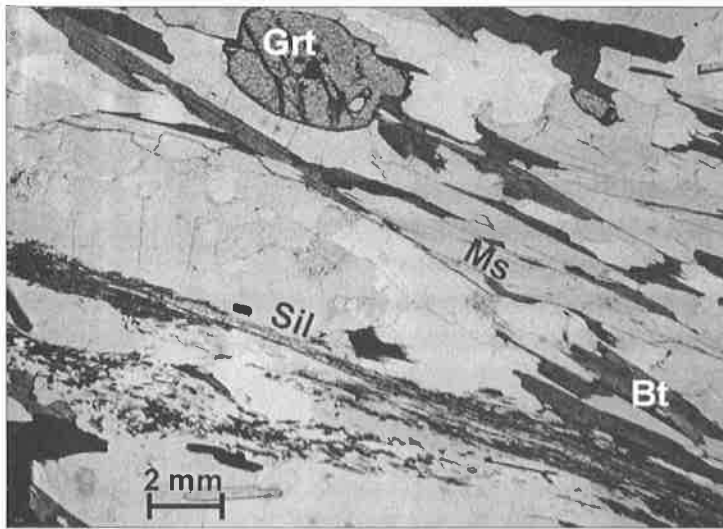


**Fig. 6.10:** Sillimanite-bearing assemblage in the metapelites from the sillimanite-migmatite zone (Gumaba Nala area). The crystals are aligned along the main S1b foliation.

### 6.2.1.5. Migmatite zone

Migmatitic paragneisses forming the core of the Gianbul dome record the highest metamorphic conditions observed along the metamorphic field gradient in the uppermost Miyar Valley (Gumba Nala; Fig. 6.3).

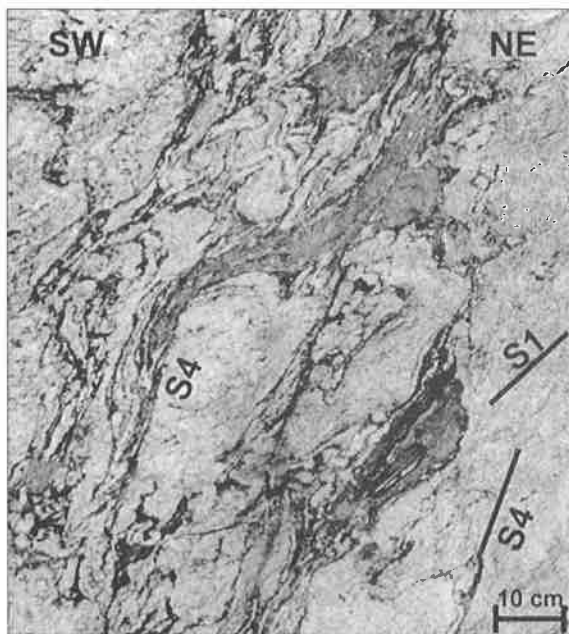


**Fig. 6.11:** Migmatite gneiss from the Gumba Nala area. The dark part corresponds to sillimanite-bearing levels. The white part represents granitic segregation. The migmatitic zone has recorded the highest grade metamorphic condition in the studied area. This zone is characterized by pervasive anatexis of the High Himalayan Crystalline Zone. Migmatization is here so intense that it is often not possible to establish whether the protholith corresponds to metasediments from the Phe Formation or to the Cambro-Ordovician granites.

This migmatite zone is characterized by the stable assemblage sillimanite + quartz + biotite + garnet + plagioclase  $\pm$  muscovite  $\pm$  K-feldspar. Except for the presence of granitic segregations, the overall mineralogy and fabric of the migmatitic paragneiss is very similar to what is observed in the sillimanite zone. Although these migmatites appear to be mainly derived from paragneiss, the intensity of partial melting hinders, in places, the identification of the protolith (Fig. 6.11). The presence of orthogneiss lenses in the migmatite zone suggests that Cambro-Ordovician granitic rocks were also involved in the Tertiary partial melting. The outer part of the migmatite zone is composed of muscovite-present assemblages, whereas the central part is delimited by a sharp muscovite-out isograd (Fig 6.12). Biotite appears to remain stable in the muscovite-absent assemblages forming the core of the migmatite dome. These observations imply that partial melting of the HHCZ metapelites took place through muscovite dehydration melting, such as determined experimentally by Patiño Douce and Harris (1998), but that the peak conditions did not allow melting through biotite

dehydration. The peak temperature reached in the centre of the migmatitic dome can thus be estimated at  $T \approx 700\text{--}850^\circ\text{C}$ , whereas the stability of sillimanite, together with the lack of kyanite, constrain the peak pressure at  $P < 10$  kbar (Fig. 6.4).

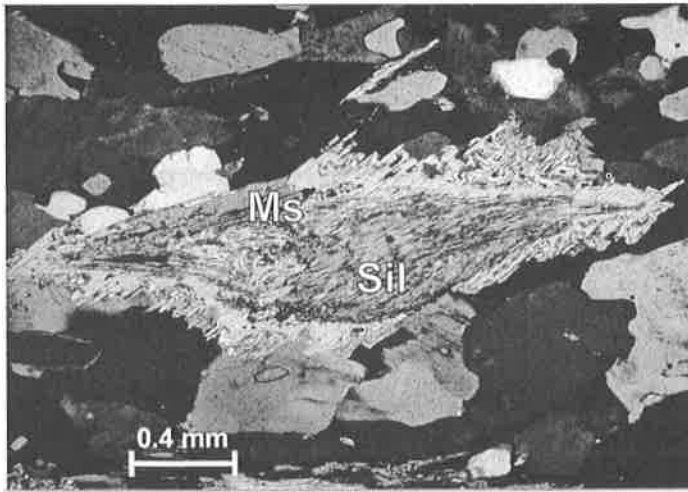


**Fig. 6.12:** Intergrowth of muscovite and fibrolitic sillimanite indicative of muscovite dehydration melting in the migmatitic paragneiss of the Miyar Valley.

## **6.2.2. Thermobarometry**

### ***6.2.2.1. Methodology***

In order to quantitatively constrain the peak P-T conditions along the Miyar section, 16 garnet-bearing samples (14 metapelites and 2 metabasites) were selected for geothermobarometry. The mineral analyses are provided in Tables A1 to A4. No chemical zoning was observed in the plagioclases, muscovites, biotites and hornblendes analysed for thermobarometry. Except for one garnet preserving a weak growth zoning, the majority of the analysed garnets show flat composition profiles testifying to chemical homogenization through diffusion at high temperatures (Fig. 6.13). Such garnets also generally show a slight increase of the  $\text{Fe} / (\text{Fe} + \text{Mg})$  ratio at the rim, indicating a limited retrograde Fe – Mg exchange with biotite during cooling (e.g. Spear, 1993). For thermobarometry calculations, such retrograde rims were avoided and the near-rim garnet composition at the lowest  $\text{Fe} / (\text{Fe} + \text{Mg})$  ratio was used together with the mean composition of the other mineral phases, in order to obtain P-T estimates approximating peak conditions. The P-T estimates were calculated by multiple equilibria thermobarometry using THERMOCALC (Powell and Holland, 1994) and the latest thermodynamic dataset of Holland and Powell (1998). The average P-T results for the Miyar section are presented in Table 6.1 and they are plotted in the KFMASH petrogenetic grid (Fig. 6.14). The peak P-T field gradients constrained by these results for the Miyar section are illustrated in Fig. 6.15.

### ***6.2.2.2. Results***

The average accuracy of the P-T results, as calculated by THERMOCALC and reported in Table 6.1, is c.  $\pm 250^\circ\text{C}$  and  $\pm 4$  kbar when considered at the 2 sigma confidence level. Although such uncertainties appear to be fairly large, it should be noted that they correspond to the overall accuracy of the P-T estimates, and that this accuracy is 5 to 10 times greater than the precision

(reproducibility) of the results (Worley and Powell, 2000). Moreover, thermobarometry results generally appear to be more robust than suggested by their accuracy calculated by rigorous statistical propagation of uncertainties (Hodges and McKenna, 1987).

Several arguments indeed suggest that the average P-T results obtained are more reliable than suggested by their relatively large calculated uncertainties (accuracy): (1) samples from comparable structural levels yield similar average P-T results (e.g. samples 1 and 2, as well as 4

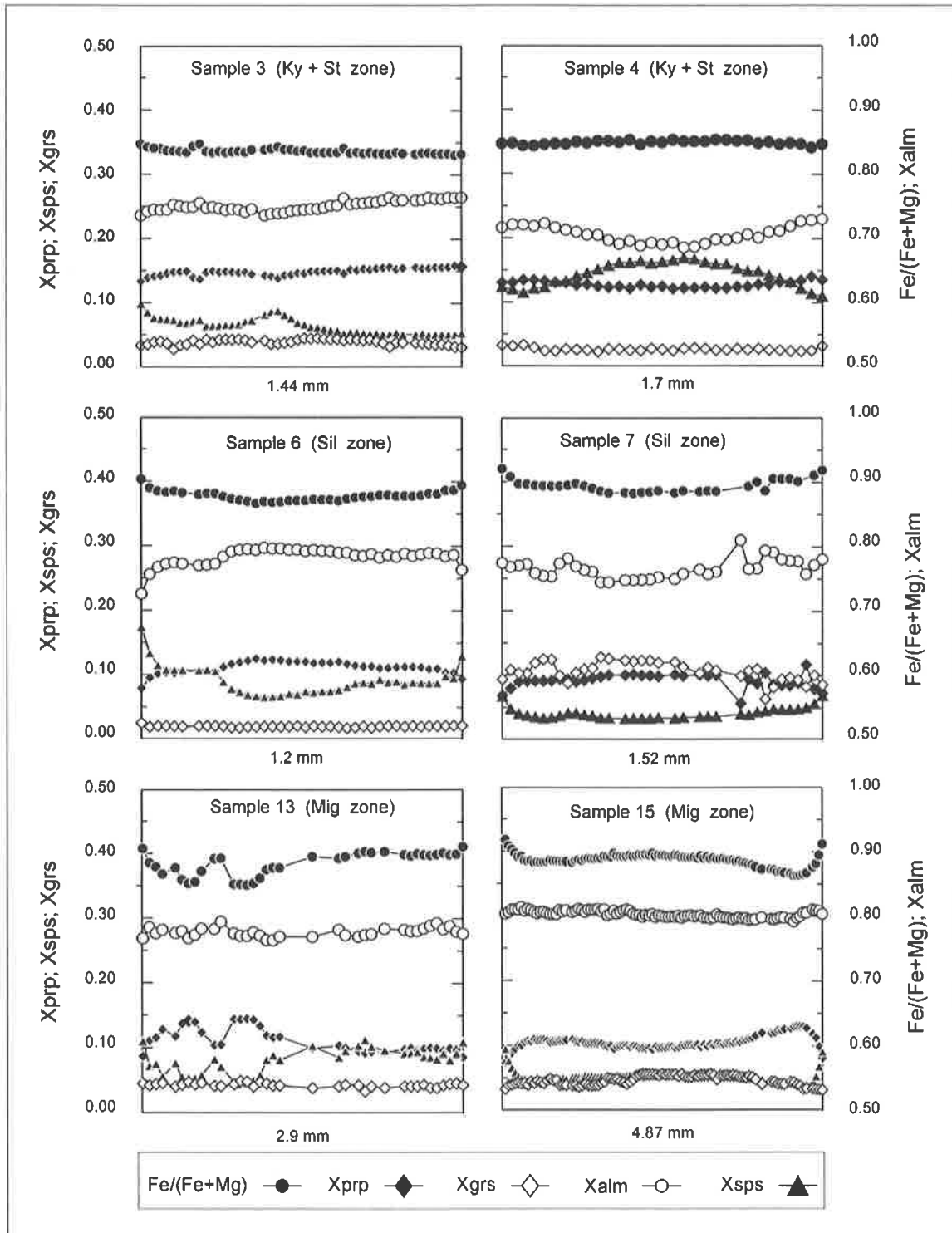


**Fig. 6.13:** Representative garnet zoning profiles from the metapelites in the Miyar Valley section (abbreviations: grs = grossular; sps = spessartine; others as in Fig. 6.4).

and 5, Table 6.1); (2) the P-T results for the various mineral zones are generally consistent with the stability of the diagnostic mineral assemblages predicted by the KFMASH petrogenetic grid calculated with the same thermodynamic dataset (Figs. 6.4 and 6.14); (3) the P-T estimates for the migmatite zone samples are in good agreement with experimentally determined partial melting conditions of Himalayan metapelites (e.g. Patiño Douce and Harris, 1998); and (4) the P-T field gradient defined by the thermobarometry results is consistent with the Barrovian metamorphic zonation mapped in the Miyar section. Considering a conservative, nominal precision of  $\pm 50^\circ\text{C}$  and  $\pm 1$  kbar, the overall consistency of the average P-T results obtained strongly suggests that they represent close estimates of the peak metamorphic conditions recorded by the studied samples. It should be noted that although samples 1 and 2 contain metabasic assemblages, their peak P-T conditions are broadly consistent with the stability conditions for the metapelitic garnet zone assemblages, as indicated by the petrogenetic grid (Figs. 6.4 and 6.14).

**Table 6.1: Average peak P-T estimates for the Miyar Valley section.**

| nbr | Samples   | Assemblage          |  | $T(^{\circ}\text{C})$ | $\sigma T$ | $P(\text{kbar})$ | $\sigma P$ | Corr  | sigfit | n | XH <sub>2</sub> O |
|-----|-----------|---------------------|--|-----------------------|------------|------------------|------------|-------|--------|---|-------------------|
|     |           | Qtz + Pl + Bt + Grt |  |                       |            |                  |            |       |        |   |                   |
| 1   | RM 98/6   | + Ep + Hbl          |  | 506                   | 49         | 6.0              | 0.9        | 0.555 | 0.56   | 6 | 1                 |
| 2   | AS 98/60  | + Ep + Hbl          |  | 525                   | 39         | 5.7              | 1          | 0.609 | 0.62   | 7 | 1                 |
| 3   | RM 98/45  | + Ms                |  | 608                   | 93         | 6.9              | 1.5        | 0.679 | 0.38   | 4 | 1                 |
| 4   | RM 98/41  | + Ms + Ky + Std     |  | 645                   | 23         | 8                | 1.1        | 0.082 | 0.3    | 7 | 1                 |
| 5   | RM 98/55  | + Ms                |  | 644                   | 99         | 8                | 1.6        | 0.756 | 0.62   | 4 | 1                 |
| 6   | RM 98/82  | + Ms                |  | 783                   | 143        | 9.2              | 2          | 0.877 | 0.83   | 4 | 1                 |
| 7   | RM 98/77  | + Ms                |  | 782                   | 150        | 10.1             | 3.3        | 0.309 | 0.4    | 3 | 1                 |
| 8   | RM 98/84  | + Ms + Sil          |  | 773                   | 144        | 8                | 2.1        | 0.793 | 0.39   | 5 | 1                 |
| 9   | RM 98/92  | + Ms                |  | 694                   | 127        | 7.4              | 1.8        | 0.824 | 0.73   | 4 | 1                 |
| 10  | RM 98/93  | + Ms + Sil          |  | 841                   | 164        | 8.7              | 2.3        | 0.822 | 0.56   | 5 | 1                 |
| 11  | RM 98/97  | $\pm$ Ms + Sil      |  | 741                   | 127        | 7.6              | 1.8        | 0.769 | 0.71   | 5 | 1                 |
| 12  | RM 98/87  | + Ms + Sil          |  | 861                   | 247        | 7.6              | 3.2        | 0.827 | 1.4    | 5 | 1                 |
| 13  | RM 99/18  | $\pm$ Ms + Sil      |  | 821                   | 150        | 8.7              | 2          | 0.837 | 0.52   | 5 | 1                 |
| 14  | AS 98/100 | $\pm$ Ms + Sil      |  | 776                   | 153        | 6.9              | 2          | 0.806 | 0.86   | 5 | 1                 |
| 15  | MS 99-1   | $\pm$ Ms + Sil      |  | 835                   | 222        | 10.2             | 33         | 0.884 | 1.34   | 5 | 1                 |
| 16  | RM 98/116 | $\pm$ Ms + Sil      |  | 789                   | 177        | 8.2              | 2.5        | 0.878 | 1.09   | 5 | 1                 |

**Note:** P-T estimates calculated with THERMOCALC (Powell and Holland 1994).  $\sigma T$  and  $\sigma P$  are the overall uncertainties at 1  $\sigma$  confidence level; Corr is the correlation between the uncertainties on P and T; n is the number of independent reactions; sigfit refers to a measure of the scatter in residuals of the enthalpies and activities normalized by their uncertainties. For all samples except RM 98/41, the P-T estimates are independent of the XH<sub>2</sub>O (set to 1) because no dehydration reactions are involved in the set of reactions constraining these results. For sample RM 98/41, the P-T estimates for reasonable XH<sub>2</sub>O values (XH<sub>2</sub>O > 0.8) remain comparable within uncertainties. The paragonite component of white micas (average K / (K + Na) = 0.89) was not included in the calculations because of unrealistically high non-ideal activities calculated by THERMOCALC. Abbreviations: Ep = epidote; Hbl = hornblende; Pl = plagioclase; Qtz = quartz; others as in Fig. 6.4.

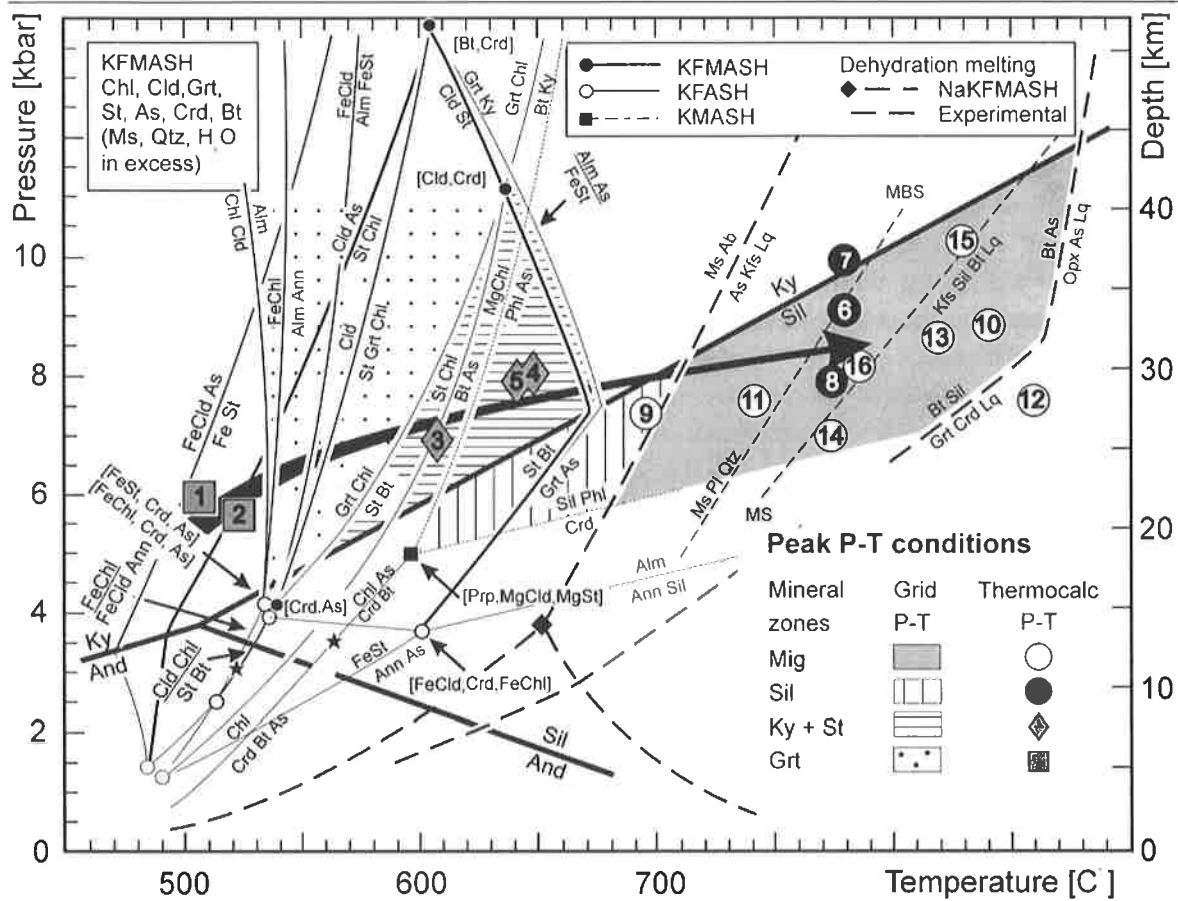


**Fig. 6.14:** Peak P-T estimates for the HHCZ of the Miyar Valley (transect A-B on Fig. 6.2), reported in a KFMASH petrogenetic grid for metapelites. The average molar fraction of Mn in the analysed garnets is c. 10 %, indicating Mn-poor assemblages satisfactorily modelled by a KFMASH system. All reactions calculated according to the thermodynamic database of Holland and Powell (1998), except the partial melting reactions. The muscovite dehydration reactions labeled "MBS" and "MS" correspond to the experimentally-determined partial melting conditions for muscovite + biotite bearing and muscovite-bearing Himalayan metapelites, respectively (Patiño-Douce and Harris, 1998). The additional muscovite and biotite dehydration melting reactions are taken from Spear et al. (1999). The black arrow represents the prograde metamorphic field gradient in the Miyar Valley. The grey arrow corresponds to the retrograde metamorphic evolution of the kyanite + staurolite zone assemblages, deduced from textural relations (see text). See Fig.6.2 for sampling locations. Abbreviations: Alm = almandine; And = andalusite; Ann = annite; As = aluminosilicate; Bt = biotite; Chl = chlorite; Cld = chloritoid; Crd = cordierite; Grt = garnet; Kfs = K-feldspar; Ky = kyanite; Lq = liquid (melt); Ms = muscovite; Opx = orthopyroxene; Phl = phlogopite; Prp = pyrope; Sil = sillimanite; St = staurolite.

The thermobarometry results indicate that from the garnet zone to the migmatite zone along the Miyar valley, the metamorphic field gradient is characterized by a gradual peak temperature increase from c. 510°C to 790°C over an horizontal distance about 20 km (Figs 6.14 and 6.15). In the hanging wall of the Miyar Thrust Zone, the peak pressure in the garnet zone is c. 5.8 kbar, indicating a burial depth about 20 km for a lithostatic gradient (0.27 kbar / km). In the footwall of the Miyar Thrust Zone, no noticeable pressure field gradient is observed within the uncertainty of the thermobarometry results. The average peak pressure in the kyanite + staurolite zone to the migmatite zone is c. 8 kbar, indicating a burial depth about 30 km for a lithostatic gradient. The pressure difference of about 2 kbar between the garnet zone and the kyanite + staurolite zone implies that a vertical displacement about 7 km has been accommodated along the extensional Khanjar Shear Zone. For the present day dip of the structure (c. 30°), this estimate translates to an extensional slip about 14 km.

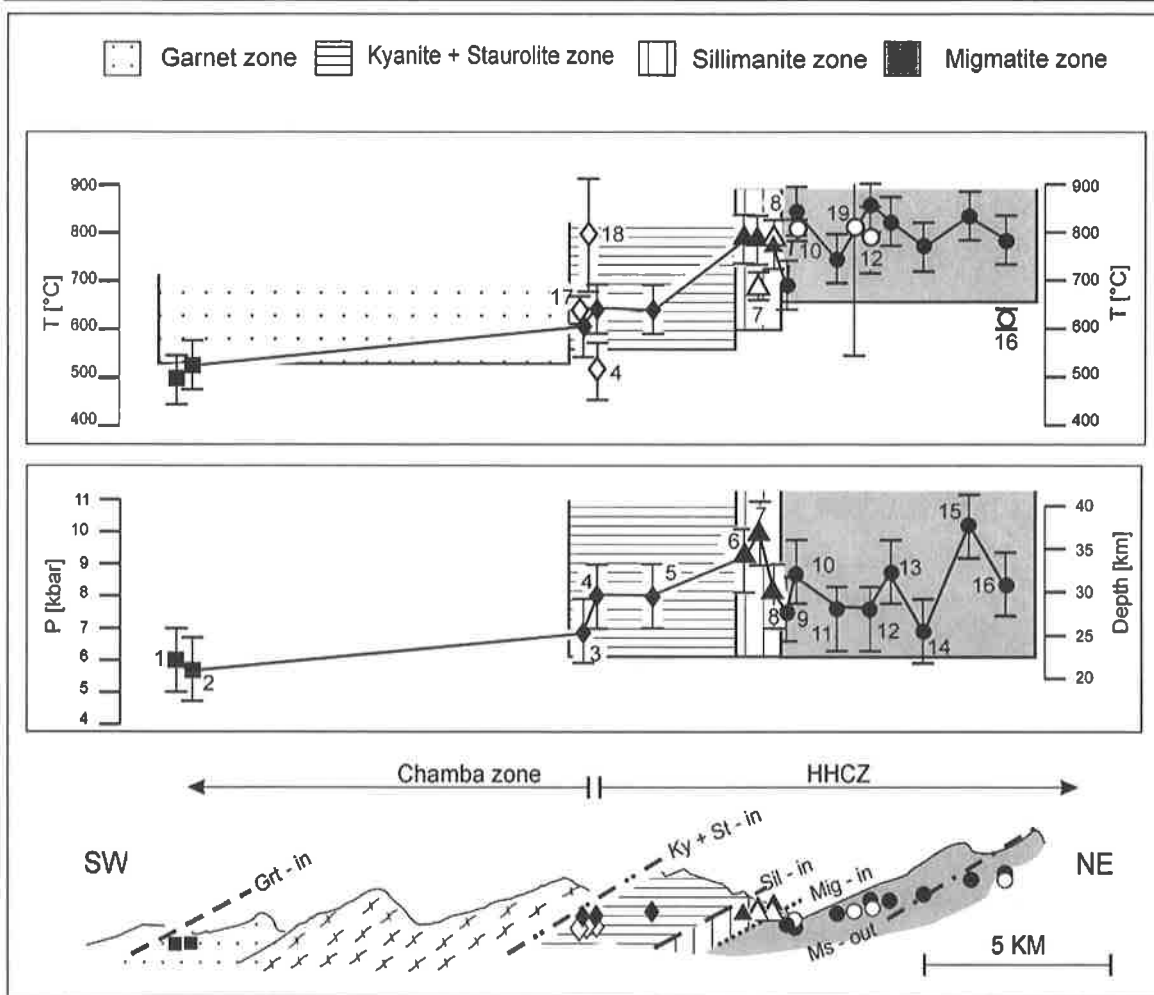


**Fig. 6.15:** Pressure and temperature profiles for the Miyar Valley section, based on the results presented in Tables 6.1 and 6.2. Fields with patterns represent the P-T range for the stability of the various diagnostic mineral assemblages, as deduced from the petrogenetic grid (Fig. 6.4). The black symbols represent multiple-equilibria P-T estimates (THERMOCALC). The white symbols correspond to the oxygen isotope thermometry results. Abbreviations: Mig = migmatite; others as in Fig. 6.4.

### 6.2.3. Oxygen isotope thermometry

In order to obtain additional independent constraints on the peak temperatures along the studied section, 9 samples were analysed for oxygen isotope thermometry. The isotopic fractionation between pairs of mineral phases is a function of the temperature of equilibration, and it is independent of the pressure. For this study, we have analysed quartz–garnet, quartz–kyanite and garnet–sillimanite mineral pairs, inasmuch as these phases are the more likely to retain peak isotopic compositions even in high-grade rocks (e.g. Moecher and Sharp, 1999; Vannay et al., 1999). The mineral separation and analytical procedures follow the approach presented in Vannay et al. (1999). The analyses were performed at the laboratories of stable isotope geochemistry at the universities of Lausanne and New Mexico (Albuquerque).

The isotopic compositions of the studied minerals are presented in Table 6.2 and Fig. 6.16. The  $\delta^{18}\text{O}$  values of quartz, garnet, and aluminosilicates are comparable with the isotopic compositions obtained by Vannay et al. (1999) for the HHCZ of the Sutlej Valley, about 150 km to the SE. These results indicate that the HHCZ preserved a characteristic isotopic composition over large distances, despite high-grade metamorphism. This isotopic composition most likely reflects the composition of the pre-metamorphic protolith and its preservation implies a lack of significant



isotopic resetting through interaction with an externally-derived (e.g. meteoric) fluid flow. The quartz-garnet and quartz-aluminosilicates fractionations are indicative of isotopic equilibration at

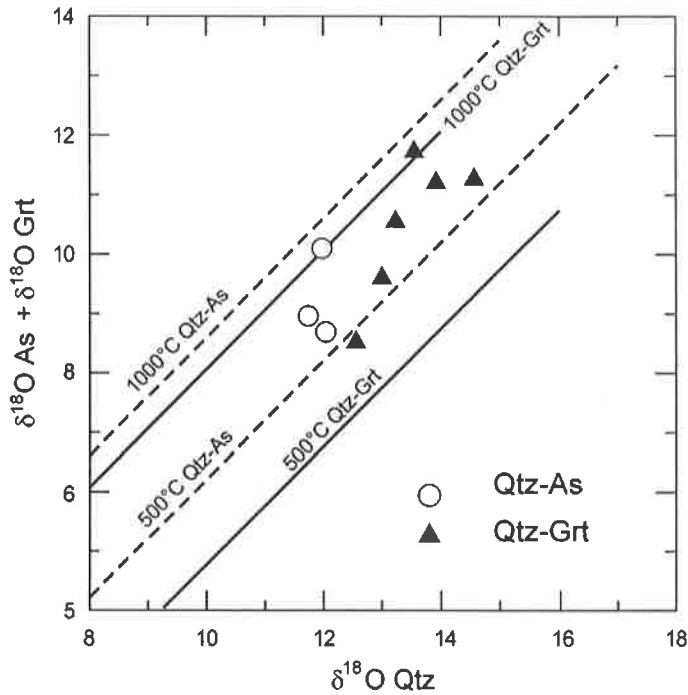


**Fig. 6.16.**  $\delta$ - $\delta$  graph for the Qtz-Grt and Qtz-As oxygen isotopic fractionations recorded in the studied samples. Temperatures based on the temperature coefficients of fractionation of Sharp (1995).

high temperatures, most likely reflecting peak conditions (Fig. 6.16). The isotopic fractionation temperatures are presented in Table 6.3, and they are reported as a function of the structural position of the samples in the studied section in Fig. 6.15. These temperatures were calculated from the  $\delta^{18}\text{O}$  values using the relation:

$$10^3 \ln \alpha (x-y) = a_{xy} 10^6 / T^2$$

where  $10^3 \ln \alpha (x-y)$  is the fractionation between two phases x and y,  $a_{xy}$  is the temperature coefficient of fractionation, and T is the temperature in Kelvin. The temperature coefficients of fractionation used in this study are:  $\alpha_{\text{Qtz-As}} = 2.25 \pm 0.2$ ,  $\alpha_{\text{Qtz-Grt}} = 3.1 \pm 0.2$  and  $\alpha_{\text{Sil-Grt}} = 0.85 \pm 0.2$  (Sharp 1995).

**Table 6.2. Oxygen isotopic compositions of analysed minerals.**

| nbr | Samples   | $\delta^{18}\text{O}$ (SMOW) [‰] |              |              |       |
|-----|-----------|----------------------------------|--------------|--------------|-------|
|     |           | Qtz                              | Grt          | Ky           | Sil   |
| 17  | RM 98/44  | 11.75 ± 0.03                     |              | 9.04 ± 0.07  |       |
| 18  | RM 98/46  | 11.99 ± 0.02                     |              | 10.10 ± 0.21 |       |
| 4   | RM 98/41  | 12.32 ± 0.27                     |              | 8.69 ± 0.04  |       |
| 7   | RM 98/77  | 13.01 ± 0.07                     | 9.65 ± 0.07  |              |       |
| 8   | RM 98/84  | 13.55 ± 0.05                     | 11.77 ± 0.06 |              | 12.53 |
| 10  | RM 98/93  | 13.93 ± 0.05                     | 11.25 ± 0.00 |              |       |
| 19  | RM 98/86  | 13.24 ± 0.12                     | 10.60 ± 0.64 |              |       |
| 12  | RM 98/87  | 14.57 ± 0.16                     | 11.82 ± 0.05 |              |       |
| 16  | RM 98/116 | 12.57 ± 0.04                     | 8.57 ± 0.04  |              |       |

**Note:** The average  $\delta^{18}\text{O}$  values relative to Standard Mean Ocean Water (SMOW) are based on two analyses (only one for Sil data). Reproducibility corresponds to 1 $\sigma$  standard deviation.

Most of the oxygen isotope thermometry results are consistent with the predictions of the petrogenetic grid for the stability of the studied metamorphic assemblages. Although quartz-garnet and quartz-sillimanite pairs from sample 5 yielded unrealistically high temperatures, a consistent temperature is obtained from the garnet-sillimanite isotopic fractionation (Table 3). This discrepancy suggests that the quartz in this sample is not in isotopic equilibrium with the other phases, probably as a consequence of isotopic resetting during cooling. Except for two samples (samples 2 and 9), the temperatures of isotopic fractionation generally show a very good agreement with the temperatures obtained by multiple-equilibria thermometry using THERMOCALC (Fig. 6.15). This consistency between results obtained by independent methods confirms that the calculated temperatures represent close estimates of peak conditions in the studied assemblages.

**Table 6.3. Oxygen isotope thermometry results for the Miyar Valley section.**

| <i>nbr</i> | Samples   | Temperatures [°C] |           |                  |           |
|------------|-----------|-------------------|-----------|------------------|-----------|
|            |           | Qtz - Grt         | Qtz - Ky  | Qtz - Sil        | Grt - Sil |
| 17         | RM 98/44  |                   | 643 ± 30  |                  |           |
| 18         | RM 98/46  |                   | 823 ± 120 |                  |           |
| 4          | RM 98/41  |                   | 519 ± 60  |                  |           |
| 7          | RM 98/77  | 693 ± 30          |           |                  |           |
| 8          | RM 98/84  | <i>1058 ± 60</i>  |           | <i>1228 ± 70</i> | 791       |
| 10         | RM 98/93  | 810 ± 20          |           |                  |           |
| 19         | RM 98/86  | 817 ± 270         |           |                  |           |
| 12         | RM 98/87  | 796 ± 70          |           |                  |           |
| 16         | RM 98/116 | 612 ± 10          |           |                  |           |

**Note:** Temperatures calculated from the isotopic compositions in Table 6.2, using the calibrations of Sharp (1995). Uncertainties correspond to  $2\sigma$  precision, calculated through standard error propagation procedure. The unrealistically high temperatures in italics reflect isotopic disequilibrium.

These results demonstrate that the metamorphic field gradient in the Miyar section is associated with a peak temperature increase from c. 500 to 750 °C, from the garnet to the migmatite zones (Fig. 6.15). The peak conditions in the migmatite zone appear to remain constant around  $800 \pm 50$  °C, in good agreement with the muscovite-dehydration melting conditions of Himalayan metapelites determined experimentally by Patiño-Douce & Harris (1998; Figs. 6.4 and 6.14). It is interesting to note that, compared to the overlying lower-grade zones, no further temperature increase is observed in the migmatite zone. As in other Himalayan sections (e.g. Pognante et al., 1987; Pognante and Lombardo, 1989; Pognante et al., 1990; Dèzes et al., 1999; Vannay et al., 1999), the maximum temperatures in the muscovite-bearing migmatites of the Miyar section appear to peak around 800°C (Fig. 6.15). We interpret this feature as the consequence of a thermal buffering controlled by the muscovite-dehydration melting.

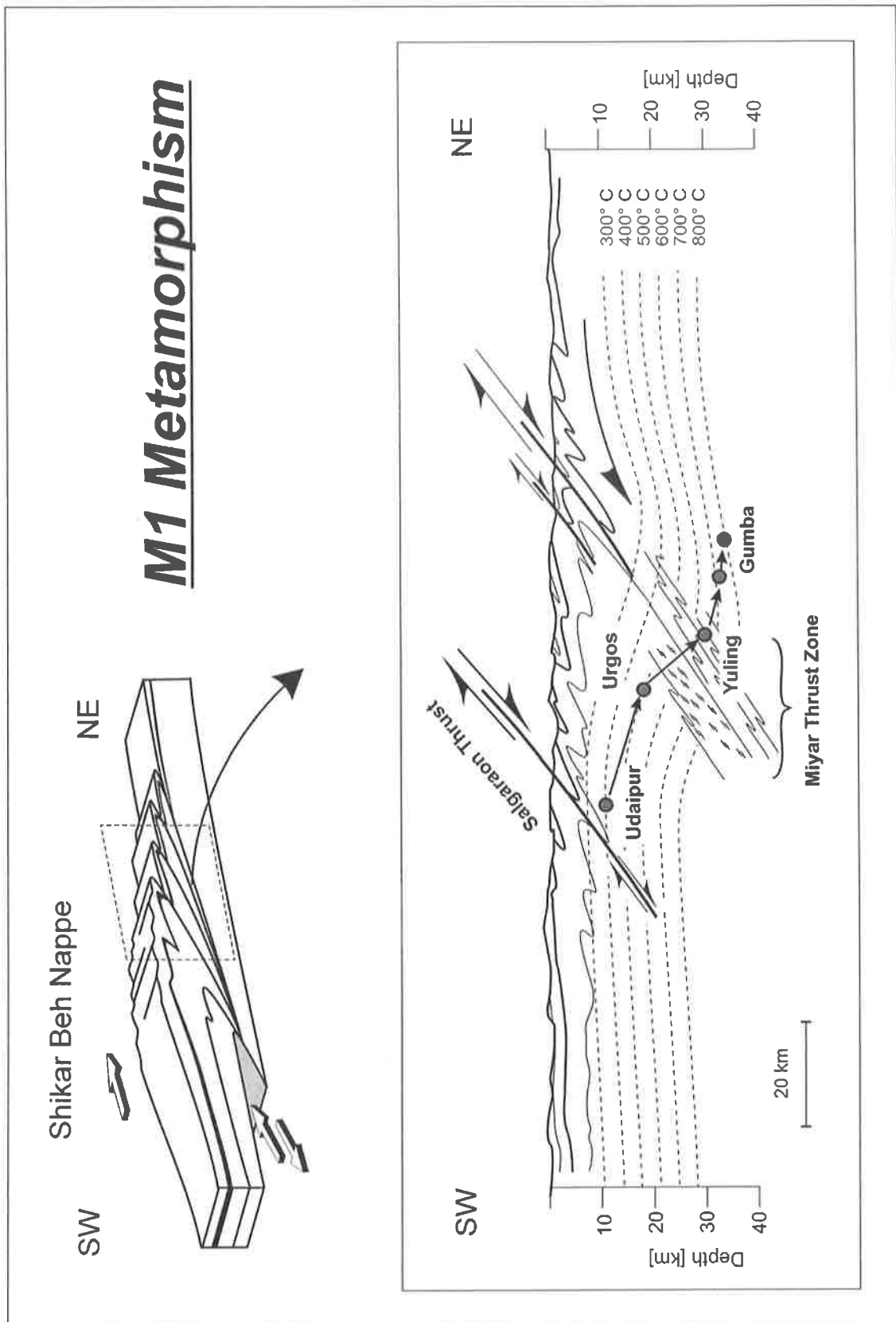


**Fig. 6.17:** Structural and thermal reconstruction for the P-T estimates of the M1 prograde Barrovian metamorphic peak conditions recorded by the metapelites from the Miyar Valley during the D1 NE-directed Shikar Beh nappe event. Temperature values are given in Table 6.1. Depth of equilibration assuming a lithostatic pressure gradient of 0.27 kbar/km. The isotherms are plotted assuming a vertical geothermal gradient of 28°C/km.

### 6.2.4. Discussion

A such Barrovian-type metamorphic field gradient, as testified by the petrographic analysis is generally the consequence of an orogenic metamorphism associated with a crustal thickening event. The presence of syntectonic garnet porphyroblasts, together with several other kinematic indicators, showing a NE-direction of rotation associates this prograde metamorphism with a crustal thickening related to the NE-directed Shikar Beh nappe emplacement. The structural observation together with the petrographic thermobarometric data indicate that the Miyar Thrust Zone represents the frontal structure of the early NE-directed Shikar Beh nappe (Fig 6.17).

### 6.2.5. Retrograde metamorphic evolution (M4)

In the Miyar section, the retrograde evolution in the footwall of the extensional Khanjar Shear Zone is well recorded in the metapelites of the kyanite zone near Yuling (Fig. 6.18). The initial stage of the retrograde history is characterized by the appearance of sillimanite, growing as a fine-

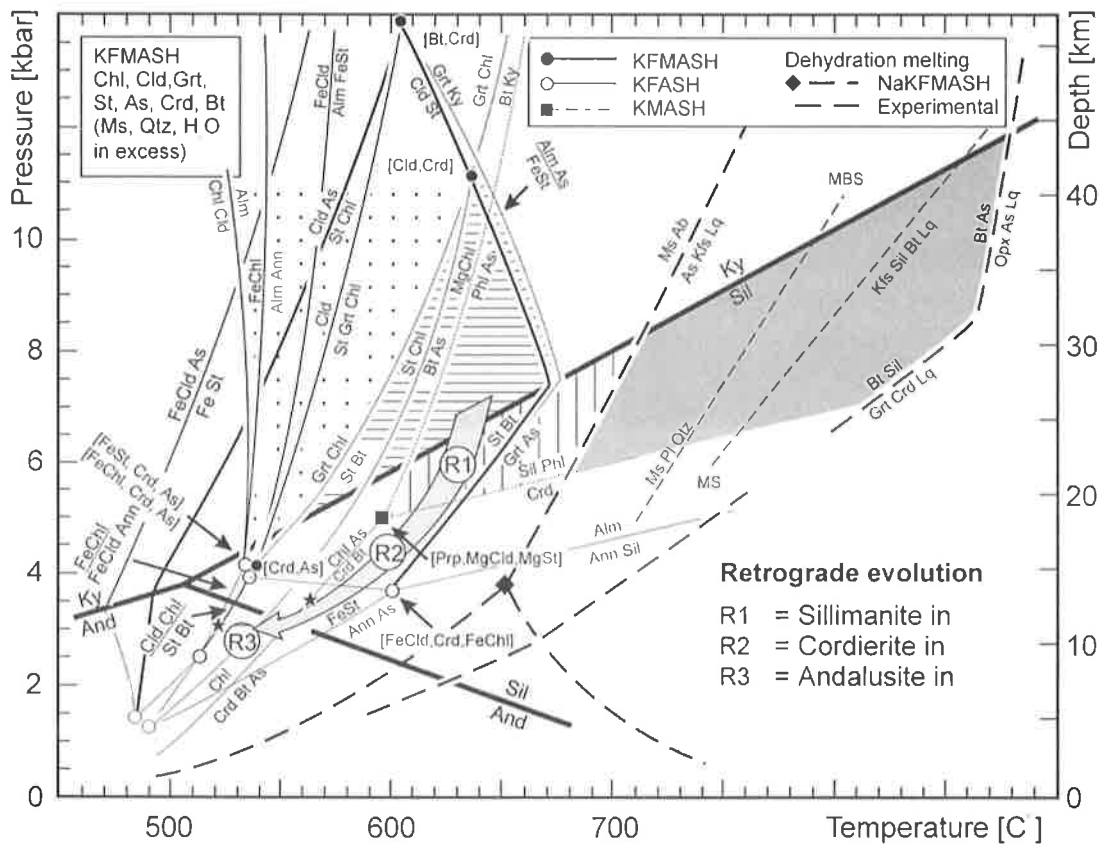


**Fig. 6.18:** Retrograde metamorphic evolution for the HHCZ of the Miyar Valley, reported in a KFMASH petrogenetic grid for metapelites. All reactions calculated according to the thermodynamic database of Holland and Powell (1998), except the partial melting reactions. The muscovite dehydration reactions labelled "MBS" and "MS" correspond to the experimentally-determined partial melting conditions for muscovite + biotite bearing and muscovite-bearing Himalayan metapelites, respectively (Patiño-Douce and Harris, 1998). The additional muscovite and biotite dehydration melting reactions are taken from Spear et al. (1999). This retrograde metamorphic evolution of the kyanite + staurolite zone assemblages is deduced from textural relations (see text). See Fig. 6.2 for sampling locations. Abbreviations: Alm = almandine; And = andalusite; Ann = annite; As = aluminosilicate; Bt = biotite; Chl = chlorite; Cld = chloritoid; Crd = cordierite; Grt = garnet; Kfs = K-feldspar; Ky = kyanite; Lq = liquid (melt); Ms = muscovite; Opx = orthopyroxene; Phl = phlogopite; Prp = pyrope; Sil = sillimanite; St = staurolite.

grained fibrolite on biotite or at the expense of kyanite (Fig. 6.19a). Cordierite is relatively abundant in some samples, where it grew as post-kinematic poikiloblasts, sometimes surrounding kyanite (Fig. 6.19b). A later stage of the retrograde evolution is recorded in some samples by the growth of andalusite as the stable aluminosilicate (Fig. 6.19c). In staurolite-bearing assemblages, staurolite generally remains stable.

The gradual succession of high-T / low-P mineral phases indicates consequently a retrograde evolution characterized by an initial stage of nearly isothermal decompression and followed by a more significant cooling (Fig. 6.18). Such a retrograde P-T path is typical of a tectonically-controlled, rapid exhumation of high-grade rocks. In the Miyar section, the exhumation of the HHCZ and the formation of retrograde mineral assemblages was largely controlled by the deformation in the Khanjar Shear Zone, as indicated by the preferential growth of fibrolitic sillimanite on the shearing surfaces of extensional C/S fabrics related to this detachment.

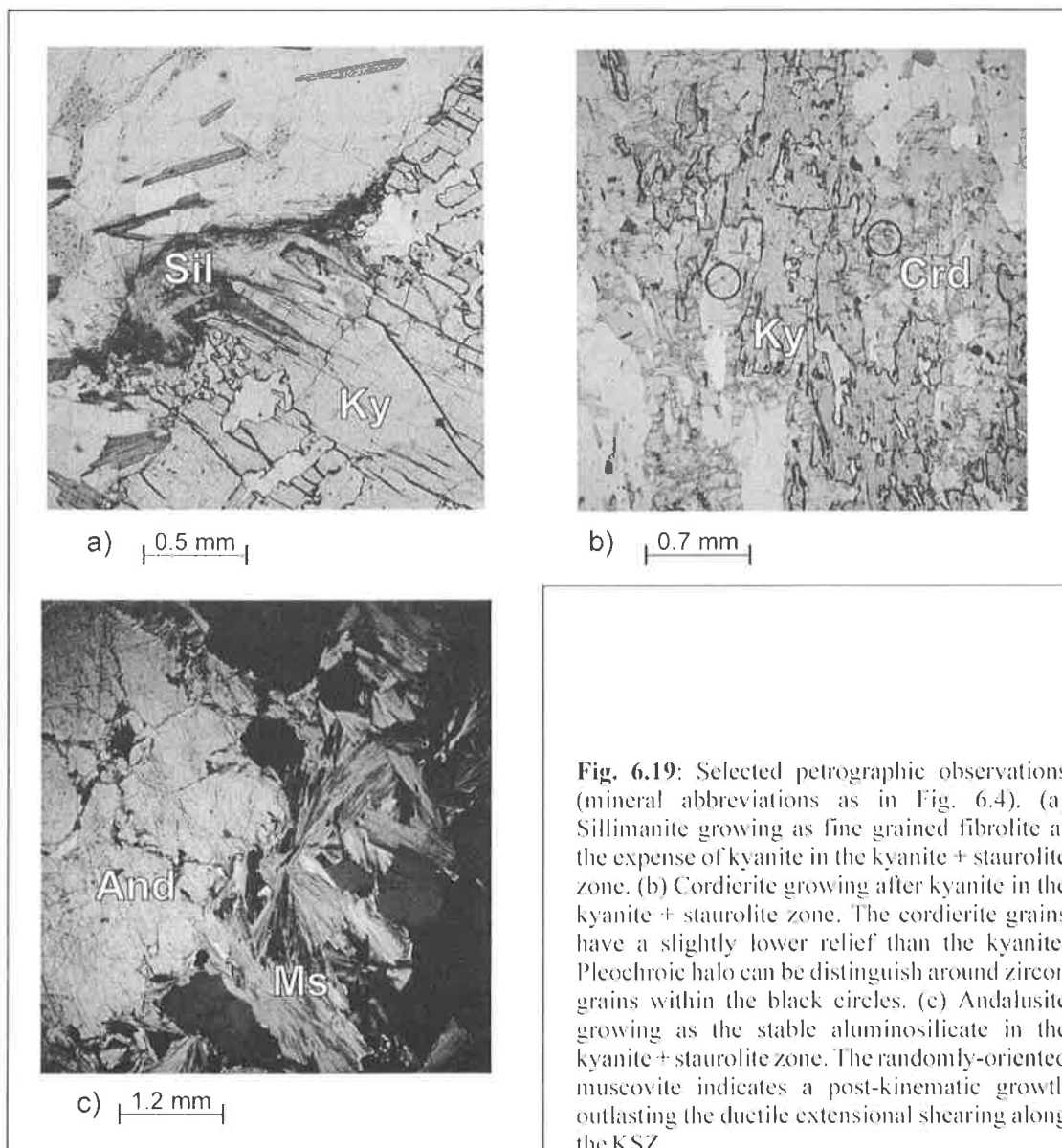


**Fig. 6.19:** Selected petrographic observations (mineral abbreviations as in Fig. 6.4). (a) Sillimanite growing as fine grained fibrolite at the expense of kyanite in the kyanite + staurolite zone. (b) Cordierite growing after kyanite in the kyanite + staurolite zone. The cordierite grains have a slightly lower relief than the kyanite. Pleochroic halo can be distinguish around zircon grains within the black circles. (c) Andalusite growing as the stable aluminosilicate in the kyanite + staurolite zone. The randomly-oriented muscovite indicates a post-kinematic growth outlasting the ductile extensional shearing along the KSZ.

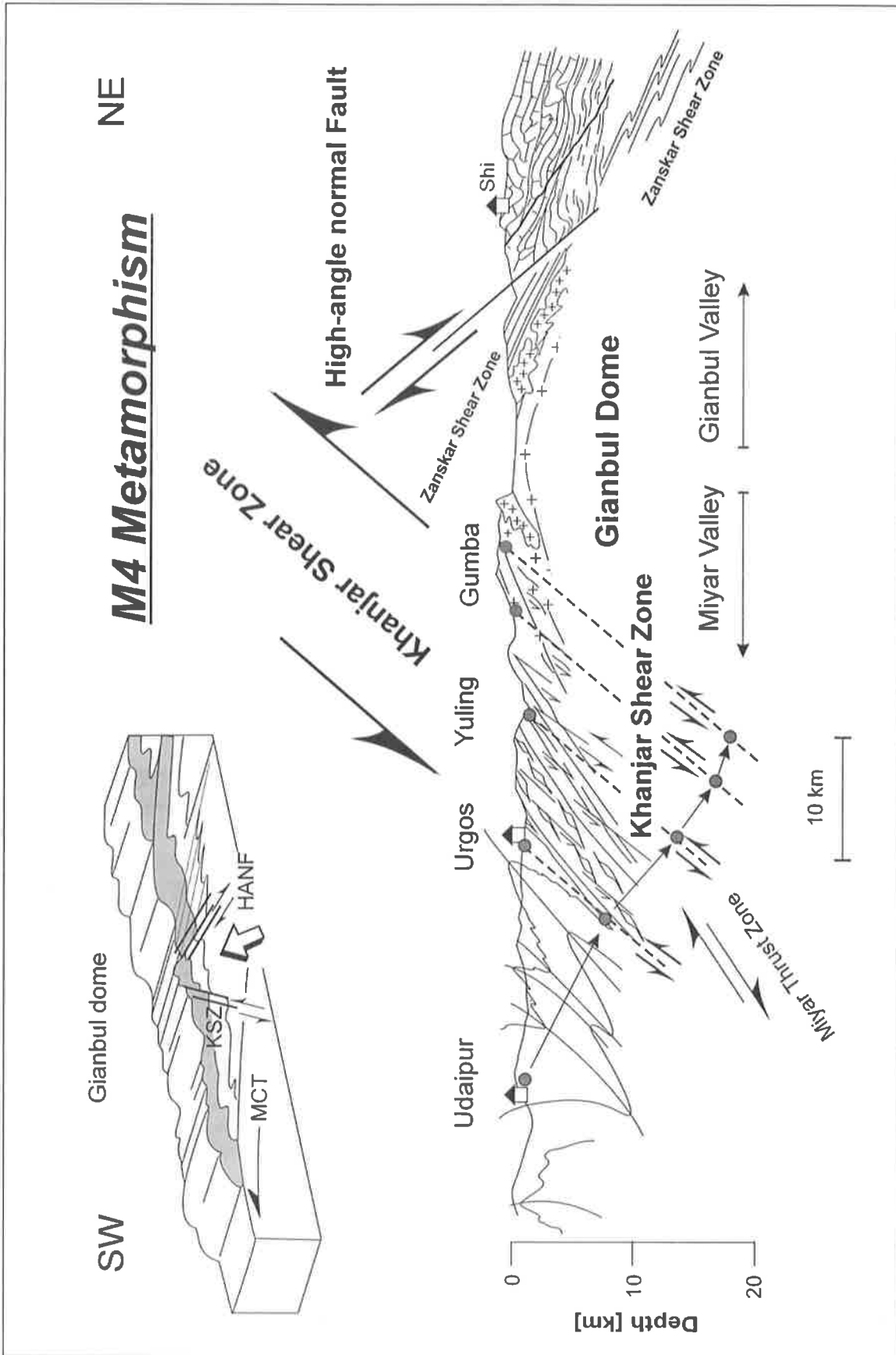


Fig. 6.20: Structural and thermal reconstruction for the M4 retrograde metamorphic conditions recorded by the metapelites from the Miyar Valley during the D4 doming phase.

### 6.3. GIANBUL VALLEY SECTION

The NE half of the Gianbul dome has been investigated by Dèzes (1999) and Dèzes et al. (1999) in the Gianbul Valley. The main structure in this later section is the Zaskar Shear Zone, which marks the transition between the high-grade metamorphic rocks of the Gianbul dome and the low-grade sediments of the Tethyan Himalaya to the NE (Figs 6.2 and 6.3). The tectono-metamorphic history in the Gianbul section is the consequence of two main events: (1) an initial phase of crustal thickening related to the emplacement of the SW-directed Nyimaling – Tsarap nappe; and (2) the subsequent exhumation of the HHCZ as a consequence of NE-directed extension along the Zaskar Shear Zone and of later doming.

#### 6.3.1. SW-directed Nyimaling –Tsarap nappe and prograde metamorphism (M2)

To the NE of the studied area, the Nyimaling-Tsarap nappe is responsible for the SW-directed transport of the low-grade sediments of the Tethyan Himalaya (Fig. 5.1; Steck et al., 1993). In contrast to what is observed in the Miyar Valley, syn-kinematic garnet and staurolite blasts in the HHCZ of the Gianbul Valley indicate a prograde metamorphism associated with a top-to-the-SW shearing (Dèzes, 1999). Consequently, the regional Barrovian metamorphism and partial melting observed in the HHCZ of the Gianbul Valley is interpreted as the consequence of the burial of this unit toward the NE, beneath the frontal part of the Nyimaling-Tsarap nappe (Fig. 6.2; Dèzes, 1999). The metamorphic field gradient in the HHCZ of the Gianbul Valley is characterized by a superposition of migmatite, sillimanite, kyanite, and garnet mineral zones, indicating a gradual and rapid decrease in metamorphic peak conditions toward the NE (Fig. 6.3).

**Table 6.4. Average peak P-T estimates for the Gianbul Valley section.**

| Sample | Assemblage          |  | T(°C) | ST  | P(kbar) | δP  | Corr  | sigfit | n | XH <sub>2</sub> O |
|--------|---------------------|--|-------|-----|---------|-----|-------|--------|---|-------------------|
|        | Qtz + Pl + Bt + Grt |  |       |     |         |     |       |        |   |                   |
| G3     | + Ms                |  | 567   | 93  | 6       | 1.4 | 0.8   | 0.46   | 4 | 1                 |
| S1     | + Ms + Std          |  | 562   | 86  | 6.7     | 1.4 | 0.74  | 0.52   | 4 | 1                 |
| K1     | + Ms                |  | 584   | 108 | 6.7     | 1.8 | 0.827 | 0.51   | 5 | 1                 |
| K2     | + Ms + Ky           |  | 634   | 89  | 7.7     | 1.5 | 0.805 | 0.37   | 5 | 1                 |
| K3     | + Ms + Ky           |  | 661   | 92  | 8.3     | 1.6 | 0.788 | 0.64   | 5 | 1                 |
| M1     |                     |  | 820   |     | 11.8    |     |       |        |   |                   |

**Note:** P-T conditions recalculated after Dèzes (1999). Procedure as in Table 1. The results for sample M1 were calculated with TWQ (Berman, 1991; Dèzes, 1999). Abbreviations as in Table 1.

The P-T conditions associated with the prograde metamorphic field gradient in the Gianbul section are summarised in Table 6.4 and presented in the petrogenetic grid of Fig. 6.21. The thermobarometry results for the samples of the garnet, staurolite, kyanite and migmatite zones are generally consistent with the predictions of the KFMASH petrogenetic grid for the stability of these mineral assemblages, considering a nominal average precision of  $\pm 50^\circ\text{C}$  and  $\pm 1$  kbar. These P-T estimates define a coherent and continuous Barrovian metamorphic field gradient, characterized by peak conditions increasing from c.  $560^\circ\text{C}$  and 6 kbar in the garnet zone, to c.  $820^\circ\text{C}$  and 11.8 kbar in the migmatite zone. The shearing of isograds at the NE border of the

Gianbul dome indicates that the frontal thrust zone of the Nyimaling-Tsarap nappe has been reactivated as an extensional structure called the Zaskar Shear Zone.

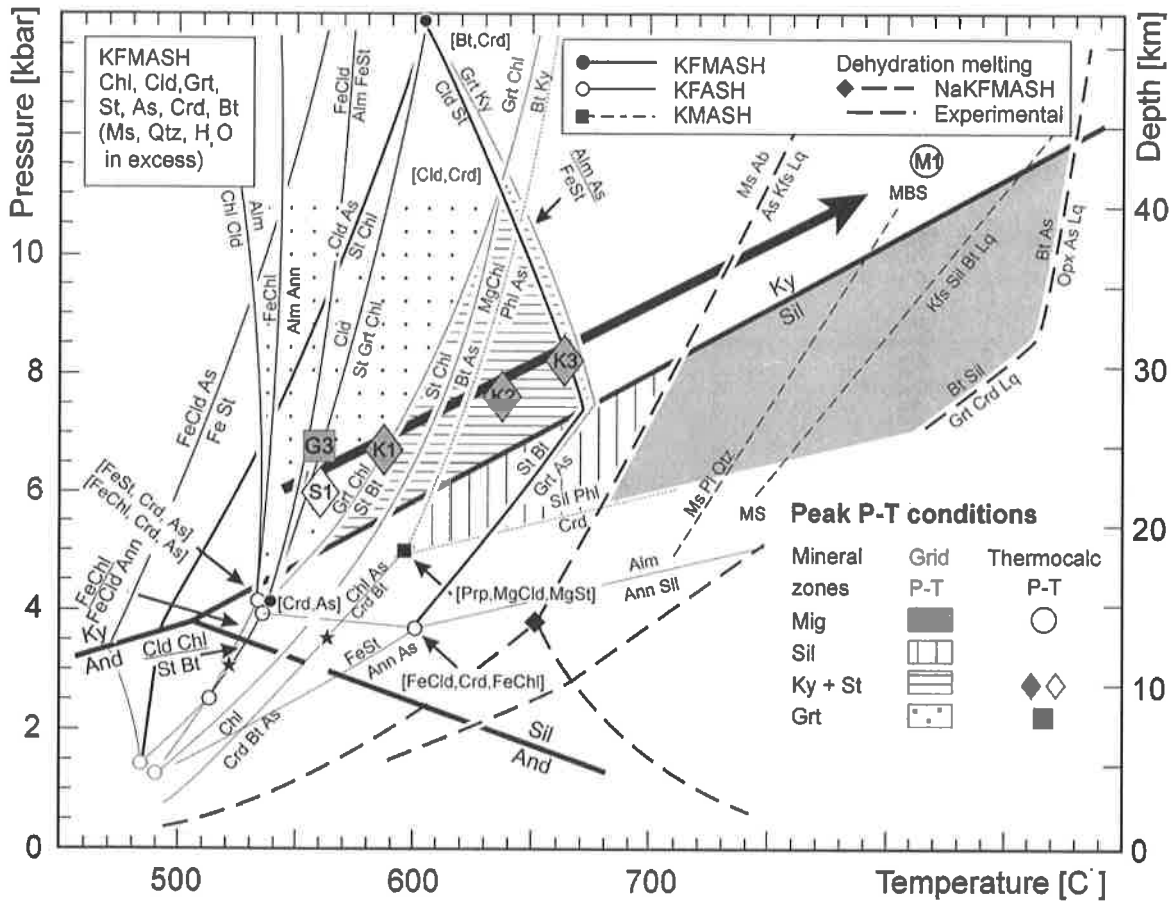


**Fig. 6.21:** Peak metamorphic conditions in the Gianbul Valley section (transect B-C on fig 6.2) recalculated after Dèzes (1999) and reported in a KFMASH petrogenetic grid (reactions as in Fig. 6.4). The black arrow represents the metamorphic field gradient based on the results presented in Table 6.4. The thermobarometry results for the samples G3, S1, K1, K2, and K3 were recalculated from the chemical analyses presented in Dèzes (1999), using THERMOCALC version 2.75 (Powell and Holland, 1994). The P-T conditions for M1 sample were calculated using TWQ (Berman, 1991; Dèzes, 1999).

### Discussion

Thermobarometry results indicate peak conditions evolving from 650°C / 7 kbar for the kyanite zone to 800°C / 12 kbar for the migmatite zone. Sigmoidal inclusion trails in M2 garnets porphyroblasts indicate a syntectonic growth during a SW-directed shearing. These observations imply that the M2 prograde metamorphism in the northern limb of the Gianbul dome is the consequence of a SW-directed crustal thickening, in contrast to the M1 tectono-metamorphic evolution in the southern limb of the dome. The M2 crustal thickening phase most likely reflects the underthrusting of the High Himalayan Crystalline Zone beneath the frontal part of the SW-directed Nyimaling – Tsarap nappe affecting the sedimentary series of the Tethyan Himalaya (Fig. 6.22).



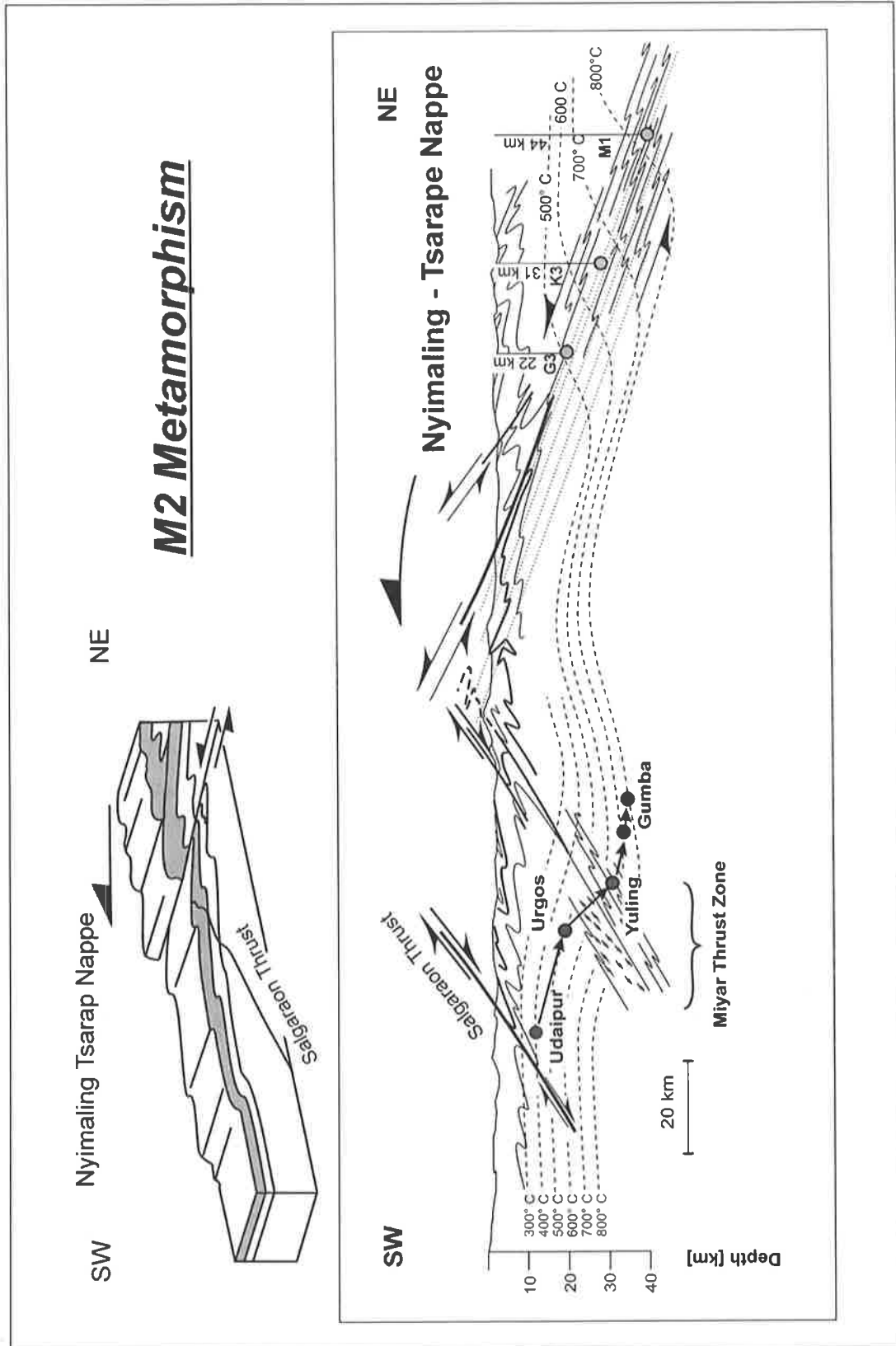


**Fig. 6.22:** Structural and thermal reconstruction for the P-T estimates of the M2 prograde Barrovian metamorphic peak conditions recorded by the metapelites from the Gianbul Valley during the D2 SW-directed Nyimaling-Tsarape nappe event. Temperature values are given in Table 6.4. Depth of equilibration assuming a lithostatic pressure gradient of 0.27 kbar/km. The isotherms are plotted assuming a vertical geothermal gradient of 28° C/km.

### 6.3.2. Zaskar Shear Zone and retrograde metamorphism (M3)

The extensional Zaskar Shear Zone (ZSZ) represents one of the most spectacular example of syn-convergence extension in the Himalaya (Gilbert, 1986; Herren, 1987; Dèzes, 1999; Dèzes et al., 1999). In the Gianbul section, the ZSZ corresponds to a c. 1 km thick mylonitic zone, separating the paragneiss of the HHCZ from the overlying low-grade sediments of the Tethyan Himalaya (Figs 6.2 and 6.3). Metamorphic isograds are sheared along the ZSZ and the kyanite to garnet isograds are now condensed within a 1 km thick section. The peak pressure difference of c. 5.8 kbar between the garnet and migmatite zones (samples G3 and M1, Fig. 6.22) indicates that c. 20 km of vertical shortening has been accommodated across the ZSZ. For the present-day dip of the structure (c. 20°), this estimate translates to an extensional slip about 60 km (Dèzes et al., 1999).

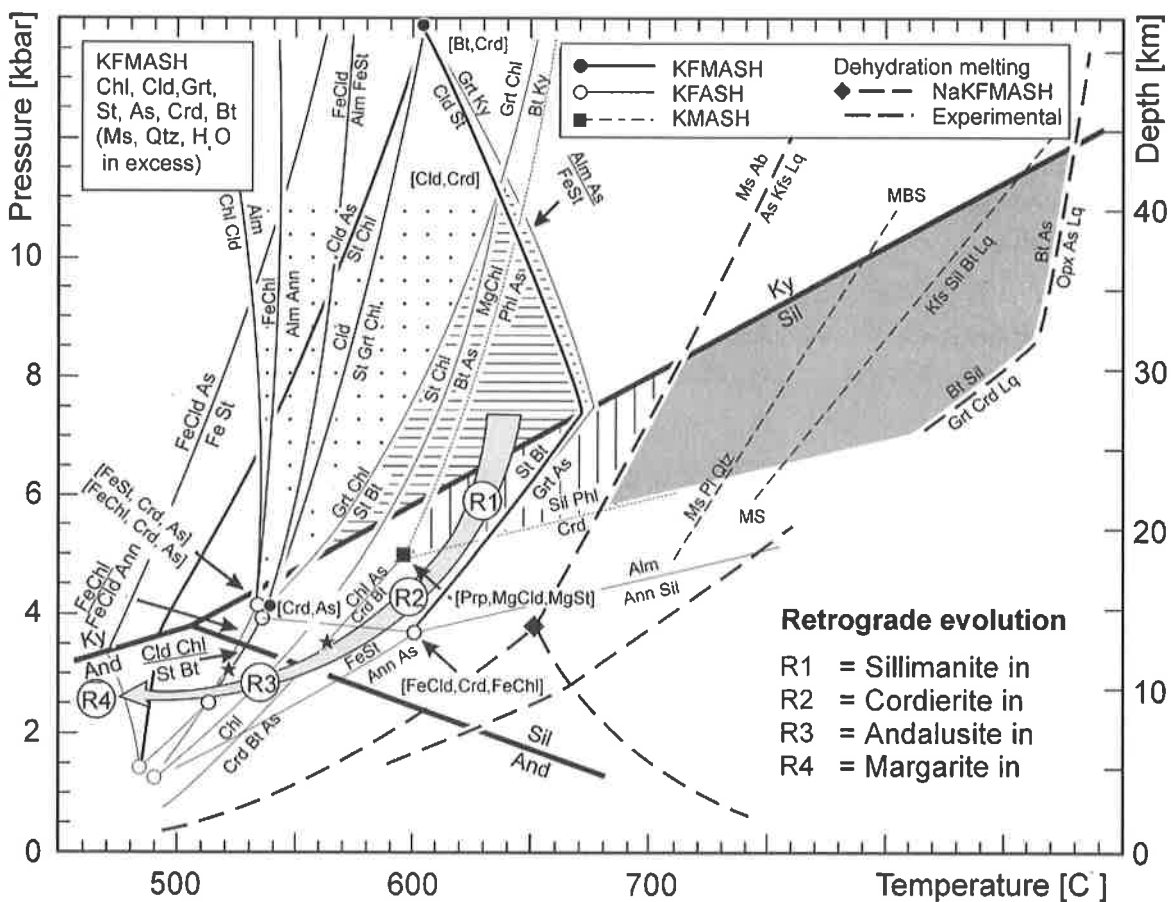


**Fig. 6.23:** Retrograde metamorphic evolution for the HHCZ of the Gianbul Valley, reported in a KFMASH petrogenetic grid for metapelites. This retrograde metamorphic evolution of the kyanite + staurolite zone assemblages is deduced from textural relations described by Dèzes (1999) (see text) (reactions as in Fig. 6.4). See Fig. 6.2 for sampling locations.

The retrograde metamorphic evolution recorded in HHCZ rocks of the Gianbul section testifies to a rapid exhumation controlled by extension along the ZSZ. This retrograde metamorphism M3, well preserved in the metapelites of the kyanite zone, is characterized by an initial phase of nearly isothermal decompression marked by the gradual appearance of fibrolitic sillimanite, cordierite,

and andalusite (Fig. 6.23; Dèzes, 1999). Geochronological results confirm a rapid extension, as they indicate that ductile shearing along the ZSZ occurred in less than  $2.4 \pm 0.2$  My, between  $22.2 \pm 0.2$  Ma and  $19.8 \pm 0.1$  Ma (Dèzes, 1999; Dèzes et al., 1999). The post-kinematic growth of andalusite with respect to the extensional structures suggests that by the end of ductile extension about 19 My ago, the samples of the Gianbul section were regrouped at a comparable structural level at a depth shallower than 10 km (Dèzes, 1999).

Early Miocene extension along the ZSZ, as well as along several other segments of the South Tibetan Detachment System (STDS), was coeval with thrusting along the MCT (Hodges et al., 1992; Coleman, 1998; Dèzes et al., 1999). To the S of the studied area, SW-directed thrusting of the HHCZ along the MCT was responsible for the creation of the High Himalayan nappe in the Kulu Valley ( Crystalline Nappe; Frank et al., 1977; Epard et al., 1995) (Fig.6.24). In the Miyar valley, this tectonic phase did not induce any major structures, although it provoked the overturning towards the south of the axial surfaces of the NE-verging folds associated with the Shikar Beh nappe (Fig. 2; Steck et al., 1999).

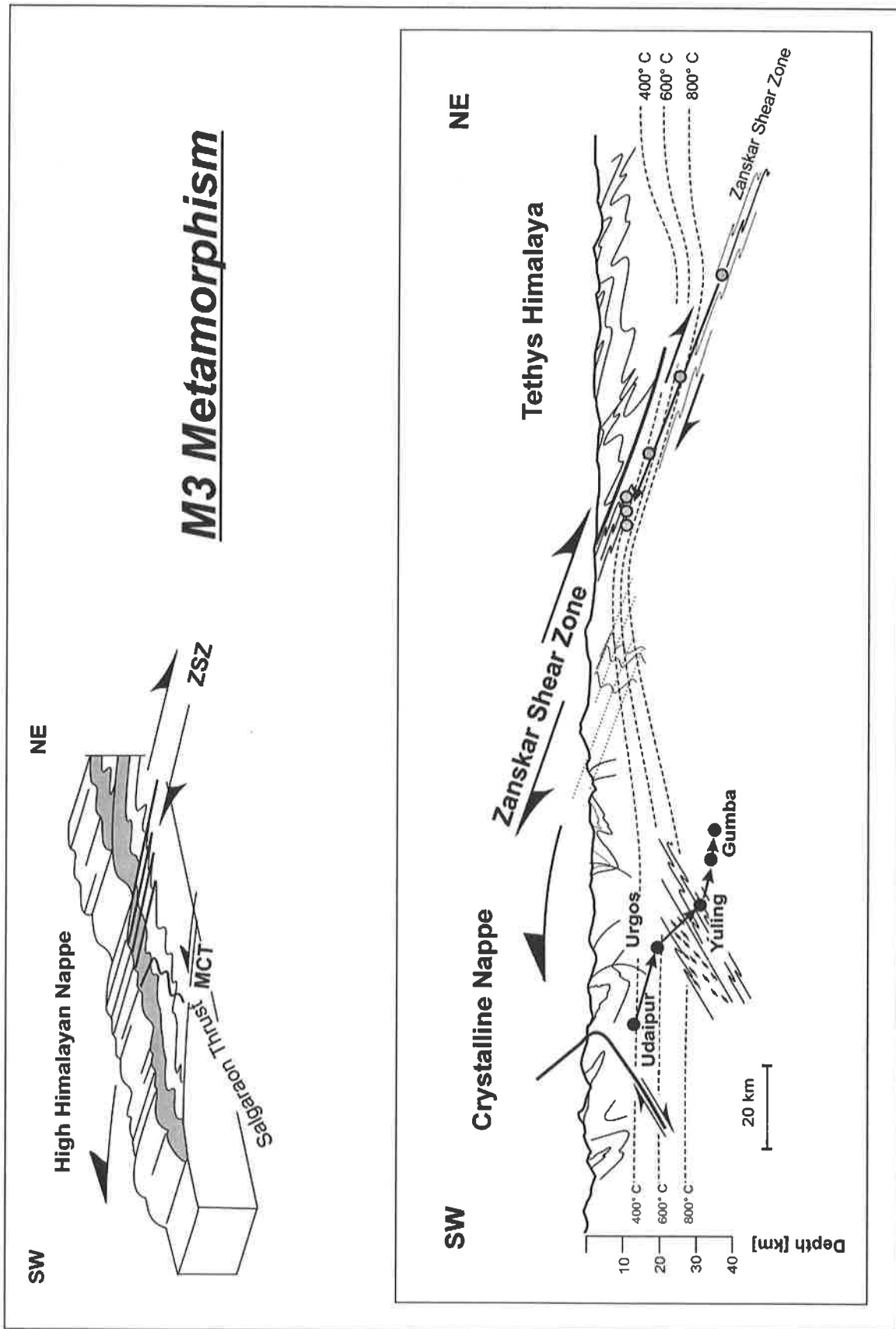


**Fig. 6.24:** Structural and thermal reconstruction for the M3 retrograde metamorphism conditions recorded by the metapelites from the Miyar Valley during the D3 exhumation phase of the High Himalayan Crystalline Zone of Zaskar

## **6.4. SYNTHESIS**

The petrographic and quantitative P-T results for the Miyar section (Figs 6.14, 6.15, and 6.18) and for the Gianbul section (Figs. 6.24 and 6.26; Dèzes et al., 1999) provide informations about the depth of burial of the studied samples, as well as about the thermal structure during the tectonic evolution of a complete transect across the Gianbul dome. On the other hand, the mapping and structural analysis of this transect (Dèzes, 1999; Dèzes et al., 1999; Steck et al., 1999) constrain its kinematic evolution. These various data can be combined to propose a semi-quantitative reconstruction of the tectono-metamorphic evolution across the Gianbul dome (Fig. 6.25).

At the onset of the India-Asia continental collision during Eocene (c. 55-50 Ma; Patriat and Achache, 1984), the passive margin of the north Indian plate was covered by a 10 to 15 km thick sedimentary sequence, intruded by Cambro-Ordovician granitic plutons (e.g. Steck et al., 1993). The first tectonic event affecting the Indian margin corresponded to an early phase of crustal thickening related to NE-directed tectonic movements (Fig. 6.27a). This D1 phase most likely took place during Early to Middle Eocene, and it led to the creation of the Shikar Beh nappe, thrusting toward the NE along the Miyar Thrust (Steck et al., 1993; 1999). As a consequence of the prograde Barrovian metamorphism M1 induced by this crustal thickening event, detrital sediments and intrusive granites at the base of the Tethyan Himalaya were gradually transformed into the paragneiss and orthogneiss now forming part of the HHCZ. Beneath the Miyar thrust, the rocks were subducted down to c. 30 km depth, where temperatures up to 750-850°C triggered partial melting (Fig. 6.14).

Between Middle Eocene and Late Oligocene, a second phase of crustal thickening was related to the SW-directed thrusting of the Nyimaling-Tsarap nappe (Fig. 6.25a). The sediments subducted beneath the frontal part of the Nyimaling-Tsarap nappe were transformed into more high-grade HHCZ paragneiss during the prograde Barrovian metamorphism M2 induced by this D2 tectonic phase. Some of these paragneisses were migmatized during subduction, as a consequence of temperatures up to c. 800°C at depths down to c. 40 km (Dèzes et al., 1999). The activation of the MCT during Early Miocene (c. 23 Ma; e.g. Frank et al., 1977; Hubbard and Harrison, 1989; Coleman, 1998) marked the onset of the tectonically-controlled exhumation of the HHCZ paragneisses and migmatites (Fig. 6.25b). In the studied transect, SW-verging folding superposed on the initial NE-verging structures of the Shikar Beh nappe testifies to the foreland-directed thrusting of the HHCZ along the MCT during this D3 phase. Syn-MCT exhumation of the HHCZ was also accompanied by c. 60 km of extension along the ZSZ, at the top of the unit, between c. 22.2 and 19.8 Ma (Dèzes, 1999; Dèzes et al., 1999). As a consequence of a nearly isothermal decompression caused by this rapid exhumation, the top of the HHCZ was affected by high-T / low-P metamorphic conditions (Fig. 6.25b). This M3 retrograde metamorphism was also accompanied by decompression melting, leading to the intrusion of granitic dykes and small plutons beneath the ZSZ.

The last tectonic phase D4 affecting the studied transect corresponds to the creation of the Gianbul dome (Fig. 6.25c). This phase probably occurred shortly after the activation of the ZSZ during Early Miocene. The doming was also associated with further extension along the Khanjar Shear Zone in the Miyar Valley. Rapid exhumation of the HHCZ in the footwall of the Khanjar Shear Zone induced a retrograde metamorphism M4, characterized by high-T / low-P conditions reached during a nearly isothermal decompression (Fig. 6.18).

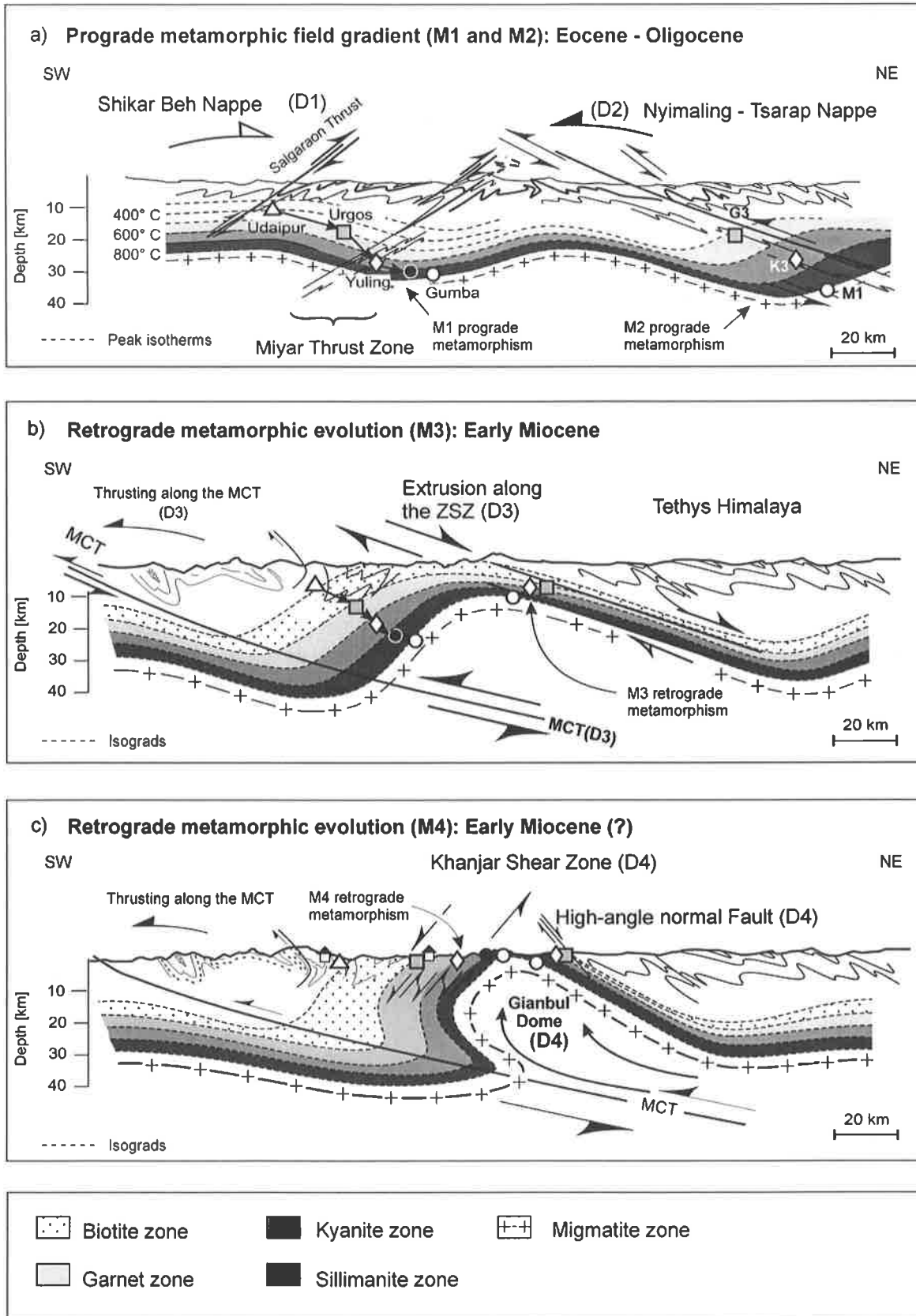


**Fig. 6.25.** Semi-quantitative reconstruction of the tectono-metamorphic evolution across the Gianbul dome, based on P-T data (Figs 6.4, 6.14, 6.18, and 6.23) and structural results. Temperature values are given in Table 6.1. Depth of equilibration assuming a lithostatic pressure gradient of 27 kbar/km.

## **6.5. CONCLUSIONS**

The tectono-metamorphic evolution of the HHCZ in the Lahul-Zaskar area can be decomposed in two important stages. The first stage corresponds to the crustal shortening, thickening and Barrovian metamorphism recorded by the sedimentary sequence of the India continental margin. This first event is related to the tectonic compression and overburden due to the collision between India and Asia at ca 50-55 Ma (Patriat and Achache 1984, Garzanti et al. 1987). The deformation consequent upon this event was accommodated by thrusting, folding and formation of both SW and NE-directed nappes (Fig. 26a and 26b). The second major phase which has affected this area is related to a syn-orogenic extension along extensional tectonic structures contributing to the exhumation of the high-grade metamorphic rocks of the High Himalayan Crystalline Zone along the MCT (Fig. 26c and 26b). This stage is expressed by the formation of ductile normal shearing, doming and brittle normal faulting. The exhumation of these deep rocks engendering the formation of the Gianbul dome (Dèzes 1999; Dèzes et al., 1999), seems to be controlled by a major syn-orogenic extensional structure, the Zaskar Shear Zone (ZSZ), which separates the High Himalayan Crystalline Zone from the low grade sediments of the Tethyan Himalayan to the NE. It appears thus that the tectono-metamorphic evolution of the HHCZ in SE Zaskar is associated with a complex tectonic history involving converging nappe structures (Shikar Beh and Nyimaling-Tsarap nappes) superimposed by opposite-directed extensional structures (ZSZ and KSZ). Consequently, although characterized by an apparently simple, symmetrical geometry and metamorphic zonation, the large-scale doming commonly observed in the HHCZ of Zaskar appear to be the consequence of a complex, polyphase tectono-metamorphic evolution composed by four major tectonic events with which are systematically associated a new distinct metamorphic history.

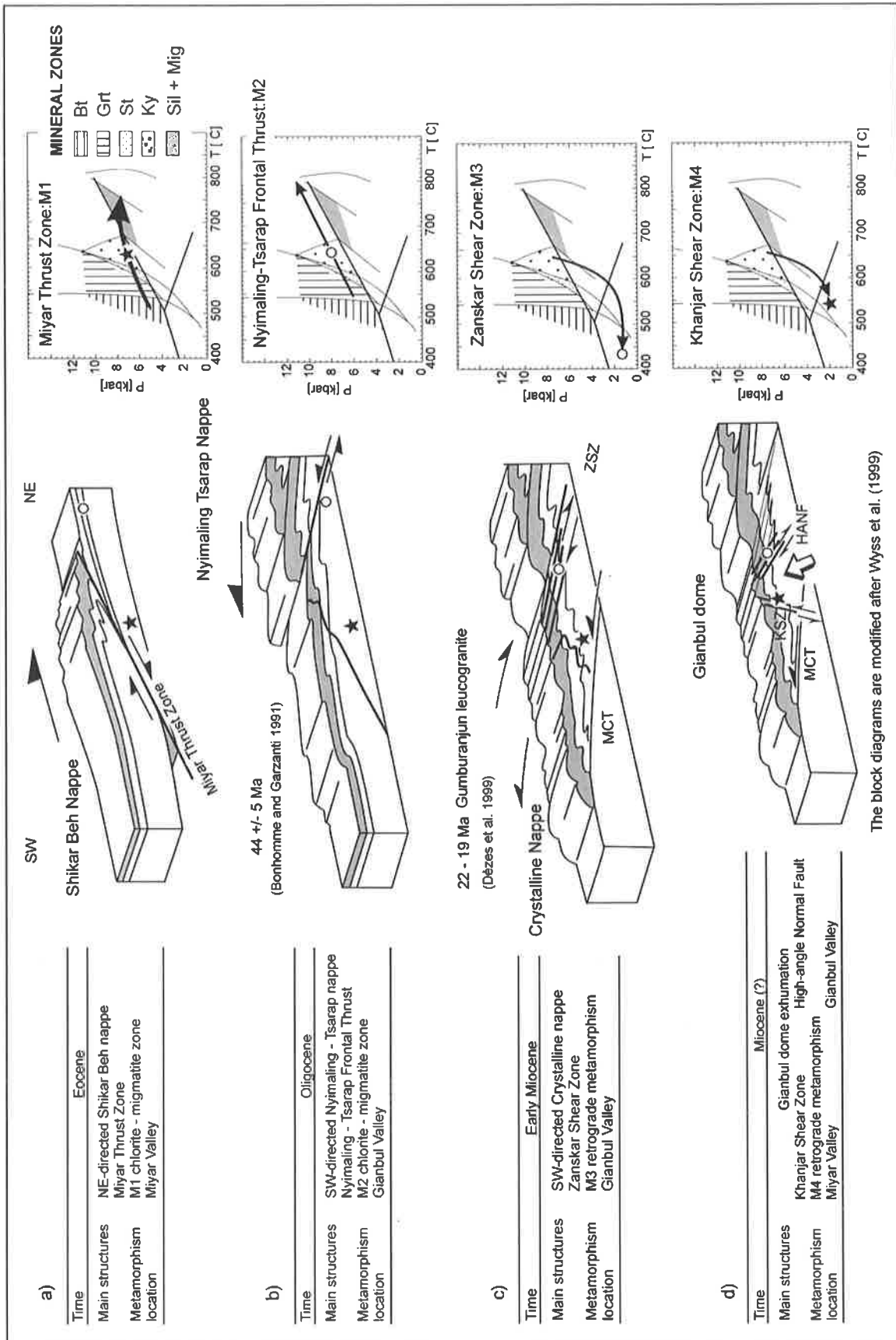


**Fig. 6.26:** Tectono-metamorphic model for the High Himalayan Crystalline Sequence in the Gianbul dome area. MCT = Main Central Thrust, ZSZ = Zanskar Shear Zone, KSZ = Khanjar Shear Zone, HANF = High-angle Normal Fault.



## **6.6. APPENDIX**

### ***Thermobarometry***

On the basis of textural evidence indicating equilibrium, 16 samples from the Miyar Valley section were selected for thermobarometry. Moreover, P-T estimates for 6 samples from the Gianbul Valley section were recalculated on the basis of their chemical analyses given in Dèzes (1999). The mineralogical assemblages for each sample are indicated in tables 1 and 2. The chemical compositions were measured at the University of Lausanne using a Cameca SX 50 electron microprobe. The analyses were performed with an acceleration voltage of 15 KV and a beam current of 30nA for garnet, 15nA for biotite, muscovite and hornblende, and 10nA for plagioclase. In order to calculate near-peak temperature estimates, the minimum Fe/(Fe + Mg) composition of each garnet was used for thermobarometry. To determine these minimum values, two composition traverses of 30-50 analyses across each garnet were systematically measured. For the other mineral phases, we measured about 10 analyses across each mineral to determine the mean composition. Representative garnet compositions at the Fe/(Fe+Mg) minimum, as well as biotite, muscovite, hornblende, and plagioclase mean compositions, are presented in Tables A1 to A4. Pressures and temperatures were calculated with the computer program THERMOCALC version 2.75 of Powell and Holland (1994). The paragonite activity calculated by the program being clearly inaccurate, we systematically withdrew this phase for the calculation of the P-T estimates.

Table A1

|                                |         | Garnet compositions at Fe/(Fe+Mg) minima |          |          |          |          |          |          |          |          |          |          |          |           |         |           |  |
|--------------------------------|---------|--|----------|----------|----------|----------|----------|----------|----------|----------|----------|----------|----------|-----------|---------|-----------|--|
| nr                             | 1       | 2  | 3        | 4        | 5        | 6        | 7        | 8        | 9        | 10       | 11       | 12       | 13       | 14        | 15      | 16        |  |
| Samples                        | RM 98/6 | AS 98/60                                 | RM 98/41 | RM 98/45 | RM 98/55 | RM 98/84 | RM 98/82 | RM 98/77 | RM 98/92 | RM 98/93 | RM 98/97 | RM 98/87 | RM 99/18 | AS 98/100 | MS 99-1 | RM 98/116 |  |
| SiO <sub>2</sub>               | 37.53   | 37.79                                    | 37.42    | 37.58    | 37.27    | 37.35    | 37.38    | 37.8     | 36.55    | 36.82    | 37.05    | 36.76    | 37.03    | 36.71     | 36.99   | 37.17     |  |
| TiO <sub>2</sub>               | 0.15    | 0.07                                     | 0.02     | 0.02     | 0.03     | 0.06     | 0.03     | 0        | 0.02     | 0.05     | 0.03     | 0.01     | 0.04     | 0.01      | 0.04    | 0.03      |  |
| Al <sub>2</sub> O <sub>3</sub> | 20.76   | 20.8                                     | 20.78    | 20.88    | 20.73    | 20.7     | 20.65    | 20.7     | 20.37    | 20.28    | 20.66    | 20.45    | 20.63    | 20.16     | 20.58   | 20.64     |  |
| Cr <sub>2</sub> O <sub>3</sub> | 0.03    | 0.02                                     | 0.06     | 0.04     | 0.02     | 0.01     | 0.02     | 0.02     | 0.04     | 0.01     | 0.02     | 0.01     | 0.02     | 0.03      | 0.01    | 0.04      |  |
| Fe <sub>2</sub> O <sub>3</sub> | 0.37    | 0.8                                      | 1.41     | 0.47     | 0.99     | 1.56     | 1.04     | 0        | 0.14     | 1.47     | 1.57     | 1.53     | 1.79     | 1.78      | 2.04    | 0.63      |  |
| FeO                            | 18.46   | 20.56                                    | 33.85    | 32.14    | 33.55    | 34.97    | 33.16    | 36.19    | 34.65    | 35.4     | 31.52    | 32.27    | 33.62    | 32.94     | 34.82   | 35.86     |  |
| MnO                            | 9.73    | 9  | 2.25     | 5.44     | 3.06     | 2.78     | 1.44     | 1.38     | 3.71     | 2.4      | 5.7      | 6.83     | 2.04     | 6.13      | 1.73    | 3.56      |  |
| MgO                            | 1.44    | 1.63                                     | 4.06     | 3.4      | 3.34     | 3.3      | 2.58     | 3        | 1.88     | 2.87     | 3.19     | 2.09     | 3.64     | 2.02      | 3.32    | 1.92      |  |
| CaO                            | 11.03   | 9.89                                     | 1.1      | 0.97     | 1.55     | 0.82     | 4.3      | 0        | 1.53     | 0.88     | 1.05     | 0.82     | 1.67     | 0.9       | 1.39    | 1.24      |  |
| Totals                         | 99.51   | 100.57                                   | 100.94   | 100.94   | 100.54   | 101.55   | 100.6    | 99.09    | 98.9     | 100.18   | 100.8    | 100.77   | 100.48   | 100.68    | 100.92  | 101.08    |  |
| Oxygens                        | 12      | 12                                       | 12       | 12       | 12       | 12       | 12       | 12       | 12       | 12       | 12       | 12       | 12       | 12        | 12      | 12        |  |
| Si                             | 3.00    | 3.00                                     | 2.98     | 3.00     | 2.99     | 2.98     | 2.99     | 3.06     | 3.01     | 2.98     | 2.97     | 2.98     | 2.97     | 2.98      | 2.96    | 3.00      |  |
| Ti                             | 0.01    | 0.00                                     | 0.00     | 0.00     | 0.00     | 0.00     | 0.00     | 0.00     | 0.00     | 0.00     | 0.00     | 0.00     | 0.00     | 0.00      | 0.00    | 0.00      |  |
| Al                             | 1.96    | 1.95                                     | 1.95     | 1.97     | 1.96     | 1.95     | 1.95     | 1.98     | 1.98     | 1.94     | 1.95     | 1.95     | 1.95     | 1.93      | 1.94    | 1.96      |  |
| Cr                             | 0.00    | 0.00                                     | 0.00     | 0.00     | 0.00     | 0.00     | 0.00     | 0.00     | 0.00     | 0.00     | 0.00     | 0.00     | 0.00     | 0.00      | 0.00    | 0.00      |  |
| Fe <sub>3</sub>                | 0.02    | 0.05                                     | 0.08     | 0.03     | 0.06     | 0.09     | 0.06     | 0.00     | 0.01     | 0.09     | 0.10     | 0.09     | 0.11     | 0.11      | 0.12    | 0.04      |  |
| Fe <sub>2</sub>                | 1.23    | 1.36                                     | 2.25     | 2.15     | 2.25     | 2.33     | 2.22     | 2.45     | 2.38     | 2.40     | 2.12     | 2.19     | 2.25     | 2.24      | 2.33    | 2.42      |  |
| Mn                             | 0.66    | 0.61                                     | 0.15     | 0.37     | 0.21     | 0.19     | 0.10     | 0.10     | 0.26     | 0.17     | 0.39     | 0.47     | 0.14     | 0.42      | 0.12    | 0.24      |  |
| Mg                             | 0.17    | 0.19                                     | 0.48     | 0.40     | 0.40     | 0.39     | 0.31     | 0.36     | 0.23     | 0.35     | 0.38     | 0.25     | 0.44     | 0.24      | 0.40    | 0.23      |  |
| Ca                             | 0.95    | 0.84                                     | 0.09     | 0.08     | 0.13     | 0.07     | 0.37     | 0.00     | 0.14     | 0.08     | 0.09     | 0.07     | 0.14     | 0.08      | 0.12    | 0.11      |  |
| Sum                            | 8       | 8  | 8        | 8        | 8        | 8        | 8        | 7.95     | 8        | 8        | 8        | 8        | 8        | 8         | 8       | 8         |  |

Table A2

| nbr<br>Samples                 | Biotite mean compositions |               |               |               |               |               |               |               |               |                |                |                |                |                 |               |                 |
|--------------------------------|---------------------------|---------------|---------------|---------------|---------------|---------------|---------------|---------------|---------------|----------------|----------------|----------------|----------------|-----------------|---------------|-----------------|
|                                | 1<br>RM 98/6              | 2<br>AS 98/60 | 3<br>RM 98/41 | 4<br>RM 98/45 | 5<br>RM 98/55 | 6<br>RM 98/84 | 7<br>RM 98/82 | 8<br>RM 98/77 | 9<br>RM 98/92 | 10<br>RM 98/93 | 11<br>RM 98/97 | 12<br>RM 98/87 | 13<br>RM 99/18 | 14<br>AS 98/100 | 15<br>MS 99-1 | 16<br>RM 98/116 |
| SiO <sub>2</sub>               | 36.59                     | 37.23         | 35.99         | 36.31         | 35.59         | 35.43         | 35.19         | 34.79         | 34.50         | 33.11          | 34.61          | 34.40          | 35.25          | 33.43           | 34.79         | 34.10           |
| TiO <sub>2</sub>               | 1.57                      | 1.44          | 1.77          | 1.71          | 1.77          | 2.49          | 2.98          | 1.67          | 2.29          | 3.44           | 2.60           | 3.09           | 1.66           | 2.99            | 2.13          | 2.48            |
| Al <sub>2</sub> O <sub>3</sub> | 16.86                     | 16.71         | 19.93         | 19.56         | 19.37         | 19.55         | 19.93         | 19.78         | 20.05         | 19.03          | 18.98          | 18.52          | 20.61          | 19.50           | 20.04         | 19.71           |
| Fe <sub>2</sub> O <sub>3</sub> | 0.00                      | 0.95          | 0.00          | 0.00          | 0.00          | 0.00          | 0.00          | 0.00          | 0.00          | 0.00           | 0.00           | 0.00           | 0.00           | 0.00            | 0.00          | 0.00            |
| FeO                            | 16.98                     | 15.36         | 17.87         | 18.21         | 19.41         | 22.33         | 22.14         | 23.92         | 23.92         | 23.26          | 20.40          | 25.27          | 22.08          | 22.89           | 23.94         | 25.81           |
| MnO                            | 0.36                      | 0.33          | 0.11          | 0.18          | 0.17          | 0.25          | 0.08          | 0.12          | 0.25          | 0.19           | 0.34           | 0.40           | 0.14           | 0.31            | 0.25          | 0.46            |
| MgO                            | 12.13                     | 13.21         | 10.50         | 10.14         | 9.82          | 6.97          | 6.52          | 6.18          | 5.36          | 5.75           | 8.36           | 5.59           | 7.06           | 4.92            | 5.28          | 4.57            |
| K <sub>2</sub> O               | 9.30                      | 9.21          | 8.68          | 8.73          | 9.29          | 8.96          | 8.82          | 9.45          | 9.17          | 8.85           | 8.98           | 9.12           | 8.82           | 9.25            | 9.28          | 8.77            |
| Totals                         | 93.80                     | 94.45         | 94.85         | 94.84         | 95.42         | 95.99         | 95.67         | 95.92         | 95.55         | 93.64          | 94.28          | 96.40          | 95.63          | 93.30           | 95.72         | 95.91           |
| Oxygens                        | 11.00                     | 11.00         | 11.00         | 11.00         | 11.00         | 11.00         | 11.00         | 11.00         | 11.00         | 11.00          | 11.00          | 11.00          | 11.00          | 11.00           | 11.00         | 11.00           |
| Si                             | 2.80                      | 2.81          | 2.71          | 2.74          | 2.70          | 2.70          | 2.69          | 2.69          | 2.67          | 2.62           | 2.68           | 2.67           | 2.69           | 2.66            | 2.69          | 2.66            |
| Ti                             | 0.09                      | 0.08          | 0.10          | 0.10          | 0.10          | 0.14          | 0.17          | 0.10          | 0.13          | 0.21           | 0.15           | 0.18           | 0.10           | 0.18            | 0.12          | 0.15            |
| Al                             | 1.52                      | 1.49          | 1.77          | 1.74          | 1.73          | 1.76          | 1.79          | 1.80          | 1.83          | 1.78           | 1.73           | 1.69           | 1.85           | 1.83            | 1.83          | 1.81            |
| Fe <sub>3</sub>                | 0.00                      | 0.05          | 0.00          | 0.00          | 0.00          | 0.00          | 0.00          | 0.00          | 0.00          | 0.00           | 0.00           | 0.00           | 0.00           | 0.00            | 0.00          | 0.00            |
| Fe <sub>2</sub>                | 1.09                      | 0.97          | 1.13          | 1.15          | 1.23          | 1.43          | 1.41          | 1.55          | 1.55          | 1.54           | 1.32           | 1.64           | 1.41           | 1.52            | 1.55          | 1.68            |
| Mn                             | 0.02                      | 0.02          | 0.01          | 0.01          | 0.01          | 0.02          | 0.01          | 0.01          | 0.02          | 0.01           | 0.02           | 0.03           | 0.01           | 0.02            | 0.02          | 0.03            |
| Mg                             | 1.38                      | 1.48          | 1.18          | 1.14          | 1.11          | 0.79          | 0.74          | 0.71          | 0.62          | 0.68           | 0.96           | 0.65           | 0.80           | 0.58            | 0.61          | 0.53            |
| K                              | 0.91                      | 0.89          | 0.83          | 0.84          | 0.90          | 0.87          | 0.86          | 0.93          | 0.91          | 0.90           | 0.89           | 0.90           | 0.86           | 0.94            | 0.92          | 0.87            |
| Sum                            | 7.81                      | 7.79          | 7.72          | 7.72          | 7.78          | 7.71          | 7.67          | 7.78          | 7.73          | 7.73           | 7.75           | 7.76           | 7.72           | 7.72            | 7.73          | 7.73            |

Table A3

| Amphibole mean compositions    |         |          | Muscovite mean compositions |          |          |          |          |          |          |          |          |          |          |           |         |           |
|--------------------------------|---------|----------|-----------------------------|----------|----------|----------|----------|----------|----------|----------|----------|----------|----------|-----------|---------|-----------|
| nbr                            | 1       | 2        | 3                           | 4        | 5        | 6        | 7        | 8        | 9        | 10       | 11       | 12       | 13       | 14        | 15      | 16        |
| Samples                        | RM 98/6 | AS 98/60 | RM 98/41                    | RM 98/45 | RM 98/55 | RM 98/84 | RM 98/82 | RM 98/77 | RM 98/92 | RM 98/93 | RM 98/97 | RM 98/87 | RM 99/18 | AS 98/100 | MS 99-1 | RM 98/116 |
| SiO <sub>2</sub>               | 43.90   | 43.39    | 45.06                       | 46.12    | 45.29    | 45.98    | 46.32    | 46.17    | 45.67    | 44.96    | 44.97    | 45.70    | 44.78    | 45.67     | 45.81   | 45.96     |
| TiO <sub>2</sub>               | 0.41    | 0.36     | 0.43                        | 0.49     | 0.58     | 0.82     | 0.95     | 0.45     | 0.54     | 0.75     | 0.71     | 0.78     | 0.73     | 0.82      | 0.26    | 0.44      |
| Al <sub>2</sub> O <sub>3</sub> | 13.92   | 15.44    | 36.62                       | 36.51    | 35.50    | 35.64    | 34.85    | 35.40    | 35.85    | 35.44    | 35.40    | 34.44    | 35.44    | 35.92     | 36.10   | 35.72     |
| Cr <sub>2</sub> O <sub>3</sub> | 0.02    | 0.05     | 0.03                        | 0.03     | 0.00     | 0.04     | 0.00     | 0.05     | 0.00     | 0.00     | 0.00     | 0.02     | 0.00     | 0.00      | 0.00    | 0.00      |
| Fe <sub>2</sub> O <sub>3</sub> | 1.41    | 2.30     | 0.00                        | 0.00     | 0.00     | 0.00     | 0.00     | 0.00     | 0.00     | 0.00     | 0.00     | 0.00     | 1.03     | 0.00      | 0.00    | 0.00      |
| FeO                            | 13.70   | 12.22    | 1.01                        | 0.81     | 1.34     | 1.30     | 1.45     | 1.34     | 1.46     | 1.33     | 1.25     | 3.00     | 1.01     | 1.28      | 1.32    | 1.30      |
| MnO                            | 0.62    | 0.44     | 0.01                        | 0.02     | 0.01     | 0.03     | 0.02     | 0.02     | 0.01     | 0.02     | 0.02     | 0.04     | 0.02     | 0.02      | 0.01    | 0.04      |
| MgO                            | 9.36    | 9.70     | 0.45                        | 0.54     | 0.76     | 0.58     | 0.71     | 0.63     | 0.48     | 0.55     | 0.70     | 0.51     | 0.75     | 0.49      | 0.49    | 0.50      |
| CaO                            | 11.97   | 11.91    | 0.01                        | 0.01     | 0.02     | 0.02     | 0.02     | 0.00     | 0.01     | 0.01     | 0.01     | 0.01     | 0.01     | 0.01      | 0.01    | 0.01      |
| Na <sub>2</sub> O              | 1.06    | 1.10     | 1.69                        | 1.52     | 1.27     | 0.83     | 0.58     | 0.60     | 0.69     | 0.71     | 0.79     | 0.86     | 0.56     | 0.58      | 0.65    | 0.66      |
| K <sub>2</sub> O               | 0.78    | 0.55     | 8.76                        | 9.10     | 9.32     | 10.10    | 10.42    | 10.56    | 10.45    | 10.34    | 10.18    | 10.15    | 9.98     | 10.67     | 10.57   | 10.44     |
| Totals                         | 97.14   | 97.46    | 94.08                       | 95.16    | 94.11    | 95.35    | 95.33    | 95.23    | 95.17    | 94.12    | 94.04    | 95.52    | 94.33    | 95.47     | 95.23   | 95.08     |
| Oxygens                        | 23.00   | 23.00    | 11.00                       | 11.00    | 11.00    | 11.00    | 11.00    | 11.00    | 11.00    | 11.00    | 11.00    | 11.00    | 11.00    | 11.00     | 11.00   | 11.00     |
| Si                             | 6.52    | 6.38     | 3.02                        | 3.05     | 3.04     | 3.06     | 3.08     | 3.08     | 3.05     | 3.04     | 3.04     | 3.06     | 3.02     | 3.04      | 3.05    | 3.07      |
| Ti                             | 0.05    | 0.04     | 0.02                        | 0.02     | 0.03     | 0.04     | 0.05     | 0.02     | 0.03     | 0.04     | 0.04     | 0.04     | 0.04     | 0.04      | 0.01    | 0.02      |
| Al                             | 2.44    | 2.68     | 2.89                        | 2.85     | 2.81     | 2.79     | 2.74     | 2.78     | 2.82     | 2.82     | 2.82     | 2.72     | 2.81     | 2.82      | 2.84    | 2.81      |
| Cr                             | 0.00    | 0.01     | 0.00                        | 0.00     | 0.00     | 0.00     | 0.00     | 0.00     | 0.00     | 0.00     | 0.00     | 0.00     | 0.00     | 0.00      | 0.00    | 0.00      |
| Fe <sub>3</sub>                | 0.16    | 0.25     | 0.00                        | 0.00     | 0.00     | 0.00     | 0.00     | 0.00     | 0.00     | 0.00     | 0.00     | 0.00     | 0.05     | 0.00      | 0.00    | 0.00      |
| Fe <sub>2</sub>                | 1.70    | 1.50     | 0.06                        | 0.05     | 0.08     | 0.07     | 0.08     | 0.08     | 0.08     | 0.08     | 0.07     | 0.17     | 0.06     | 0.07      | 0.07    | 0.07      |
| Mn                             | 0.08    | 0.06     | 0.00                        | 0.00     | 0.00     | 0.00     | 0.00     | 0.00     | 0.00     | 0.00     | 0.00     | 0.00     | 0.00     | 0.00      | 0.00    | 0.00      |
| Mg                             | 2.07    | 2.12     | 0.05                        | 0.05     | 0.08     | 0.06     | 0.07     | 0.06     | 0.05     | 0.06     | 0.07     | 0.05     | 0.08     | 0.05      | 0.05    | 0.05      |
| Ca                             | 1.90    | 1.88     | 0.00                        | 0.00     | 0.00     | 0.00     | 0.00     | 0.00     | 0.00     | 0.00     | 0.00     | 0.00     | 0.00     | 0.00      | 0.00    | 0.00      |
| Na                             | 0.31    | 0.31     | 0.22                        | 0.20     | 0.17     | 0.11     | 0.08     | 0.08     | 0.09     | 0.09     | 0.10     | 0.11     | 0.07     | 0.08      | 0.08    | 0.09      |
| K                              | 0.15    | 0.10     | 0.75                        | 0.77     | 0.80     | 0.86     | 0.89     | 0.90     | 0.89     | 0.89     | 0.88     | 0.87     | 0.86     | 0.91      | 0.90    | 0.89      |
| Sum                            | 15.37   | 15.33    | 7.00                        | 6.98     | 7.00     | 6.99     | 6.98     | 7.00     | 7.01     | 7.01     | 7.01     | 7.03     | 6.98     | 7.00      | 7.01    | 7.00      |

Table A4

| nbr<br>Samples                 | Plagioclase mean compositions |               |               |               |               |               |               |               |               |                |                |                |                |                 |               |                 |
|--------------------------------|-------------------------------|---------------|---------------|---------------|---------------|---------------|---------------|---------------|---------------|----------------|----------------|----------------|----------------|-----------------|---------------|-----------------|
|                                | 1<br>RM 98/6                  | 2<br>AS 98/60 | 3<br>RM 98/41 | 4<br>RM 98/45 | 5<br>RM 98/55 | 6<br>RM 98/84 | 7<br>RM 98/82 | 8<br>RM 98/77 | 9<br>RM 98/92 | 10<br>RM 98/93 | 11<br>RM 98/97 | 12<br>RM 98/87 | 13<br>RM 99/18 | 14<br>AS 98/100 | 15<br>MS 99-1 | 16<br>RM 98/116 |
| SiO <sub>2</sub>               | 46.84                         | 47.72         | 65.07         | 66.17         | 64.45         | 65.51         | 55.01         | 65.17         | 62.68         | 63.63          | 63.60          | 66.65          | 62.13          | 63.45           | 64.93         | 66.21           |
| TiO <sub>2</sub>               | 0.02                          | 0.00          | 0.00          | 0.00          | 0.00          | 0.00          | 0.00          | 0.00          | 0.00          | 0.00           | 0.00           | 0.00           | 0.00           | 0.00            | 0.00          | 0.00            |
| Al <sub>2</sub> O <sub>3</sub> | 33.04                         | 33.01         | 21.30         | 21.23         | 22.09         | 21.74         | 28.26         | 22.16         | 23.10         | 22.13          | 21.99          | 21.13          | 23.41          | 22.81           | 22.38         | 21.58           |
| CR <sub>2</sub> O <sub>3</sub> | 0.00                          | 0.00          | 0.00          | 0.00          | 0.00          | 0.08          | 0.00          | 0.00          | 0.00          | 0.00           | 0.00           | 0.00           | 0.00           | 0.00            | 0.00          | 0.00            |
| Fe <sub>2</sub> O <sub>3</sub> | 0.16                          | 0.07          | 0.72          | 0.14          | 0.22          | 0.12          | 0.20          | 0.23          | 0.12          | 0.09           | 0.11           | 0.13           | 0.06           | 0.06            | 0.07          | 0.09            |
| CaO                            | 16.21                         | 15.91         | 2.37          | 2.44          | 3.25          | 2.61          | 10.43         | 0.00          | 4.41          | 3.19           | 3.28           | 1.83           | 4.96           | 3.78            | 2.64          | 2.59            |
| Na <sub>2</sub> O              | 2.14                          | 2.41          | 10.38         | 10.04         | 9.76          | 10.07         | 5.39          | 9.60          | 9.15          | 9.89           | 9.76           | 10.55          | 8.80           | 9.40            | 9.89          | 10.09           |
| K <sub>2</sub> O               | 0.07                          | 0.03          | 0.22          | 0.07          | 0.22          | 0.12          | 0.15          | 0.24          | 0.20          | 0.17           | 0.18           | 0.16           | 0.19           | 0.36            | 0.41          | 0.26            |
| Totals                         | 98.48                         | 99.15         | 100.06        | 100.09        | 99.98         | 100.25        | 99.44         | 97.40         | 99.66         | 99.10          | 98.92          | 100.45         | 99.54          | 99.86           | 100.32        | 100.82          |
| Oxygens                        | 8.00                          | 8.00          | 8.00          | 8.00          | 8.00          | 8.00          | 8.00          | 8.00          | 8.00          | 8.00           | 8.00           | 8.00           | 8.00           | 8.00            | 8.00          | 8.00            |
| Si                             | 2.18                          | 2.20          | 2.87          | 2.90          | 2.84          | 2.87          | 2.49          | 2.91          | 2.79          | 2.83           | 2.84           | 2.91           | 2.77           | 2.81            | 2.85          | 2.89            |
| Ti                             | 0.00                          | 0.00          | 0.00          | 0.00          | 0.00          | 0.00          | 0.00          | 0.00          | 0.00          | 0.00           | 0.00           | 0.00           | 0.00           | 0.00            | 0.00          | 0.00            |
| Al                             | 1.81                          | 1.80          | 1.11          | 1.10          | 1.15          | 1.13          | 1.51          | 1.17          | 1.21          | 1.16           | 1.16           | 1.09           | 1.23           | 1.19            | 1.16          | 1.11            |
| Cr                             | 0.00                          | 0.00          | 0.00          | 0.00          | 0.00          | 0.00          | 0.00          | 0.00          | 0.00          | 0.00           | 0.00           | 0.00           | 0.00           | 0.00            | 0.00          | 0.00            |
| Fe <sub>3</sub>                | 0.01                          | 0.00          | 0.02          | 0.01          | 0.01          | 0.00          | 0.01          | 0.01          | 0.00          | 0.00           | 0.00           | 0.00           | 0.00           | 0.00            | 0.00          | 0.00            |
| Ca                             | 0.81                          | 0.79          | 0.11          | 0.11          | 0.15          | 0.12          | 0.51          | 0.00          | 0.21          | 0.15           | 0.16           | 0.09           | 0.24           | 0.18            | 0.12          | 0.12            |
| Na                             | 0.19                          | 0.22          | 0.89          | 0.85          | 0.84          | 0.86          | 0.47          | 0.83          | 0.79          | 0.85           | 0.84           | 0.89           | 0.76           | 0.81            | 0.84          | 0.85            |
| K                              | 0.00                          | 0.00          | 0.01          | 0.00          | 0.01          | 0.01          | 0.01          | 0.01          | 0.01          | 0.01           | 0.01           | 0.01           | 0.01           | 0.02            | 0.02          | 0.01            |
| Sum                            | 5.01                          | 5.01          | 5.01          | 4.98          | 5.00          | 4.99          | 4.99          | 4.93          | 5.01          | 5.02           | 5.01           | 4.99           | 5.00           | 5.01            | 5.00          | 4.99            |

## CHAPTER 7: MECHANISM OF THE GIANBUL DOME FORMATION

The peak metamorphic conditions reached in the High Himalayan Crystalline Zone of Zaskar are comparable to what is observed in most sections across the metamorphic core zone all along the range. Such P-T results indicate that the High Himalayan Crystalline Zone represents a part of the Indian plate sedimentary cover that has been metamorphosed up to partial melting conditions, as a consequence of peak temperatures up to about 750 °C at subduction depths around 30 km (e.g. Pêcher, 1989; Vannay & Hodges, 1996; Dèzes et al. 1999; Vannay et al. 1999; Wyss 2000). In the central and south-eastern parts of the Himalaya, the High Himalayan Crystalline Zone corresponds mainly to a NE-dipping monoclinial slab cropping out in the frontal part of the range, as a consequence of a tectonic exhumation controlled by combined thrusting along the MCT and extension along the South Tibetan Detachment System detachments (e.g. Hodges et al. 1992, 1996; Vannay & Hodges, 1996; Wyss et al. 1999).

In the NW Himalaya, however, the geological setting contrasts significantly from what is observed for more than 1400 km to the SE. In the Himalaya of Zaskar, the high-grade gneisses of the High Himalayan Crystalline Zone mainly crop out in a more internal part of the orogen as a large-scale dome structure. Between the Kulu and Chenab Valleys, the hanging wall of the MCT consists mainly of low- to medium grade metasediments (Chamba zone), connected to the upper-Precambrian to lower-Cambrian sediments forming the base of the Tethyan Himalaya, and separating the High Himalayan Crystalline Zone of Zaskar from the comparable high-grade rocks cropping out in the frontal part of the range further to the SE (Figs. 3.1 and 5.1). A major characteristics of this High Himalayan Crystalline Zone of Zaskar is the presence of several large-scale gneiss domes, cored by Cambro-Ordovician granitic gneisses and/or Tertiary migmatites and leucogranites (e.g. Kündig, 1989; Searle et al. 1999). This particular setting implies that the exhumation of high-grade rocks in this part of the range was for a large part controlled by doming. Large-scale doming appears thus to have played a significant role in the exhumation of high-grade rocks in this part of the range, but the cause of doming remains debated.

The origin of the gneiss domes is classically attributed to three processes: diapirism, interference patterns, and metamorphic core complex-type extension. Each one of these processes allows the formation of domal structures in a geologically favourable context to their respective development. Erosion is an other factor which has to be taken into account in the processes of doming. It is often assumed that erosion is a rather slow process of exhumation. Nevertheless this factor cannot be ignored as a permanent factor contributing to the exhumation processes. Moreover, in the mountainous, wet, and tectonically active regions like in the frontal part of the Himalayan range, the surficial erosion can locally be a very fast process (Ring et al., 1999). This observation suggest a cause and effect relationship between the rate of erosion and the velocity of the exhumation process.

In order to check these models, we may consider the following points according to the structural history and the peak metamorphic conditions reached in the Gianbul dome: (1) the 35 km of displacement along the Zaskar Shear Zone; (2) the constraints on the age and duration of extensional tectonic movements along the Zaskar Shear Zone (from 22.2 Ma. to 19.8 Ma.), and (3) the overall convergent orogenic setting of the studied area.

Considering the density contrast between the paragneiss and the numerous Cambro-Ordovician granitic plutons and Tertiary migmatites cropping out in the High Himalayan Crystalline Zone of Zaskar, Kündig (1989) proposed that doming could be the consequence of diapirism. Diapirism of granitic gneiss appears, however, as a relatively slow process; for a 5 km thick orthogneiss dome covered by 10 km of (meta)sediments, for example, Ramberg (1981) calculated that it takes about 14 Ma for the dome to increase its amplitude from 0.01 to 2.25 km, and that the subsequent rate of diapiric ascent is c. 0.8 mm / yr. In contrast, a minimum of 12 km of differential vertical movement occurred across the Zaskar Shear Zone between 22.2. and 19.8 Ma (Dèzes et al. 1999), implying that the vertical movement of the High Himalayan Crystalline Zone rocks forming the Gianbul Dome took place at an average rate in excess of 5 mm/yr. Recent researches on ascent and emplacement of granitic magmas (Paterson and Vernon, 1995; Grocott and Wilson, 1997) suggest that the significance of diapiric ascent of granitic magma has to be minimized because granitic diapirs rise relatively slowly due to viscosity constraints imposed by crustal material (Clemens et al., 1997). Besides, Vigneresse and Clemens (2000) affirm that the density contrast between magma and surroundings is not sufficient to induce diapirism or fractures. According to these authors, pluton formation appears to be controlled by local structures rather by intrinsic magma properties. It consequently appears that diapirism alone could not account for the rapid exhumation and cooling of the High Himalayan Crystalline Zone of Zaskar, such as constrained by P-T path and geochronological data (e.g. Dèzes et al. 1999; Walker et al. 1999).

A superposition of folding phases can also lead to domal structures (Ramsay, 1962 and 1967). The formation of a such structure by superimposed folding implies that the axial traces of both shortening phases are more or less perpendicular. The geological situation of the studied area being strongly controlled by a NE-SW compressional, it would be necessary to invoke a significant E-W shortening to form a domal interference patterns. Consequently, a superposition of folding phases appears to be an unlikely mechanism because there is no field structural evidences for a significant E-W shortening.

The geometry, metamorphic zonation, and extensional tectonic contacts characterizing the Himalayan gneiss domes, like the Gianbul dome, are features reminiscent of metamorphic core complexes such as observed in the North American Cordillera, suggesting that they could be the consequence of isostatic uplift in the footwall of an extensional detachment (e.g. Chen et al. 1990). The metamorphic core complex-type dome can be explained by the rise of the ductile crust toward surface under detachment zone. This process is a direct consequence of the gravitational collapse of the sedimentary cover previously thickened during an orogen. Thermal relaxation consecutive with this thickening involves a viscosity drop in the lower part of the crust. The isostatic readjustment following the gravitational collapse of the higher crust allows the creep and the rise of the lower crust towards the surface by isostatic compensation. A dome thus develops in the footwall zone of detachment. One of the characteristic of the metamorphic core complexes is that they were exhumed during a crustal scale extensional event. In contrast to classical metamorphic core complexes, however, the Himalayan gneiss domes developed within an overall convergent orogenic setting. Consequently, the mechanism of dome formation in the north-western part of the Himalaya of India can not be compared to the metamorphic core complex-type formation.

Several recent models suggest that the exhumation of the High Himalayan Crystalline Zone, associated with combined thrusting along the MCT and extension along the South Tibetan Detachment System, reflects a ductile extrusion of these high-grade, low-viscosity paragneisses and migmatites, controlled by gravity forcing and/or by the underthrusting of the Indian plate (e.g. Beaumont et al. 2001; Vannay & Grasemann, 2001, and references therein). According to the channel flow numerical model by Beaumont et al. (2001), two significant parameters controlling

the site of high-grade rocks extrusion in the orogen are the erosion rate at the orogenic front and the rheological strength of the upper crustal rocks overlying the channel. The numerical simulations by Beaumont et al. (2001) suggest that efficient erosion and strong upper crust induce extrusion in the frontal part of the range, such as observed along most of the Himalaya, whereas reduced erosion and weaker upper crust can lead to doming and extrusion in a more internal part of the range. This latter scenario appears consistent with what is observed in the NW Himalaya, where the lack of high-grade metamorphic rocks in the hanging wall of the MCT between the Beas and Chenab rivers (=low-grade metasediments of the Chamba zone, Fig. 3.1), strongly suggests reduced erosion in the frontal part of the orogen compared to the rest of the chain, possibly because of a lack of major river in the Chamba area. As a consequence, the high-grade rocks of the High Himalayan Crystalline Zone could have been forced to extrude in a more internal part of the orogen, to eventually "pierce" through the Tethyan Himalaya sedimentary cover as large-scale domes (Fig. 6.25). The presence of the pre-existing local structures such as the Miyar Thrust Zone could have facilitated the extrusion of the deep metamorphic rocks in a more internal part of the range.



## CHAPTER 8: CONCLUSIONS

Together with the results of Dèzes (1999), Dèzes et al., (1999) and Steck et al., (1999), the new structural and thermobarometric constraints presented in this study allow to propose a reconstruction of the tectono-metamorphic evolution of the High Himalaya in the Lahul-Zaskar region. Four main stages of metamorphic crystallisation characterizing the metamorphic evolution can be correlated with the four major tectonic events which have built the actual geometry of the High Himalaya in this part of the range. Structural and metamorphic data indicate consequently that the tectonometamorphic evolution of the High Himalaya in Lahul – Zaskar region is associated with a complex tectonic history involving converging nappe structures (Shikar Beh and Nyimaling – Tsarap nappes) superimposed by opposite-directed extensional structures (Zaskar Shear Zone and Khanjar Shear Zone). This tectono-metamorphic can be summarized in the following way: (1) a first phase of crustal shortening, thickening and Barrovian metamorphism is recorded by the sedimentary sequence of the India continental margin. The deformation relative to this event was accommodated by thrusting, folding and formation of both NE and SW -directed nappes; (2) a second major phases is related to a syn-orogenic extension along extensional tectonic structures contributing to the exhumation of the high-grade metamorphic rocks of the High Himalayan Crystalline Zone. This stage is expressed by the formation of ductile normal shearing, doming and brittle normal faulting and is responsible of the new retrograde metamorphic assemblages testifying of a significantly pressure drop.

The structural analysis highlights that the main structures observed in the Miyar Valley are associated with NE-directed compressional movements documented by kinematic indicators preserved within the NE-directed Miyar Thrust Zone. The crystallisation/deformation relationships observed within this thrust zone indicate that the NE-directed movements are synchronous with a Barrovian-type metamorphic field gradient, evolving from chlorite zone to the SW to amphibolite-migmatite zone to the NE. Such a Barrovian metamorphic field gradient can only be explained by a significant overload coming from the SW. That obliges us to interpret the Miyar Thrust Zone and the associated metamorphism as testifying to the overthrusting of a NE-directed nappe. In the Tandi-Khoksar area, such an interpretation has been proposed for the first time by Steck et al. (1993). Indeed, these authors explain the NE-directed vergence of the Tandi syncline and the high-grade metamorphism observed in the Khoksar area as the consequence of the NE-directed Shikar Beh nappe emplacement. Equivalent NE-directed structures have also been highlighted in the Spiti Valley (Steck et al., 1998; Wyss et al., 1999). In all these regions, the structural interference patterns between the NE-directed structures and the classical SW-directed structures indicate that the NE-directed structures associated with the Shikar Beh nappe emplacement correspond to the oldest Himalayan structures. These overall observations allow to trace the NE-directed Shikar Beh nappe over a distance of 200 km from the Miyar Valley to the NW to the Spiti Valley to the SE. Fieldworks carried out in the Sutlej Valley (Vannay and Grasemann 1998) indicate that the NE-directed Shikar nappe doesn't seem to extend eastward beyond the Spiti Valley. On the other hand, we can not rule out that the Shikar Beh nappe extends further to the north-west. In these regions, several observations seems to indicate that some NE-directed described structures could be interpreted as equivalent to the NE-directed Shikar Beh structures. It appears consequently that the Shikar Beh nappe has to be considered as a major geological feature in the north-western part of the Himalaya of India. The presence of this opposite-directed nappe in this part of the range could also explain the significant differences we observed in the north-western part of the Himalaya of

India such as the particular metamorphic zonation in the frontal part of the range or as the sudden termination of the cylindrical geometry of the Himalayan orogen in this part of the range

The main goal of this work was to constrain the tectono-metamorphic evolution of the south-eastern limit of the High Himalayan Crystalline Zone in the Miyar Valley area. Our structural data, together with the petrographic investigations, demonstrated that the transition between the low-grade metamorphic Chamba Zone and the high-grade metasediments of the High Himalayan Crystalline Zone corresponds to a major shear zone which initially acted as a ductile thrust zone (Miyar Thrust Zone) late reactivated as a ductile extensional shear zone (Khanjar Shear Zone). The nearly isothermal decompression, expressed by the appearance of new typical retrograde metamorphic assemblages in the kyanite zone, in the footwall of the Khanjar Shear Zone, suggests a rapid exhumation of the high-grade metamorphic rocks exposed to the north of the Khanjar extensional shear zone. Several structural descriptions from the Kilar-Saichu area, further to the west, reveal SW-directed extensional structures in the transition zone between the Chamba Zone and the High Himalayan Crystalline Zone (Frank et al., 1995; Stephenson et al., 2001). The presence of these structures also testifies of a NE-directed extrusion of the High Himalayan Crystalline Zone of Zaskar with respect to the Chamba Zone. Consequently, it appears that the particular metamorphic zonation in the NW part of the Himalaya of India, characterized by a gradual decrease of the metamorphic grade towards the SW, is mainly controlled by tectonics.

On the metamorphic map presented on the Fig. 6.2, we note that the metamorphic isograds turn around the dome. However, although characterized by an apparently simple, symmetrical geometry, and metamorphic conditions on both side of the dome, the structural and metamorphic investigations carried out in the Miyar Valley together with comparable data from the Gianbul Valley, reveal that the large scale doming observed in Zaskar-Lahul area is the consequence of a complex and polyphase tectono-metamorphic evolution composed by four major tectonics events with which are systematically associated a new and distinct metamorphic history.

## ACKNOWLEDGEMENTS

When I was student, I already dreamed about the imposing and majestic landscapes of Himalaya, looking at the Himalayan pictures exposed in the hall of the Institute. I listened attentively to the fantastic accounts of the Himalayan Ph. D. students. Thanks to the Prof. Albrecht Steck, my dream became reality. I wish to express to him my profound gratitude for having given me the possibility to carry out, first my master, and then my Ph.D. research in a such beautiful areas of the Himalaya. I thank him for his constant support during all my studies and for the confidence he has invested in me during our long years of collaboration.

My work was also closely followed by the Dr. Jean-Claude Vannay and by the Prof. Jean-Luc Eparad. Both of them deeply contributed to the achievement of this research project.

Jean-Claude has constantly shared his knowledge and I have learned a lot from him. His enthusiasm and his motivation were the indispensable motor in the advance of my work. Without his support, this work would certainly not have been also agreeable to realize. I am also deeply obliged towards Jean-Claude for the critical comments, suggestions, the linguistic revision, and the advises in the writing of the manuscript, particularly in the metamorphic chapter. Shall he be assured of my infinite gratitude.

Jean-Luc greatly supervised my structural analysis and contributed thus a lot to the improvement of the tectonic part of the manuscript. Their advises and comments were very much appreciated. Jean-Luc also was the indispensable moral support when my motivation was dropping.

Combining the experience and the skills of these three people, I could not imagine better working conditions and I was very pleased to collaborate with them during all my thesis.

I would like also to particularly thank the Prof. Henri Masson and the Prof. Bruno Lombardo who accepted to be the experts for my thesis, and to share their geological experience with myself.

I also thank the Dr. François Bussy for supervising microprobe works, the Prof. Johannes Hunziker and the Dr. Jorge Spangenberg for supervising isotopic analyses, Dr. Mike Cosca for Ar/Ar works and Laurent Nicod for preparation of thin and polished sections.

I am also deeply obliged for the help and enthusiasm of my colleagues Emmanuel Marclay, Micha Schlup and Olivier Zingg. My sincere thanks for having shared with me unforgettable moments during field works in the Himalaya.

Pierre Dèzes also provide me a lot of information from the northern part of my field of investigation. He was always ready to shared with me his great Himalayan experience.

I also sincerely wish to thank Martin Wyss and Matthieu Girard who, throughout their discussion, have also participated to the achievement of this project.

George Mascle and the people of the French embassy in Delhi are thanked for discussion and for helping with samples transport.

I am equally grateful to Prehm Singh Negi, his family and his horses for their infrastructural support and for the long cold himalayan evening we spend around a salutary fire. His kindness and his resourcefulness were indispensable in a lot of difficult moments. Shall he be assured of my infinite gratitude.

I also want to thank Raffaele Virgilio Geronimo L., Dominique R., Andreas M., David G., Nicolas K., Piercarlo G., Alain M., Christian S., Elisabeth C., François B., François R., Gilles B., Huguette G., Jens F., Neija N., Nicolas G., Philippe F., Pierre-François E., Sebastien B., Sebastien P., Sylvain R and Vincent B.

I would finally like to heartily thank my wife, Catherine, who not only supported the stressful moments which precedes the end of a thesis but who also shared with me two field seasons in the Himalaya. Many thanks.

This study was financed by the Swiss National Science Foundation (FNRS grants 20-45063.95 and 20-52165.97) and the Herbette Foundation of the University of Lausanne.

## BIBLIOGRAPHY

- Argand, E., 1916. Sur l'arc des Alpes Occidentales, *Eclogae Geologicae Helvetiae*. 14, 145-204
- Argand, E., 1924. La Tectonique de l'Asie. Extrait du compte-rendu du XIII Congrès géologique international, Bruxelles 1922, 372 p.
- Auden, J.B., 1937. Traverses in the Himalaya. *Records of the Geological Survey of India* 69, 123-167.
- Bassoulet, J.P., Boulin, J., Colchen, M., Marcoux, J., Mascle, G., Montenat, C., 1980. L'évolution des domaines téthysiens au pourtour du Bouclier indien du Carbonifère au Crétacé. Translated Title: Evolution of Tethyan domains around the Indian Shield, from the Carboniferous to the Cretaceous. *Mémoires du B.R.G.M.* 115, 180-198.
- Baud, A., Arn, R., Bugnon, P., Crisimel, A., Dolivo, E., Escher, A., Hammerschlag, J.G., Marthaler, M., Masson, H., Steck, A., Tietche, J.C., 1982. Le contact Gondwana--Peri-Gondwana dans le Zaskar oriental (Ladakh, Himalaya). Translated Title: The Gondwana-peri-Gondwana contact in eastern Zaskar, Ladakh, Himalayas. *Bulletin de la Société Géologique de France*. 24; 341-361.
- Baud, A., Gaetani, M., Garzanti, E., Fois, E.E., Nicora, A., Tintori, A., 1984. Geological observations in southeastern Zaskar and adjacent Lahul area (northwestern Himalaya). *Eclogae Geologicae Helvetiae*. 77, 171-197.
- Beaumont, C., Jamieson, R.A., Nguyen, M.H., Lee, B., 2001. Himalayan tectonics explained by extrusion of a low-viscosity crustal channel coupled to focused surface denudation. *Nature* 414, 738-742.
- Berman, R.G., 1991. Thermobarometry using multi-equilibrium calculations : a new technique with petrological applications. *Canadian Mineralogist* 29, 833-855.
- Berthelsen, A., 1953. On the geology of the Rupshu District, N. W. Himalaya; a contribution to the problem of the central gneisses. *Bulletin of the Geological Society of Denmark* 12. 350-414.
- Bhatt, D.K., Kumar, G., 1980. Discovery of conodonts in the Cambrian of Spiti, Tethys Himalaya. *Current Science (Bangalore)*. 49, 357-358.
- Bonhomme, M., Garzanti, E., 1991. Age of metamorphism in the Zaskar Tethys Himalaya (India). *Géologie Alpine, Mémoire H.S.* 16, 15-16.
- Brookfield, M.E., 1993. The Himalayan passive margin from Precambrian to Cretaceous times. *Sedimentary Geology* 84,1-35.
- Burchfiel, B.C., Chen, Z., Hodges, K.V., Liu, Y., Royden, L.H., Deng, C., Xu, J., 1992. The South Tibetan Detachment System, Himalayan orogen; extension contemporaneous with and parallel to shortening in a collisional mountain belt. *Geological Society of America Special Paper* 269, 41pp.
- Burchfiel, B.C., Royden, L.H., 1985. North-South extension within the convergent Himalayan region. *Geology*, 13, 679-682.
- Burg, J.-P., Chen, G.M., 1984. Tectonics and structural zonation of southern Tibet, China. *Nature* 311, 219-223.

- Caby, R., Pêcher, A., Le Fort, P., 1983. Le grand chevauchement central himalayen; nouvelles données sur le métamorphisme inverse à la base de la Dalle du Tibet. *Revue de Geologie Dynamique et de Geographie Physique* 24, 89-100.
- Chemenda, A.I., Mattauer, M., Malavieille, J., Bokun, A.N., 1995. A mechanism for syn-collisional rock exhumation and associated normal faulting; results from physical modelling. *Earth and Planetary Science Letters*. 132, 225-232.
- Chen, Z., Liu, Y., Hodges, K.V., Burchfiel, B.C., Royden, L.H., Deng, C., 1990. The Kangmar Dome: a metamorphic core complex in southern Xizang (Tibet). *Science* 250, 1552-1556.
- Clemens, J.D., 1998. Observations on the origins and ascent mechanisms of granitic magmas. *Journal of the Geological Society of London* 155, 843-851.
- Clemens, J.D., Petford, N., Mawer, C.K., 1997. Ascent mechanisms of granitic magmas: causes and consequences. In: *Deformation-enhanced fluid transport in the Earth's crust and mantle* (ed Holness, M.B.), London, Chapman and Hall, 144-171.
- Colchen, M., Mascle, G., Van-Havert, T., 1986. Some aspects of collision tectonics in the Indus suture zone, Ladakh. In: *Collision tectonics*. (eds, Coward, M.P., Ries, A.C.), Geological Society of London, Special Publications 19, 173-184.
- Coleman, M.E., 1996. Orogen-parallel and orogen-perpendicular extension in the central Nepalese Himalayas. *Geological Society of America Bulletin*. 108, 1594-1607.
- Coleman, M.E., 1998. U-Pb constraints on Oligocene-Miocene deformation and anatexis within the Central Himalaya, Marsyandi valley, Nepal. *American Journal of Science* 298, 553-571.
- Dainelli, G., 1933-1934. Spedizione italiana de Filippi nell'Himalaia, Caracorum e Turchestan cinese (1913-1914). Risultati geologici e geografici. Vol 2. La serie dei Terreni I and 2, Zanichelli, Bologna, 1-1105.
- Dèzes, P., 1999. Tectonic and metamorphic evolution of the Central Himalayan domain in southeast Zaskar (Kashmir, India). *Mémoires de Géologie*. Lausanne 32, 149 pp.
- Dèzes, P., Vannay, J.-C., Steck, A., Bussy, F., Cosca, M., 1999. Synorogenic extension: quantitative constraints on the age and displacement of the Zaskar Shear Zone (NW Himalayas). *Geological Society of America Bulletin* 111, 364-374.
- Draganits, E., Grasemann, B., Frank, W., Miller, C., Wiesmayr, G., 1998. The sedimentary protoliths of the HHC in the Chamba-Lahaul area, NW-Himalayas, India. 13th Himalaya-Karakoram-Tibet international workshop; abstract volume. *Geological Bulletin*, University of Peshawar. 31, 58-60.
- Epard, J.-L., Steck, A., Vannay, J.-C., Hunziker, J., 1995. Tertiary Himalayan structures and metamorphism in the Kulu Valley (Mandi-Khoksar transect of the western Himalaya) - Shikar Beh Nappe and Crystalline Nappe. *Schweizerische Mineralogische und Petrographische Mitteilungen* 75, 59-84.
- Escher, A., Beaumont, C., 1997. Formation, burial and exhumation of basement nappes at crustal scale; a geometric model based on the western Swiss-Italian Alps. *Journal of Structural Geology*. 19, 955-974.
- Eskola, P., (1939). Die metamorphen Gesteine. In: *Die Entstehung der Gesteine*. (eds Barth, F.W., Correns, C.W., Eskola, P.) Verlag von Julius Springer, Berlin, 263-407.
- Ferrara, G., Lombardo, B., Tonarini, S., Turi, B., 1991. Sr, Nd and O isotopic characterisation of the Gomphu La and Gumburanjun leucogranites (High Himalaya). *Schweizerische Mineralogische und Petrographische Mitteilungen* 71, 35-51.

- Frank, W., Baud, A., Honegger, K., Trommsdorff, V., 1987. Comparative studies on profiles across the Northwest Himalayas. In: The anatomy of mountain ranges. (eds Schaer, J.-P., Rodgers, J.), Princeton University Press, 261-275.
- Frank, W., Grasemann, B., Guntli, P., Miller, C., 1995. Geological Map of the Kishtwar-Chamba-Kulu Region (NW Himalaya, India). *Jahrbuch der Geologischen Bundesanstalt* 138, 299-308.
- Frank, W., Hoinkes, G., Miller, C., Purtscheller, F., Richter, W., Thoeni, M., 1973. Relations between metamorphism and orogeny in a typical section of the Indian Himalayas; NW-Himalaya; S-Lahul, Kulu; Himachal Pradesh; first comprehensive report. *Tschemaks Mineralogische und Petrographische Mitteilungen* 20, 303-332
- Frank, W., Miller, C., Grasemann, B., 1995. Ar/Ar-ages of detrital micas and paleogeographic provenance of Proterozoic clastic sediments in the Himalayas. In: 10th Himalaya-Karakorum-Tibet workshop; abstract volume.
- Frank, W., Thoni, M., Purtscheller, F., 1977. Geology and petrography of Kulu - South Lahul area. *Colloques Internationaux du Centre National de la Recherche Scientifique* 268, 147-172.
- Fuchs, G., 1982. The geology of western Zaskar. *Jahrbuch der Geologischen Bundesanstalt Wien*. 125, 1-50.
- Fuchs, G., 1987. The geology of southern Zaskar: evidence for the autochthony of the Tethys zone of the Himalaya. *Jahrbuch der Geologischen Bundesanstalt Wien*. 130, 465-491.
- Fuchs, G., 1989. Arguments for the autochthony of the Tibetan Zone: discussion. *Eclogae geologicae Helvetiae* 82, 685-692.
- Fuchs, G., 2001. Sedimentary facies patterns of Zaskar - indications of geodynamic events. *Journal of Asian Earth Sciences*. 19.p 19
- Fuchs, G., Linner, M., 1995. Geological traverse across the western Himalaya; a contribution to the geology of eastern Ladakh, Lahul, and Chamba. *Jahrbuch der Geologischen Bundesanstalt Wien*. 138, 655-685.
- Gaetani, M., Garzanti, E., Jadoul, F., 1985. Main structural elements of Zaskar, NW Himalaya (India). *Rendiconti della Societa Geologica Italiana*. 8, 3-8.
- Gaetani, M., Garzanti, E., Tintori, A., 1990. Permo-Carboniferous stratigraphy in SE Zaskar and NW Lahul (NW Himalaya, India). *Eclogae geologicae Helvetiae* 83, 143-161.
- Gansser, A., 1964. *Geology of the Himalayas*. London, John Wiley and Sons, 289p.
- Gansser, A., 1980. The significance of the Himalayan suture zone. *Tectonophysics* 62, 37-52.
- Gapais, D., Pêcher, A., Gilbert, E., Ballèvre, M., 1992. Synconvergence spreading of the Higher Himalaya Crystalline in Ladakh. *Tectonics* 11, 1045-1056.
- Garzanti, E., Baud, A., Mascle, G., 1987. Sedimentary record of the northward flight of India and its collision with Eurasia (Ladakh Himalaya, India). *Geodinamica Acta*. 1, 297-312.
- Garzanti, E., Van Haver, T., 1988. The Indus clastics; forearc basin sedimentation in the Ladakh Himalaya (India). *Sedimentary Geology* 59, 237-249.
- Gilbert, E., 1986. Evolution structurale d'une chaîne de collision: Structures et déformations dans le Nord de la plaque indienne en Himalaya du Ladakh [Doctoral thesis] Université de Poitiers, 225 p.
- Girard, M. 2001. Metamorphism and tectonics of the transition between non metamorphic Tethyan Himalaya sediments and the North Himalayan Crystalline Zone (Rupshu area, Ladakh, NW India). *Mémoires de Géologie*. Lausanne (in press), 100 pp.

- Girard, M., Bussy, F., 1999. Late Pan-African magmatism in the Himalaya: new geochronological and geochemical data from the Ordovician Tso Morari metagranites (Ladakh, NW India). *Schweizerische Mineralogische und Petrographische Mitteilungen* 79, 399-418.
- Girard, M., Steck, A., Thelin, P., 1999. The Dutung-Thaktote extensional fault zone and nappe structures documented by illite crystallinity and clay-mineral paragenesis in the Tethys Himalaya between Spiti river and Tso Morari, NW India. *Schweizerische Mineralogische und Petrographische Mitteilungen* 79, 419-430.
- Griesbach, C.L., 1891. Geology of the Central Himalaya. Memoir of the Geological Survey of India XXIII. 1-232
- Griesbach, C.L., 1891. Geology of the Central Himalaya. Memoir of the Geological Survey of India XXIII. 1-232
- Grocott, J., Wilson, J., 1997. Ascent and emplacement of granitic plutonic complexes in subduction-related extensional environments. In: *Deformation-enhanced fluid transport in the Earth's crust and mantle* (ed Holness, M.B.), London, Chapman and Hall, 173-195
- Grujic, D., Casey, M., Davidson, C., Hollister, L.S., Kuendig, R., Pavlis, T.L., ; Schmid, S.M, 1996. Ductile extrusion of the Higher Himalayan Crystalline in Bhutan; evidence from quartz microfabrics. *Tectonophysics*. 260, 21-43.
- Guillot, S, Hodges, K.V., Le Fort, P, Pêcher, 1994. New constraints on the age of the Manaslu Leucogranite; evidence for episodic tectonic denudation in the central Himalayas. *Geology (Boulder)*. 22, 559-562.
- Guntli, P., 1993. Geologie und Tectonik des Higher und Lesser Himalaya im Gebiet von Kishtwar, SE Kashmir (NW Indien). [Dissertation Nr. 10211 thesis] ETHZ, 198 p.
- Hanmer, S., 1986. Asymmetrical pull-aparts and foliation fish as kinematic indicators. *Journal of Structural Geology*. 8, 111-122.
- Hanmer, S., Passchier, C., 1991. Shear-sense indicators; a review. *Geological Survey of Canada*. 72 pp.
- Harrison, T.M., Mahon, K.I., Guillot, S, Hodges, K.V., Le Fort, P, Pêcher, A., 1995. New constraints on the age of the Manaslu leucogranite; evidence for episodic tectonic denudation in the central Himalaya; discussion and reply. *Geology (Boulder)*. 23, 478-480.
- Hayden, H.H., 1904. The Geology of Spiti, with part of Bashahr and Rupshu: Memoir of the Geological Survey of India, 26, p. 1-129.
- Herren, E., 1987. Northeast-southwest extension within the Higher Himalayas (Ladakh, India). *Geology* 15, 409-413.
- Hodges, K.V., 2000. Tectonics of the Himalaya and southern Tibet from two perspectives. *Geological Society of America Bulletin*. 112; 324-350.
- Hodges, K.V., McKenna, L.W., 1987. Realistic propagation of uncertainties in geologic thermobarometry. *American Mineralogist* 72, 671-680.
- Hodges, K.V., Parrish, R.R., Housh, T.B., Lux, D.R., Burchfiel, B.C., Royden, L.H., Chen, Z., 1992. Simultaneous Miocene extension and shortening in the Himalayan Orogen. *Science* 258, 1466-1470.
- Hodges, K.V., Parrish, R.R., Searle, M.P., 1996. Tectonic evolution of the central Annapurna Range, Nepalese Himalayas. *Tectonics*. 15, 1264-1291
- Holland, T.J. and Powell, R., 1998. An internally consistent thermodynamic data set for phases of petrological interest. *Journal of Metamorphic Geology* 16, 309-343.



- Honegger, K., 1983. Strukturen und Metamorphose im Zaskar Kristallin. [Dissertation Nr. 7456 thesis] ETHZ, 117 p.
- Honegger, K., Dietrich, V., Frank, W., Gansser, A., Thoeni, M., Trommsdorff, V., 1982. Magmatism and metamorphism in the Ladakh Himalayas (the Indus-Tsangpo suture zone). *Earth and Planetary Science Letters* 60, 253-292.
- Hubbard, M.S., Harrison, T.M., 1989.  $^{40}\text{Ar}/^{39}\text{Ar}$  age constraints on deformation and metamorphism in the Main Central Thrust Zone and Tibetan Slab, eastern Nepal Himalaya. *Tectonics* 8, 865-880.
- Hughes, N.C., Jell, P.A., 1999. Biostratigraphy and biogeography of Himalayan Cambrian trilobites. *Special Paper Geological Society of America*. 328, 109-116.
- Khan, A., Raghavendra, R., Ganju, J.L., Sankaran, V., 1971. Discovery of invertebrate and vertebrate fossils from Upper Murree Formation of Palkhai Syncline near Udhampur, Jammu and Kashmir State, India. *Journal of the Palaeontological Society of India* 16, 16-21.
- Kündig, R., 1989. Domal structures and high-grade metamorphism in the Higher Himalayan Crystalline, Zaskar Region, north-west Himalaya, India. *Journal of Metamorphic Geology* 7, 43-55.
- Leake, B.E., and 21 co-authors, 1997. Nomenclature of amphiboles: report of the subcommittee on amphiboles of the International Mineralogical Association, Commission on New Minerals and Mineral Names. *The Canadian Mineralogist* 35, 219-246.
- Lydekker, R., 1878. Notes on the Geology of Kashmir, Kishtwar and Pangi. *Records of the Geological Survey of India* 11, 30-64
- Lydekker, R., 1883. The geology of the Kashmir and Chamba Territories, and the British district of Khagan. *Memoir of the Geological Survey of India* 22, 108-112.
- Massey, J.A., Harmon, R.S., Harris, B.W., 1994. Constrating retrograde oxygen isotope exchange behaviour and implications: examples from the Langtang Valley, Nepal. *Journal of metamorphic Geology* 12, 261-272.
- McElroy, R., Cater, J., Roberts, I., Peckham, A., Bond, M., 1990. The structure and stratigraphy of SE Zaskar, Ladakh Himalaya. *Journal of the Geological Society of London* 147, 989-997.
- Moecher, D.P., Sharp, Z.D., 1999. Comparison of conventional and garnet-aluminosilicate quartz O isotope thermometry: insights for mineral equilibration in metamorphic rocks. *American Mineralogist* 84, 1287-1303.
- Najman, Y., Garzanti, E., 2000. Reconstructing early Himalayan tectonic evolution and paleogeography from Tertiary foreland basin sedimentary rocks, northern India. In: *Special focus on the Himalaya* (eds Geissman, J.W., Glazner, A.), *Geological Society of America Bulletin* 112, 435-449.
- Nanda, M.M., Singh, M.P., 1977. Stratigraphy and sedimentation of the Zaskar area, Ladakh and adjoining parts of the Lahaul region of Himachal Pradesh. *Himalayan Geology* 6, 365-388.
- Parrish, R.R., Hodges, K.V., 1996. Isotopic constraints on the age and provenance of the Lesser and Greater Himalayan sequences, Nepalese Himalaya. *Geological Society of America Bulletin*. 108, 904-911.
- Patel, R.C., Singh, S., Asokan, A., Manickavasagam, R.M., Jain, A.K., 1993. Extensional tectonics in the Himalayan Orogen, Zaskar, NW India. In: *Himalayan Tectonics* (eds Treolar, P.J., Searle, M.P.), *Geological Society of London, Special Publication* 74, 445-459.

- Paterson, S.R., Vernon, R.H., 1995. Bursting the bubble of ballooning plutons; a return to nested diapirs emplaced by multiple processes. *Geological Society of America Bulletin* 107, 1356-1380.
- Patiño Douce, A.E., Harris, N., 1998. Experimental Constraints on Himalayan Anatexis. *Journal of Petrology* 39, 689-710.
- Patriat, P., Achache, J., 1984. India-Eurasia collision chronology has implications for crustal shortening and driving mechanism of plates. *Nature* 311, 615-621.
- Pêcher, A., 1989. The metamorphism in the central Himalaya. In: *Himalayan metamorphism* (eds Barnicoat, A.C., Treloar, P.J.), *Journal of Metamorphic Geology* 7, 31-41.
- Pêcher, A., 1991. The contact between the higher Himalaya crystallines and the Tibetan sedimentary series; Miocene large-scale dextral shearing. *Tectonics*. 10, 587-598.
- Pêcher, A., Bouchez, J.L., Le Fort, P., 1991. Miocene dextral shearing between Himalaya and Tibet. *Geology (Boulder)*. 19, 683-685.
- Pickett, J., Jell, J., Conaghan, P., Conaghan, P., Powell, C., Dowell, C., 1975. Jurassic invertebrates from the Himalayan Central Gneiss. *Alcheringa*. 1, 71-85.
- Platt, J.P., 1984. Secondary cleavages in ductile shear zones. *Journal of Structural Geology*. 6, 439-442.
- Platt, J.P., Vissers, R.L.M., 1980. Extensional structures in anisotropic rocks. *Journal of Structural Geology*. 2, 397-410.
- Pognante, U., Castelli, D., Benna, P., Genovese, G., Oberli, F., Meier, M., Tonarini, M., 1990. The crystalline units of the High Himalayas in the Lahul Zaskar region (northwest India) : metamorphic-tectonic history and geochronology of the collided and imbricated India plate. *Geological Magazine* 127, 191-116.
- Pognante, U., Genovese, G., Lombardo, B., Rossetti, P., 1987. Preliminary data on the High Himalayan Crystallines along the Padum-Darcha Traverse (South-Eastern Zaskar, India). *Rendiconti della Società Italiana di Mineralogia e Petrologia* 42, 95-102.
- Pognante, U., Lombardo, B., 1989. Metamorphic evolution of the High Himalayan Crystallines in SE Zaskar, India. In: *Himalayan metamorphism* (eds Barnicoat, A.C., Treloar, P.J.). *Journal of Metamorphic Geology*. 7, 9-17.
- Powell, C.M.A., Conaghan, P.J., 1973. Polyphase deformation in Phanerozoic rocks of the Central Himalayan Gneiss, Northwest India. *Journal of Geology* 81, 127-143.
- Powell, R., Holland, T., 1994. Optimal geothermometry and geobarometry. *American Mineralogist* 79, 120-133.
- Ramberg, H., 1981. The role of gravity in orogenic belts. In: *Thrust and Nappe Tectonics* (eds McClay, K.R., Price, N.J.), *Geological Society of London, Special Publication* 9, 125-140.
- Ramsay, J.G., 1962. The geometry and mechanics of formation of "similar" type folds. *Journal of Geology*. 70, 309-327.
- Ramsay, J.G., 1967. *Folding and fracturing of rocks*. McGraw-Hill, New York. 568 p.
- Rattan, S.S., 1973. Stratigraphy and sedimentation of the Chamba area, Western Hiamchal Pradesh. *Himalayan Geology*. 3, 231-248.
- Ring, U., Brandon, M.T., Willett, S.D., Lister, G.S., 1999. Exhumation processes. In: *Exhumation processes; normal faulting, ductile flow and erosion* (eds Ring, U., Brandon, M.T., Willett, S.D., Lister, G.S.), *Geological Society Special Publications* 154, 1-27.

- Robertson, A., Degnan, P., 1994, The Dras arc complex; lithofacies and reconstruction of a Late Cretaceous oceanic volcanic arc in the Indus suture zone, Ladakh Himalaya. *Sedimentary Geology* 92, 117-145.
- Robyr, M., Vannay, J.C., Epard, J.L., Steck, A., 2002. Thrusting, extension and doming during the polyphase tectonometamorphic evolution of the High Himalayan Crystalline Zone in NW India. *Journal of Asian Earth Sciences*. in press
- Schaerer, U., Hamet, J., Allegre, C., 1984. The Transhimalaya (Gangdese) plutonism in the Ladakh region; a U-Pb and Rb-Sr study. *Earth and Planetary Science Letters* 67, 327-339.
- Searle, M.P., 1986. Structural evolution and sequence of thrusting in the High Himalayan, Tibetan-Tethys and Indus suture zones of Zaskar and Ladakh, western Himalaya. *Journal of Structural Geology* 8, 923-936.
- Searle, M.P., Cooper, D.J.W., Rex, A.J., 1988. Collision tectonics of the Ladakh-Zaskar Himalaya. In: *Tectonic evolution of the Himalayas and Tibet* (eds Shackleton, R.M., Dewey, J.F., Windley, B.F.), *Philosophical Transactions of the Royal Society of London, Series A: Mathematical and Physical Sciences* 326, 117-150.
- Searle, M.P., Waters, D.J., Dransfield, M.W., Stephenson, B.J., Walker, C.B., Walker, J.D., Rex, D.C., 1999. Thermal and mechanical models for the structural and metamorphic evolution of the Zaskar High Himalaya. In: *Continental Tectonics* (eds Mac Niocaill, C., Ryaan, P.D.), *Geological Society of London, Special Publications* 164, 139-156.
- Searle, M.P., Waters, D.J., Rex, D.C., Wilson, R.N., 1992. Pressure, temperature and time constraints on Himalayan metamorphism from eastern Kashmir and western Zaskar. *Journal of the Geological Society of London*. 149, 753-773.
- Sharp, Z.D., 1995. Oxygen isotope geochemistry of the Al<sub>2</sub>SiO<sub>5</sub> polymorphs. *American Journal of Science*. 295, 1058-1076.
- Spear, F., 1993. *Metamorphic phase equilibria and pressure-temperature-time paths*. Mineralogical Society of America. Monograph series, Washington DC, 799 pp.
- Spear, F., Kohn, M.J., Cheney, J.T., 1999. P-T paths from anatexis pelites. *Contributions to Mineralogy and Petrology* 134, 17-32.
- Spring, L., 1993. Structures gondwaniennes et himalayennes dans la zone tibétaine du Haut Lahul - Zaskar oriental (Himalaya indien). *Mémoires de Géologie Lausanne*. 14, 148 p.
- Spring, L., Bussy, F., Vannay, J.-C., Hunon, S., Cosca, M.A., 1993. Early Permian granitic dykes of alkaline affinity in the Indian High Himalaya of upper Lahul and SE Zaskar; geochemical characterization and geotectonic implications. In: *Himalayan Tectonics* (eds Treolar, P.J., Searle, M.P.), *Geological Society of London, Special Publication* 74, 251-264.
- Spring, L., Masson, H., Stutz, E., Thelin, P., Marchant, R., Steck, A., 1993. Inverse metamorphic zonation in very low-grade Tibetan zone series of SE Zaskar and its tectonic consequences (NW India, Himalaya). *Schweizerische Mineralogische und Petrographische Mitteilungen* 73, 85-95.
- Spring, L., Crespo-Blanc, A., 1992. Nappe tectonics, extension, and metamorphic evolution in the Indian Tethys Himalaya (Higher Himalaya, SE Zaskar and NW Lahul). *Tectonics* 11, 978-989.
- Srikantia, S.V., Bhargava, O.N., 1976. An outline of the structure of the area between the Rohtang Pass in Lahaul and the Indus Valley in Ladakh. *Journal of Geological Survey of India*. 41, 193-204.

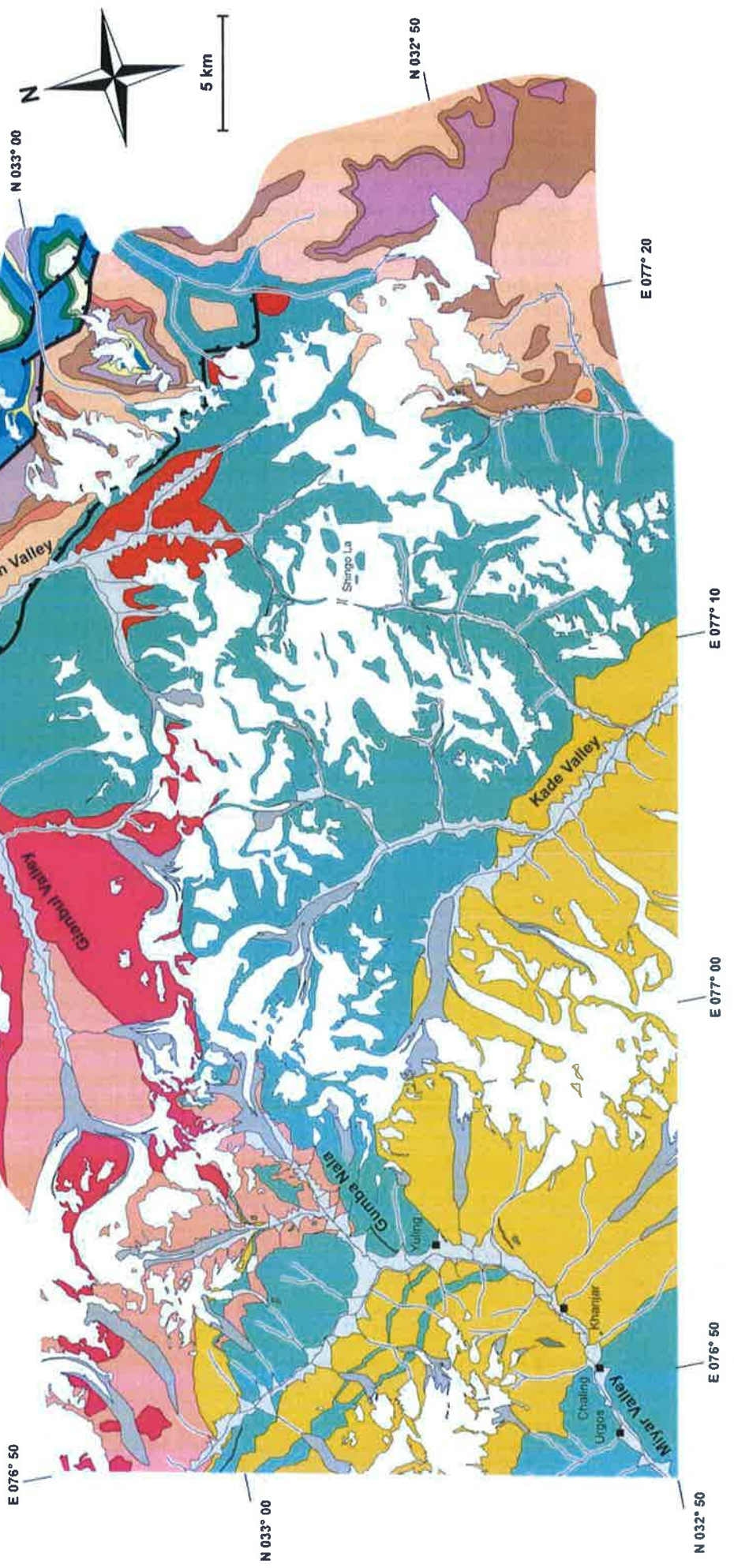
- Srikantia, S.V., Bhargava, O.N., 1979. The Tandi Group of Lahaul - its geology and relationship with the Central Himalayan Gneiss. *Journal of Geological Society of India*, 20, 531-539
- Srikantia, S.V., Ganesan, T.M., Rao, P.N., Shina, P.K., Tirkey, B., 1980. Geology of the Zaskar area, Ladakh Himalaya. In: *Himalayan Geology* (ed Nautiyal, S.), 1009-1033.
- Stäubli, A., 1989. Polyphase metamorphism and the development of the Main Central Thrust. *Journal of Metamorphic Geology* 7, 73-93.
- Steck, A., Epard, J.-L., Robyr, M., 1999. The NE-directed Shikar Beh Nappe: A major structure of the Higher Himalaya. *Eclogae geologicae Helvetiae* 92, 239-250.
- Steck, A., Epard, J.-L., Vannay J.-C., Hunziker, J., Girard, M., Morard, A., Robyr M., 1998. Geological transect across the Tso Morari and Spiti areas: the nappe structures of the Tethys Himalaya. *Eclogae geologicae Helvetiae* 91, 103-122.
- Steck, A., Spring, L., Vannay, J.-C., Masson, H., Bucher, H., Stutz, E., Marchant, R., Tièche, J.-C., 1993. Geological transect across the northwestern Himalaya in eastern Ladakh and Lahul (a model for the continental collision of India and Asia). *Eclogae geologicae Helvetiae* 86, 219-263.
- Steck, A., Spring, L., Vannay, J.-C., Masson, H., Bucher, H., Stutz, E., Marchant, R., Tièche, J.-C., 1993. The tectonic evolution of the northwestern Himalaya in eastern Ladakh and Lahul, India. In: *Himalayan Tectonics* (eds Treolar, P.J., Searle, M.P.), Geological Society of London, Special Publication 74, 264-276.
- Stephenson, B.J., Searle, M.P., Waters, D.J., Rex, D.C., 2001. Structure of the Main Central Thrust zone and extrusion of the High Himalayan deep crustal wedges, Kishtwar-Zaskar Himalaya. *Journal of the Geological Society of London*. 158, 637-652.
- Stephenson, B.J., Waters, D.J., Searle, M.P., 2000. Inverted metamorphism and the Main Central Thrust: field relations and thermobarometric constraints from the Kishtwar Window, NW Indian Himalaya. *Journal of Metamorphic Geology* 18, 571-590.
- Stoliczka, F., 1866. Summary of Geological Observations during a visit to the Provinces -Rupshu, Karnag, South Ladakh, Zaskar, Suroo and Dras- of western Tibet. *Memoir of the Geological Survey of India* 4, 337-354.
- Stutz, E., 1988. Geologie de la chaine de Nyimaling aux confins du Ladakh et du Rupshu (NW-Himalaya, Inde); evolution paleogeographique et tectonique d'un segment de la marge nord-indienne. *Memoires de Geologie Lausanne*. 3, 149 pp.
- Stutz, E., Steck, A., 1986. La terminaison occidentale du cristallin du Tso Morari (Haut-Himalaya; Ladakh meridional, Inde); subdivision et tectonique de nappe. *Eclogae geologicae Helvetiae* 79, 253-269.
- Stutz, E., Thoeni, M., 1987. The lower Paleozoic Nyimaling Granite in the Indian Himalaya (Ladakh); new Rb/ Sr data versus zircon typology. *Geologische Rundschau* 76, 307-315.
- Thöni, M., 1977. Geology, structural evolution and metamorphic zoning in the Kulu Valley (Himachal Himalayas, India) with special reference to the reversed metamorphism. *Mitt. Ges. Geol. Bergbaustud, Osterr.* 24, 125-187.
- Valdiya, K.S., 1980. Geology of Kumaun Lesser Himalaya. Wadia Institute of Himalayan Geology. Dehra Dun, India, 291 p.
- Vance, D., Harris, N., 1999. Timing of prograde metamorphism in the Zaskar Himalaya. *Geology* 27, 395-398.

- Vannay, J.-C., 1993. Geologie des chaines du Haut-Himalaya et du Pir Panjal au Haut-Lahul (NW Himalaya, Inde); paleogeographie et tectonique. *Memoires de Geologie Lausanne*. 16, 148 pp.
- Vannay, J.-C., Grasemann, B., 2001. Himalayan inverted metamorphism and syn-convergence extension as a consequence of a general shear extrusion. *Geological Magazine* 138, 253-276.
- Vannay, J.-C., Hodges, K.V., 1996. Tectonometamorphic evolution of the Himalayan metamorphic core between the Annapurna and Dhaulagiri, central Nepal. *Journal of Metamorphic Geology* 14, 635-656.
- Vannay, J.-C., Sharp, Z.D., Grasemann, B., 1999. Himalayan inverted metamorphism constrained by oxygen isotope thermometry. *Contributions to Mineralogy and Petrology* 137, 90-101.
- Vannay, J.-C., Steck, A., 1995. Tectonic evolution of the High Himalaya in Upper Lahul (NW Himalaya, India). *Tectonics* 14, 253-263.
- Vigneresse, J.L., Clemens, J.D., 2000. Granitic magma ascent and emplacement: neither diapirism nor neutral buoyancy. In: *From the Arctic to the Mediterranean: Salt, Shale and Igneous Diapirs in and around Europe* (eds Vendeville, B., Mart, Y., M.T., Vigneresse, J.L.), Geological Society Special Publications 174.
- Walker, J.D., Martin, M.W., Bowring, S.A., Searle, M.P., Waters, D.J., Hodges, K.V., 1999. Metamorphism, melting, and extension : age constraints from the High Himalayan Slab of southeast Zaskar and northwest Lahaul. *Journal of Geology* 107, 473-495.
- Whittington, A., Harris, N.B.W., Ayres, M.W., Foster, G., 2000. Tracing the origins of the western Himalaya; an isotopic comparison of the Nanga Parbat massif and Zaskar Himalaya. In: *Tectonics of the Nanga Parbat syntaxis and the western Himalaya*, Geological Society Special Publications. 170, 201-218.
- Wiesmayr, G., Grasemann, B., 1999. Balanced cross-section and depth-to-detachment calculations for the Tethyan Himalaya (Spiti, N India); where is the crystalline basement of the Higher Himalaya? *Journal of Conference Abstracts* 4/1, EUG 10. p51
- Worley, B., Powell, R., 2000. High-precision relative thermobarometry : theory and worked example. *Journal of Metamorphic Geology* 18, 91-101.
- Wyss, M., 1999. Structural geology and metamorphism of the Spiti valley-eastern Lahul-Parvati valley area, Himachal Himalaya (India). Thèse de doctorat, Université de Lausanne, 183 p.
- Wyss, M., 2000. Metamorphic evolution of the northern Himachal Himalaya: phase equilibria constraints and thermobarometry. *Schweizerische Mineralogische und Petrographische Mitteilungen* 80, 317-350.
- Wyss, M., Hermann, J., Steck, A., 1999. Structural and metamorphic evolution of the northern Himachal Himalaya, NW India (Spiti-eastern Lahul-Parvati valley traverse). *Eclogae geologicae Helveticae* 92, 3-44.

**Plate A:** Geological map of the NW Lahul – SE Zaskar. The geological mapping of the north-western part of the map was led by Dèzes (1999). Because of the lack of detailed topographical map of this region, the geological map is based on satellite imagery.

- Phe Formation (Precambrian-Lower Cambrian)
- Graphitic-quartzitic horizon (Phe Formation)
- Phe Formation (migmatites)
- Karsha Formation (Lower to Middle Cambrian)
- Kurgiakh Formation (Middle to Upper Cambrian)
- Thaple Formation (Ordovician)
- Muth Formation (Devonian)
- Lipak Formation (Lower Carboniferous)

- Po + Guanmachidam Formation (Carboniferous to Lower Permian)
- Panjal Traps (Middle Permian)
- Kuling Formation (Upper Permian)
- Lilang Formation (Triassic)
- Kade orthogneiss (ca. 470 Ma)
- Tertiary Leucogranites (22 Ma)
- Metabasitic lenses
- Normal faults



- No. 28 HÜRLIMANN A., BESSON-HURLIMANN A and MASSON H. 1995. Stratigraphie et tectonique de la partie orientale de l'écaïlle de la Gummfluh (Domaine Briançonnais des Préalpes). 132 pp. 62 text-figs., 39 pl., 6 maps.
- No. 29 DOBMEIER C. 1996. Die variskische Entwicklung des südwestlichen Aiguilles Rouges Massives (Westalpen, Frankreich). 191 pp. 70 text-figs., 18 tables., 1 map.
- No. 30 BAUD A., POPOVA I., DICKINS J.M., LUCAS S. and ZAKHAROV Y. 1997. Late Paleozoic and early Mesozoic circum-Pacific events : biostratigraphy, tectonic and ore deposits of Primorye (far East Russia). IGCP Project 272. 202 pp., 71 text-figs., 48 pls.
- No. 31 ARMANDO G. 1999. Intracontinental alkaline magmatism : geology, petrography, mineralogy and geochemistry of the Jebel Hayim Massif (Central High Atlas, Morocco). 106 pp. 51 text-figs., 23 tab., 1 map.
- No. 32 DEZES P. 1999. Tectonic and metamorphic evolution of the Central Himalayan Domain in Southeast Zaskar (Kashmir, India). 145 pp., 89 text-figs., 1 map.
- No. 33 AMODEO F. 1999. Il Triassico terminale- Giurassico del Bacino Lagonegrese. Studi stratigrafici sugli Scisti Silicei della Basilicata (Italia meridionale). 160 pp., 50 text-figs., 10 pl.
- No. 34 SAVARY J. and GUEX J. 1999. Discrete biochronological scales and Unitary Associations: Description of the BioGraph computer program. 282 pp. 21 text-figs.
- No. 35 GIRARD M. 2001 . Metamorphism and tectonics of the transition between non metamorphic Tethyan Himalaya sediments and the North Himalayan Crystalline Zone (Rupshu area, Ladakh, NW India). 96 pp., 7 pl.
- No. 36 STAMPFLI G. M. 2001. Geology of the western Swiss Alps, a guide-book. 195 pp., 67 text-figs., 7 pl.
- No. 37 REY D. 2002. Shear2F, un logiciel de modélisation tectonique. 52 pp., 122 text-figs.
- No. 38 TEMGOUA E. 2002. Les accumulations ferrugineuses actuelles de bas de versants en zone forestière humide du Sud-Cameroun. Evolutions pétrologiques des faciès et des éléments traces en relation avec le cuirassement. 134 pp., 83 text-figs., 4 pl.
- No. 39 RAKUS M. and GUEX J. 2002. Les ammonites du Jurassique Inférieur et Moyen de la dorsale Tunisienne. 217 pp., 109 text-figs., 33 pl.
- No. 40 ROBYR M. 2002. Thrusting, extension and doming in the High Himalaya of Lahul-Zaskar area (NW India). 126 pp., 62 text-figs. 1 map.



# Mémoires de Géologie (Lausanne)

- No. 1\* BAUD A. 1987. Stratigraphie et sédimentologie des calcaires de Saint-Triphon (Trias, Préalpes, Suisse et France). 202 pp., 53 text-figs., 29 pls.
- No. 2 ESCHER A., MASSON H. and STECK A. 1988. Coupes géologiques des Alpes occidentales suisses. 11 pp., 1 text-figs., 1 map.
- No. 3\* STUTZ E. 1988. Géologie de la chaîne Nyimaling aux confins du Ladakh et du Rupshu (NW-Himalaya, Inde). Evolution paléogéographique et tectonique d'un segment de la marge nord-indienne. 149 pp., 42 text-figs., 11 pls. 1 map.
- No. 4 COLOMBI A. 1989. Métamorphisme et géochimie des roches mafiques des Alpes ouest-centrales (géoprofil Viège-Domodossola-Locarno). 216 pp., 147 text-figs., 2 pls.
- No. 5 STECK A., EPARD J.-L., ESCHER A., MARCHANT R., MASSON H. and SPRING L. 1989 Coupe tectonique horizontale des Alpes centrales. 8 pp., 1 map.
- No. 6 SARTORI M. 1990. L'unité du Barrhorn (Zone pennique, Valais, Suisse). 140 pp., 56 text-figs., 3 pls.
- No. 7 BUSSY F. 1990. Pétrogenèse des enclaves microgrenues associées aux granitoïdes calco-alcalins: exemple des massifs varisque du Mont-Blanc (Alpes occidentales) et miocène du Monte Capanne (Ile d'Elbe, Italie). 309 pp., 177 text-figs.
- No. 8\* EPARD J.-L. 1990. La nappe de Morcles au sud-ouest du Mont-Blanc. 165 pp., 59 text-figs.
- No. 9 PILLOUD C. 1991. Structures de déformation alpines dans le synclinal de Permo-Carbonifère de Salvan-Dorénaz (massif des Aiguilles Rouges, Valais). 98 pp., 59 text-figs.
- No. 10\* BAUD A., THELIN P. and STAMPFLI G. 1991. (Eds.). Paleozoic geodynamic domains and their alpidic evolution in the Tethys. IGCP Project No. 276. Newsletter No. 2. 155 pp.
- No. 11 CARTER E.S. 1993 Biochronology and Paleontology of uppermost Triassic (Rhaetian) radiolarians, Queen Charlotte Islands, British Columbia, Canada. 132 pp., 15 text-figs., 21 pls.
- No. 12\* GOUFFON Y. 1993. Géologie de la "nappe" du Grand St-Bernard entre la Doire Baltée et la frontière suisse (Vallée d'Aoste -Italie). 147 pp., 71 text-figs., 2 pls.
- No. 13 HUNZIKER J.C., DESMONS J., and HURFORD AJ. 1992. Thirty-two years of geochronological work in the Central and Western Alps: a review on seven maps. 59 pp., 18 text-figs., 7 maps.
- No. 14 SPRING L. 1993. Structures gondwaniennes et himalayennes dans la zone tibétaine du Haut Lahul-Zanskar oriental (Himalaya indien). 148 pp., 66 text-figs., 1 map.
- No. 15 MARCHANT R. 1993. The Underground of the Western Alps. 137 pp., 104 text-figs.
- No. 16 VANNAY J.-C. 1993. Géologie des chaînes du Haut-Himalaya et du Pir Panjal au Haut-Lahul (NW-Himalaya, Inde). Paléogéographie et tectonique. 148 pp., 44 text-figs., 6 pls.
- No. 17\* PILLEUIT A. 1993. Les blocs exotiques du Sultanat d'Oman. Evolution paléogéographique d'une marge passive flexurale. 249 pp., 138 text-figs., 7 pls.
- No. 18 GORICAN S. 1994. Jurassic and Cretaceous radiolarian biostratigraphy and sedimentary evolution of the Budva Zone (Dinarides, Montenegro). 120 pp., 20 text-figs., 28 pls.
- No. 19 JUD R. 1994. Biochronology and systematics of Early Cretaceous Radiolaria of the Western Tethys. 147 pp., 29 text-figs., 24 pls.
- No. 20 DI MARCO G. 1994. Les terrains accretés du sud du Costa Rica. Evolution tectonostratigraphique de la marge occidentale de la plaque Caraïbe. 166 pp., 89 text-figs., 6 pls.
- No. 21\* O'DOGHERTY L. 1994. Biochronology and paleontology of Mid-Cretaceous radiolarians from Northern Apennines (Italy) and Betic Cordillera (Spain). 415 pp., 35 text-figs., 73 pls.
- No. 22 GUEX J. and BAUD A. (Eds.). 1994. Recent Developments on Triassic Stratigraphy. 184 pp.
- No. 23 BAUMGARTNER P.O., O'DOGHERTY L., GORICAN S., URQUHART E., PILLEUIT A. and DE WEVER P. (Eds.). 1995. Middle Jurassic to Lower Cretaceous Radiolaria of Tethys: Occurrences, Systematics, Biochronology. 1162 p.
- No. 24 REYMOND B. 1994. Three-dimensional sequence stratigraphy offshore Louisiana, Gulf of Mexico (West Cameron 3D seismic data). 215 pp., 169 text-figs., 49 pls.
- No. 25 VENTURINI G. 1995. Geology, Geochronology and Geochemistry of the Inner Central Sezia Zone. (Western Alps - Italy). 183 pp. 57 text-figs, 12 pls.
- No. 26 SEPTFONTAINE M., BERGER J.P., GEYER M., HEUMANN C., PERRET-GENTIL G. and SAVARY, J. 1995. Catalogue des types paléontologiques déposés au Musée Cantonal de Géologie, Lausanne. 76 pp.
- No. 27 GUEX, J. 1995. Ammonites hettangiennes de la Gabbs Valley Range (Nevada, USA). 130 pp., 22 figs., 32 pl.

\*: out of print ..... (continued inside)

Order from **Institut de Géologie et Paléontologie,**  
**Université de Lausanne. BFSH-2. CH-1015, SWITZERLAND.**  
<http://www-sst.unil.ch/publications/memoires.htm> Fax: (41) 21-692.43.05  
Bank Transfer: Banque Cantonale Vaudoise 1002 Lausanne  
Account Number: **C.323.52.56** Institut de Géologie, rubrique: Mémoires  
Price CHF 30 per volume except volume 23 (CHF 100). The price doesn't include postage and handling.  
- Please do not send check -